Université de Strasbourg

UNIVERSITÉ DE STRASBOURG

École Doctorale des Sciences de la Vie et de la Santé STRASBOURG

ÉCOLE DOCTORALE SCIENCES DE LA VIE ET DE LA SANTE

[Institut de Génétique et de Biologie Moléculaire et Cellulaire]

THÈSE présentée par :

[Jia SONG]

soutenue le : **26 Février 2020**

pour obtenir le grade de : **Docteur de l'université de Strasbourg**

Discipline/ Spécialité : Biophysique

Caractérisation de l'entrée en sénescence en utilisant les mutant de longévité et l'intervention concernant les facteurs de vieillissement ERC et ROS

THÈSE dirigée par :

[M. Gilles CHARVIN]	Directeur de recherche, université de Strasbourg

RAPPORTEURS :

[Mme. P-Y.J. WU]	Directeur de recherche, Université de Rennes 1
[M. Z. XU]	Chargé de recherches, Université de Sorbonne

AUTRES MEMBRES DU JURY :

[M.M. MENDOZA]	Chargé de recherches, IGBMC

This report is dedicated to all the person that I have encountered during my thesis, my parents faraway, my friends who have been accompanied me aboard.

Remerciements

I would like to thank specially the researcher Dr. Sandrine MORLOT for helping me enormously during my thesis. And all the lab members: Audrey MATIFAS, Basile JACQUEL, Sophie QUINTIN, Théo ASPERT, for their warm and kind help during my doctoral period. Finally, the team leader Dr. Gilles CHARVIN for allowing me to pursue my thesis in the host laboratory.

Last but not least, those who helped me to advance my work, though their names are not listed below.

I'm very grateful for all your inspirations.

Table of content

Chapter I

Introduction

1. The importance of studying ageing for both biological and social issues

Ageing is a complex and inevitable process which has raised scientists' attention to investigate questions such as: how the ageing induces diseases in later life. We are facing ageing as a physiological issue. Because when people ages, they become vulnerable to age-related diseases (for instance: cancer) and show an increase in morbidity and mortality. In addition, the proportion of elder population is increasing, and this may trigger serious social issues for instance: the increasing need for social security and heavy social burden. From the United Nation World Population Prospect, the population aged more than 60 years old has reached one billion in 2018 and was 12.8% of the world-wide population. If continuing the trend of population ageing, in 2100, the population aged more than 60 years old may reach three billion and the proportion could double to 27.3% (Figure 1.1). Studies on ageing and age-related diseases can help to find solutions to make people live a longer and healthier life meanwhile release the stress coming from the population ageing for the future generations.

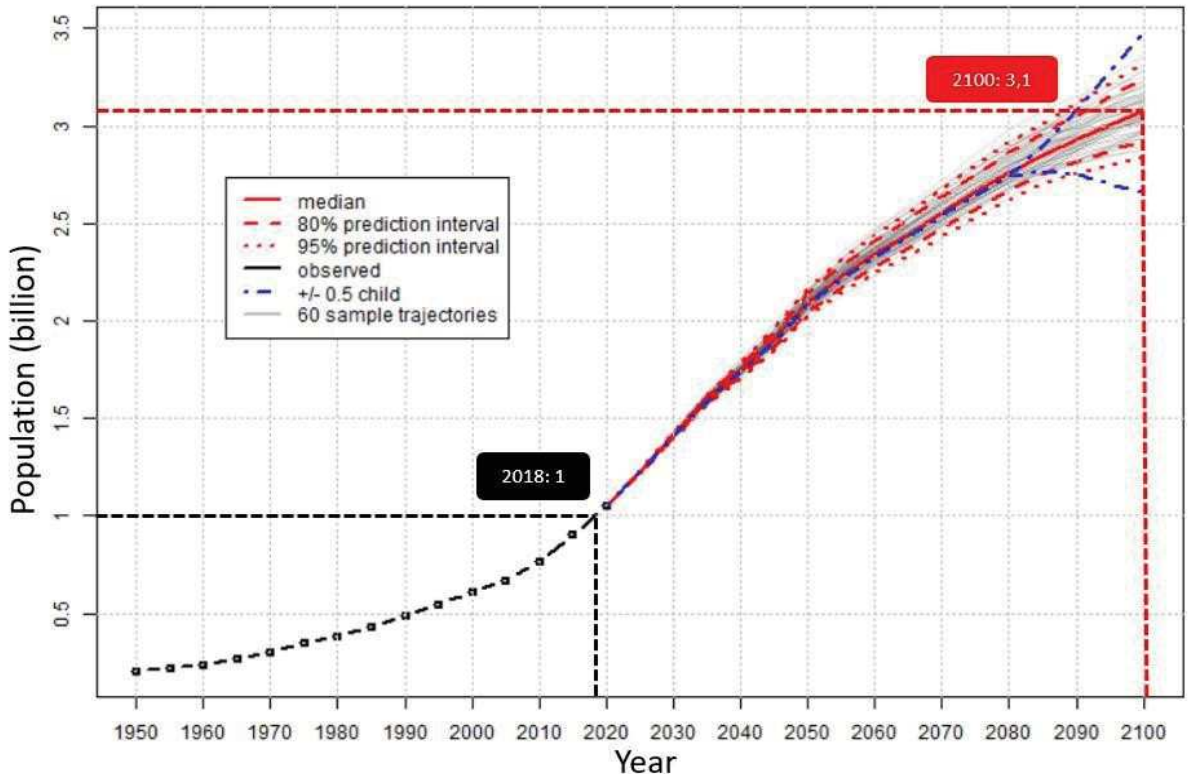

Figure 1.1 Graph of population (aged 60 and over) evolution over time based on real data and estimation

The graph shows estimates and probabilistic projections of the world population aged 60 and over (on the right) from 1950 to 2100. The population projections are based on the probabilistic projections of total fertility and life expectancy at birth. The figure displays the probabilistic median, and the 80 and 95 percent prediction intervals of the probabilistic population projections, as well as the (deterministic) high and low variant (+/- 0.5 child). (@2019 United Nations, DESA, Population Division. World Population Prospect 2019: https://population.un.org/wpp/)

2. Evolutionary understanding of ageing phenomena

2.1 Natural selection reduced with age

Study for ageing has been carried out for centuries. The first book 'The Canon of Medicine' which offered instructions for 'care of the aged' was written by Avicena (980-1037). From 19th century, when Darwin proposed the theory of biological evolution, researchers try to answer the questions: why do different organisms have a short or a long lifespan? Why must they grow old and die?

During the 1940s to 1950s, Evolutionary biologists started to realize that ageing may not evolve for the purpose of evolution, instead ageing might be a consequence of evolution.

Different traits are evolved to better survive, yet such traits may be the reason to induce ageing.

The natural selection force is reduced to maintain function and fitness in old age due to lack of reproductive capacity at later life (Figure 2) (Fabian and Flatt 2011) .Thus the selection at late life is inefficient, this decrease of selection force is the fundamental basis for the evolutionary theories of ageing.

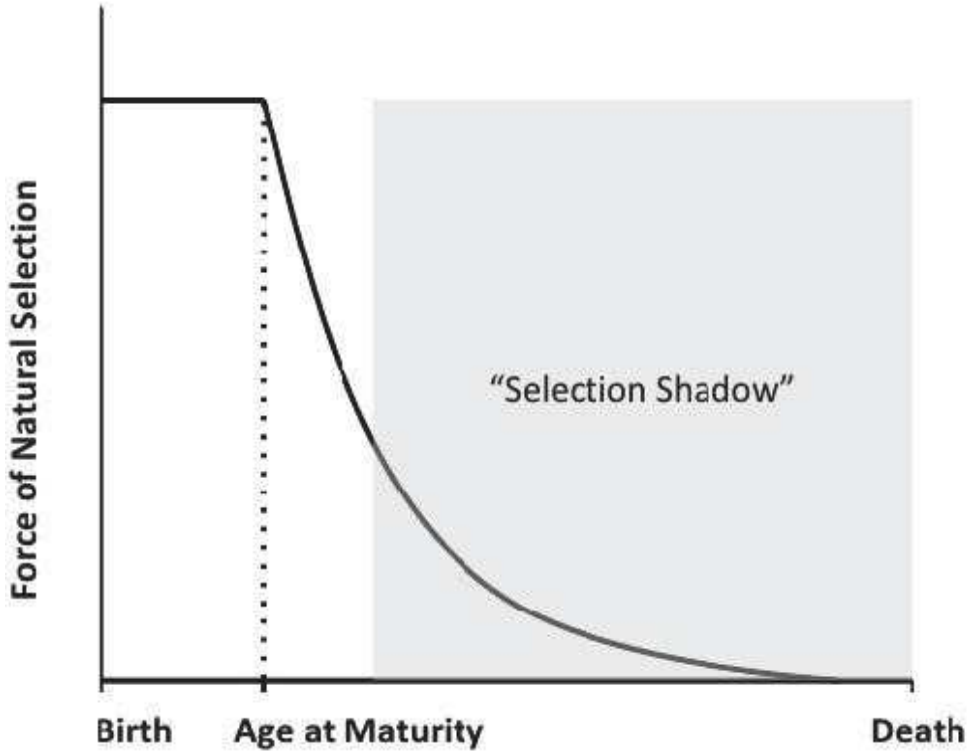

Figure 1.2 the selection force throughout the whole lifespan (Fabian and Flatt 2011)

The force of natural selection act on the population through survivors and reproduction. It is maintained at high level before reproductive maturity then starts to decrease as the reproductive capacity decline with ageing.

According to the evolutionary readout, to maintain a population, the force of selection is happening throughout its birth to death. However, once the individual pass the reproductive period, the natural selective force will not work on the individual who gone-through selection, because those beneficial mutations will not be inherited to the offspring due to the loss of reproductive capacity at old age. However, if a selection happened before the individual pass the reproductive period. Beneficial mutation may pass onto the offspring and lead to an evolutionary reservation of such beneficial mutation.

Taking Huntington disease as an example, in the study of an evolutionary biologists, Haldane (Haldane 1941). He pointed out that under the force of natural selection, the beneficial mutation (whose gene dominate the disease onset has changed) were presumably selected and their age of onset is delayed to the age of thirty. Yet, it has been speculated that the same disease was a disease of infancy for sinanthropus (Fisher 1931). It has also been proposed that such disease would not be efficiently eliminated by natural selection because most people suffering such disease may not succeed the natural selection and would have already died. Therefore, ageing phenomena may be evolved under similar mechanism due to insufficient natural selection force. The deleterious genes that negatively affect the organism at old age may not be selected against and therefore inherit to the descendants.

2.2 Mutation accumulation and antagonistic pleiotropy ageing theories

Current evolutionary explanations of ageing are based on former mentioned conceptual theory that natural selection become weak at advanced age. Two major evolutionary theories were raised: Medawar's mutation accumulation theory (Medawar 1946, Medawar 1952) and William's antagonistic pleiotropy theory (Williams 1957).

The mutation accumulation hypothesis is based on the genomic mutations or alleles which play a neutral role when selection is strong at early age. However, these genes may exhibit deleterious effects later in life (Figure 1.3A). These mutations or alleles are selected and inherited to off-springs at the age of reproduction before late-life negative effects become apparent. Consequently, ageing become an inevitable result of accumulation of mutations that exhibit deleterious effects after reproduction and eventually lead to increasing mortality in later life.

The antagonistic pleiotropy theory of ageing was proposed by Williams under the inspiration of Medawar's idea. He argued that mutations or alleles might have dual or pleiotropic (multiple) functions. They may be favored by selection and exhibiting beneficial effects during early age but become detrimental towards later life (Figure 1.3B). The beneficial effects at early age outweigh their detrimental effect at late ages. Therefore, it was proposed that ageing to be a maladaptive byproduct of selection for survival and reproduction during youth.

These two theories of ageing are not mutually exclusive and may be coordinated to generate 'grow old' phenomenon. The main difference between the two theories is that for mutation accumulation, the negative mutations are passively pass onto the descendants, while antagonistic pleiotropy actively select negative mutations on purpose during early age (Le Bourg 2001).

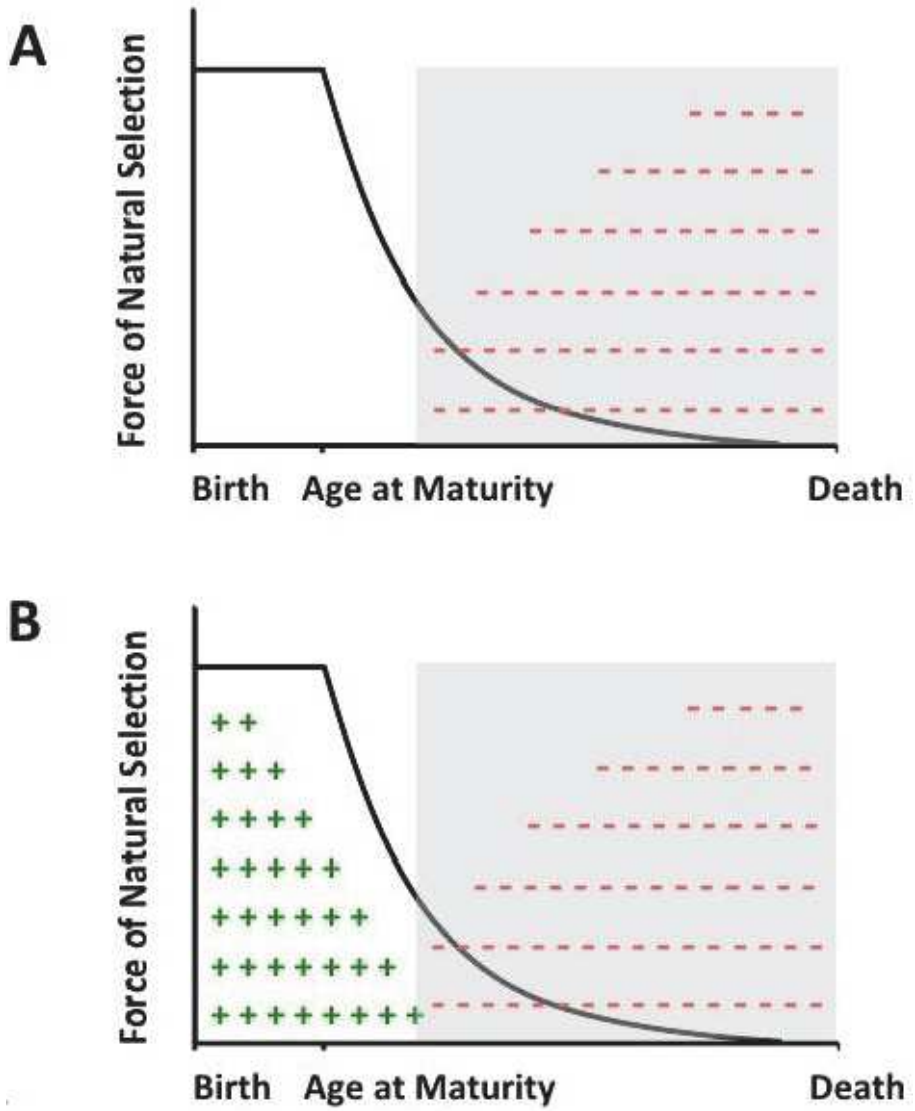

Figure 1.3 Mutation accumulation and antagonistic pleiotropy

A: Medawar's mutation accumulation theory of ageing. Due to lack of efficient selection force at late life, harmful genetic effects are maintained in the population which result in an accumulation of mutations which lead to ageing phenomenon.
B: Williams's antagonistic pleiotropy theory of ageing. Genes exhibiting multiple functions may be conserved and selected due to natural selection force at early age by reproduction. Such genes may become negatively impact on ageing at late life.

2.3 Disposable soma theory

Under the light of antagonistic pleiotropy ageing theory, in 1977, British biologist Thomas Kirkwood proposed the well-known disposable soma theory of ageing (Kirkwood 1977). The theory is based on the observation that reproduction of an individual consumes much larger energy than simple survival. He proposed that the organism have limited energy, therefore a trade-off relationship is between reproductive activities and the maintenance of the non-reproductive activities. The soma indicates the somatic material.

The authors are agreeing that 'the disposable soma theory is, in a sense, a special case of Williams's pleiotropic gene hypothesis [antagonistic pleiotropy theory].' Because in this case, the genes involved in pleiotropic functions are narrowly defined for reproductive development and soma maintenance. This group of genes regulate the energy consummation direction. The beneficial effect is due to energy saving effect in soma and redirect to reproductive functions. The detrimental effect is that ultimately this may lead to loss of soma integrity at old age (Kirkwood and Holliday 1979).

Both supportive and opposite observations for disposable soma theory of ageing are found from scientific research. For instance, bamboo is a long-lived plant can grow typically twenty to sixty years, some may even exceed more than a hundred years (Janzen 1976). They form large clonal field covering hundreds of square meters by vegetative growth from the root (rhizomatous asexual growth). However, the bamboo can also endure massive flowering through 'sexual' reproduction at a certain local region for more than a year once in their life. Then they die (Keeley and Bond 1999). This special fruiting cycle may be related to the disposable soma theory that sexual reproduction is more energetic consuming than asexual growth. It is also supported by the study of c. elegans that longevity can be extended by prevent mating but not gametogenesis. However, in other studies of c. elegans, a long-lived mutant daf-2 show active fertile individual and extend its lifespan for about 2-fold. This observation is not in line with disposable soma theory. Suggesting that other factors apart from nutrition and reproductive energy consummation are involved in longevity regulation.

These evolutionary theories remain an ideal theory which are not totally scientifically proved. They are raised according to the biological observation and scientific research. Therefore, the questions mentioned above remain unsolved. The biologists have investigated ageing from

organismal, cellular and molecular scales in order to answer such questions. Hopefully, by unraveling the underlying mechanisms contribute to ageing phenomenon, may help us to the better understanding of the emergence of ageing and avoid the high morbidity due to ageing. Eventually may even lead to the extension of lifespan.

3. Ageing, a complex and multifactorial process

Ageing is a complex and multifactorial process which has been characterized as a progressive loss of physiological integrity that leads to increasing mortality in parallel to an increase in morbidity (Case and Deaton 2017). In another word, after an organism become reproductively available, the ageing begins. To understand the ageing process, experiments and observations are performed on a wide range of animals and human as well. The gradual and subtle modifications accumulate during ageing make the readout of ageing process difficult. Taking an example from human, it is difficult to define at what age can we consider an individual as 'aged'? What are the significant features to define an aged individual? In addition, due to the individual heterogeneity, the rate of ageing may be different among individual within the same population. There may be old individual but in a healthy state whereas relatively young individual in a pathogenic condition. Whether the pathogenic condition is due to the old age or an exogenous pathogen? Due to the complexity of ageing, many observations and common traits between various species are compared to build up a general understanding of ageing.

3.1 Common ageing trends summarized by studies across species

In 1908, the German physiologist, Max Rubner, discovered a correlation between metabolic rate, body size, and longevity (Rubner 1908). By comparing five domestic animals and human, he calculated the energy expended per mass over the maximum lifespan of each animal (except for human). Although the body weight can be 50000-fold different, the amount of energy expended per mass per lifespan does not vary more than 1.5-fold between species. In another word, regardless of species or total body size, a given mass of tissue expends a given amount of energy per lifetime. The interpretation of this interesting result was that organisms contain a limited amount of 'vital principle'. The faster they consume the energy, the sooner they die.

It is reasonable that if an animal is big in size (body mass), it may contain more 'vital principle' and energy potential to live longer. Even though this definition of 'vital principle' was not

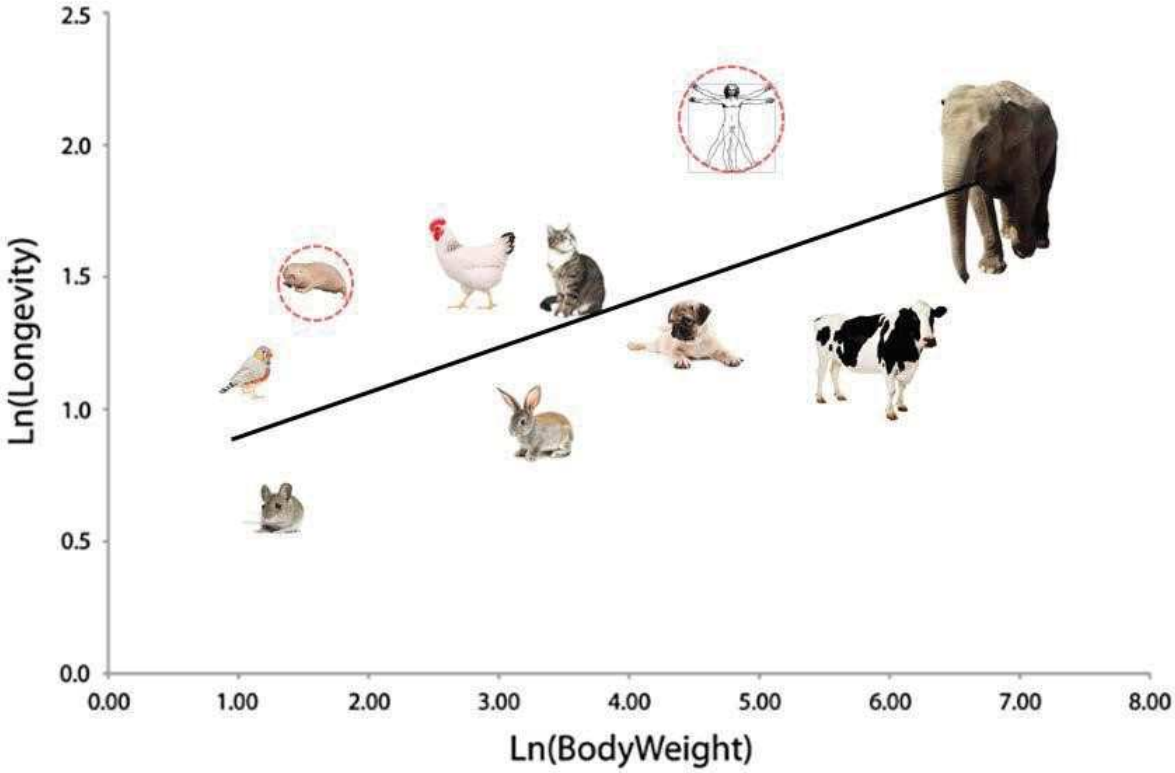

Figure 1.4 Longevity is plotted according to body weight adapted from (Morgan, Mc Cartney et al. 2013)

The correlation between body weight (Ln) and longevity (Ln) determined by various animals, the outlier animals are circled by dashed red line. They are separately naked mole rat and human.

scientifically uncovered, the positive correlation between body mass and longevity across various species has been observed as well (Figure 1.4).

This work led to the theory of 'rate of living' proposed by Pearl (Pearl 1928). Raymond Pearl, an American biologist, suggested that a high metabolic rate should lead to a faster ageing because biochemical reactions are faster. Many exceptions have been observed, for instance the marsupials show a lower basal metabolic rate than mammals of similar size, yet marsupials live shorter than mammals (Austad 2010). Also, the birds have high basal metabolic rates compare with mammals. According to the theory of "rate of living", they should be short-lived compare to similar-size mammals, yet they can live up to four-fold longer (Holmes and Austad 1995). Later, this theory was further questioned due to the methodology used to measure metabolic rates. The metabolic rates were measured by total oxygen consumption. However, larger size organisms such as elephants may consume more oxygen than smaller size organisms such as mice during the same period. If the metabolic rate were corrected by body mass, the correlation between metabolic rate and longevity could no longer be established (Figure 1.5) (Magalhães, Costa et al. 2007).

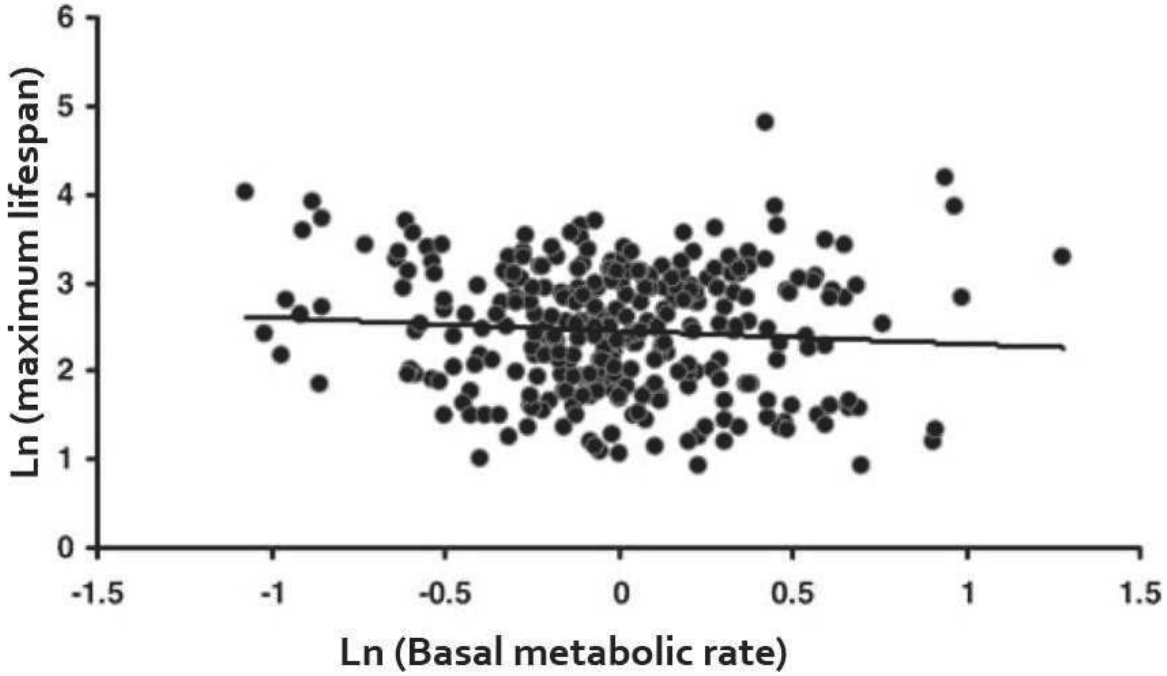

Figure 1.5 No significant correlation between metabolic rate and maximum lifespan adapted from (Magalhães, Costa et al. 2007)

Ln-transformed relationship between basal metabolic rate and maximum lifespan in different mammals. The statistics are collected from mammals (n=300). The correlation is not statistically significant.

Other factors, such as growth (Blagosklonny and Hall, 2009) and development (Magalhães, Costa et al. 2007), have been related to ageing. It has been found that, independently to the body size, developmental time is strongly associated with maximum adult life span (Figure 1.6) (Prothero 1993).

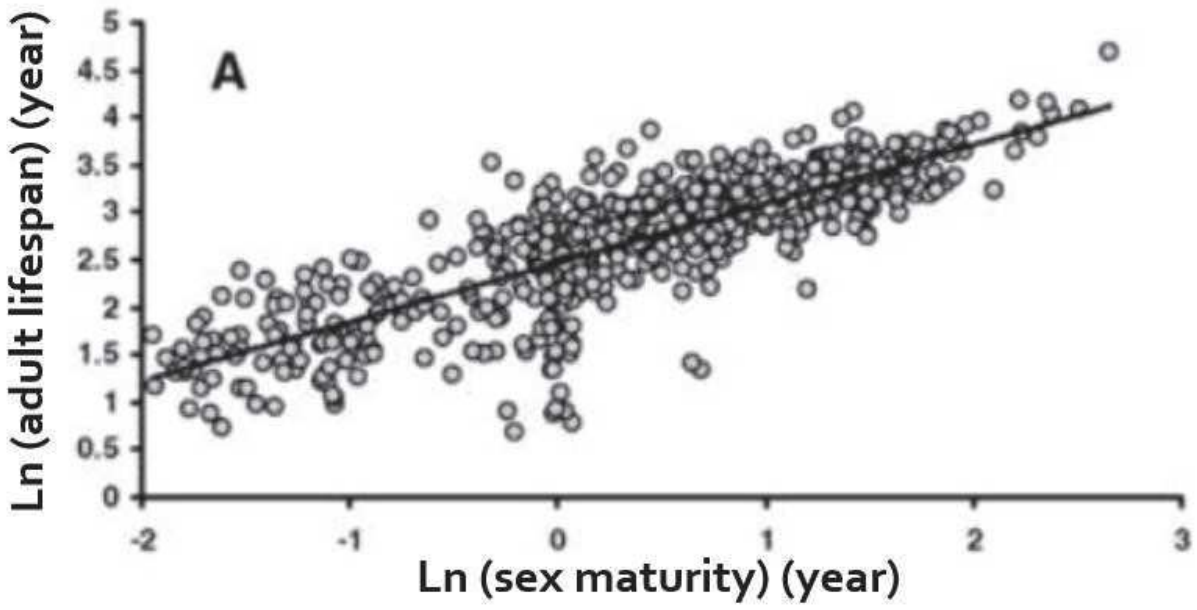

Figure 1.6 Correlation between sex maturity and adult lifespan adapted from (Magalhães, Costa et al. 2007)

Ln-transformed relationship between maturity time and adult lifespan. The statistics are collected from mammals (n=606). The correlation is statistically significant.

This correlation suggests that species exhibiting longer lifespan tend to spend longer time for reproductive maturation. It is reasonable considering that long-lived species are generally larger in size, hence it takes longer time for large-size animals to grow and become sexually mature for reproduction.

To summarize, body mass and time for reproductive maturity contribute to longevity (Figure 1.7). Other factors such as the growth rate have been found correlated to longevity as well. These examples illustrate some obvious common features of ageing process by pooling and analyzing statistics and data from various phylogenies.

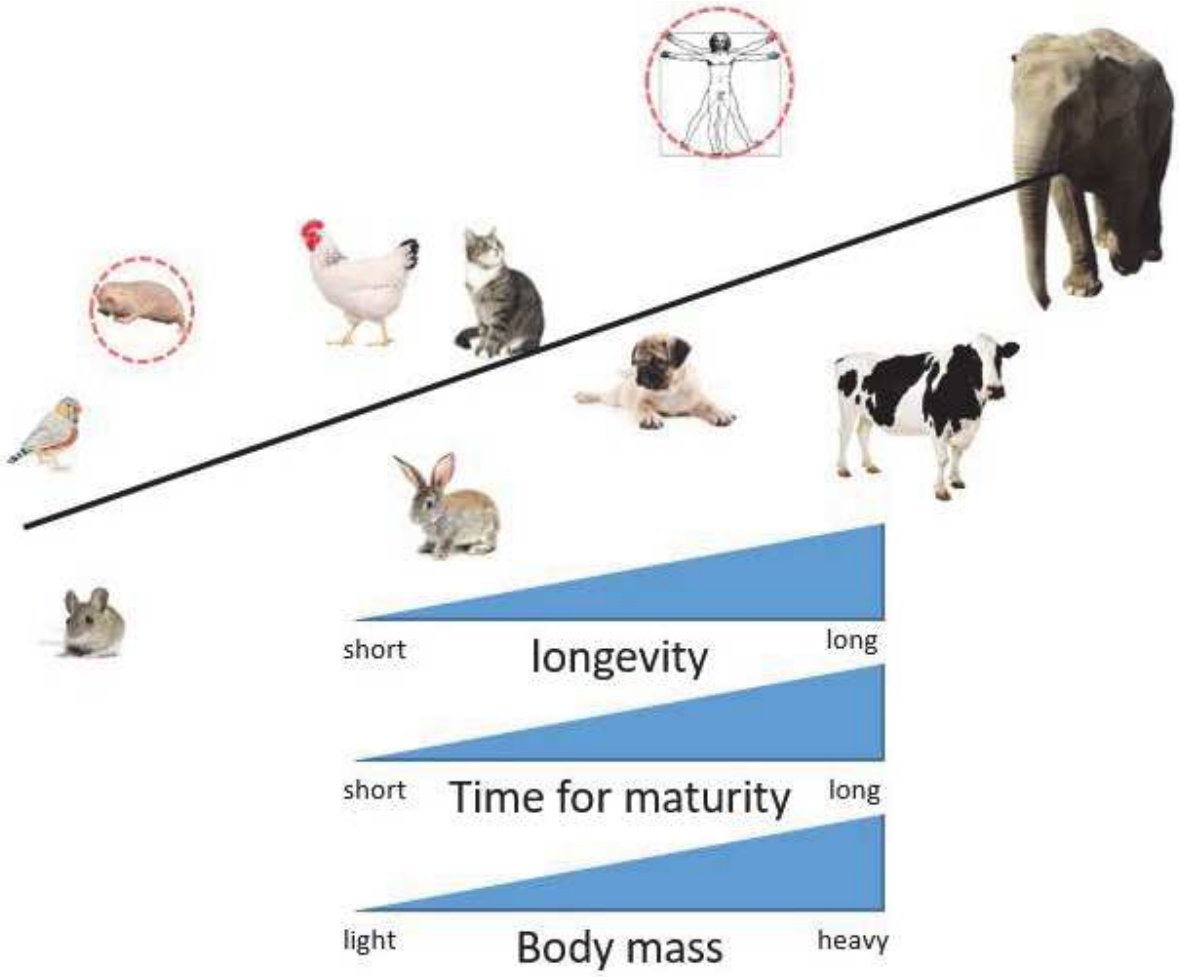

Figure 1.7 Summary of common traits observed across species

Body mass and time for sexual maturity are two traits observed along with longevity distribution across various species.

3.2 Divers organism models for ageing studies in the laboratory

Based on ageing studies across species, scientists have highlighted several interesting animals which are extensively used for investigating ageing mechanisms in the laboratory. One of the most widely used model is the rodent. Since mouse belongs to the mammal and shares on average 85% of similarity with the human genome protein coding-regions (Jang, Hua et al. 1999), many molecular and cellular mechanisms of ageing studies are carried out between young and old individuals in mice (Figure 1.8) (Kõks, Dogan et al. 2016). Due to ethical issue, such studies cannot be performed on human. Therefore, using similar mammal animal models may help to gain more information of the ageing progress on a smaller: organelle, cellular and even molecular

scales. Interventions such as dietary condition (Anderson, Shanmuganayagam et al. 2009, Pifferi, Terrien et al. 2018), environmental factors may be performed on mouse to understand the impact of exogenous factors to longevity (Xie, Neff et al. 2017, Wang, Cao et al. 2018).

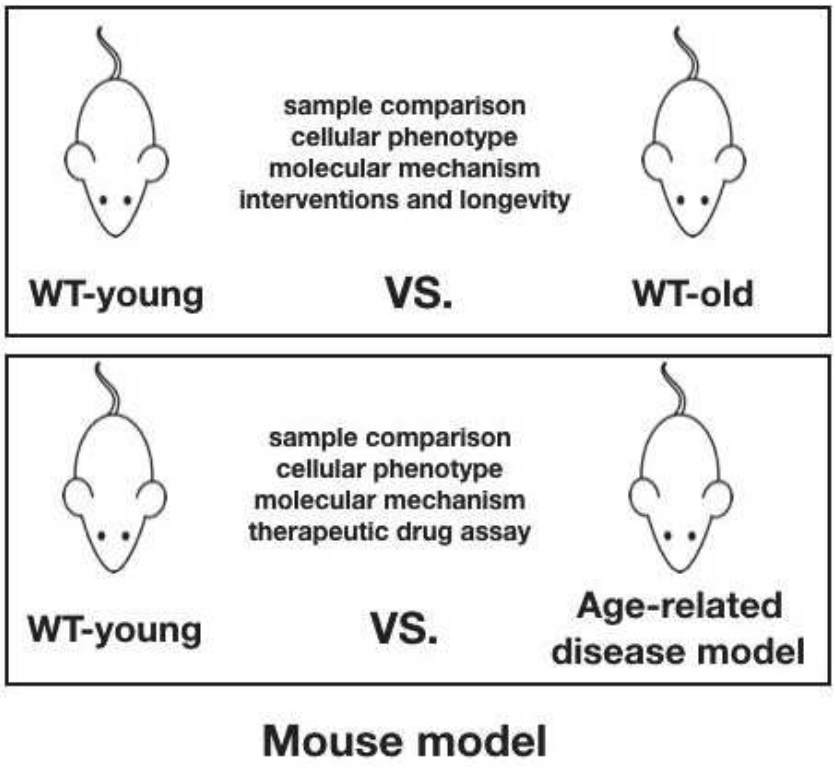

Figure 1.8 Schematic mouse model application for ageing study
Direct comparison for understanding the cellular and molecular mechanism between young and old individuals can be performed on mouse. By establishing age-related disease models on mouse, scientists can investigate the cellular and molecular mechanisms and even searching for potential therapeutic treatment.

Scientists can also establish age-related disease models on mouse to unraveling the pathogenic progression through-out the whole body and developing therapeutic approaches for clinical assay. For instance, many cancers are induced on mouse model by xenograft to observe the tumor malignancy, progression of cancer and even the metastasis. The understanding of each steps on molecular mechanisms, could lead to the potential medical treatment development.

There is other rodent model, for instance, one of the rodent family: naked mole rat has caught the attention of biologists due to its exceptionally long lifespan compared to other animals with similar size. It showed outlier behavior and deviated from the predicted correlation between longevity and body mass. Naked mole rat is a good example (red circle

in Figure 1.7) It has been proved to be the most long-lived rodent (28 years old kept in lab)

Figure 1.9 Naked mole rat
Photos of naked mole rat. (John Brighenti/Flickr/CC; .Frans Lanting/Getty Images)

(Figure 1.9) (Buffenstein 2005).

Due to the complexity of the multicellular mammal ageing progress, it is also important to understand cellular and molecular mechanisms of ageing process in animal models that are simpler. For instance, the nematode model: c. elegans and the simplest single-cell eukaryotic organism: budding yeast. The lifespan of c. elegans is approximately two to three weeks. It has fully sequenced genome, well-developed genetic methods and transparent body. Importantly, there are mutations that exhibiting longevity alteration which may extend the lifespan to more than 10 times long (Reis, Bharill et al. 2009). By studying the mechanisms underlying such lifespan alteration in simple model may help to complete further understanding in more complex organism such as human ourselves. As for the microorganism model: budding yeast, the lifespan of S. cerevisiae is approximately twenty-five generations about 2 days. It is fully sequenced and has established mature methods for genetic manipulation. The advantage of using single-cell microorganism to investigate ageing

thematic is multiple. It may minimize the influence of signal transduction issue from other cells compare to multicellular organism; easy to be conserved in the laboratory and may provide large amount of population statistics due to its small size and short period of generation time. In addition, due to its eukaryotic characteristics, many important conserved

molecular pathways, such as nutrient sensing (Conrad, Schothorst et al. 2014, González and Hall 2017) and metabolism mechanisms (Baccolo, Stamerra et al. 2018) can be studied in parallel to complete the understanding in complex eukaryotic organisms.

Not only above mentioned model organisms, but also non-human primates (Colman, Anderson et al. 2009, Colman 2018), dogs (Chapagain, Range et al. 2018), drosophila (He and Jasper 2014), zebrafish (KISHI 2004) are used for laboratory ageing research. Since ageing and longevity are difficult concepts to tackle due to the biodiversity and complexity of nature. Therefore, to gain more general understanding of ageing, diverse organism models are needed to be investigated.

4. Cellular senescence is a good starting point to understand ageing

4.1 The difference between ageing and senescence

The term 'senescence' is often used for describing ageing phenomena too. However, its meaning should not be confused with 'ageing'. Ageing describes a whole progressive process whereas the senescence is used to define the period when organism starts to show deteriorated function. Because the senescence often defines the organism subjected to more lethal change which leads to death, therefore the senescence is usually used for ageing phenomena at later life. The difference between ageing and senescence will be discussed in the following paragraph.

Taking one specific example to help differentiating the two terms. When an adolescent grows up to adult, this process can be called ageing, the physiological function is rather maturing than failing during the process. Yet such process cannot be termed as senescence because the physiological function is not weakening. In another example, for an old man who is at his 70s. He may show grey hair, loose and wrinkle skin, attenuation of vision, audition and even organ failure. This is due to the decline of physiological function at old age, both reparative and regenerative capacities are limited. Thus, such process can be termed as both ageing and senescence for the fact that both his age increase (ageing) and organism starts to show deteriorated function (senescence).

Lastly, the senescence may be triggered by other reason than simply ageing. For instance, when a person was infected by HIV virus and the immune system become deficient. The whole body may undergo a senescence process while the organism become weakening due to the disease.

4.2 Ageing occur at different scales

The concept of ageing and senescence can be applied to different organisms and at diverse scales. There is organ ageing which indicates the loss of regenerative capacity, and limited ability responding to stress (Khan, Singer et al. 2017). For these multicellular scales of ageing process, it is hard to delimit a temporal moment where the senescence start (Figure 1.10). Therefore, the 'organismal senescence' and 'organ senescence' are simply used to define the fact of 'grow old' and are like 'organismal ageing' and 'organ ageing'. Now if we take cellular ageing and cellular senescence for example. The cellular ageing in general defines the whole process of cell accumulates maturity, gradually declines its physiological function, reduces the resistance to environmental stress and becomes more and more vulnerable then finally dead. 'Cellular senescence' is clearly defined as an irreversible cell cycle arrest that occurs during cellular ageing. This term was firstly used to describe the loss of proliferative capacity of human fibroblast after successive divisions during its final stage in the study of & Moorhead fifty years ago (Hayflick and Moorhead 1961). While cellular ageing describes the whole progressive process including cellular senescence until cell death and cellular senescence refer to the specific phase when cell undergoes irreversible arrest.

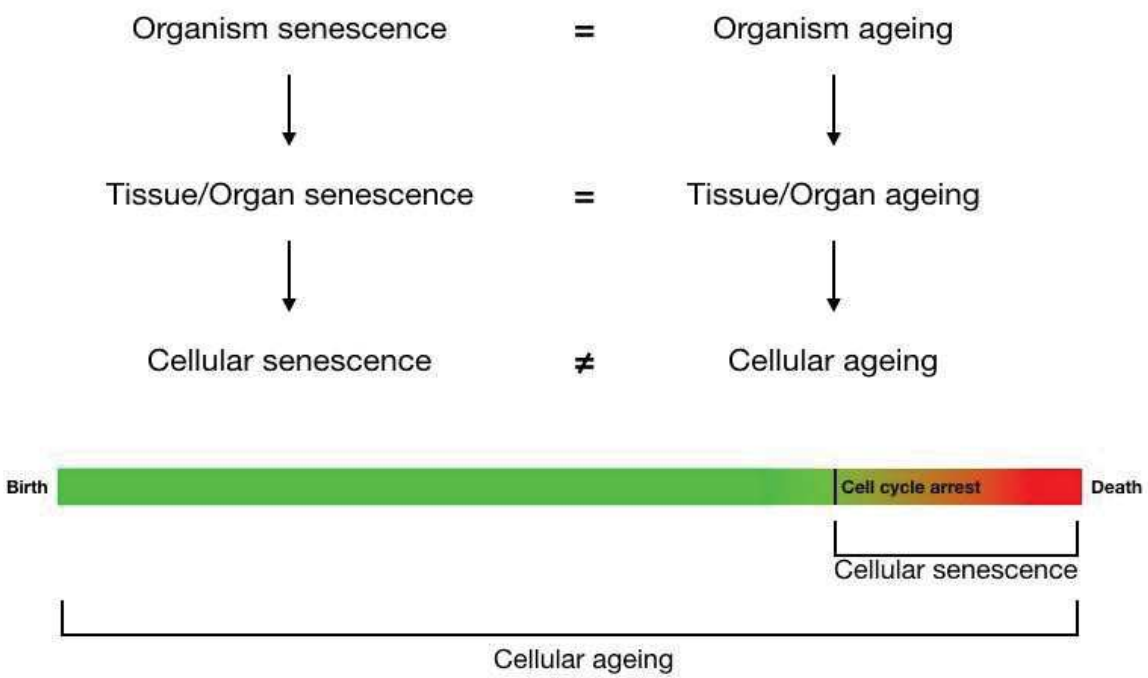

Figure 1.10. Summary of different scales of ageing

The obvious differences are not clear between ageing and senescence at higher scale. Yet cellular senescence is defined differently to cellular ageing. While the cellular ageing indicates the whole process and cellular senescence starts from the irreversible cell cycle arrest.

4.3 Discovery of cellular senescence

Cellular senescence was firstly studied by Hayflick half a century ago (Hayflick and Moorhead 1961), he observed that normal cells end up their lives by entering senescence state. After

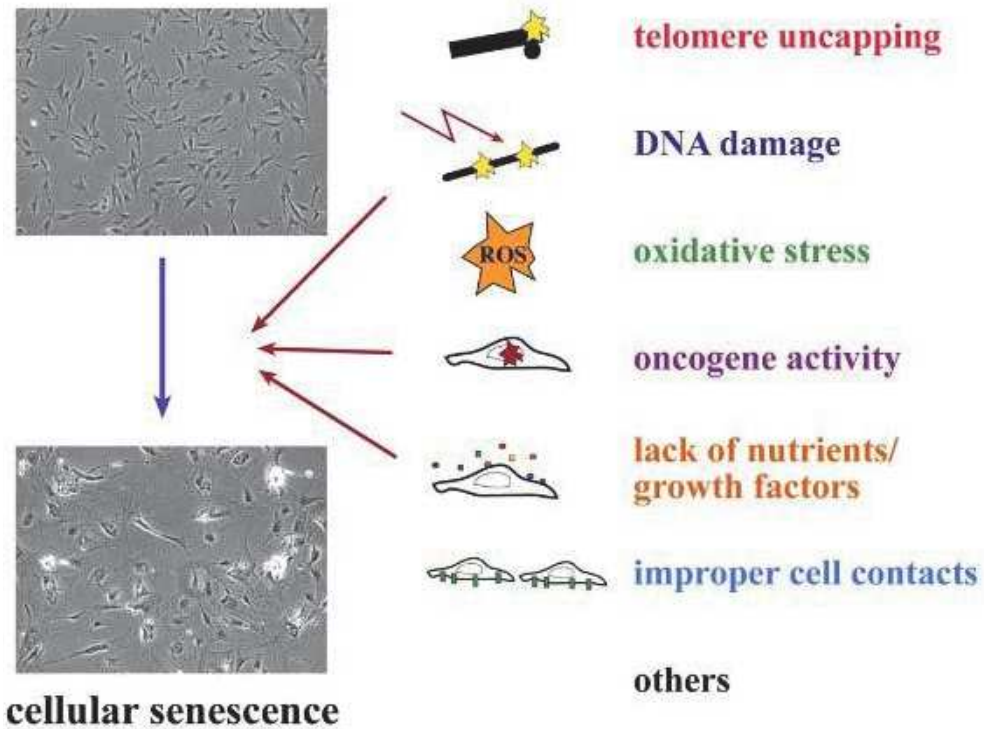

Figure 1.11. The signals activating senescence

Multiple types of stress can induce cells to undergo senescence.

several passages, the cells undergo a non-dividing arrest is defined as Hayflick limit (Hayflick 1965). Later when investigating the mechanisms that induce cellular senescence, both intrinsic and extrinsic factors were found to trigger senescence-like cell cycle arrest (Figure 1.11) (Ben-Porath and Weinberg 2004). The senescent cells show differences in cell structure including volume enlargement, morphological change to a flattened shape, gene expression pattern tremendously altered, etc. (Shelton, Chang et al. 1999).

The cell cycle progression is under the regulation of cell cycle promoter genes (E2F; Cyclin D1, p16, etc.) and cell cycle inhibitory genes (p21, pRB, CDK4, etc.) (Ren, Cam et al. 2002, Trimarchi and Lees 2002). When cell cycle promoter genes are down-regulated or the inhibitory genes are up-regulated, the cell cycle will be arrested. There are two major cellular senescence pathways that trigger cell cycle arrest. p53 and retinoblastoma protein (pRb) which act to restrain the cell cycle progression and induce a senescent-like arrest (Shay, Pereira-Smith et al. 1991). Inactivation of p53 tumor suppressor protein leads to rapid tumor development (Symonds, Krall et al. 1994). Similar observations by disrupting pRb signaling pathway are observed in different types of human tumors (Xu, Cairns et al. 1993).

4.4 Mechanisms underlying cellular senescence

4.4.1 Cellular senescence can be induced by intrinsic stimuli

Telomere shortening

After the discovery of cellular senescence by Hayflick and Moorhead, scientists were urged to search for the underlying molecular mechanisms. During the 1970s, the length of non-coding sequence at the end of chromosome has caught the attention of scientists. This region seems to reduce after each cell cycle due to incomplete replication (Olovnikov 1971, Watson 1972). These observations led to the hypothesis of DNA terminal region shortening induce the Hayflick limit. After the structure of telomere were elucidated (Greider and Blackburn 1987), the theory of telomere shortening is confirmed to be the reason triggering cellular senescence that observed by Hayflick and Moorhead in 1961 (Vaziri, Schächter et al. 1993).

Telomere is a repetitive segment of DNA sequence that locate to the end of chromosome. In mammals it contains repetitive sequence (TTAGGG)n (Moyzis, Buckingham et al. 1988) (Figure 1.12). In human the telomere is varied in size from ten to fifteen kb (Moyzis,

Buckingham et al. 1988, Allshire, Dempster et al. 1989). The function of the telomere is to protect ends of DNA from degradation, fusion and recombination, this function is also called capping. Telomere can also help to favor the DNA replication (Shiels, Kind et al. 1999). Telomere serves as acritical intrinsic 'clock' which after each round of cell cycle, it lost 40-100 base pairs of DNAs (Vaziri, Schächter et al. 1993). Therefore, when telomere become critically short, the DNA damage response is activated and cell cycle cease to progress (Di Leonardo, Linke et al. 1994, Allsopp, Chang et al. 1995, Hemann, Strong et al. 2001, Hahn and Weinberg 2002). This is the reason of cellular senescence observed by Hayflick and Moorhead.

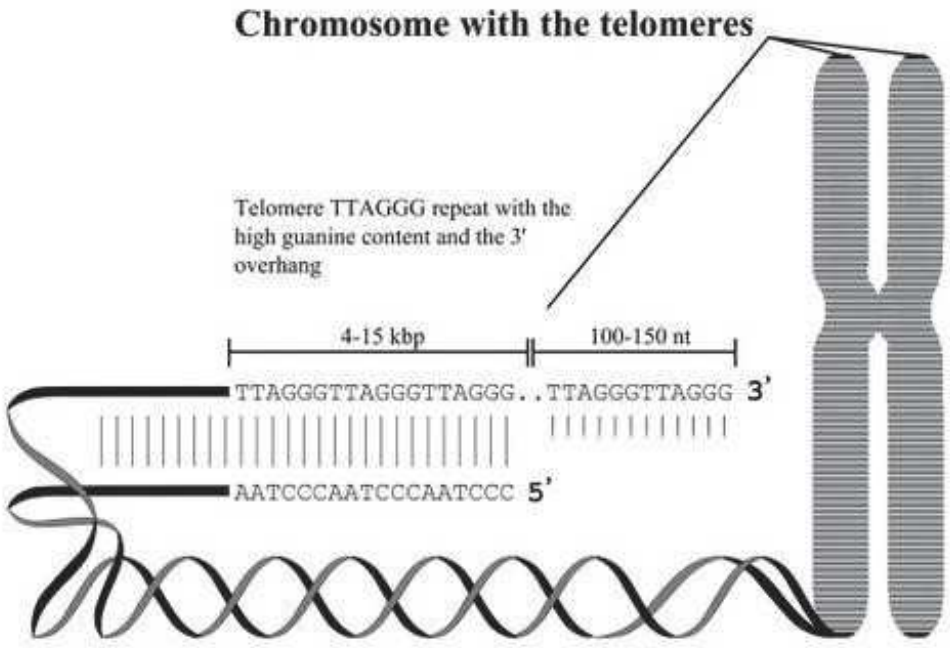

Figure 1.12. Structure of telomere

Maintenance of telomere length is under the regulation of DNA polymerase enzyme called telomerase (Greider and Blackburn 1987). Maintaining the length of telomere can extend the replicative limit, and its length is proportional to the replicative capacity. In germline cells, the telomerase is expressed whereas in somatic cells showing less dividing capacity, the telomerase is not expressed. Therefore, the telomere length is related to the proliferative capacity. In an earlier study when human fibroblasts from different donors were compared, the initial telomere length can predict the replicative capacity of corresponding cells in vitro (Allsopp, Vaziri et al. 1992). Telomere is like a cellular clock which determines the cellular age by its length.

How do shortened telomere signal senescence? There are two theories. First is called telomere position effects (TPE) which combines the telomere shortening with gene expression change (Shay and Wright 2005). When telomere is long, the genes near telomeres are silenced due to chromatin structure near telomere. As cell loss the length of telomere, the subtelomeric region may loss the silencing and alter the gene expression pattern which further affect cellular and organelle functions .(Baur, Zou et al. 2001)However, more and more evidence show that the cell cycle arrest is due to a DNA-damage induced response. Which leads to the second theory of telomere shortening-induced cellular senescence mechanism: DNA damage response (DDR) activation. During replication, telomere region is shortened due to newly synthesized strand after each cell cycle. The protein complex 'shelterin' existed to stabilize telomere region is disrupted and expose the telomere end (Griffith, Comeau et al. 1999), then DNA double strand break signal will be sensed and activates the DNA repair mechanism (Sedelnikova, Horikawa et al. 2004, Victorelli and Passos 2017). Study has shown that deleting the component of 'shelterin' complex, the proteins involved in DDR such as 53BP1, the Mre11 complex and H2A.X and Rad 17 can be induced (Takai, Smogorzewska et al. 2003). Consistent with this study, in senescent cells the DDR effector proteins such as γ-H2AX, RAD17, CHK1 phosphorylation were found accumulated to the uncapping telomere regions (di Fagagna, Reaper et al. 2003). Such DDR can result in activation of cellular senescence pathways including the DNA repair, cell-cycle arrest which will be introduced below.

4.4.2 Cellular senescence can be induced by various stress

Shortly afterward, it has been shown that telomere shortening is not the only pathway that induce cellular senescence, the up-stream mechanism that induce telomere shortening is not restricted to cell cycle progression solely. Various exogenous stressors (Di Leonardo, Linke et al. 1994, Toussaint, Medrano et al. 2000) and oncogene activations (Serrano, Lin et al. 1997) can lead to a similar growth arrest called pre-mature cellular senescence, because the emergence of such phenotype appear long before they reach Hayflick limit during their 'early ages' (Figure 1.13). This 'pre-mature cellular senescence' can be triggered by a single double strand break of DNA (Di Leonardo, Linke et al. 1994), by stimuli such as (Venable, Lee

et al. 1995), by intrinsic pRb oncogene activation (Kiyono, Foster et al. 1998), by oxidative stress such as hyperoxia (Honda and Matsuo 1992) etc.

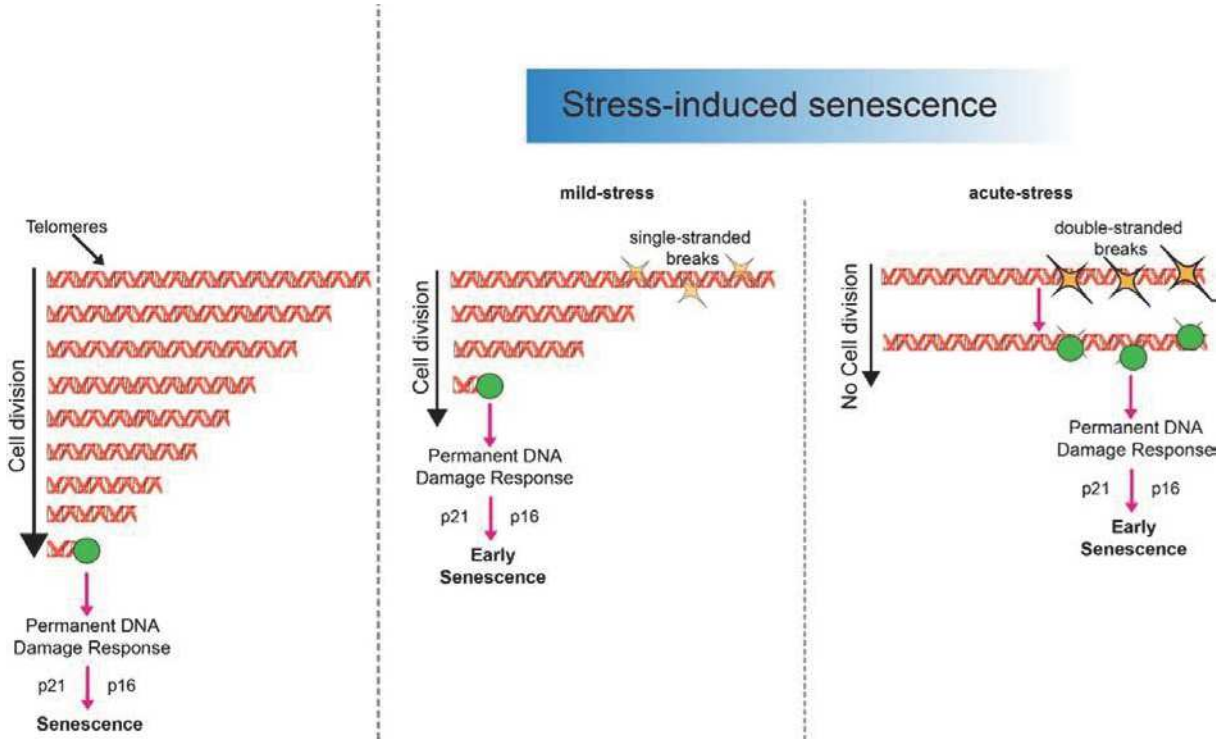

Figure 1.13 Length-independent telomere damage.

Telomere shortening that occurs naturally with each round of cell division ultimately leads to chromosome ends becoming exposed and activating a DNA damage response, which results in a permanent arrest known as replicative senescence. However, recent evidence suggests that telomeres may serve as highly sensitive sensors of stress. It is known that mild oxidative stress causes single-stranded breaks to accumulate at telomeres, leading to accelerate shortening and premature cell cycle arrest. However, it is possible that acute stresses induce telomere double-stranded breaks which are not efficiently repaired. This results in a persistent DDR signaling, preventing cells from undergoing further rounds of replication irrespective of their telomere length, a state which can also be called “telomere length-independent senescence”. (Victorelli and Passos 2017)

It is important to emphasize that stress listed above can also be released from inside the cell. For instance, the production of reactive oxygen species (ROS) may be generated from mitochondria through respiration (Murphy 2009) and from exogenous oxidant such as Ceramide. The other stress such as DDR can also be originated from inside the cell by telomere shortening or under the treatment of ionizing radiation (Santivasi and Xia 2014). A comparison of phenotypes between replicative senescence and pre-mature senescence shows that they share similar features such as morphological changes, gene expression pattern, mitochondrial DNA deletion, telomere shortening, low energy metabolism, etc. (Toussaint, Medrano et al. 2000). These observations indicate that cellular senescence is a

homeostasis mechanism when cells are exposed to stress (either intrinsic or extrinsic) and prevent from further proliferation. Some important molecular pathways that trigger senescence under various stimuli are discussed below to better understand the current cellular senescence models.

ROS

It is then proposed that telomere shortening can be triggered by exposure to oxidative stress (Von Zglinicki 2002). It has been proposed that the characteristic G/C rich of telomere region is causing high sensitivity to oxidative stress (Sitte, Merker et al. 1998, Kawanishi and Oikawa 2004). Other stimuli such as H2O2, hyperoxia (von Zglinicki, Saretzki et al. 1995), obesity, cigarette smoking (Valdes, Andrew et al. 2005), and even psychological stress can induce higher oxidative stress and lower telomerase activity, therefore generate telomere shortening and cellular senescence (Epel, Blackburn et al. 2004).

DDR

The up-stream stimuli that trigger DDR-induced senescence include ionizing radiation, topoisomerase inhibitors, and chemotherapeutic drugs for cancer treatment (Robles and Adami 1998, Roninson 2003), which induce Double Strand Breaks (DSBs). DSBs are potent senescence inducer, it has been estimated that a single DSB is sufficient to trigger a senescence growth arrest (Di Leonardo, Linke et al. 1994).

Extensive study on DNA damage response triggered by telomere shortening induce cellular senescence. The telomere shortening independent stress can also trigger DNA damage activation, cell cycle arrest and DNA repair etc. The importance of DDR induced cellular senescence is the severity of the damage demonstrating persistent DDR signaling not transient DDR activation (Campisi and Di Fagagna 2007). Summarized in the review, the DNA damage response has a broad network from its sensory complexes, signaling transduction to DNA repair effectors. Many downstream pathway effectors are shared in telomere-shortening inducing DDR.

Oncogene activation

Cellular senescence can also be triggered by oncogene activation, the first observed oncogene induced senescence is by RAS, a cytoplasmic mitogenic signaling pathway transducer (Serrano, Lin et al. 1997). The overexpression of the RAS activates the MAP (Mitogen-Activated Protein) kinase signaling pathway, which cause uncontrolled proliferation (Pearson, Carbone et al. 2000). The high level of RAS has shown can stimulate a high level of p16 (Maldonado, Timmerman et al. 2004) inducing cell cycle arrest and senescence by pRb signaling pathway. Some oncogenes activation lead to strong mitogenic activity can cause DNA damage and persistent DDR activation. This may be possibly caused by inappropriate replicon firing and replication fork collapse during the fast cell cycle progression. Such DDR induction by oncogene activation can trigger cellular senescence by p53-mediated signaling pathway. There are also studies showing DDR-independent senescence induction by oncogene activation (Freund, Patil et al. 2011). No matter which kind of initial oncogenic stimuli, the central cellular senescence inducing pathways: p53 and pRb are engaged downstream to arrest cell cycle.

This kind of observation is consistent with the tumorigenesis suppression theory of cellular senescence. In conclusion, the cellular senescence is triggered by uncontrolled genome instability and lack of integrity: the telomere shortening which damage the chromosome end region, DNA damage induced by various stimuli and even the oncogenic mutations. Cellule senescence seems to be a homeostatic mechanism to confront the stress-induced loss of genome integrity and prevent the malignant transformation.

4.4.3 Cellular senescence can be delayed by caloric restriction Caloric restriction

The various stress that have been discussed all play negative roles on cell functioning and accelerate the cellular ageing process. This ‘stress’ is a well-established model to result in lifespan elongation. Caloric restriction (CR), a significant reduction of calorie intake without malnutrition increases lifespan. It has been suggested that CR is a classic intervention of longevity and is conserved in most species across different lineages (Partridge and Gems 2002). In a CR feeding organism, less senescent cells were observed compare to control (Krishnamurthy, Torrice et al. 2004, Jurk, Wang et al. 2012). The exact molecular mechanisms

leading to less senescent cell accumulation is not well elucidated. Yet several speculations were proposed due to recent scientific research observations.

In a multi-cellular mechanism, caloric restriction have been found to reduce the ROS production (Sohal, Ku et al. 1994, Sohal and Weindruch 1996), lowering of the metabolic rate which then leads to a less production of ROS and related oxidative damages, reduce the protein and DNA damage (López-Lluch and Navas 2016), etc. Not only reducing the deleterious stress, CR can also promote the defense mechanisms against oxidative stress (Mercken, Crosby et al. 2013, Luo, Chiang et al. 2017) and activate DNA repair mechanisms (Lee, Tsai et al. 2011). Therefore, it has been speculated that cellular senescence may be delayed under CR feeding condition.

Apart from delaying the cellular ageing process, it was suggested that by better eliminating the damaged cells by autophagy may also cause less accumulation of senescent cells (Meydani, Das et al. 2016, Yang, Licastro et al. 2016).

4.5 Senescence-Associated-Secretary-Phenotype (SASP)

4.5.1 Phenotype of SASP

What cells do when they become senescent? During the early 21st century, more and more studies have demonstrated a typical senescent cell category which can secrete cytokine and chemokine to the extracellular environment nearby (Herbig, Ferreira et al. 2006, Coppé, Patil et al. 2008, Coppé, Desprez et al. 2010). This is called SASP (Senescence-Associated-Secretory-Phenotype). When cells ages and after the cell entry into senescence state, the senescent cells can remain metabolically activate and undergo major changes in protein expression and secretion, ultimately developing the SASP (Kuilman and Peeper 2009). Massive changes were observed between non-senescent and SASP cells based on the chromatin structure and mRNA expression profile (Kulaeva, Draghici et al. 2003, Narita 2007). These changes were more and more studies for the following years, categories of SASP are uncovered, including the nuclear structure alteration (Mehta, Figgitt et al. 2007, Righolt, van't Hoff et al. 2011), DNA damage activation (di Fagagna 2008, Borodkina, Shatrova et al. 2014), growth arrest under the p53/pRb signling pathway (Campisi 2005,

Campisi and Di Fagagna 2007), and reduction of cytoplasmic proteolytic capacity (Chondrogianni and Gonos 2004), increase of reactive oxygen species (Kuilman, Michaloglou et al. 2010, Passos, Nelson et al. 2010, Correia-Melo and Passos 2015), and the secreted cytokine and chemokine(Herbig, Ferreira et al. 2006, Coppé, Patil et al. 2008, Coppé, Desprez et al. 2010).

4.5.2 SASP cell characteristics

Morphological characteristics

Senescent cells cease to divide and dramatic change into a flattened and enlarged shape. They show increasing adhesion to extracellular matrix and loss the cell to cell connection (Ben-Porath and Weinberg 2004).

DNA damage activation

Senescent cell has special biomarkers, two of them that are commonly used. The first marker is based on the increasing acidity in senescence cell therefore β-galactosidase activity may stain senescent cell in blue. Another feature of senescent cell is called persistent DNA damage response (DDR). DDR activation marker has been used to uncover senescent cells from advanced-age tissue.

Central pathways of cellular senescence by cell cycle inhibition

In senescent cells, both p53 and pRb are the central tumor suppressor proteins that can be activated (figure). Both proteins are transcriptional regulators. For p53, the telomere dysfunction can trigger a p53-mediated DNA damage response (Itahana, Dimri et al. 2001, di Fagagna, Reaper et al. 2003, di Fagagna, Teo et al. 2004). Overexpression of oncogenic RAS (one the most common oncogenes, its overexpression can ultimately lead to cancer) can also trigger the p53-dependent damage response by producing high levels of DNA-damaging ROS (Irani, Xia et al. 1997). The p53 protein can be activated by a post-translational modification which produces a set of proteins involved in DNA repair pathway, ultimately leads to cell cycle arrest, cellular senescence or cellular apoptosis (Jin and Levine 2001). pRB physically bind to E2F family transcription factors. This complex can bind to E2F-regulated-promoter

regions and recruit histone deacetylases (HDACs) for gene repression (Harbour and Dean, 2000 (Harbour and Dean 2000). However, when pRb are phosphorylated by Cdk activity, the E2F-dependent gene expression are enabled. The E2F regulate genes that involved in DNA replication, synthesis of DNA, cyclins E and A. Therefore, the activation of hypo-phosphorylated pRb can block the cell cycle progression from entering S phase and induce cell cycle arrest.

Even though various stimuli can induce senescence response, these two central pathways p53 and pRb are responsible for the senescence growth arrest (Bringold and Serrano 2000).

Other characteristics

It seems that when senescent cell is under SASP state, both genetic and phenotypic profiles are different from its original state. Its nuclear structure, gene expression, protein profile and even metabolism are altered. More and more studies are focusing to answer questions regarding SASP and unravel its contribution to ageing.

4.6 Positive effect induced by senescent cells

Cellular senescence is a key mechanism that prevent the tumorigenesis, proposed by scientists (Prieur and Peeper 2008). Because in the study of Hayflick, they found that for those cells who bypass this process, though at a very low frequency, are prone to be malignant cells which is oncogenesis in vitro (Hayflick 1965).Ever since this observation, the biologists propose that this is a direct demonstration to prove that cellular senescence is a cancer-suppressive mechanism (Campisi 2013) (Figure 14). Though cancer is not a simple limitless replicating cell, it acquires several biological capabilities such as resistance to apoptosis, insensitivity to growth signaling, angiogenesis to support the cancer growth (Hanahan and Weinberg 2000). Unlimited proliferative capacity is one of the necessities for oncogenesis. However, the gaining of stemness a crucial step because the tumorigenesis is raised due to the accumulation of mutations over time. Therefore, unlimited dividing can be a leading source to provide mutation accumulation for malignancy.

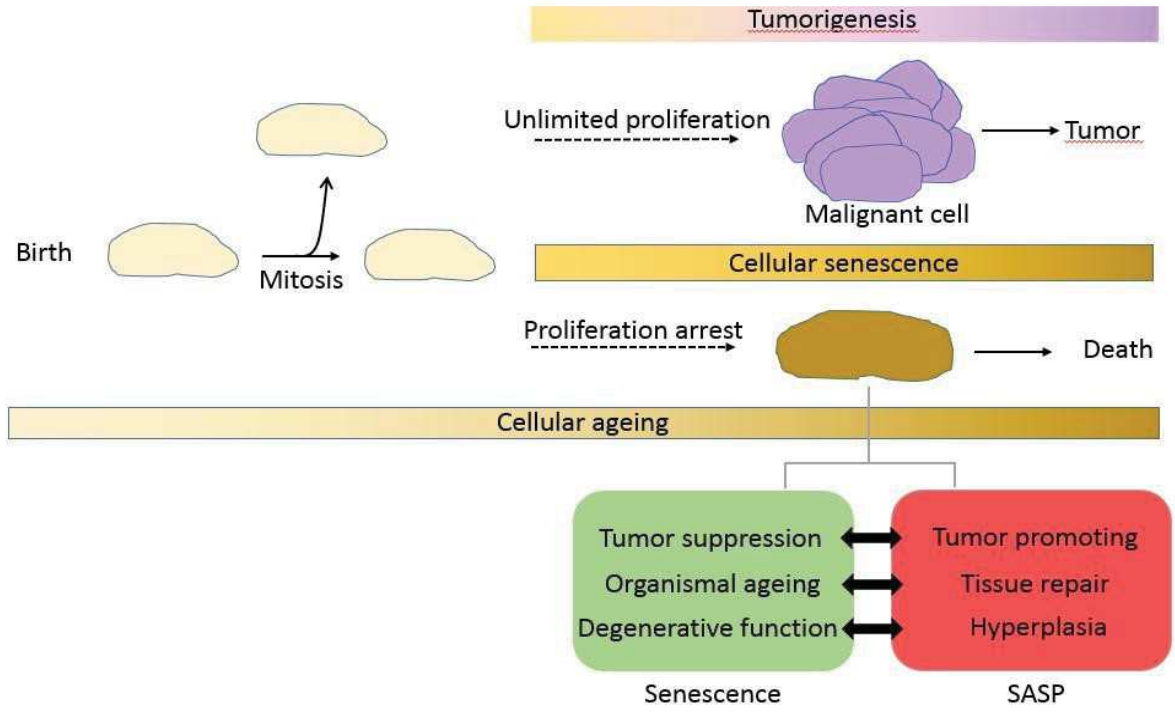

Figure 1.14: Cellular senescence is a tumor suppressive mechanism.

This graphic represents the opposition between rumor promotion and suppression during ageing under the regulation of cellular senescence. The controversial functions of senescent cell discussed below under cellular senescence mechanism are presented.

4.7 Negative effects induced by senescent cells in advanced-age-state

Up until now, scientists cannot explain why the senescent cell demonstrate secretory phenotype that cytokine and chemokine are secreted to the extracellular environment. Theoretical speculations are proposed based on their pro-inflammatory phenotypic performance in the review of (Borodkina, Deryabin et al. 2018). Firstly, in vivo SASP can serve as a signal to attract immune cells for self-elimination. Secondly, the proteins that can alter the extracellular matrix can favor the migration of immune cell. Thirdly, the secreted growth factor can induce the neighbor region for new cell generation to replace the senescent cell. These processes may be less effective when the individual ages, which results in negative effects: the accumulated senescent cells and the emergence of chronic inflammatory focus. Indeed, the hypotheses above were partially proved. Age related chronic disease often origin from where senescent cell accumulated. For instance, cardiovascular and neuro-degenerative diseases.

The presence of senescent cells promotes the proliferation of non-senescent cells (Giri and Ittmann 2000). Alteration of tissue microenvironment by senescent cells can promote the progression of premalignant cell development (Campisi 2005). Therefore, cellular senescence can promote carcinogenesis progression.

4.8 Origins for organ ageing, organismal ageing and age-related diseases

With better understanding of cellular senescence and age-related studies, scientists have proposed cellular theory of ageing which connect cellular senescence to organismal ageing. There are three major arguments that directly links cellular senescence to organismal ageing. In the review of Collado et al. 2007 (Collado, Blasco et al. 2007), two reasons were argued. Firstly, the senescent cells persist and accumulated in aged tissue over time (Dimri, Lee et al. 1995). Secondly, the regenerative stem cells senesce and loss its replicative capacity as well. For these two reasons, the theoretical hypothesis is following the same principle, that all cells age. Not only differentiated cells senesce which result in organ structural perturbation, but also proliferative stem cells exhaust and limit the regenerative capacity, finally aggravated organismal ageing. Followed by the SASP discovery, it becomes clear that senescent cells may lead to other above-mentioned consequences. DNA damage activation (di Fagagna 2008, Borodkina, Shatrova et al. 2014), and reduction of cytoplasmic proteolytic capacity (Chondrogianni and Gonos 2004), increase of reactive oxygen species (Kuilman, Michaloglou et al. 2010, Passos, Nelson et al. 2010, Correia-Melo and Passos 2015), and the exposure of secreted cytokine and chemokine (Herbig, Ferreira et al. 2006, Coppé, Patil et al. 2008, Coppé, Desprez et al. 2010). In the review of Jeyapalan and Sedivy, 2008 (Jeyapalan and Sedivy 2008), the authors argued a third reason that cellular senescence can trigger organismal ageing because typical age-related diseases such as cardiovascular disease, atherosclerosis and osteoarthritis arise at where presenting more senescent cells in our body. Suggesting the vulnerability of organismal ageing in front of age-related diseases is caused by senescent cells.

4.9 Clearance of senescent cells – a new therapeutic way against ageing

Due to these observations, a new therapeutic pathway is proposed. Studies start to focus on the clearance of senescent cells, because it provides therapeutic opportunities (Tchkonia, Zhu et al. 2013). And indeed, clearance of senescent cells of mouse starting from one year

of age delay tumorigenesis, attenuate age-related deterioration and extend lifespan (Baker, Childs et al. 2016).

4.10 Senescent cell is in support of pleiotropic antagonist theory of ageing

Three major conflicts regarding effects of senescent cells were proposed (Rodier and Campisi 2011, Campisi 2013). The first conflict is that both tumor suppression and tumor promotion can be induced under the effects of senescent cells. When cell becomes senescent, it avoids limitless proliferation which signify that at this stage tumor suppression is achieved by cellular senescence mechanism. However, when senescent cells once exhibit the SASP phenotype, the tumor promotion can be triggered due to its inflammatory characteristic and creating microenvironment to favor the metastasis. The second conflict is that both organ/organismal ageing and tissue repair can be induced under the impact of senescent cells. The accumulated senescent cells trigger organ structural dysfunction and stem cell exhaustion. Meanwhile, by gaining SASP phenotype, the senescent cells secrete cytokine and chemokine which may favor the cell growth and tissue repair. The third conflict is like the previous one, except that this conflict is occurring at a higher organelle scale. The degenerative function of organ can be induced by senescent cells. At the same time, hyperplasia (which increased cell production in a normal tissue or organ) can be promoted by chronic inflammation under the impact of senescent cells. These controversial observations indicate that cellular senescence is an antagonistic pleiotropic phenomenon. Because cellular senescence has multiple functions, certain functions may be beneficial at earlier stage of life, then it becomes detrimental due to these functions during later life.

5. Budding yeast as a cellular ageing model

The importance of understanding on cellular senescence leads to the investigation on cellular ageing progression. One of the classic cellular ageing models is the microorganism -- budding yeast. The host laboratory focuses on this model organism for understanding the cellular ageing process.

Budding yeast is the simplest eukaryotic organisms that the genome was entirely sequenced since the 1996 (Bassett Jr, Basrai et al. 1996). It contains organelles and functions like other eukaryotic cells such as mammalian cells. Due to its conserved eukaryotic characteristic, it is a powerful tool to help investigating the complex molecular mechanisms in multi-cellular higher eukaryotic. Let alone the simplest eukaryotic single-cell organism, there are also enormous studies on genetics of budding yeast.

Budding yeast is easy to perform genetic modifications and economically maintained in the laboratory. The collections of singe-gene deleting mutants (Giaever and Nislow 2014) and targeted gene GFP fused collections (Huh, Falvo et al. 2003) are well established and can be used as powerful genetic tools for ageing investigation. For instance, budding yeast single-gene deleting mutant collection has been used to screen the genes involved in longevity regulation (Fabrizio, Hoon et al. 2010).

Most of the ageing study on budding yeast is based on two models: replicative and chronological ageing. They are two powerful models for understanding both mitotic cellular ageing and post-mitotic cellular ageing.

5.1 Two ageing models in budding yeast

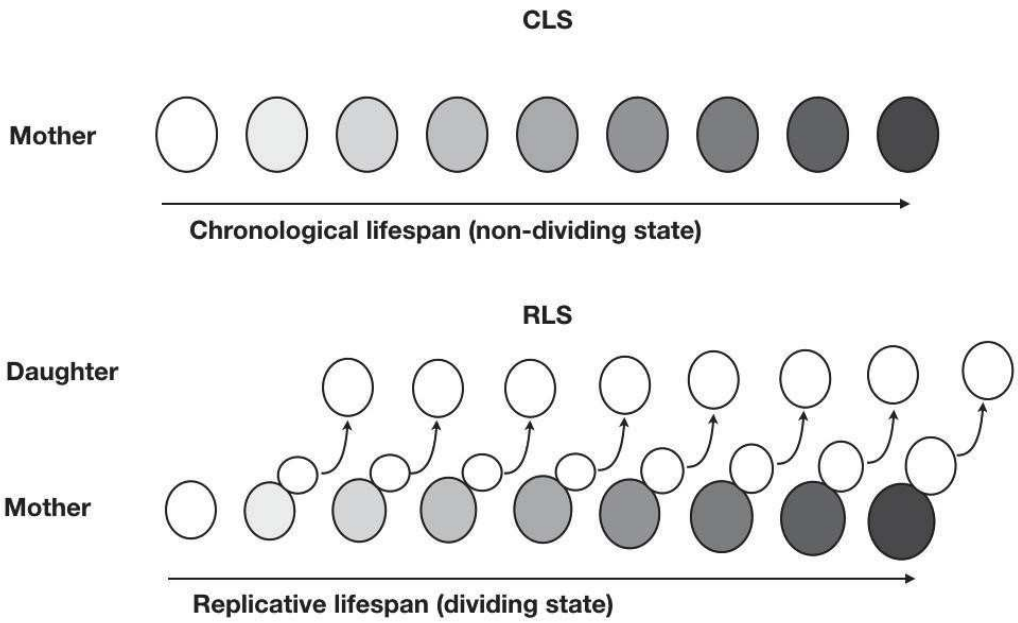

Figure 1.15. Schematic graph for Yeast Chronological and Replicative Ageing

CLS is measured by the length of time cells in a stationary culture can remain viable. The period for the cell remains viable is defined as chronological lifespan.
RLS in yeast is measured by the number of mitotic divisions that can arise from a single mother cell. The number of generated daughters is defined as replicative lifespan.

There are two ageing models that has been established to investigate cellular ageing process by budding yeast: chronological ageing and replicative ageing (Figure 1.15).

The chronological ageing is defined by the viability that a cell maintained under non-dividing state for ageing process. When the budding yeast is under non-dividing state, it may be metabolically active. During this ageing process, damages can also be accumulated and eventually lead to cell death (Longo, Shadel et al. 2012). The chronological longevity is measured by the period when mother yeast is viable.

The replicative ageing is defined by the number of daughter yeasts that a mother yeast can generate. Due to asymmetric dividing pattern of budding yeast (Mortimer and Johnston 1959, Chang and Drubin 1996), scientists observe that mother yeast gradually gain in size and accumulate damages. The mother yeast can give birth to daughters exhibiting average

dividing capacity same as young mother. However, the daughters from very old mothers show reduced dividing capacity (Kennedy, Austriaco et al. 1994). These observations suggest mother yeast increase in age and accumulate damages which restrict the inheritance to daughters. At last, mother yeast may lose the capacity for damage restriction which generate short-lived daughters.

So far, the relationship between replicative lifespan and chronological lifespan is not clearly understood. Significant overlap of genes participating in replicative ageing and chronological ageing are not detected (Burtner, Murakami et al. 2011). However, trend has been observed that chronologically aged cells have a reduced RLS; and a period of stationary phase can reduce RLS (Ashrafi, Sinclair et al. 1999). Both damaged proteins (Arlia-Ciommo, Piano et al. 2014, Saarikangas and Barral 2015) and genome instability (Bitterman, Medvedik et al. 2003, Hu, Chen et al. 2014) are observed during both ageing processes.

5.2 Chronological lifespan and non-dividing/post-mitotic cell model

Chronological ageing is also called post-mitotic ageing. As the term indicated, its lifespan is measured by the period when mother yeast survived under a non-replicative condition. And this process is generally a time scale of weeks. This study is mostly estimated under calorie restriction condition, mimicked by starvation (Longo, Shadel et al. 2012); in the absence of caloric restriction chronological ageing can also be investigated (Nagarajan et al., 2014). During chronological ageing, the accumulated damages cannot be diluted through cell division, but must be turned over and renewed. Therefore, chronological lifespan (CLS) might be related to the capacity of stress resistance (MacLean, Harris et al. 2001).

Molecular mechanisms involved in calorie restriction (Arlia-Ciommo, Leonov et al. 2018), quiescence (Leonov, Feldman et al. 2017) and autophagy (Tyler and Johnson 2018) are investigated using chronological ageing model.

5.2.1 Approaches to study chronological lifespan in budding yeast

To induce a non-dividing state is typically induced by growing yeast cells into the post-diauxic state (Longo, Gralla et al. 1996). The post-diauxic phase is when cells deplete extracellular glucose from medium. At this time, the growth rate will drastically be decreased and switch

to a mitochondrial respiratory metabolism. The cells will consume ethanol generated previously during fermentation (Werner-Washburne, Braun et al. 1996). Gradually the yeast cells will enter a stationary phase where they are kept at non-dividing state. According to the variety of medium provided, this state can be maintained under 2 to 10 days (Figure 1.16 adapted from (Longo, Shadel et al. 2012)).

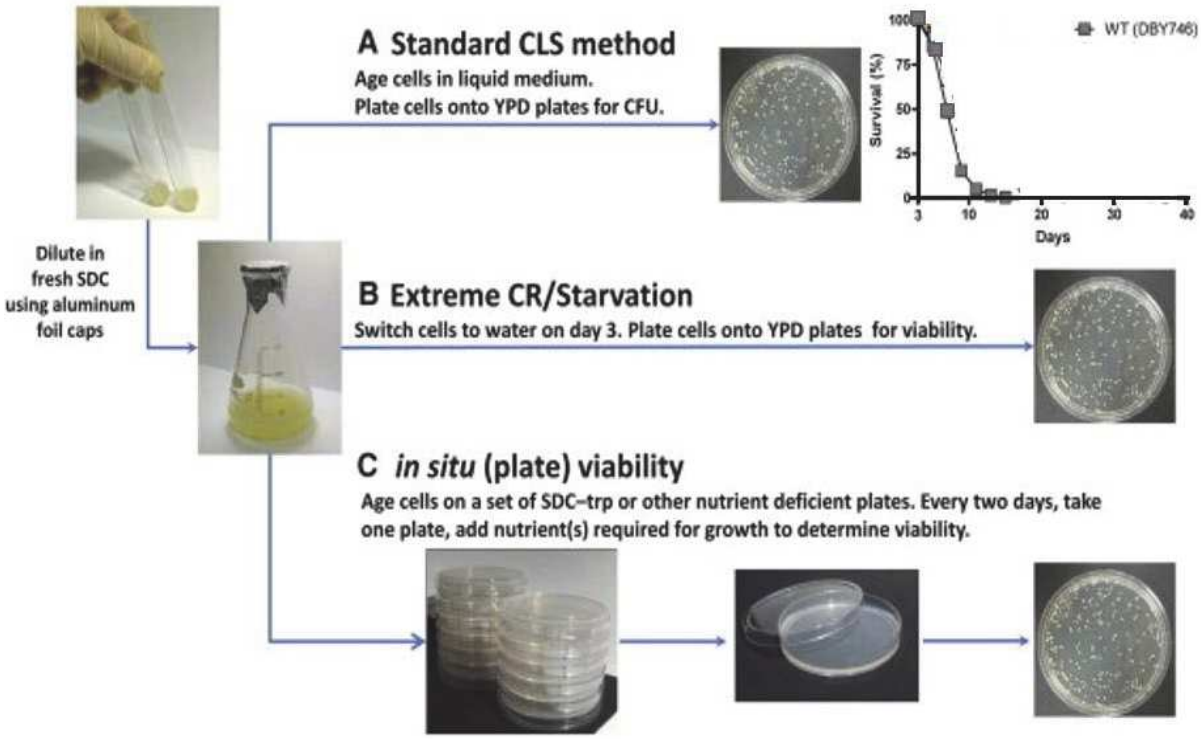

Figure 1.16. Induction of yeast chronological ageing

After an overnight culture, cells grow until they reach post-diauxic phase, then plated onto starvation medium (A); for extreme starvation, cells grown after 3 days will be plated onto starvation medium (B); for testing different carbon sources (or other medium condition), using nutrient deficient plates or selectif medium for viability determination (C). Caloric restriction as the most reproducible approach to extend longevity, has been extensively studied in budding yeast to understand the molecular network in response to nutrient deficiency. As explained above, during stationary phase, the cell may be maintained under a low metabolic rate and increase a variety of stress-resistance pathways.

5.3 Replicative ageing lifespan and dividing-/mitotic ageing model

The replicative ageing is the successive dividing process of a mother cell from birth to death. The measurement of RLS is calculated by counting the number of generated daughters (Mortimer and Johnston 1959). On average, twenty-five daughters can be reproduced by a mother yeast, and the whole process may take generally four to five days. While the mother

yeast ages, the daughters show rejuvenated phenotype of recovered dividing potential (Jazwinski 1990, Kennedy, Austriaco et al. 1994). This rejuvenating capacity is lost in extremely old mothers before death. These observations lead to the assumption of accumulated 'ageing factors' which result in senescence and promote ageing. Those daughters show rejuvenated phenotype are born without the inheritance of 'ageing factors.

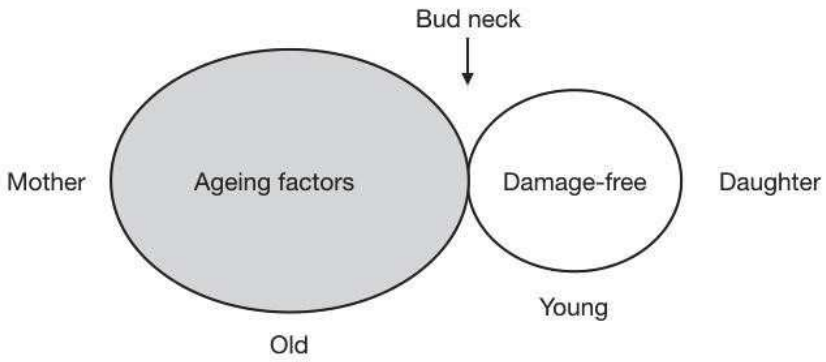

Figure 1.17 Asymmetric division between mother and daughter in a budding pattern

The mother and daughter cells are morphologically different. Internal cytoplasmic content including proteins and organelles are asymmetrically segregated to generate damage-free rejuvenated daughter, whereas mothers retain damages and ageing factors.

Replicative ageing of budding yeast is a model of mitotic ageing. During the mitotic ageing process, the yeast show asymmetry between mother and daughter (Hartwell 1971). Such establishment of polarization leads to the emergence of daughter cells by budding along with cytoplasmic content asymmetric segregation including proteins which leads to distinct gene-expression pattern and even variation of pH (Figure 1.17) (Okada, Kusunoki et al. 2017) (Henderson, Hughes et al. 2014, Yang, McCormick et al. 2015).

Mitotic ageing model is useful for further investigation in other asymmetric dividing model such as stem cell of higher organisms. Molecular mechanism such as nutrient sensing pathway (Conrad, Schothorst et al. 2014), cell cycle progression (Kraikivski, Chen et al. 2015) and ageing process (Steinkraus, Kaeberlein et al. 2008) are investigated in replicative ageing.

5.3.1 Approaches to study replicative lifespan in budding yeast

To investigate the replicative ageing process of budding yeast, specific approaches are required to overcome the difficulty. There are two major difficulties: the number of mother

yeast is relatively small within one population (Figure 1.18). If the initial cell number is 1, after N generations, there will be only one mother yeast at the age of N, while the daughters' population can be up to 2^N-1. Therefore, there is limited number of mother yeast within a bulk of mixed cell culture. The second difficulty is due to the cell-to-cell variety within the isogenic population. The cells are undergone different pace of ageing. This can be easily revealed by a survival curve (Figure 1.19). The mothers die at different ages, suggesting a

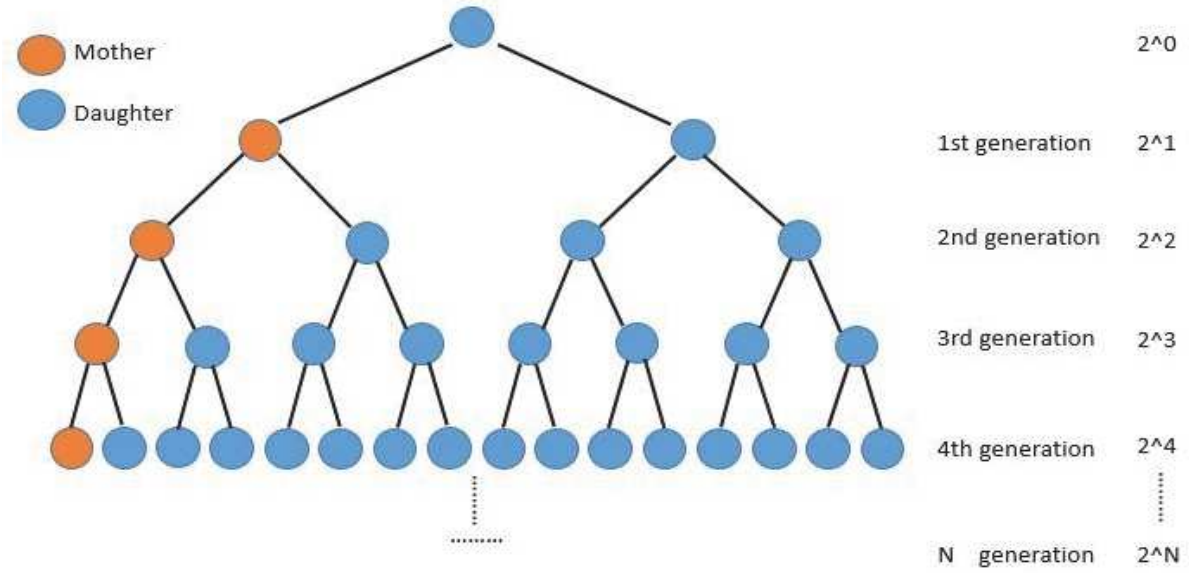

Figure 1.18 Representative scheme to describe mother and daughter cell number in the population

Initiated from one single cell, after N generation, the population may reach 2^N of cells. The mother at the age of N is still one.
heterogeneous ageing process. Due to the multifactorial causal factors leading to the cellular senescence, we could expect subpopulations showing diverse ageing process.

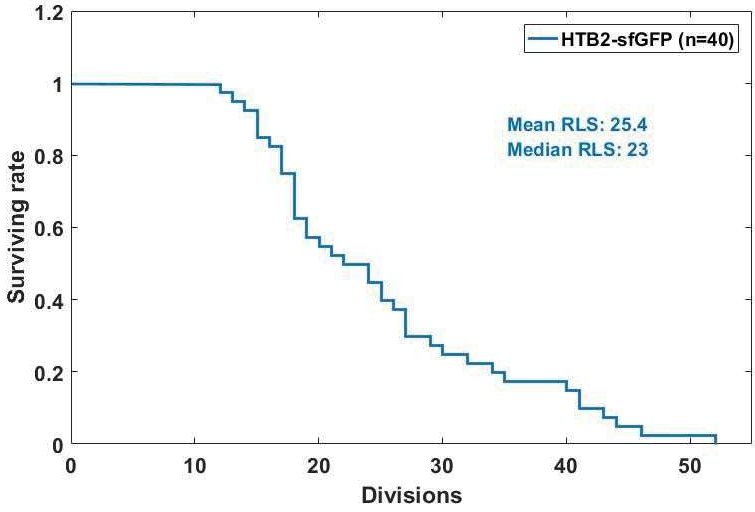

Figure 1.19 Survival curve of a histone reporter strain

The survival curve gradually decreases not in a linear pattern. The curve shows that cells die at various ages.

To rise above the first difficulty, conventional approach to study replicative ageing process is by micro-dissection (Mortimer and Johnston 1959, Steffen, Kennedy et al. 2009). Using a fine needle to remove each daughter from a single mother (Figure 1.20), and this process should be repeated several times to obtain enough number of mother yeasts for reliable statistical analysis. Therefore, this approach requires a big amount of time, patience and repeated work. In addition, when shifting to nighttime, the cells are conserved at lower temperature to delay the division. Hence, interruptions are induced during the whole ageing process. This approach is suitable for quantifying the replicative ageing survivorship and phenotypic events of mother yeast, yet internal molecular dynamic cannot be monitored.

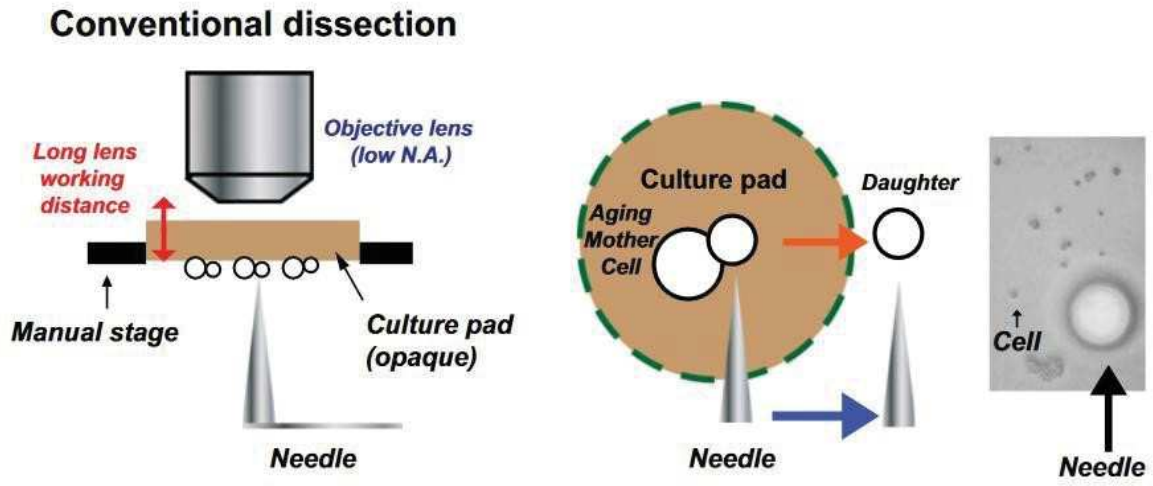

Figure 1.20 Schematic graphic demonstrating micro-dissection (Lee, Vizcarra et al. 2012)

Using the micro needle, the daughter cells are removed away from the ageing mother cell.

A second major approach to enrich the mother cell number for ageing study is by mother-specific fixation system. Both physical fixation by biotin-magnetic column and genetic modification by limiting daughter's division (Lindstrom and Gottschling 2009, Sinclair 2013) are applied to increase the mother population, yet such method is preferentially for population analysis. In addition, the study for ageing process can be only measured by time but not by division. This approach is suitable for population analysis of molecular dynamic by collecting mother cells at various time points. Yet the cell-to-cell variety cannot be precluded. In addition, real-time dynamic for molecular evolution cannot be monitored.

Nowadays, a new type of technique using microfluidic system is rapidly developed in the field for investigating more detailed ageing process. This approach provides a stable fluidic micro-environment to minimize the cellular growth space (Figure1.21A). As shown in the figure, single cell ageing process can be monitored (Fehrmann, Paoletti et al. 2013). This study was performed using microfluidic device developed by the host laboratory. The host laboratory mainly focuses on the application of micro-fluidic system for ageing process investigation. In 2013, using 'cavity' design, single mother yeast can be trapped and monitored for real-time ageing dynamic studies (Figure 1.21B). Later, this device is improved by a high throughput design (Figure 1.22). More mother yeast can be trapped and monitored for ageing studies. Combining with computational analysis: data processing, automated segmentation and cell mapping, both single-cell and population analysis can be performed. Using microfluidic system to investigate ageing process become a new trend, when searching 'microfluidic' as a keyword for budding yeast' publications on PubMed, the increment of publication is almost linear during the past decades starting from 1997.

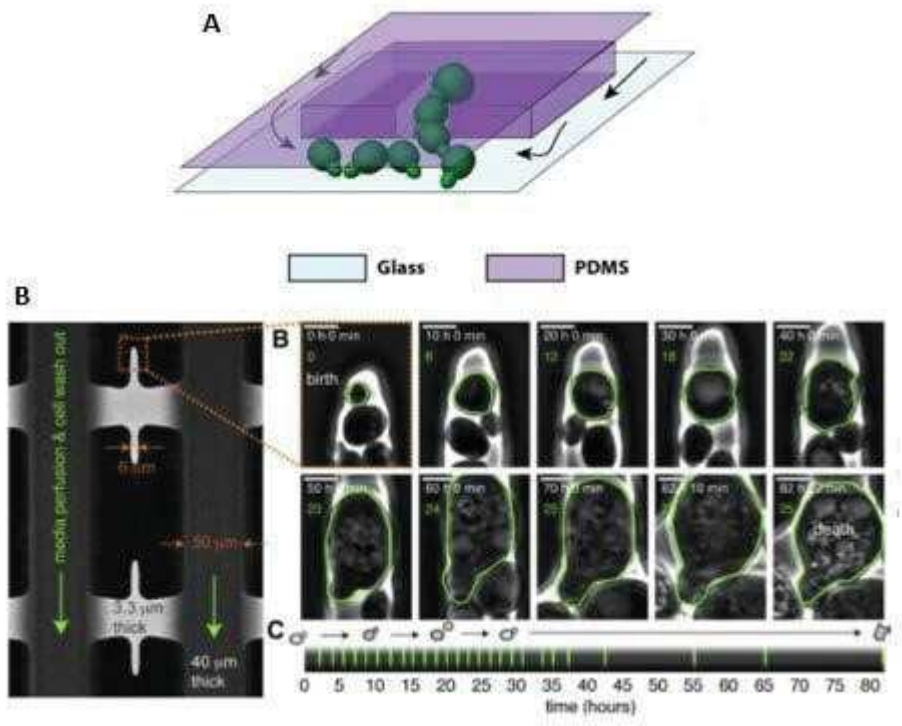

Figure 1. 21 Microfluidic system allowing single cell successive monitoring

A: Using PDMS (silicone) and glass coverlid to form a designed micro-environment, this space can allow single cell growth. 3D scheme of the cavity design shows that liquid medium can be provided for cell growth. (Chen, Crane et al. 2017)
B: The real image of the cavity design on the left, the right panel shows a mother yeast captured at the tip. RLS is monitored along with the successive division. Each green line corresponding to the division time. A full replicative lifespan trajectory is presented. (Fehrmann, Paoletti et al. 2013)

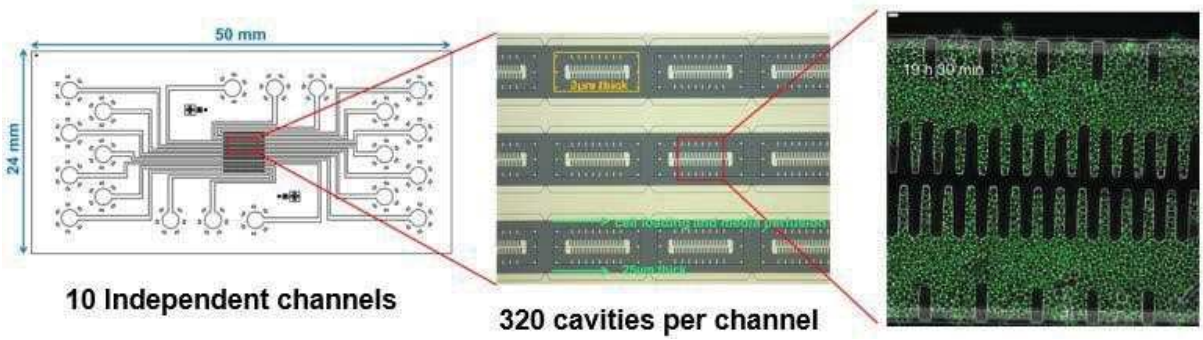

Figure 1.22 High-throughput design improvement for mother cell capture (by Dr. Morlot)

The cavity designed is repeated. In total 320 cavities per channel. There are ten independent channels on a single microfluidic chip.

As a conclusion, following the development of new approaches, more and more precise and detailed molecular mechanisms can be investigated. According to different needs, various

methodologies can be applied to answer those questions. Due to the focus on replicative ageing for my doctoral thesis subject, more related information will be introduced.

6. Ageing factors and the regulation

Identification of damages and ageing factors that induce ageing in mother yeast is crucial for the investigation of ageing process. It has been suggested that factors accumulated in mother cytoplasm is determinant (Egilmez and Jazwinski 1989). Later, it has been observed that when mother ages, the daughters are born damage-free and show average dividing capacity same as young mother cell (Kennedy, Austriaco et al. 1994). Such observation lead to the speculation that damages are restrain in mother and not inherited to the daughters. Some ageing factors will be briefly introduced.

6.1 ERC

Early in 1997, scientists have proposed that ERC is an ageing factor (Sinclair and Guarente 1997). ERC is short for Extrachromosomal rDNA circles, as its name, the molecule is issued from rDNA repetitive loci located on chromosome XII of budding yeast. Its accumulation leads to the ageing phenotype in mother and its clearance in daughter leads to the rejuvenation of age. When monitoring the replicative ageing process of mother yeast, the mothers show more accumulated ERC, whereas the daughters are born ERC-free. There are on average 150 to 200 repetitive rDNA copies on the chromosome XII, this repetitive category of rDNA is the may reason that rDNA gene may be excised from the chromosome and form ERC by homologous recombination (Park, Defossez et al. 1999).

These molecules are like plasmid, it contains rDNA gene copies excised from the chromosome and can be self-replicated under the regulation of ARS origin following each cell cycle. In addition, the induction of ERC accumulation leads to a shorter lifespan. Not only the ERC accumulation itself, the increasing rDNA loci instability in some mutants may also induce ERC accumulation and ageing phenotype (Sinclair, Mills et al. 1997). However, how ERC accumulation induce ageing phenotype is not understood yet. How the ERC accumulation leads to ageing is not confirmed, speculations of protein titration theory has been proposed.

In addition, the mechanism of ERC asymmetric retention between mother and daughter cells is not fully understood. Yet there are studies demonstrating that asymmetric segregation between mother and daughter is achieved by a diffusion barrier located at the bud neck by

forming a filtering net (Shcheprova, Baldi et al. 2008, Wloka, Nishihama et al. 2011, Denoth-Lippuner, Krzyzanowski et al. 2014). The ERC molecules are speculated to be tethered to the Nuclear Pore Complex (NPC) embedded in the nuclear envelope of mother nucleus. It has been speculated that due to the large size of the assembly, the narrow bud neck and fast cell division might serve to limit the leakage of ERC to daughter cell (Gehlen, Nagai et al. 2011).

6.2 Oxidative stress and damages accumulation

Reactive Oxygen Species (ROS) has been considered as one of the major factors to induce ageing in budding yeast (Harman 1992). ROS is a group of molecules that discovered originally during mitochondrial aerobic respiration by electron leakage (Chance and Sies 1979). Later, scientists confirmed that the production of ROS is mainly from mitochondria and NADPH oxidase (Longo, Gralla et al. 1996, Rinnerthaler, Büttner et al. 2012). This group of molecules is highly reactive, short-lived and can induce DNA damage (Salehi, Behboudi et al. 2018), protein aggregation (Vasconcellos, Dutra et al. 2016) and lipid peroxidation (Ayala, Muñoz et al. 2014), they can basically react indiscriminately to all macromolecules (Labuschagne and Brenkman 2013) some damages may be irreversible.

Following a series of reductive reactions by antioxidant enzymes (Birben, Sahiner et al. 2012), the ROS may be reduced to H2O or converted to oxygen to avoid further damages. However, the respiratory metabolism is crucial for providing energy in aerobic organism. Therefore, ROS accumulation during ageing is inevitable for aerobic microorganism. In addition, environmental stimuli such as heat stress (Davidson, Whyte et al. 1996), UVA radiation (Kozmin, Slezak et al. 2005) can cause ROS accumulation and oxidative damages.

It has been proposed that ROS increase during ageing, yet direct evidence has not been reported. A recent study has observed an increase of oxidative stress at early age but not throughout the whole RLS (Kniess and Mayer 2016). In addition, mild oxidative stress triggering longevity extension have been observed in the study of host laboratory (Goulev, Morlot et al. 2017). Therefore, whether oxidative stress leads to direct causal link for ageing is debatable. Yet the accumulative damages issued from oxidative stress and other basic cell activity may be a more direct reason for triggering senescence and deleterious ageing effects (Aguilaniu, Gustafsson et al. 2003, Erjavec, Larsson et al. 2007).

6.3 Others

There are also other ageing factors, such as dysfunctional organelles: dysfunctional mitochondrion, vacuole that are specifically retained in mother yeast to promote daughter rejuvenation. The mechanisms of the polarity establishment and maintenance of these ageing factors are crucial for regulating replicative ageing.

7. Previous work of host laboratory and my thesis project

As previously described, the laboratory focuses on understanding the molecular mechanisms involved in cellular homeostasis by using special customized microfluidic device. One of the topics is to study the replicative ageing process.

In 2013, using the microfluidic device of cavity design, single cells' replicative ageing trajectories were collected (Figure1.23A). If we take the single cell, we can observe a sharp cell cycle extension at a certain age of the mother. This is represented by a transition from green to red. We can observe that the cell cycle extension is indeed abrupt, which is different from conventional speculation that cell cycle may be gradually declined. However, when we align the cells according to the birth, the abrupt cell cycle extension (color bar from green to red) is not synchronized due to cell heterogeneity.

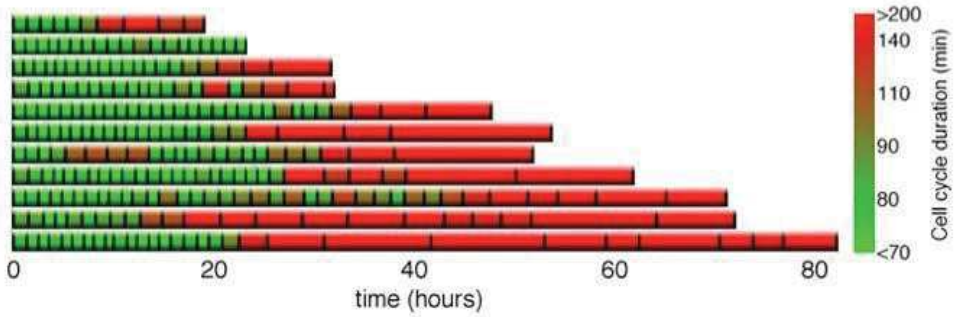

Figure 1.23 Single cell cycle duration trajectory aligned by birth

The cell cycle duration is presented by color and length. Short cell cycle in green, long cell cycle in red. Each line corresponds to a single mother cell cycle duration trajectory. The transition from green to red is very abrupt and this transition happens at different ages showing individual heterogeneity.

We then align all the mother trajectories according at the cell cycle extension point, we found that RLS can be distinguished into two phases. The young phase, where the mothers show regular cell cycle duration. And the old phase, when the mothers show irreversible cell cycle slowdown, the cell cycle become irregular and extended (Figure1.24). This sharp cell cycle extension is defined as the Senescence Entry Point (SEP). Previously the cellular senescence has been used to define a permanent cell cycle arrest. This SEP is a breaking point to define an irreversible cell cycle slow-down. The two phases can be called pre-SEP and post-SEP, respectively.

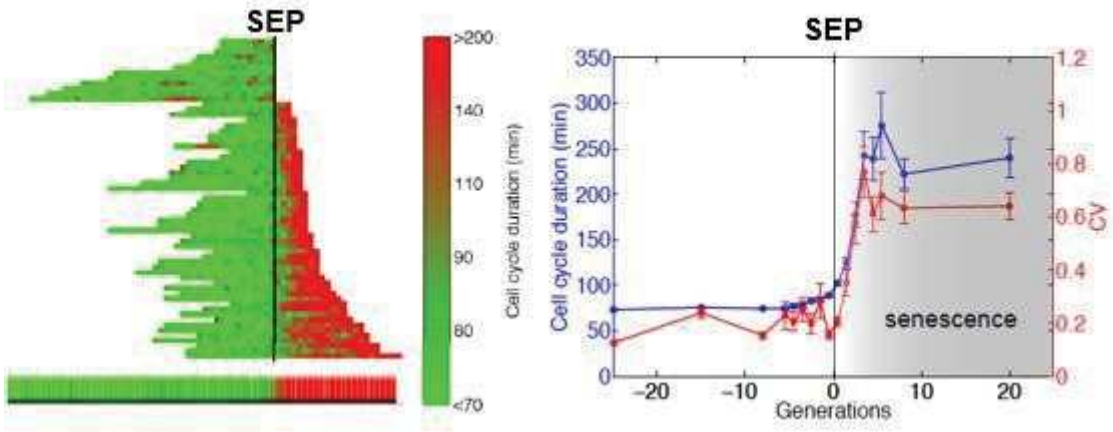

Figure 1.24 Definition of SEP by abrupt cell cycle slowdown breaking point

The left panel shows single cell trajectories aligned by cell cycle extension. Obvious change of color from green to red can be observed.

The right panel shows a statistical analysis of the mothers. The cell cycle duration evolution is drawn in blue, the coefficient of variation is drawn in red. The definition of SEP is determined according to the dividing frequency change using MATLAB.

8. My thesis project

The understanding of the mechanisms underlying this cell cycle slowdown may help us to further understand its contribution to ageing process. During my thesis, I tried to investigate the SEP and replicative ageing from 3 major perspectives.

Firstly, from cell cycle point of view to understand its cell cycle phase rearrangement upon SEP, whether cell cycle checkpoints are activated?

Secondly, using the long-lived mutants to investigate the dynamic of SEP. For instance, whether SEP is delayed in long-lived mutants and how. These long-lived mutants may be involved in different mechanisms by modulating the accumulation of ageing factors (ERC accumulation, oxidative stress). By investigating the SEP transition and longevity in these mutants, the ageing process of corresponding mutants including SEP transition and nuclear homeostasis can be compared and studied.

Thirdly, it has been proposed that ROS and oxidative damages accumulate during the ageing process, yet the real-time dynamic remains unclear. Using the microfluidic system, we expect to monitor the evolution of redox homeostasis and whether it could contribute to the SEP?

Chapter II

Result part 1

Characterization of SEP from the perspective of cell cycle regulation

1 Cell cycle phase quantification upon SEP

1.1 Specific background

In previous work of Dr. Fehrmann, he has observed the sudden cell cycle extension during replicative lifespan. It is interesting to understand how cell cycle is extended from cell cycle phases' perspective (Figure 2.1). Is a certain phase or are all the phases of the cell cycle extended? And how are they redistributed in elongated cell cycle? When cell cycle is elongated in post-SEP period, how cell cycle phases are rearranged?

Figure 2.1 The cell cycle phase extension upon SEP event

A normal cell cycle is constituted by 4 phases including G1, S, G2/M and late mitosis (Anaphase). During post-SEP, the whole cell cycle duration extended. The cell cycle phases may be rearranged after SEP.

1.1.1 Cell cycle progression in budding yeast

Cell cycle is defined as the period between successive divisions of a cell. A duplicate of genetic material should be synthesized and divide into the daughter cell at the end of this cell cycle. They are separately S phase for DNA synthesis, M phase for mitosis. Then G1 is the first gap phase after mitosis before entry of S phase, the second gap phase is after S phase and before entering M phase (Figure 2.2). The core of cell cycle regulatory mechanism is the oscillatory cyclin complexes. The cyclin complexes can be enzymatically activated and phosphorylate numerous substrates that are involved in a specific phase. Different cyclins are activated at different phases. Therefore, they are classified in four classes according to their corresponding activity to the specific phase.

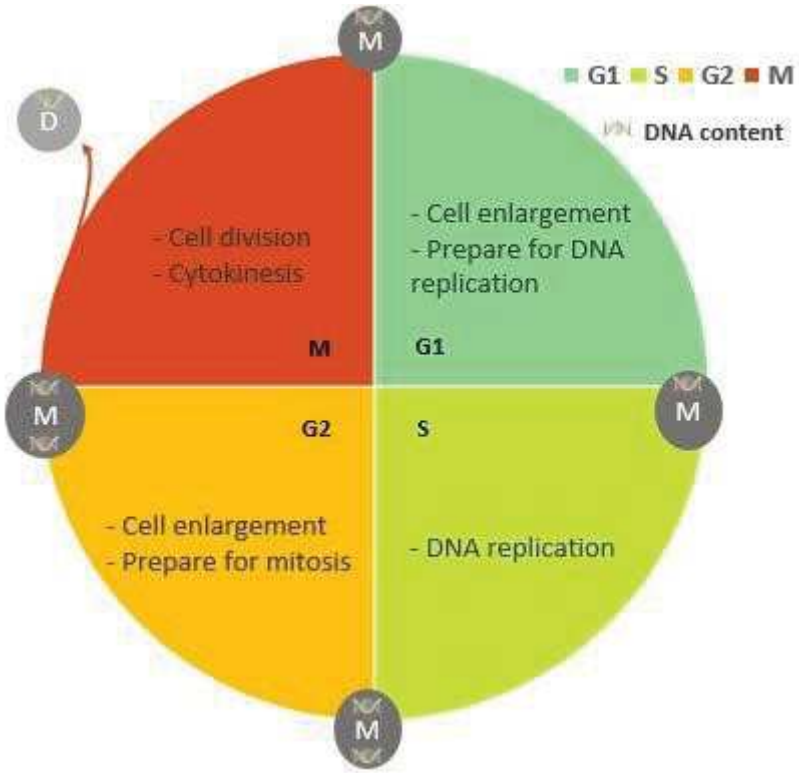

Figure 2.2 Cell cycle phase functions within one cell cycle

The cell cycle is consisted of four phases. The G1 phase when the cell enlarges in size and prepare for the DNA replication of next phase. The S phase is when the DNA duplicated. The G2 phase corresponds to the cell size enlargement and prepare for the mitosis. The M phase is short for the mitosis phase corresponding to the cell division. Eventually, after a full cell cycle, the mother cell generates a newly born daughter cell.

1.1.2 Cell cycle checkpoint activation in budding yeast

Throughout the whole cell cycle, the Mitosis takes relatively short period of time. The cell spends most of the time preparing for the division. This period is also called interphase. During interphase (G1, S and G2), cells pass through numerous checkpoints (Figure 2.3) (Hartwell and Weinert 1989). For instance, during G1 the cell check whether it was in an appropriate size, the energy reserve was favorable and DNA integrity before launch the DNA duplication of S phase. During G2 phase, the cell will check DNA replication and search for DNA damage before proceeding to M phase. During Mitosis, the cell will check sister-chromatid correctly attaching to the kinetochore.

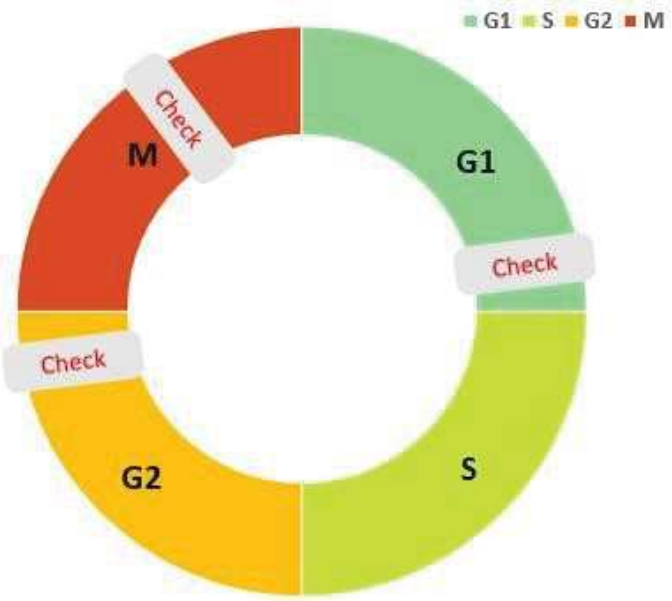

Figure 2.3 Cell cycle phases and the checkpoints on the cell cycle scheme

There are three cell cycle checkpoints within one cell cycle for budding yeast. The 'Start' checkpoint happens at late G1 phase before the DNA starts replication to avoid DNA mal duplication. The second checkpoint is the DNA damage checkpoint which serve to examine the DNA duplication and DNA damage after DNA duplicated before mitosis. The third checkpoint is the spindle pole checkpoint which serve to verify the chromosomal attachment before DNA separation. These cell cycle checkpoint may halt the cell at different phases when errors are detected and assure the proper cell cycle progression.

The checkpoint system of cell cycle is very crucial for maintaining the cell integrity. If the checkpoint is activated by an error, the cell will be halted at that stage. If disorder occur to these checkpoint mechanisms, grave consequences may lead to cell death or even disease such as cancer for mammals (unconstrained cell cycle).

1.1.3 Identification of targeted mother cells show SEP transition

The ageing process of HTB2-sfGFP reporter strain can be monitored by time lapse microscopy, hence the cell cycle duration trajectory of mother yeasts is analyzed (Figure 2.4A). Mother yeasts undergo SEP transition are selected by first manually counting the cell cycle duration and then perform a data analysis on MATLAB software (Figure 2.4B, 2.4C).

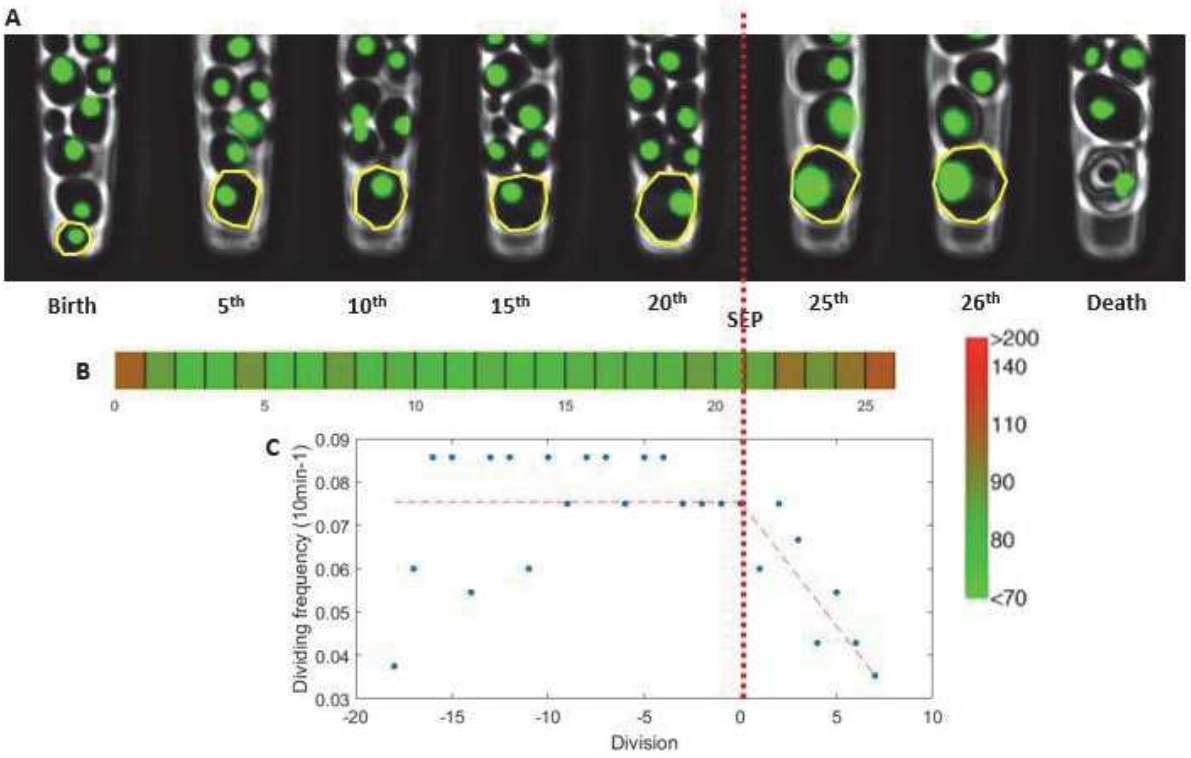

Figure 2.4 Cell cycle duration trajectory and the determination of SEP in a mother cell

A: representative mother yeast HTB2-sfGFP reporter strain full RLS trajectory is monitored under epifluorescence microscopy by performing time lapse ageing experiment.
B: The cell cycle duration trajectory of the mother yeast is manually analyzed by counting the number of frames for each cell cycle. The cell cycle duration trajectory of full RLS is shown by color code bar. In green the short cell cycle duration and in red the long cell cycle duration. A phase of extended cell cycle duration is observed at late RLS and delimited by dashed red line.
C: The frequency of cell division is calculated based on cell cycle duration. Using piece-wise linear regression code, the SEP can be determined by searching for the most abrupt point when the dividing frequency starts to decrease using 'findSEP_Jia' code in MATLAB software.

To determine the SEP moment, there is a customized function called 'findSEP_Jia'. The code performs the analysis by firstly transform the cell cycle duration into dividing frequency (Figure 2.4C), then using the piecewise linear regression to determine the breaking point where dividing frequency decreased most significantly. This breaking point is the SEP moment which corresponding to the abrupt cell cycle duration extension.

After analyzing the cell cycle duration trajectories of mother yeasts, all the mother yeast exhibiting SEP transition are collected (Figure 2.5).

1.1.4 Approach of cell cycle phase quantification using HTB2-sfGFP marker strain

To quantify the cell cycle phase duration, the host laboratory has developed a method by using fluorophore protein fused to C terminal of HTB2 histone gene (one of the histone nucleosome subunit H2b protein) (Garmendia-Torres, Tassy et al. 2018). This single marker allows to discriminate cell cycle phases, based on the tight temporal correlation between histone synthesis and DNA replication process (Figure 2.6) (Heintz, Sive et al. 1983, Sittman, Graves et al. 1983, Baumbach, Stein et al. 1987, Nelson, Ye et al. 2002). The fluorophore protein is super folder GFP (sfGFP) which can mature rapidly to avoid artefact and represent accurate histone level dynamic.

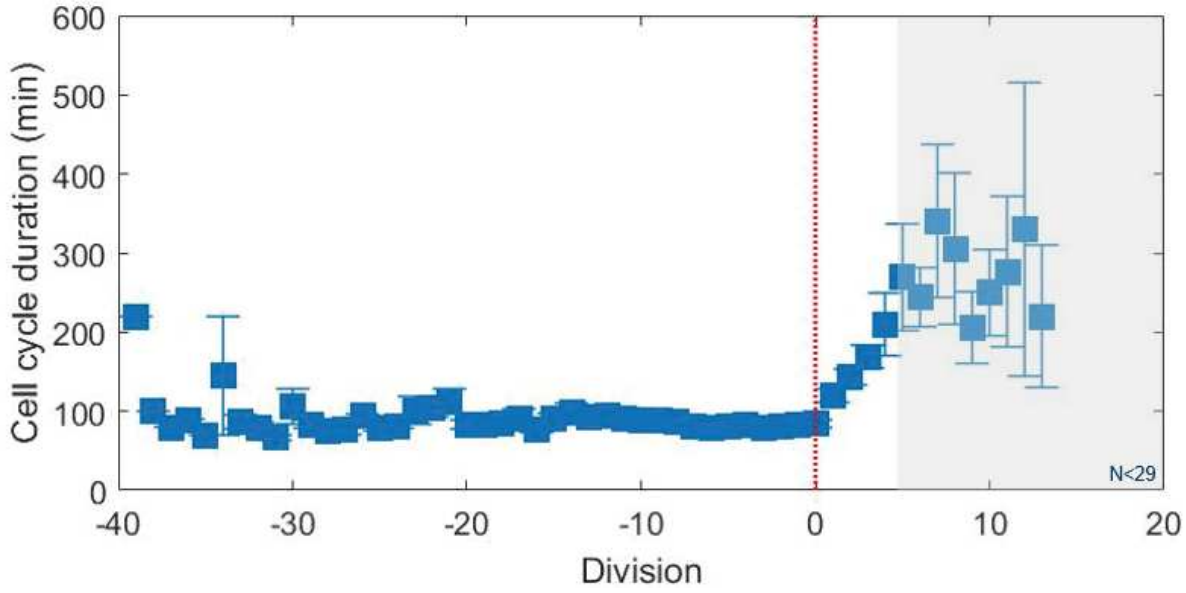

Figure 2.5 Pooling mothers by SEP alignment

The cell trajectories are pooled according to SEP moment delimited by dashed red line (N=58). Evolution of cell cycle duration is showing good correlation to previous publication of Fehrmann et al., 2013. The legend indicates the mean ±standard error on mean.

The fluorescence signal curve can be then analyzed for cell cycle phase quantification since the fluorescence signal can represent distinct cell cycle phases according to the fluorescence profile. The S phase corresponds to the increasing slope of the fluorescence profile and the late mitosis (anaphase) is manifested by the chute of histone fluorescence. The G1 and G2 phases are represented by stable fluorescence profile respectively before S phase and mitosis. The transition points between each phase are determined by using customized piecewise linear regression approach. This approach for cell cycle phase quantification has been already developed and applied in the publication for exponentially growing population using the same HTB2-sfGFP reporter strain (Garmendia-Torres, Tassy et al. 2018).

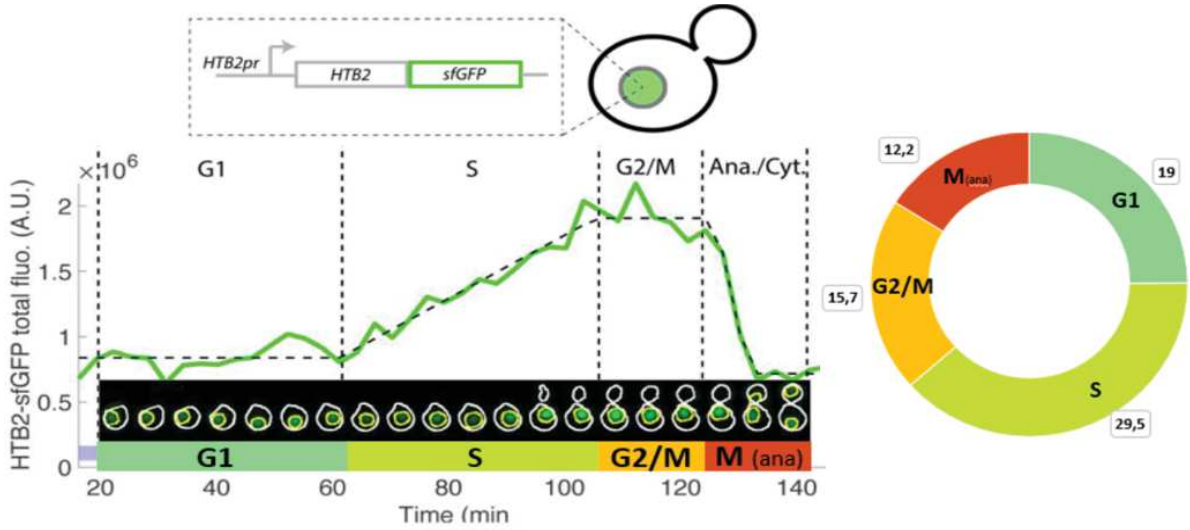

Figure 2.6 Cell cycle phase quantification by HTB2-sfGFP fluorescence reporter (adapted to Garmendia-Torres, Tassy et al. 2018)

The super folder GFP fluorophore is fused to the C-terminal of endogenous HTB2 histone gene. The fluorescence of histone protein level can be thus measured in real-time following the cell cycle progression. The fluorescence signal profile can be used to quantify cell cycle phases base on the piecewise linear regression analysis. Various phases and corresponding to different fluorescence signal profile is shown on the fluorescence plot. According to previous publication (Garmendia-Torres, Tassy et al. 2018), the cell cycle phase distribution in young mother yeast has been measured (upper right).

1.2 Result

1.2.1 Cell cycle phase generally elongated upon SEP

The HTB2-sfGFP reporter strain is monitored under microfluidic device for the cell cycle phase quantification experiment. This experiment is different to the ageing experiment with a higher frequency of time lapse-frame to increase the precision of fluorescence following the cell cycle progression. The mother yeasts exhibiting SEP transition are collected. Based on the above-mentioned method, cell cycle phase durations are quantified by fluorescence profile analysis (Figure 2.7). According to the automated detected fluorescence chute at the end of each cell cycle, it can be used for calculating the cell cycle duration. The SEP of these mother cells are determined by 'findSEP' MATLAB customized function. All the cell cycle phases are quantified by aligning all the cells at SEP.

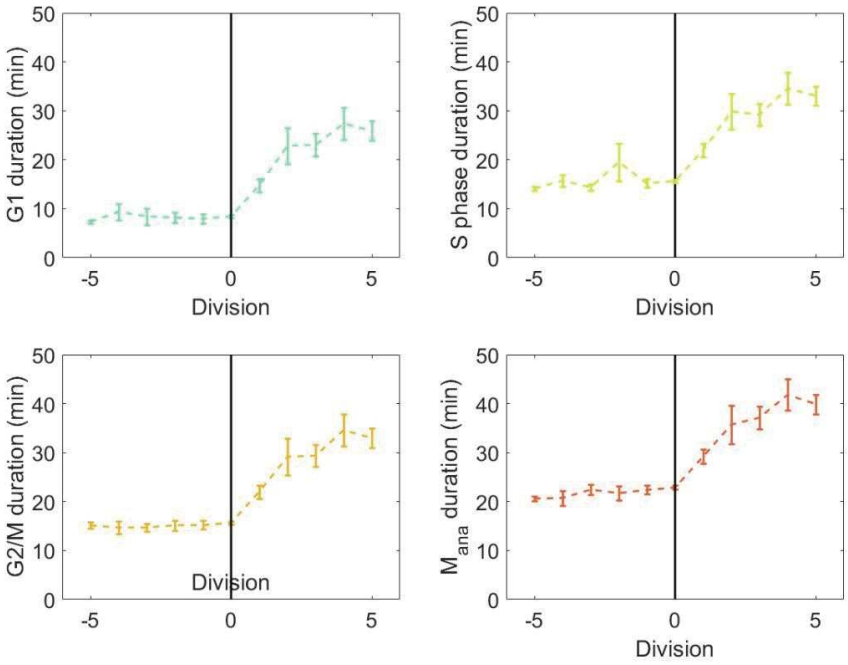

Figure 2.7 Evolution of cell cycle phase-duration upon SEP using automated analytic approach

The evolution of cell cycle phase duration is analyzed in automated-detected mother cells enduring the SEP transition. Different cell cycle phases are shown in various color: G1 in light green, S in light yellow, G2/M in orange, anaphase in red. The averaged pre-SEP cell cycle phase durations are respectively: 8.5, 15.5, 15.5, and 23 minutes. The SEP transition is represented by black line at 0 (x axe). The legend indicates the mean ±standard error on mean.

The evolution of each cell cycle phase duration is shown in the figure 2.7. Five divisions before and after SEP are presented. All the cell cycle phases are elongated after the SEP transition. However, if we look at the average cell cycle phase duration before SEP, for G1, S, G2/M and anaphase, they are respectively 8.5, 15.5, 15.5, and 23 minutes. The cell cycle phase measurement during pre-SEP period is not in line with the result obtained from exponentially growing (mostly pre-SEP) cells (Garmendia-Torres, Tassy et al. 2018). Adding all the phases together, the entire cell cycle duration 62.5-minute is obviously shorter than average pre-SEP cell-cycle-duration 76 minutes. In addition, the quantification of cell cycle phases is significantly different to the result obtained from exponentially growing cells. As a conclusion, the automated detection for cell cycle duration quantification and SEP determination is not reliable based on the histone H2b protein fluorescence level solely. Therefore, manually intervention is needed to provide more precision for cell cycle phase quantification upon SEP.

The cell cycle phase-duration are separately: 8.5, 15.5, 15.5, and 23 minutes for G1, S, G2/M and anaphase. The whole cell cycle duration is around 62 minutes. The whole measurement is shorter than the quantification obtained from exponentially growing cells. The data of exponentially growing cells has been previously published in the work of Dr. Garmendia-Torres by using the same HTB2-sfGFP reporter (Garmendia-Torres, Tassy et al. 2018). The only exception is the G2/M phase which shows comparable duration in both pre-SEP and exponentially growing cell population. The inconsistency while using the same method and obtain a different result might be due to an error for determination of the cytokinesis, therefore both G1 and anaphases are abnormal.

Another possibility that the cell cycle duration is much shorter than 76 minutes from exponentially growing cells (Garmendia-Torres, Tassy et al. 2018) might be due to the mal-detection of each cell cycle division. The automated detection for each cell division is based on fluorescence peak and the automated determination for SEP is based on sudden extension of cell cycle duration. These criteria may lead to a determination of the SEP at an extremely short cell cycle duration which follows by an elongated cell cycle duration. Therefore, both cell cycle duration and the moment of SEP maybe inaccurate. Both SEP and the cell cycle cytokinesis must be correctly determined. To better quantify the cell cycle

phase duration at the SEP transition, both cell division and SEP are thus determined manually.

Using an alternative approach for precise cell cycle phase quantification. Eventually by pooling more cell cycles, the quantification of averaged cell cycle phase duration may provide more precision (Figure 2.8). However, this method can only compare the difference between all pre-SEP and post-SEP cells, but it cannot demonstrate the dynamic evolution of all the cell cycle phases.

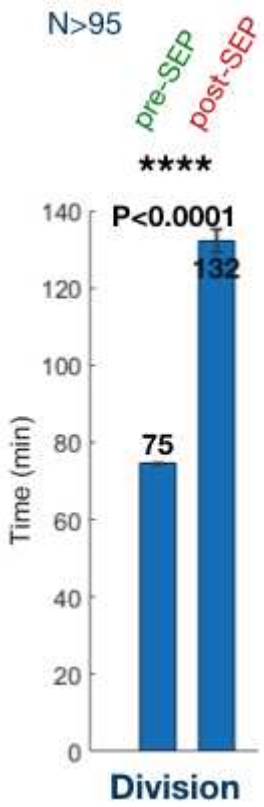

Figure 2.8 Histogram comparison of cell-cycle-duration between pre-SEP and post-SEP cell population

By pooling all the cell cycles before and after SEP, the averaged cell cycle duration is quantified between the two population (pre-SEP, post-SEP; N>95). Distinct cell cycle duration after SEP is observed by comparing averaged full cell cycle duration. The legend indicates the mean ±standard error on mean.

Based on the fluorescence profile, the fluorescence signal of all these cell cycles are analyzed by piecewise linear regression in order to quantify the cell cycle phase duration. The result is shown below (Figure 2.9). The cell cycle phase-duration are separately compared, they all show significant increase after SEP for all the phases. The measurement of the cell-cycle-phase is comparable between exponentially growing cells and pre-SEP cells population. From exponentially growing cells, the average G1, S, G2/M and anaphase phases' duration are

respectively 19, 29.5, 19.7, 12.2 minutes; while from pre-SEP cells, the corresponding cell-cycle-phase quantification are respectively 14, 32, 16 and 13 minutes. The two sets of quantification show relatively comparable result. However, since the two measurement are performed in two different cell population, for instance, the statistical analysis of comparison is not performed for further distinction.

Among these phases, compare to the post-SEP cells, the G1-phase-duration increases for more than 3-fold. The other phases: S, G2/M and anaphase show about 1.5-fold increment (Figure 2.9). All these phases lead to a total 1.8-fold increment from the cell cycle level. It seems that G1 phase is mostly affected phase among all the cell cycle phases.

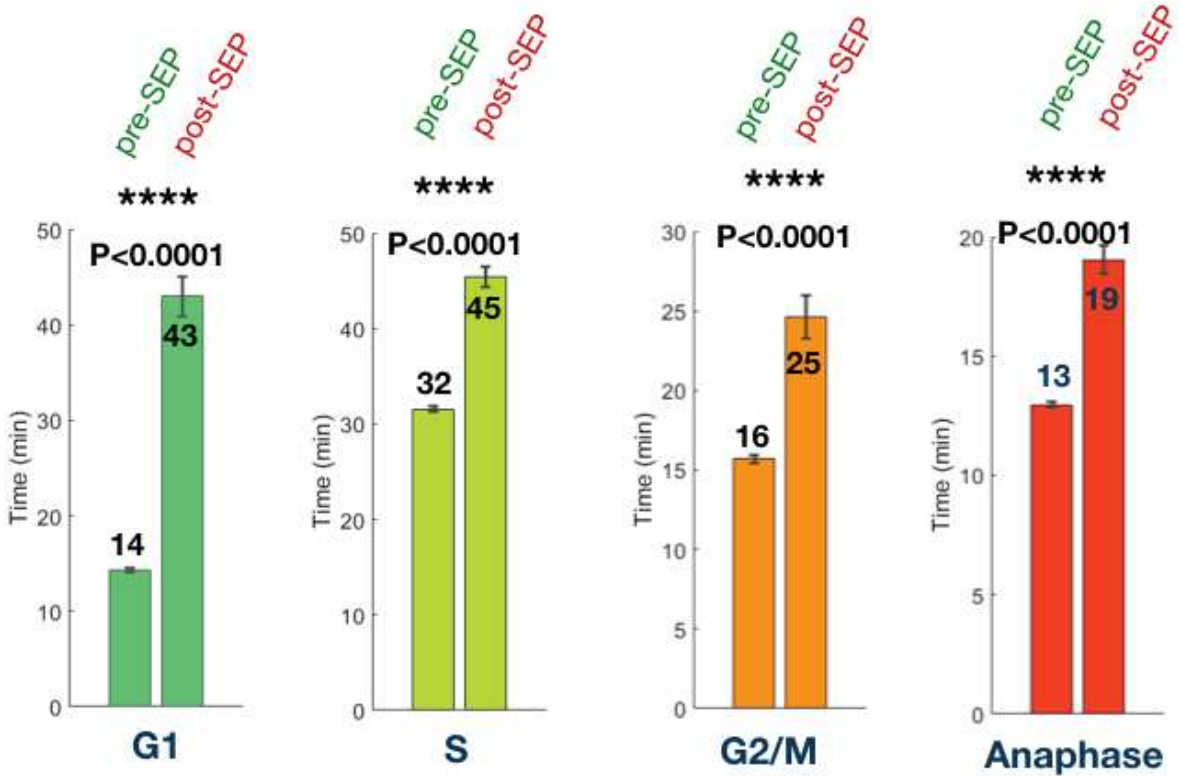

Figure 2.9 Comparison of cell-cycle-phase-duration quantified in both pre-SEP and post-SEP cell population by histogram

The histogram of various phase duration comparison before and after SEP. The legend indicates the mean ±standard error on mean. (pre-SEP, post-SEP; N>95)

2 Alternative marker for cell cycle phase measurement upon SEP

2.1 Specific background

Because of abnormal histone protein fluorescence accumulation during post-SEP period, it is reasonable to ask whether the measurement of cell cycle phase duration using HTB2-sfGFP

reporter after SEP is still reliable. Therefore, using a non-histone cell cycle phase reporter to monitor the cell cycle phase after SEP is performed to confirm the measurement of post-SEP cell cycle phase quantification.

I used the G1 phase marker WHI5-GFP reporter strain and performed the same time-lapse cell cycle phase quantification experiment under epi-fluorescence microscope. Whi5 protein is a transcription factor regulator that shuttles between cytoplasm and nucleus during the cell cycle. Whi5 is imported at the end of the cell cycle before cytokinesis and exported more than 50% from the nucleus prior to the Start of DNA replication (Figure 2.10) (Liu, Wang et al., 2015). The G1 phase duration measured by Whi5 nuclear residence do not correspond exactly to the G1 phase duration measured by H2b protein, because Whi5 proteins are exported from nucleus before DNA replication started. However, the oscillatory dynamic of Whi5 can reveal relatively G1 phase duration and has been an excellent reporter of cell cycle dynamics (Schmoller et al., 2015; Neurohr et al., 2018). It has been measured that G1 phase duration is approximately 13,7 minutes in a mother cell population of the same cell strain background cultured in the similar medium (Liu, Wang et al., 2015), this value is for reference only.

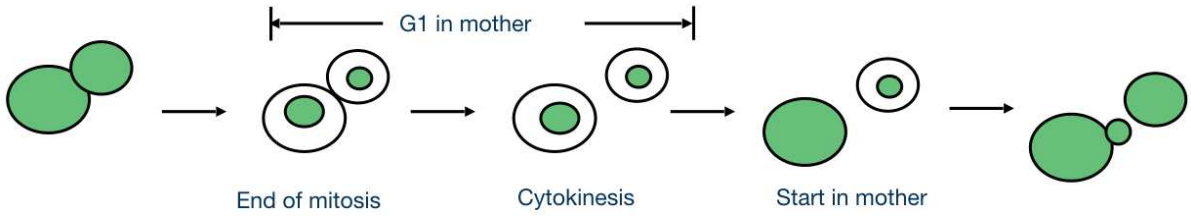

Figure 2.10 Schematic Whi5 protein oscillatory shuttling between cytoplasm and nucleus adapted from (Liu, Wang et al. 2015) in WHI5-GFP reporter
Schematic presentation of whi5 protein (green) location during the cell cycle. Right after the mitosis, the whi5 protein are translocated into nucleus before cytokinesis. They are exported from nucleus before Start of S phase. Whi5 protein is a good cell cycle G1 phase reporter.

2.2 Result

2.2.1 Whi5-GFP reporter strain reveals significant G1 phase elongation upon SEP

Ageing time-lapse experiment on WHI5-GFP strain was performed. Due to the short period of time (13.7 mins) that whi5 reside in the nucleus, the interval of frames allowing may be very short. Therefore, the single cell trajectories of mother yeast are analyzed manually using

ImageJ. During the cell cycle progression, whi5 protein can be seen clustered in the nucleus and then diffused into the cytoplasm before S phase (Figure 2.11). After analyzing the cell cycle duration trajectory, mother cells exhibiting SEP transition are identified (Figure 2.12).

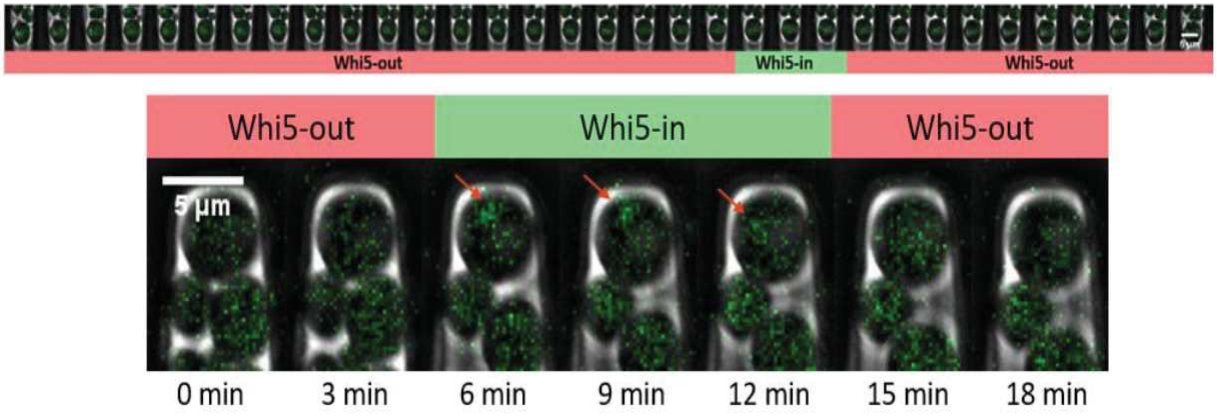

Figure 2.11 Whi5 protein evolution during the whole cell cycle in a pre-SEP mother cell

The sequential images of a full cell cycle progression for WHI5-GFP reporter strain. To better visualize the Whi5 protein nuclear cluster, the zoom-in images are provided. The red arrow indicates the Whi5 protein nuclear residence.

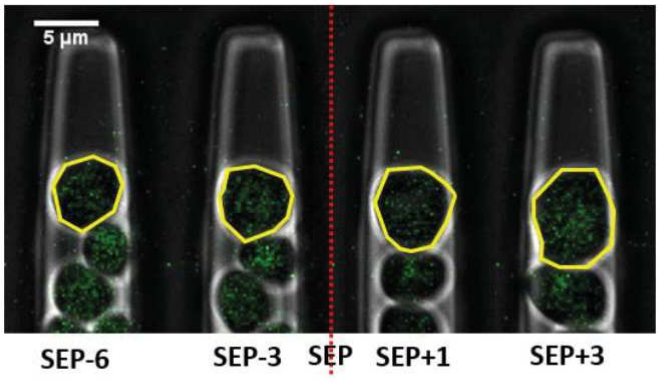

Figure 2.12 Mother yeast show SEP transition (WHI5-GFP)

Mother cell of WHI5-GFP reporter strain exhibiting SEP transition are shown in the figure, the red dashed line indicates the SEP.

After collecting all the mother yeast performing SEP transition, the number of frames showing WHI5-GFP reporter cell cycle duration and nuclear localization of G1 phase are counted by eye using ImageJ software. As the result, both cell cycle duration and G1 phase duration measured by Whi5 protein nuclear clustering are compared in pre-SEP and post-

SEP cells (Figure 2.13). The cell cycle duration shows a general increase of about 2.4-fold during post-SEP period, whereas the relative G1 phase shows an increment of about 5.4-fold. The cell cycle duration before SEP is about 84 minutes and it increases to 200 minutes after SEP. The G1 phase duration increases from 9 minutest up to 49 minutes. This measurement shows slightly larger increment after SEP compare to the measurement of HTB2-sfGFP reporter strain. This can be explained by a larger effective of post-SEP mother cells in WHI5-GFP reporter strain. When analyzing the cell-cycle-phase duration by HTB2-sfGFP reporter strain, some abnormal fluorescence pattern towards the end of replicative

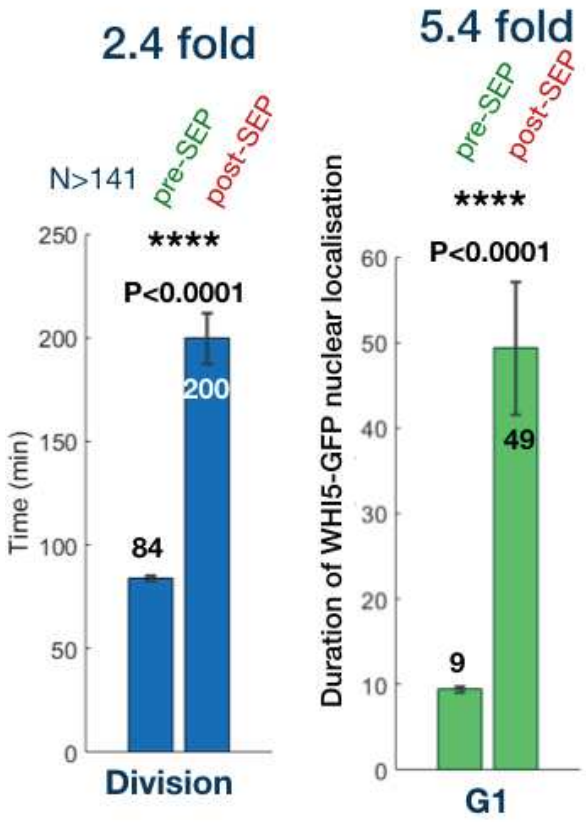

Figure 2.13 Cell cycle duration and relative G1 phase duration in WHI5-GFP reporter strain
Both cell cycle and relative G1 phase durations are quantified in pre-SEP and post-SEP mother yeasts. The legend indicates the mean ±standard error on mean. (pre-SEP, post-SEP; N>141)

lifespan are ruled out. Therefore, the number of post-SEP cell cycles that included in the analysis is much more in the WHI5-GFP reporter strain, especially some cell cycles shown at the end of lifespan. Consequently, the late life cell cycles are included for analysis and contribute to a higher post-SEP increment for WHI5-GFP reporter strain.

The result comparing pre-SEP and post-SEP population indicates that G1 phase is indeed showing significant elongation, the S/G2/M phases contribute to much less increment

(Figure 2.13). Even though the time window of G1 phase measured between HTB2-sfGFP and whi5-GFP are different, we observe the same cell cycle phase distribution pattern after SEP. We can conclude that the result of HTB2-sfGFP reporter strain is probably correct and all the phases are increased after SEP. And it seems that G1 phase is indeed extended mostly after the SEP transition. Similar conclusion has been made in the work of Noerohr et al., 2018 using Whi5 marker strain. In his work, he also proved that more and more whi5 protein are clustered in nucleus before death. Based on the significant G1 phase duration elongation towards the end of lifespan and along with other investigations, they have proposed that cell growth (corresponding to G1 phase) before Start checkpoint is crucial for cell cycle regulation at the end of lifespan, and the G1/S phase transition is the proximal cause for cell death. Combining with our result, the proportion of G1 phase to the whole cell cycle is about ⅑ at pre-SEP and become ¼ during post-SEP. This further suggests the significant role of G1 phase during ageing.

3 Histone and DNA quantification upon SEP

3.1 Specific background

3.1.1 Histone level increment is concomitant to SEP

As mentioned above, the histone protein level starts to increase from SEP. This observation has been extensively described in the cooperative project with Dr. Morlot's work of the host lab (Morlot et al., 2019). When using histone protein as nuclear marker, we observed previously that both histone level and nuclear size are increased after SEP (Figure 2.14). Yet the oscillatory pattern is still maintained during post-SEP.

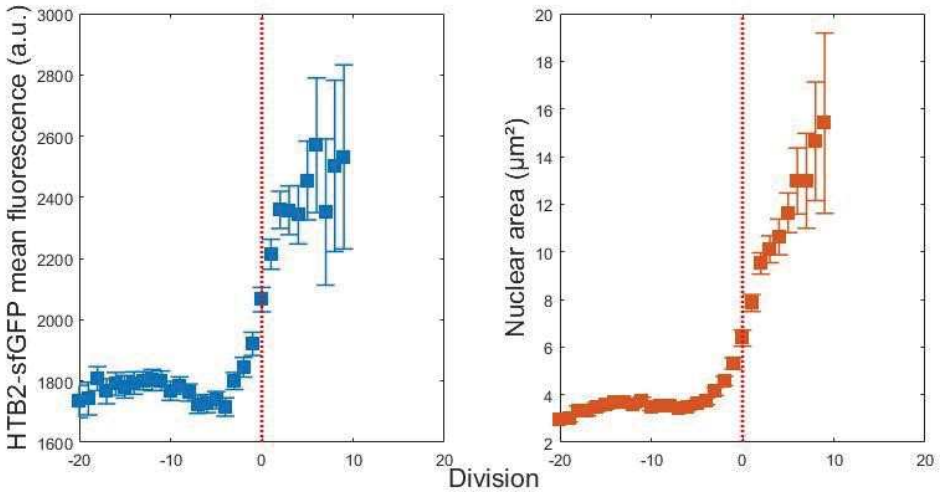

Figure 2.14 Histone protein expression and nuclear size increment aligned by SEP in mother cells

When aligning mother yeasts by SEP (red dashed line), the averaged HTB2-sfGFP fluorescence and nuclear size both increase abruptly concomitant to the SEP. The legend indicates the mean ±standard error on mean. (pre-SEP, post-SEP; N>40)

According to HTB2-sfGFP marker, both G1 and S phases' durations are showing tremendous increase after the SEP. In addition to the observation that Htb2 protein basal level starts to accumulate since SEP. The tight link between histone and DNA has been proved in previous literatures (Heintz, Sive et al. 1983, Sittman, Graves et al. 1983, Baumbach, Stein et al. 1987, Nelson, Ye et al. 2002). Therefore, Htb2 histone protein is selected to be used for cell cycle phase quantification in our approach.

3.1.2 DNA quantification by DAPI staining in microfluidic system

To understand the DNA quantity variation during ageing process, DAPI staining experiment was performed in microfluidic device. By the end of a microfluidic experiment, the yeast cells at various ages are retained in the microfluidic chip. Then the cells are stained by DAPI, the fluorescence levels corresponding to the quantity of DNA can be measured in yeast cells at different ages (Figure 2.15).

The age of mother yeast is determined using previously monitored time-lapse experiment. To ensure the measurement of nuclear DNA quantity by DAPI, five stacks of planes are collected to screen the whole cell volume. To avoid the artefact of DAPI signal from mitochondrial DNA, the nuclear DAPI fluorescence signal is measured within the nuclear contour determined by histone protein (Figure 2.15).

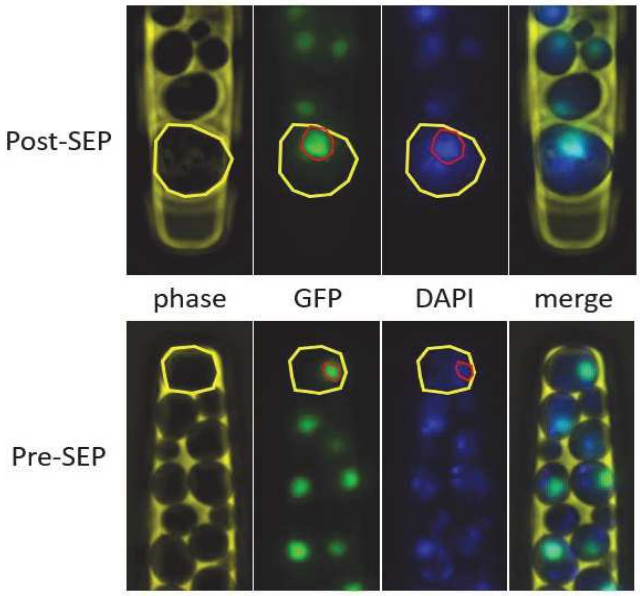

Figure 2.15 DAPI dye reveals DNA quantity in pre-SEP and post-SEP budding yeast in microfluidic device

Both pre-SEP and post-SEP mothers are shown in the figures. The cell contour in yellow is determined by automated cell contour detection of phase channel. Nuclear contour in red is determined by histone protein localization. DAPI fluorescence level inside the nuclear

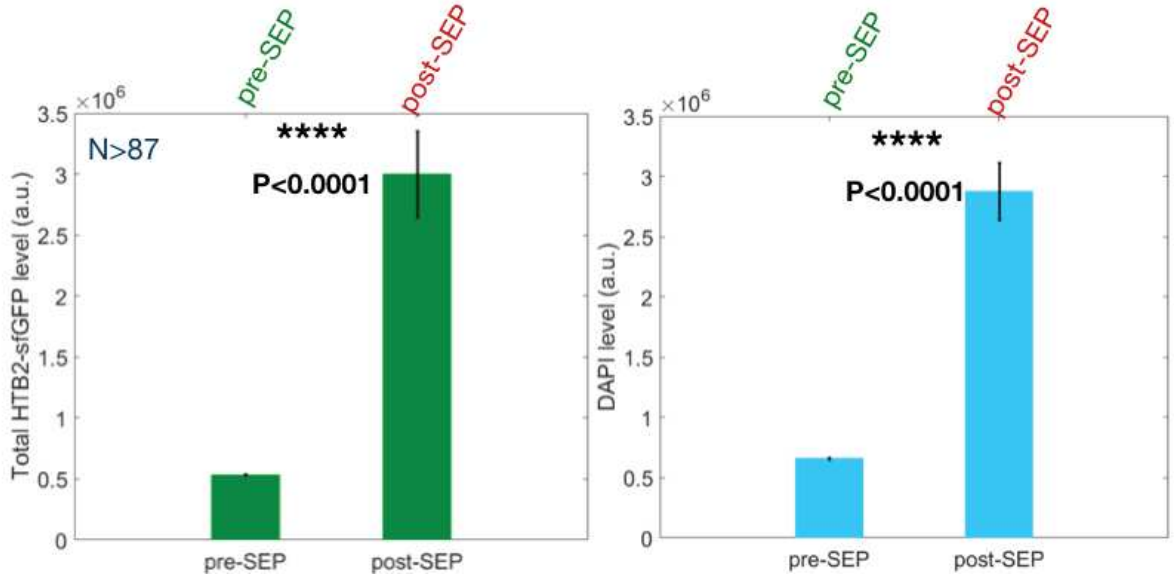

Figure 2.16 HTB2-sfGFP and DAPI fluorescence signal comparison in pre-SEP and post-SEP population

The histogram graphic of HTB2-sfGFP and DAPI fluorescence before and after SEP. The legend indicates the mean ±standard error on mean. (pre-SEP, post-SEP; N>87)

Based on this methodology, the nuclear DNA quantity corresponding to different mother yeast ages can be measured.

3.2 Result

3.2.1 Both histone and DNA quantity are increased upon SEP

DAPI fluorescence signal is increased when mother yeast ages, and the increment seems to start from SEP transition (Figure 2.16). It rises to 4-fold, which is like the increasing rate of histone protein level.

The DNA quantity accumulation after SEP shows a large variation compared to pre-SEP population. To monitor the dynamic of DNA quantity increment after SEP, the DAPI fluorescence of post-SEP mother at different age are analyzed. Considering the SEP transition as age 0, following each round of cell division the post-SEP mother's age increase to 1,2,3… The DAPI fluorescence increasing dynamic after SEP can be shown by aligning these post-SEP mothers according to their age. However, the increment did not show any pattern, the distribution of the DAPI fluorescence become irregular suggesting that each mother cell after SEP become very heterogeneous for their nuclear DNA quantity.

I then asked whether such DNA increase is scaled with histone increase in post-SEP population.

3.2.2 The scaling between DNA and histone are uncoupled after SEP

To compare the scaling between histone and DNA in both pre-SEP and post-SEP population, histone vs. DNA quantity of mother yeast is plotted (Figure 2.17).

Young pre-SEP population presented by the green hexagons, the cells are well restricted in the scaling between histone and DNA. According to the pre-SEP population, a linear correlation is fitted for revealing the correlation between histone and DNA. The result suggests that 70% of the cells can adapt to the linear fitting. The post-SEP cells are then compared in red stars. They show a much larger variety of both histone and DNA increase. And the increase of post-SEP cells seem to show slightly less DNA increase than histone increase, because the stars are mostly found below the linear fitting of pre-SEP population.

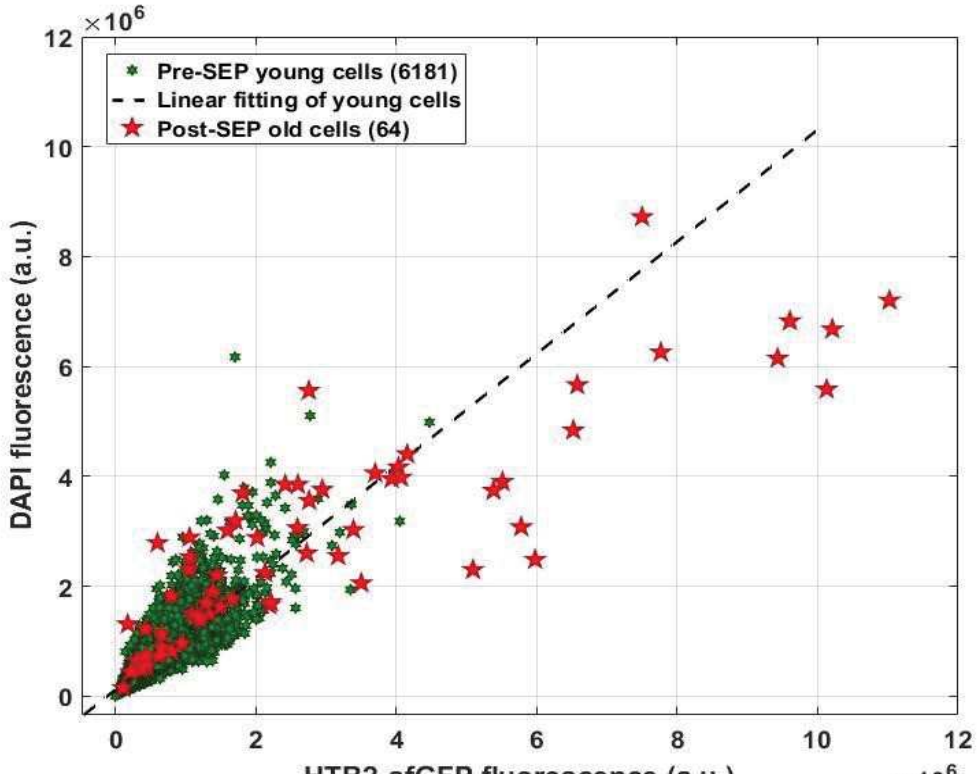

Figure 2.17 Comparison of DAPI vs. HTB2-sfGFP fluorescence in pre-SEP and post-SEP populations

DAPI vs. HTB2-sfGFP fluorescence is shown in the graphic, the pre-SEP population is presented by green hexagons, the linear fitting according to the pre-SEP population is estimated and shown in black dashed line. The goodness of the fit: SSE: 4.093e+14; R-square: 0.703; Adjusted R-square: 0.7029; RMSE: 2.574e+05. The post-SEP population is presented by red stars.

To better compare the maintenance of scaling between histone and DNA quantity during post-SEP period, the ratio of HTB2-sfGFP and DAPI fluorescence is calculated. The groups of ratios from both pre-SEP and post-SEP are plotted into smoothed distribution for better visualization (Figure 2.18). From the figure, we could observe that the peak of ratio distribution is relatively overlaid. By Mann–Whitney–Wilcoxon statistical test to compare these two sets of data, the P-value equals 0.24 suggesting that equal median is not rejected at the default 5% significance level. The two groups of data show identical median. As a conclusion, though the post-SEP cells show much more variety in both histone and DNA quantity, the scaling between histone and DNA is uncoupled after SEP.

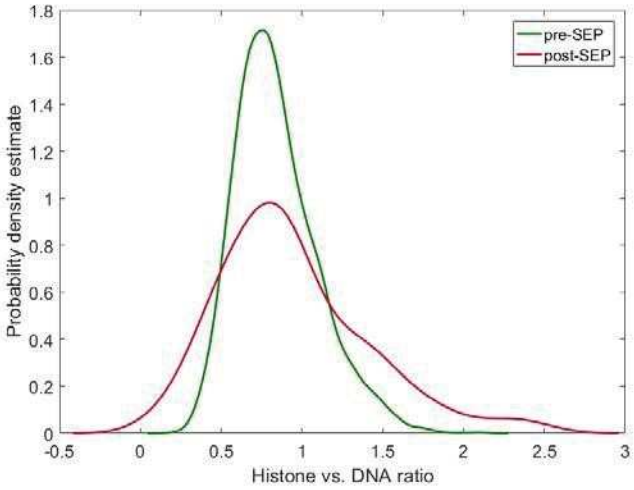

Figure 2.18 Smoothing estimate of pre-SEP and post-SEP population based on the HTB2-sfGFP vs. DAPI fluorescence ratio

The smoothed distribution of histone and DNA ratio in pre-SEP and post-SEP. The two groups of ratios are calculated by HTB2-sfGFP versus DAPI fluorescence and visualized by a Kernel smoothing function using MATLAB. Statistical test suggests the two groups of ratios between pre-SEP and post-SEP population is identical, the two sets of data have identical median.

4 DNA damage cell cycle checkpoint action upon SEP

4.1 Specific background

As DNA and histone quantity become more variable after SEP, the increased S/G2/M phase-duration become reasonable. We then speculate whether this raise is due to DNA damage response (DDR) activating as cell cycle checkpoint which then slow down the cell cycle progression after SEP?

4.1.1 Potential DDR activation markers

We chose to use DDR activation marker strains: DDC2-GFP and RNR3-GFP (Figure 2.19A). Ddc2 protein is the DNA damage sensor protein which forms a focus to locate the DNA

damage site. GFP fusion strain of Ddc2 has been used in the literature for detecting DDR activation in permanent cell cycle blocked cells (Figure 2.19B) (Goulev, Morlot et al. 2017). The Rnr3 is an isoform of RNR-complex, RNR complex is the ribonucleotide-diphosphate reductase to transform NTP into dNTP. After the DNA damage is sensed and during reparation, dNTP is required. Rnr3 is a downstream effector of DNA damage response which involved in DNA synthesis. DNA synthesis is downstream to a DDR activation signal. This RNR3-GFP fusion strain has been used to reveal the DDR activation in early telomere shortened mutant by counting the RNR3-GFP burst frequency (Figure 2.19B) (Xie, Jay et al. 2015).

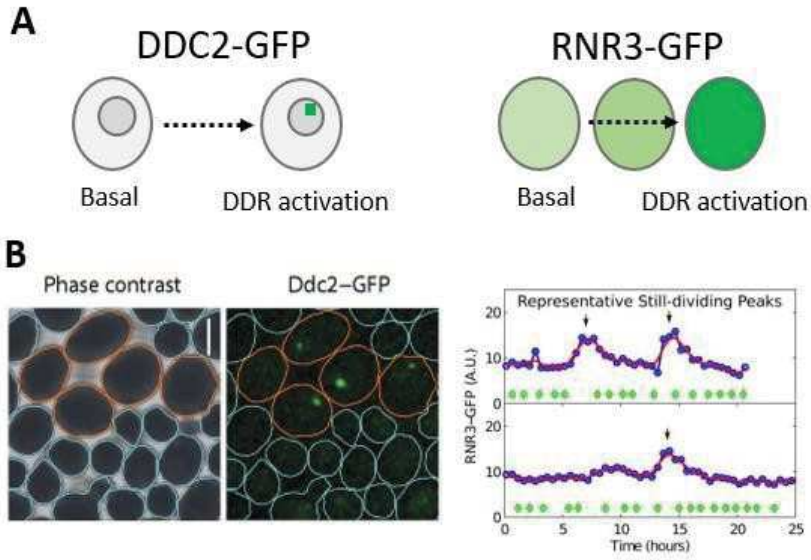

Figure 2.19 DDR activation markers: DDC2-GFP and RNR3-GFP

A: Schematic DDR activation fluorescence response of DDC2-GFP and RNR3-GFP reporter strains. The green color indicates the location and the quantity of the protein expression upon DDR.
B: Example of DDC2-GFP reporter strain for revealing DNA damage-induced cell cycle arrest after H2O2 treatment, the cell shows a persistent fluorescence focus (Goulev, Morlot et al. 2017). Example of RNR3-GFP reporter strain for revealing DDR activation in mutant, the cell shows fluorescence burst upon DDR (Xie, Jay et al. 2015).

4.1.2 Verification of DDR reporters in microfluidic system

Both reporter strains are treated under H2O2 and zeocin antibiotic for inducing DDR activation. When treating DDC2-GFP marker strain with H2O2 to trigger DNA damage. It is difficult to track the foci due to the loss of focus and weak signal (Figure 2.20). In addition, the time lapse frequency or the excitation light cannot be further increased to avoid photo-damage of laser. According to these observations in microfluidic device, we found that DDC2-GFP is not the ideal marker strain for DDR activation.

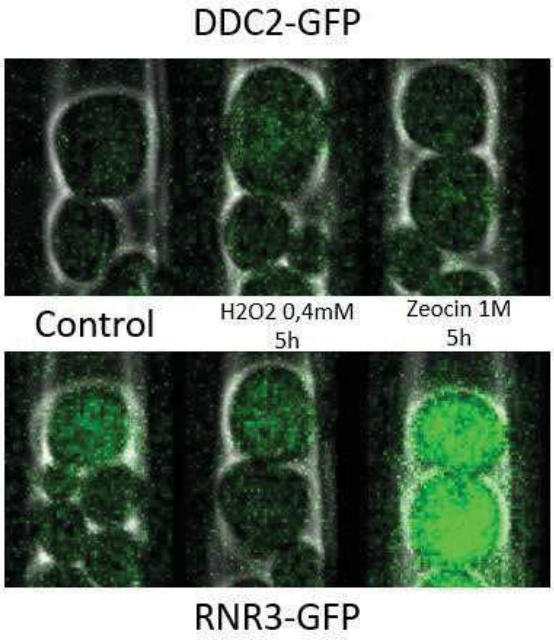

Figure 2.20 DDR induced in DDR reporter strain in microfluidic system

The reporter strains are treated under both H2O2 0.4mM concentration and zeocin 1M concentration for 5 hours. The time lapse ageing experimental setting is used for this test. The upper panel are the representative images of DDC2-GFP reporter strain, and lower panel RNR3-GFP. From left to right, the image is the result of different treatment: control, H202 0.4mM for 5h zeocin 1M for 5h. The fluorescence burst that observed in RNR3-GFP treated by zeocin is the most significant increase. The DDC2-GFP loci can rarely be observed.

On the contrary, the RNR3-GFP shows a long-last (more than 1 hour) fluorescence burst along with cytoplasmic Rnr3 overexpression. It can be easily detected in microfluidic system.

In addition, zeocin antibiotic seems to be the most efficient DDR-inducing agent (Figure 2.20). Therefore, from the positive control, RNR3-GFP reporter strain is used for the DDR activation and the RNR3-GFP fluorescence signal under the zeocin antibiotic treatment is set as positive control reference.

4.2 Result

4.2.1 Establishment of DDR activation threshold

The determination of DDR activation for RNR3-GFP marker strain is slightly tricky due to heterogeneous basal level of RNR3-GFP in individual cells (Figure 2.21). The average fluorescence signal is 464.9 ± 21 a.u. (standard deviation) in control experiment. RNR complex is periodically expressed due to the dNTP requirement at S phase for DNA synthesis.

The cell shows oscillatory Rnr3 expression pattern. In a population, the cell cycle is not synchronized, this makes it difficult to set-up a threshold for DDR activation.

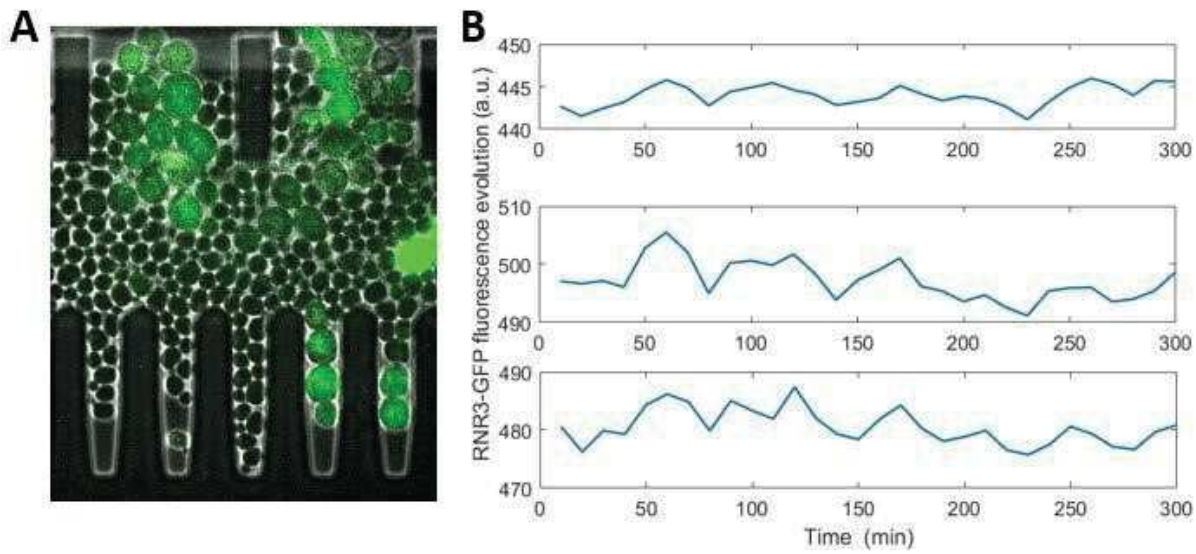

Figure 2.21 Heterogeneous RNR3-GFP basal level in control condition

A: The photo of RNR3-GFP reporter strain under control condition showing heterogeneous fluorescence basal level.
B: The representative trajectories of RNR3-GFP in the same experiment are shown. The average fluorescence level is 464.9 with an error of 21 a.u. (standard deviation).

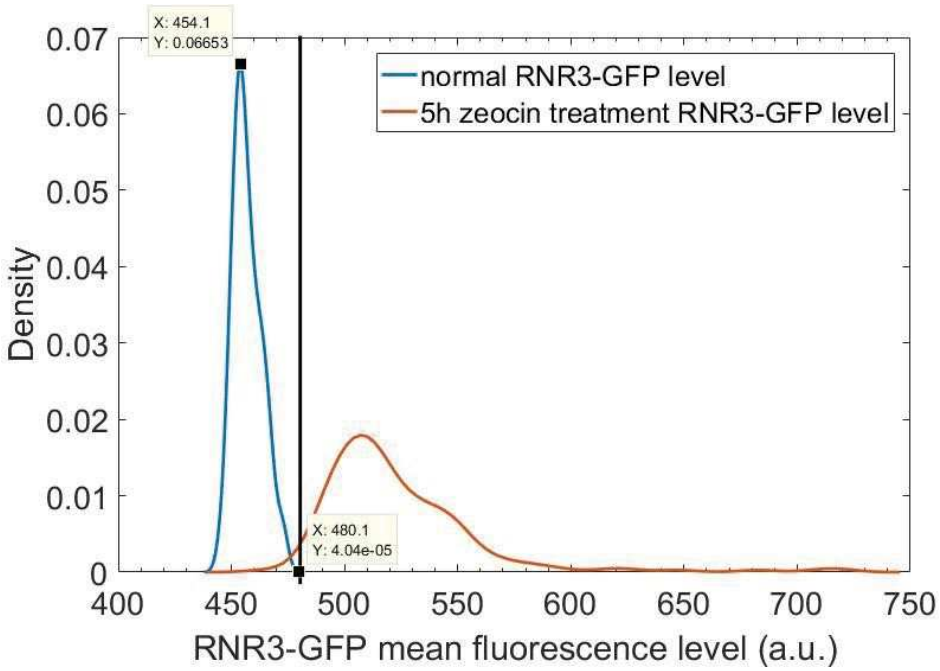

Figure 2.22 DDR activation threshold in RNR3-GFP reporter strain

The smoothed distribution of RNR3-GFP reporter strain under both control and positive control groups are shown in blue and orange, respectively. Based on the control fluorescence signal, the threshold is determined to avoid false DDR activation. The threshold is set by maximum fluorescence minus the median fluorescence level of control condition: 480-454=26a.u.

The fluorescence distribution of control is drawn in blue and the positive control in orange. We can observe that fluorescence level of positive control group is indeed increased compare to control group yet overlap can still be noticed. Thus, the determination of DDR activation threshold is set to avoid DDR false activation. The threshold of DDR activation is determined by maximum minus median RNR3-GFP fluorescence level measured under control condition as shown from the figure above (Figure 2.22). The difference between 480.1 and 454.1 is 26 a.u. Therefore 26 a.u. is set to be DDR activation threshold, any increment reaches 26 a.u. will be considered as a DDR activation.

4.2.2 SEP is not exclusively caused by DDR activation

The ageing process of reporter strain RNR3-GFP is monitored under time lapse experiment. The full mother yeast fluorescence level profile is quantified (Figure 2.23). Based on determined threshold (26 a.u.), 2 out of 69 mother cells show an increment of fluorescence larger than the threshold. Meaning that only 3% of cells are DDR activated during the ageing process revealed by RNR3-GFP marker. Out of the two cells, one shows DDR activation before SEP and the other after SEP. Most of the cell (97%), 67 out of 69 do not show a DDR activation throughout the whole RLS (Figure 2.24).

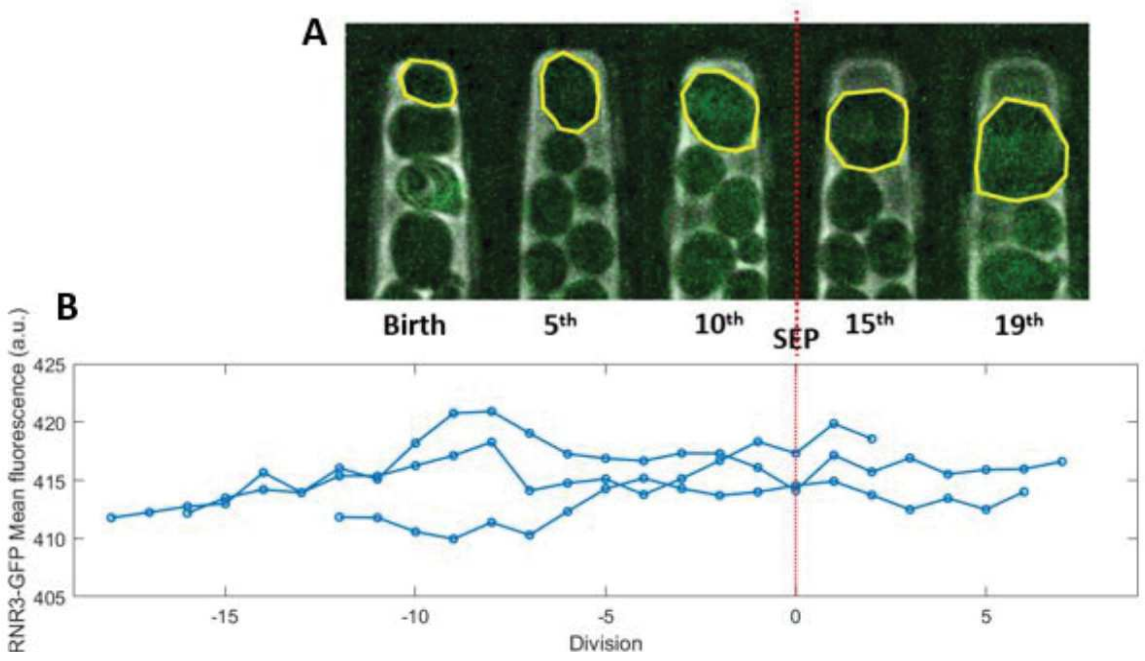

Figure 2.23 RNR3-GFP Single cell full RLS trajectories
A: Sequential images of RNR3-GFP reporter strain full lifespan, the SEP is presented by red dashed line.
B: The trajectories of fluorescence level evolution during ageing are aligned by SEP, each dot indicates the averaged fluorescence level of each cell cycle.

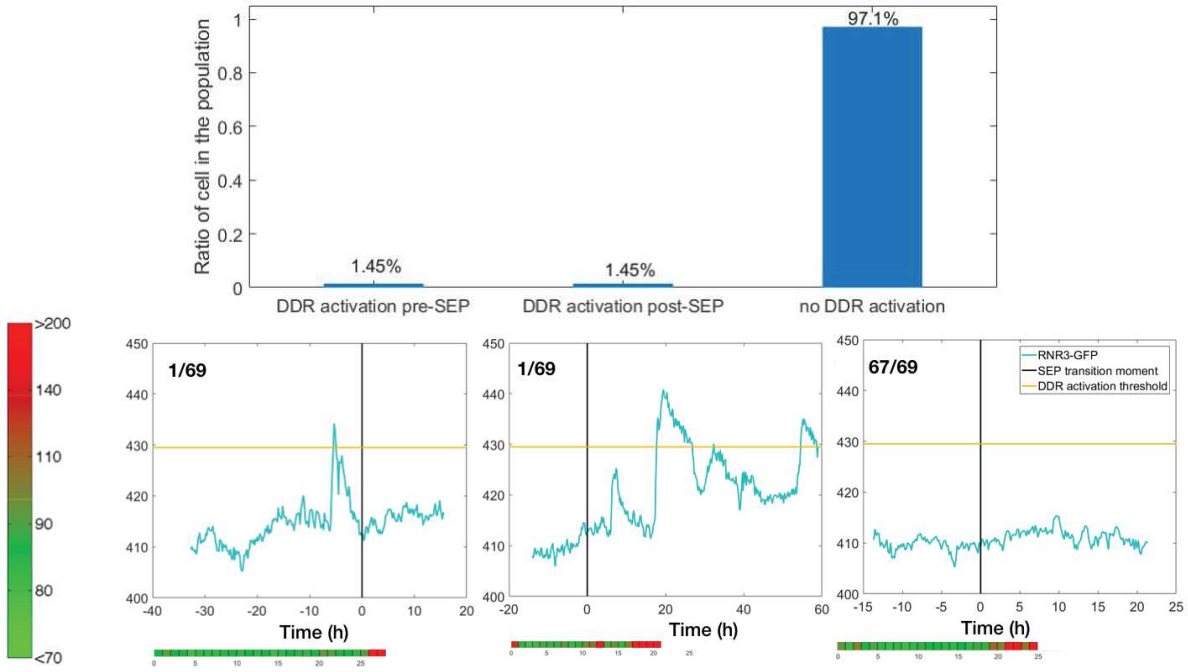

Figure 2.24 DDR activation proportion during RLS revealed by RNR3-GFP marker

Histogram graphic of DDR activated population fraction before and after SEP. One cell (1/69) shows DDR activation before SEP and the other one (1/69) after SEP. Most of the cells (67/69) 97.1% show no DDR activation during SEP transition.

The corresponding fluorescence trajectory profile of the full RLS is shown in the panel below. The SEP of each mother cell is shown in black line. The activated threshold is marked by orange line. The cell cycle duration trajectory presented by color bar of corresponding cell is shown below each fluorescence profile.

According to the RNR3-GFP reporter, it strongly suggests that SEP is not exclusively caused by DNA damage, because most of the cells are not DDR activated throughout their lifespan. This may be: firstly, due to the enormous DNA damage induction when cells were treated by zeocin at 1M for 5 hours for positive control; secondly, due to downstream DDR pathway effector Rnr3 protein may not be sensitive enough to reveal minor DDR signal. Therefore, weak DDR activation during normal ageing process may be less shown by RNR3-GFP reporter. To verify this hypothesis, more sensitive DDR activation reporter is needed to be tested for ageing experiment.

4.2.3 More DNA damage signals are observed after SEP in later RLS

However, an increment of RNR3-GFP signal at late life period can be observed, though it is below the DDR activation threshold (Figure 2.25). If we pool all the fluorescence level of RNR3-GFP cells aligned by the SEP moment. We can observe a slight increase of RNR3-GFP

level after the SEP transition to the late lifespan of mother yeast. Yet this increment is still below the determined DDR activation threshold.

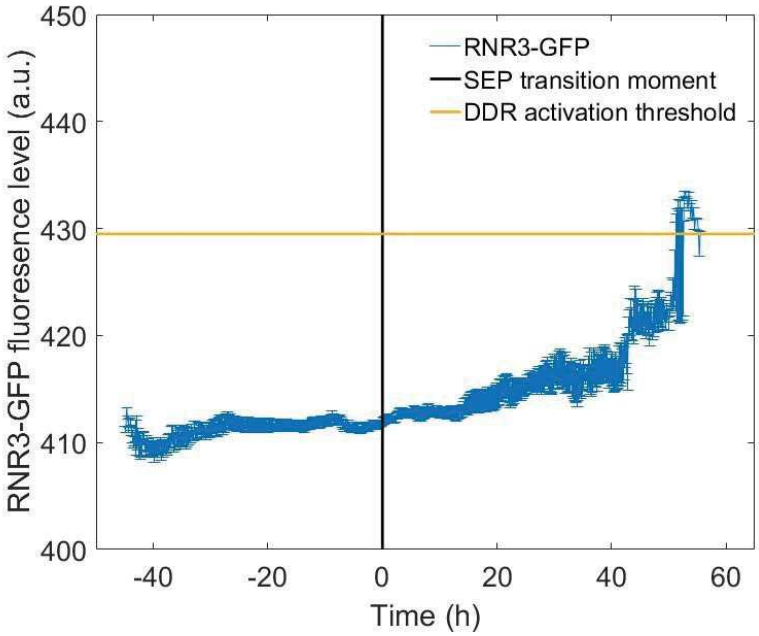

Figure 2.25 RNR3-GFP fluorescence level aligned by SEP transition moment

Fluorescence of RNR3-GFP are pooled and aligned by SEP to reveal the evolution of DDR activation throughout the whole replicative lifespan. The SEP is indicated by black line, the DDR activation threshold is shown in orange. The averaged fluorescence evolution is plotted in blue. The legend indicates the mean ±standard error on mean. (N=69)

Yet the RNR3-GFP fluorescence increment before death may be explained by increasing DNA damage happening at the end of lifespan. This observation is in line with previously published work on the study of DNA damage in replicative ageing context (Novarina, Mavrova et al. 2017). In their work, more DNA damage signals revealed by Rad52 foci (DNA damage sensor) can be observed at old age compare to young cells, and this work has proposed that such increment might be due to less efficient DNA repair mechanism as the cell ages.

Chapter III

Result part 2:

SEP characterization in long-lived context

1 Characterization of SEP in long-lived mutant fob1 by limited ERC generation

1.1 Specific background

1.1.1 Regulatory elements on ribosomal DNA gene

The ERC is a double strand plasmid-like circular DNA that contains ribosomal large subunit 35S and small subunit 5S (Figure 3.1). 35S corresponding to the large ribosomal subunit for which the replication is under the regulation of pol I complex; and 5S encoded the ribosomal small subunit is replicated by polymerase III. The transcriptional direction of these two genes are opposite as indicated on the figure. There is a fork block protein Fob1 bind between the two genes and serve to prevent bi-directional transcription. (Figure 3.1). A rDNA gene is around 9.1 kb. The tandem repeats of rDNA on chromosome XII can be as long as 1.4Mb due to repetitive rDNA genes.

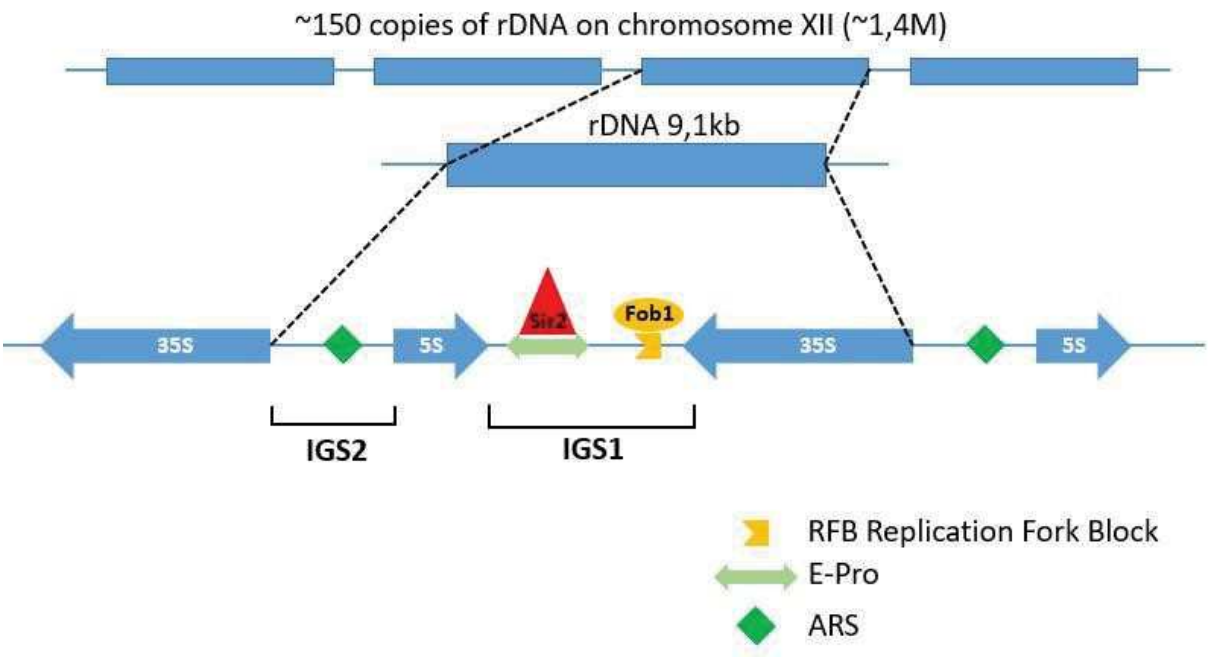

Figure 3.1 Regulatory elements on rDNA repetitive loci

35S and 5S ribosomal coding genes are shown in blue, with the corresponding transcription orientation. In green the ARS signal allows the auto-replication. In light green is the E-pro site where Sir2 protein can bind to this region and induce silencing. The Fob1 fork block binding site is in orange. Fob1 fixation allows single direction transcription of 5S gene. IGS1 and IGS2 stands for the two intergenic space (sequence). A rDNA gene is around 9.1 kb. The tandem repeats of rDNA on chromosome XII can be as long as 1.4Mb.

The excision of ERC is induced DNA homologous recombination repair. DNA binding proteins including transcription polymerases and fob1 proteins collapse from rDNA loci and induce double strand break. The cell may detect such break and when repairing by homologous recombination, the unequal copy number between sister chromatid may lead to ERC excision and eventually repair rDNA repetitive loci and ERC may be excised.

The ERC formation is related to the exposed rDNA that show transcriptional accessibility. Because when the rDNA repetitive loci are transcriptional activated, the proteins may bind onto the DNA and eventually lead to rDNA repetitive gene excision when DNA collision happens. The excised rDNA tandem DNA circle -- ERC which contain an auto-replicative origin sequence (ARS) region for which the replication can be originated. This allows the ERC molecule to be duplicated along each cell cycle. Once the ERC excised, it has been speculated that ERC will be replicated for each cell cycle because of its RAS replicative origin. Therefore, the excised ERC may be accumulated exponentially after each cell cycle (Figure 3.2). The mainstream hypothesis of ERC-induced toxicity phenomenon is based on the titration of transcriptional factors which spare excessive regulatory proteins on ERC and eventually it may become lethal when the number of ERC become outrageous in aged mother yeast.

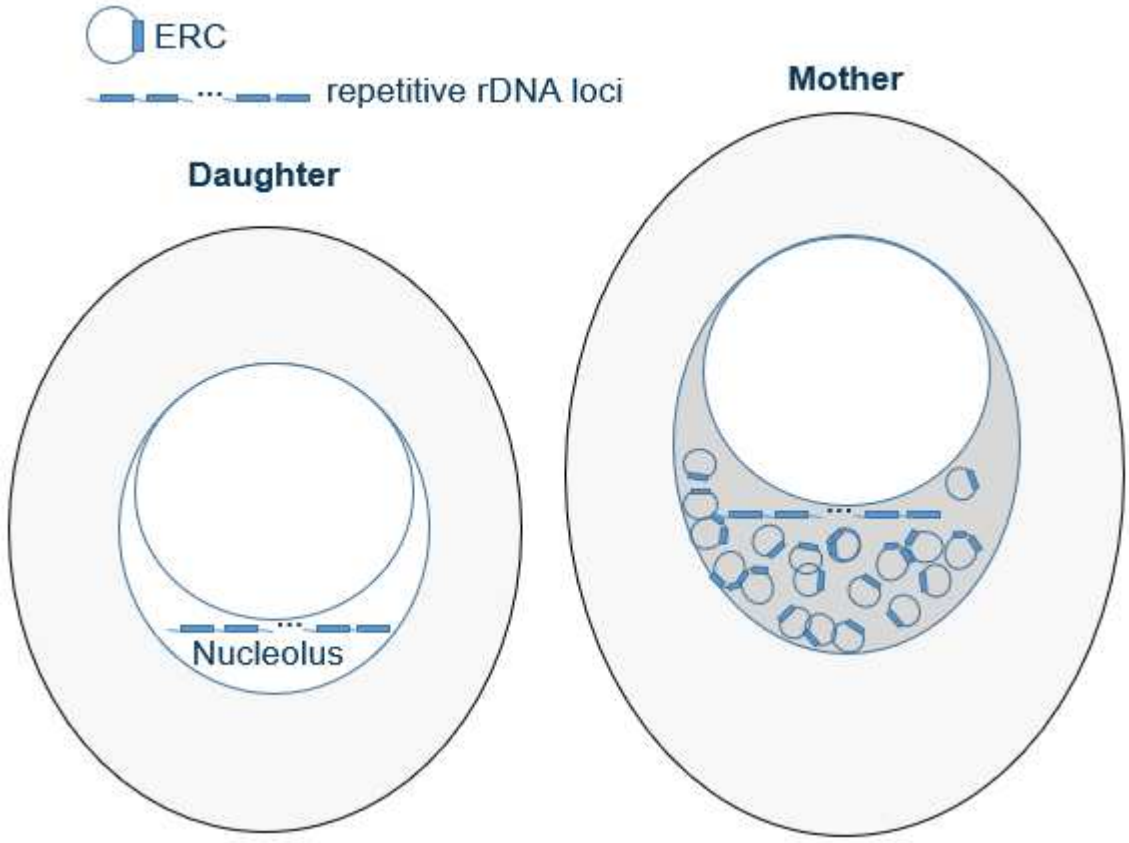

Figure 3.2 Schematic ERC molecule in both daughter and aged mother cells
The schematic rDNA and ERC localization figure in daughter cell and aged mother cell. The blue block indicates the ribosomal coding gene. The repetitive rDNA loci locate in the nucleolus region. As the mother ages, more and more ERCs are formed and may induce death eventually.

The protein Fob1 is a DNA binding protein specific to the rDNA region for transcription regulation and its known to induce DSB and ERC formation. It has been reported that fob1Δ mutant show less ERC accumulation due to less ERC formation and longer RLS compare to WT. This might be due to less ERC-induced toxicity.

1.1.2 Regulation of ERC biogenesis and rDNA stability by chromosome remodeling

There are about 150-200 tandem copies of rDNA genes, yet not all of them are accessible for transcription. This accessibility is under the regulation of chromosome structure and function, more precisely the epigenetic histone post-translational modifications, such as: by covalent modification on histone residues such as acetylation or deacetylation on lysine etc.

These modifications can induce rDNA silencing and increase transcriptional accessibility by chromosome remodeling (Srivastava, Srivastava et al. 2016).

For rDNA loci, its nucleosome can be remodeled under the control of enzyme exhibiting histone deacetylase activity via Sir2 (Buck, Sandmeier et al. 2002, Huang and Moazed 2003). Deleting Sir2 gene can reduce silencing therefore increase the transcriptional accessibility around the repetitive rDNA region. This exposure may further affect the ERC formation under the influence of rDNA stability. Indeed, in sir2Δ, the cell exhibits high rDNA instability and rapidly form large amount of ERC (Kobayashi, Horiuchi et al. 2004, Kobayashi and Sasaki 2017). This mutant show significantly shortened RLS.

1.1.3 The relationship between rDNA/ERC and SEP (work in (Morlot, Song et al. 2019)

Previously in the lab, the work of Dr. Morlot (Morlot et al., 2019) has revealed the direct relationship between SEP and the ageing factor ERC. By using a rDNA/ERC marker, she found that SEP may be a consequence of ERC accumulation (Figure 3.3).

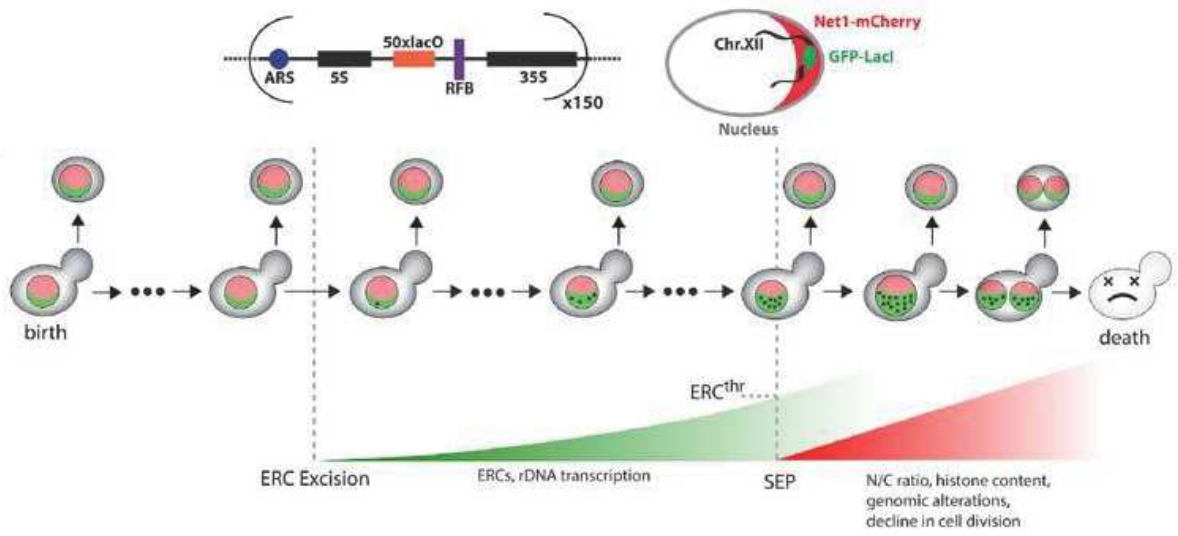

Figure 3.3 SEP is a consequence of ERC accumulation revealed by ERC-LacO & GFP-LacI reporter strain

A schematic figure of ERC accumulation prior to the SEP over the course of ageing. The green zone represents nucleolar region of nucleus; the black dot indicates the ERC molecule. The reporter strain used for rDNA/ERC is shown on the figure. As the ERC copy number reaches a certain threshold, the SEP happens and eventually the cell death.

She has used the reporter strain of ERC/rDNA to monitor its copy number during ageing (Figure 3.3). Each rDNA gene is inserted with repetitive LacO sequence so that LacI-GFP can bind to the rDNA/ERC molecule and reveal green fluorescence signal. The ERC accumulation

starts shortly after birth. When the quantity of ERC reaches a threshold, SEP is triggered. In addition, the statistical estimation of fluorescence signal indicates an exponential increase within each division. This observation suggests that fluorescence signal increment is indeed issue from the extrachromosomal ERC gene copies. Therefore, once ERC is excised, the duplication starts as cell ages. Eventually, at the end of lifespan, the quantity of ERC can reach a size of 1.6-fold of yeast genome.

One of the mutants showing less ERC accumulation is the long-lived fob1Δ mutant. As the SEP is related to ERC accumulation, whether SEP is delayed and how the SEP become in fob1Δ mutant can be asked.

1.2 Result

1.2.1 Fob1 mutant shows prolonged RLS in microfluidic system

Deleting Fob1 protein leads to RLS extension, this has been reported in the literatures since 1999 (Defossez, Prusty et al. 1999, Kobayashi 2003). Fob1Δ mutants with and without histone nuclear marker (HTB2-GFP) are used for time lapse ageing experiment. We confirmed that fob1Δ mutant is long-lived in our microfluidic system (Figure 3.4).

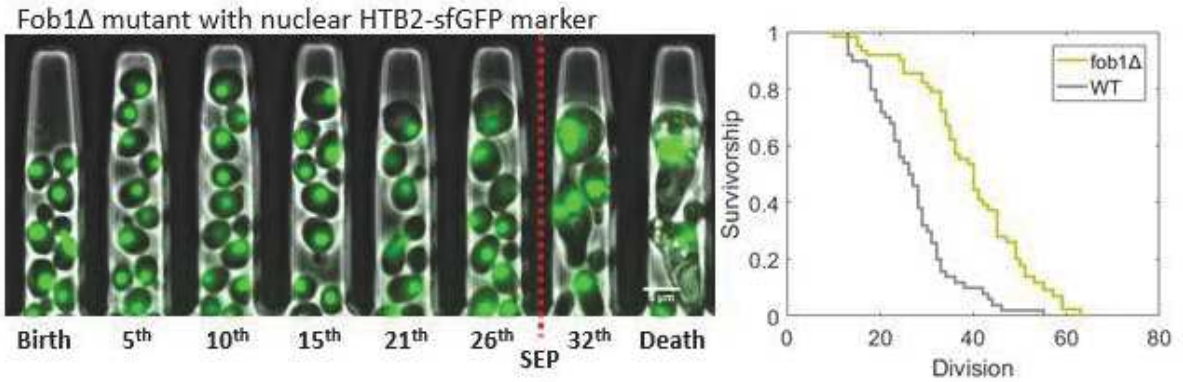

Figure 3.4 Fob1 Δ mutant indeed show longer RLS than WT

The representative ageing trajectory of fob1Δ mutant with nuclear marker is shown in the left panel. The mother replicative lifespan is measured and compare to WT. Significant increase of RLS can be observed (WT (27.5) N=130; fob1Δ (39) N=63).

1.2.2 Probabilistic SEP event by limiting ERC excision in fob1Δmutant

Surprisingly, we observe two distinct cell fate in fob1Δ mutant, there are cells die with and without SEP (Figure 3.5).

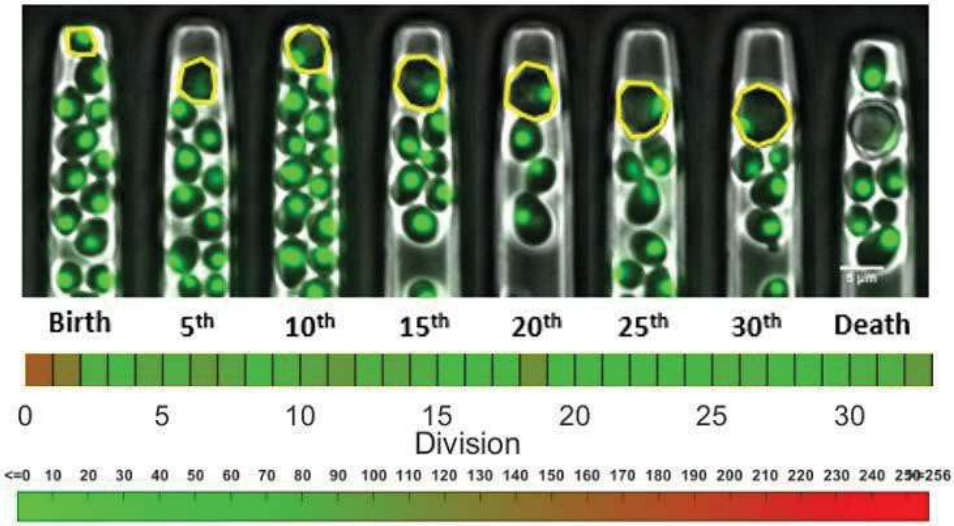

Figure 3.5 Fob1Δ mutant show long-lived mother cell age without SEP

Representative fob1Δ mutant show no-SEP ageing pattern. Both sequential images and cell cycle duration trajectory is shown below. The average cell cycle duration is ~80 minutes per division throughout the whole lifespan.

In WT population, the SEP is triggered in most of the mother yeast, about 85% of cells die with SEP (N=90, with-SEP=77, no-SEP=13) (Figure 3.6). Yet in fob1Δ mutant, up to 63% of cells (N=56, with-SEP=21, no-SEP=35) die without SEP transition, these cells are thus defined as no-SEP subpopulation. They show significantly longer RLS (45) compare to WT (27.5). In this fob1Δ no-SEP subpopulation, the nuclear size is relatively constant and do not show

enlargement before cell death (Figure 3.5). This suggests that ERC copy numbers of no-SEP cells may not be increased as in with-SEP population. The mother yeast may be died in an ERC-free status. This hypothesis is indeed confirmed by Dr. Morlot's complementary work by directly using rDNA/ERC reporter in a fob1Δ mutant. When monitoring the ERC signal throughout the whole lifespan in no-SEP cells, the fluorescence signal shows a constant level.

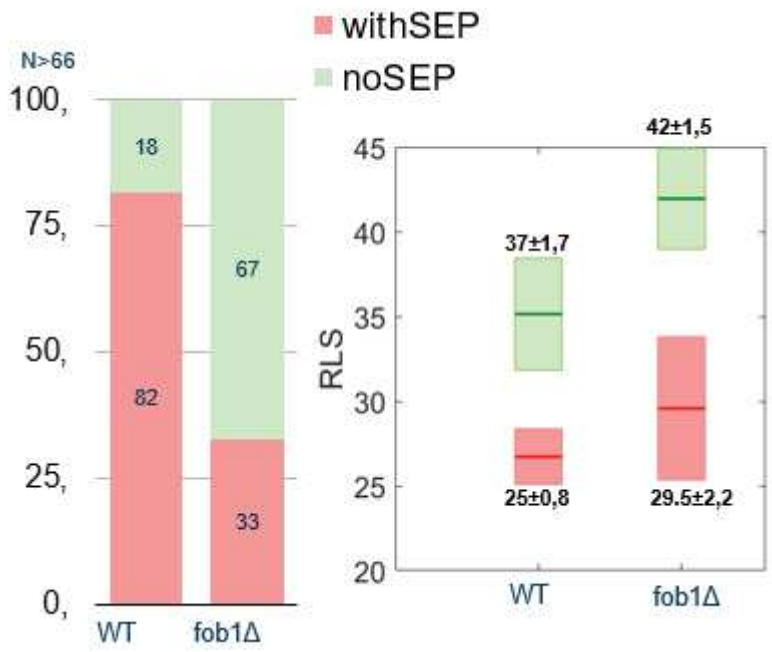

Figure 3.6 Distribution of with-SEP and no-SEP population

The histogram distribution of with-SEP and no-SEP population in both WT and fob1Δ mutant. The legend indicates the percentage proportion of the two subpopulations. The boxplot figure indicates each subpopulation replicative lifespan. The legend indicates the mean ±standard error on mean. (N>66)

For fob1Δ with-SEP subpopulation, there is 37% of mother yeast undergo SEP transition and they show slightly longer RLS than the WT. I then asked whether the SEP in both fob1Δ and WT is happening at the same time. Statistical Mann–Whitney–Wilcoxon test for both full RLS and SEP are compared between WT and fob1Δ with-SEP subpopulation (Figure 3.7).

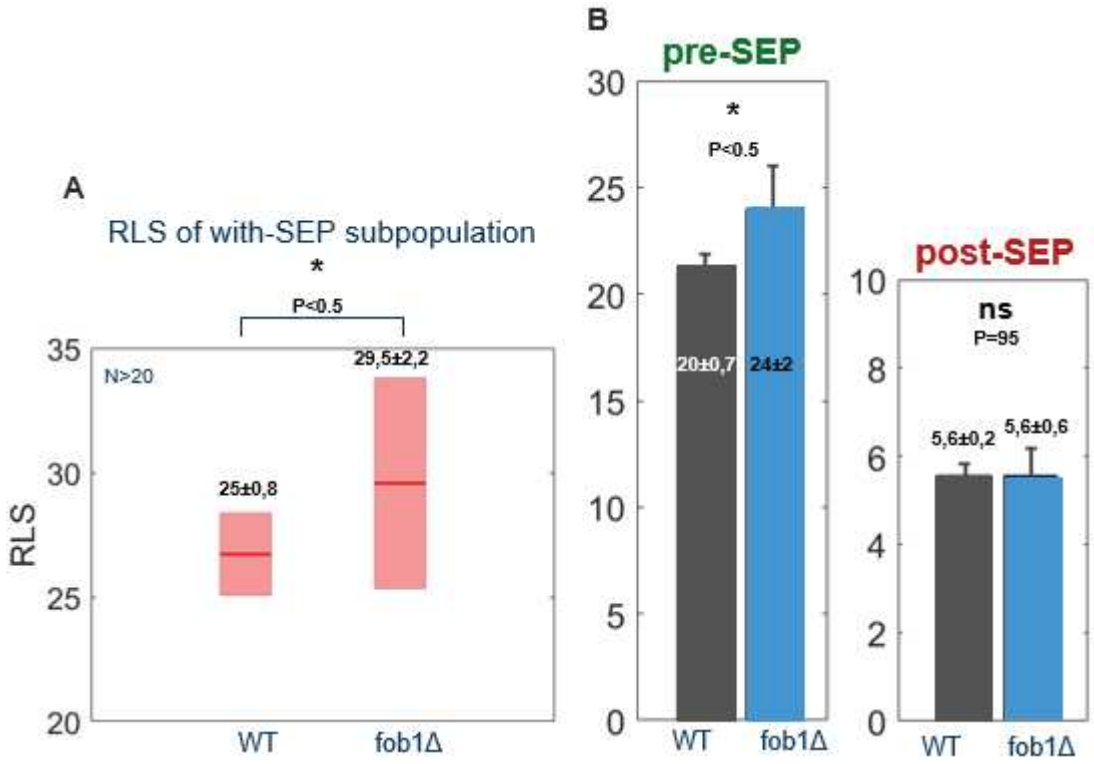

Figure 3.7 Comparison of SEP onset and RLS of subpopulation

A: The boxplot graph of with-SEP subpopulation in both fob1Δ and WT. The with-SEP cells of fob1Δ strain shows slightly longevity extension. The legend indicates the mean ±standard error on mean. (N>20)

B: The histogram graph of SEP comparison in both fob1Δ and WT. The SEP of fob1Δ mutant (24) is prolonged compare to WT (21). The post-SEP lifespan is identical in both backgrounds. The legend indicates the mean ±standard error on mean.

It seems that SEP is delayed in fob1Δ mutant and the extended SEP mainly contribute to the longevity extension in with-SEP subpopulation. The post-SEP period of both fob1Δ and WT do not show distinct lifespan. From this result, two factors contribute the fob1Δ longevity extension. Firstly, the no-SEP cells which is most of the whole population, live significantly longer; secondly, the with-SEP cells show delayed SEP also extend RLS. Taking together, it seems that fob1Δ mutant by limiting the ERC formation largely reduce the SEP probability in the population. Two distinct cell fate of fob1Δ population, suggests that ERC excision regulated by Fob1 protein may be a probabilistic event during the ageing process.

1.2.3 SEP characterisation in with-SEP subpopulation of WT and fob1Δ

To further compare the SEP between WT and fob1 with-SEP subpopulation. Both cell cycle duration, histone fluorescence increment and nuclear cytoplasmic ratio are compared (Figure 3.8). It seems that SEP exhibit identical characteristics between WT and fob1Δ mutant.

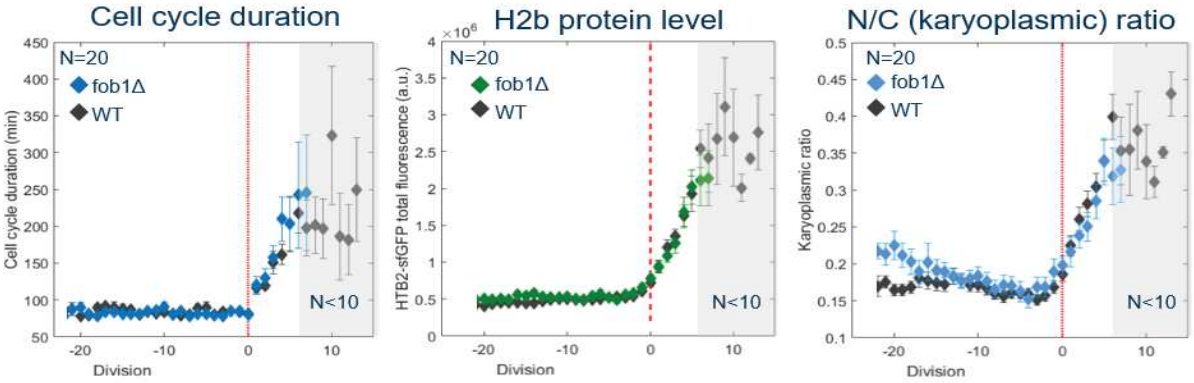

Figure 3.8 Comparison of SEP characteristics in fob1Δ and WT

The evolution of cell cycle duration, HTB2-sfGFP and N/C ratio in fob1Δ and WT (aligned by SEP). The error bar indicates ±standard error on mean. (N=20 for both strains) The SEP is indicated by a dashed red line and located to the zero of x-axe. The grey area indicates less effective at late life due to mother cell death.

This observation validate that SEP observed in fob1Δ with-SEP population is like the SEP observed in WT population. Even though SEP is similar, the cell cycle duration of fob1Δ (84) is longer than WT (76) for young pre-SEP cells. This difference must be crucial for survivorship of WT in savage environment. It has been proposed in the study of microorganism that fast growth of the population is crucial for nutrient and space occupation and competition. This maybe the one of the reasons that long-lived fob1Δ mutant cannot override WT strain.

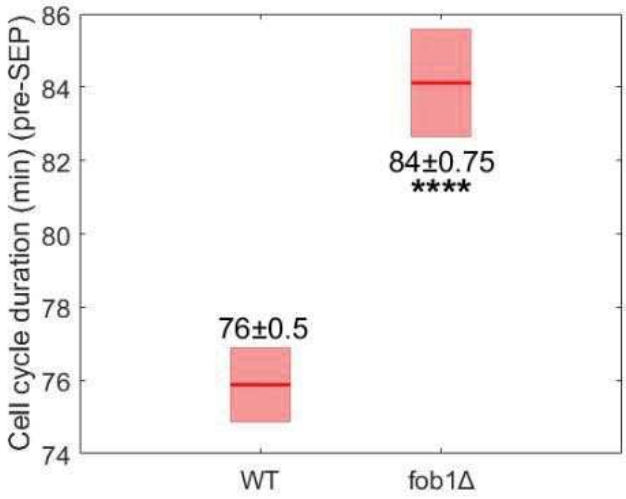

Figure 3.9 Comparison of cell cycle duration between WT and fob1Δ

The boxplot graph compares the cell cycle duration og WT and fob1Δ mutant. (N=338)

2 Characterization of SEP in long-lived mutants by perturbing ERC mother-daughter segregation

2.1 Specific background

2.1.1 Regulatory elements for ERC asymmetric segregation between mother and daughter cells

As the number of ERC increases, it becomes crucial for the mother yeast to generate ERC-free daughters for which their ages are reset to zero (Kennedy, Austriaco et al. 1994). One of the mechanisms that has been elucidated which involved in the ERC asymmetric segregation is by tethering to mother nuclear pore complex (NPC) under the regulation of SAGA complex (Denoth-Lippuner, Krzyzanowski et al. 2014). SAGA complex is short for Spt-Ada-Gcn5-Acetyltransferase complex. It is one of the major transcriptional regulator complexes for gene expression. The SAGA complex is constituted of 18 subunits and regulate chromosomal structure by histone post-translational modification. Its enzymatic activities include histone acetylation by Gcn5 complex and histone de-ubiquitination by mDUB module (Figure 3.10A) (Yan and Wolberger 2015).

It has been further uncovered that in the SAGA mutant, ERC can abnormally propagate from mother to daughter yeast (Figure 3.10B) (Denoth-Lippuner, Krzyzanowski et al. 2014). These mutants (SAGA component deleting mutants) lacking ERC anchorage capacity exhibit longer RLS than WT. The authors proposed that SAGA complex serve to enhance ERC anchorage on NPC and restrict its segregation to daughter cell. I then chose the SAGA mDUB module mutants: sgf73Δ and ubp8Δ mutants which are known to be long-lived and has been investigated previously (McCormick, Mason et al. 2014).

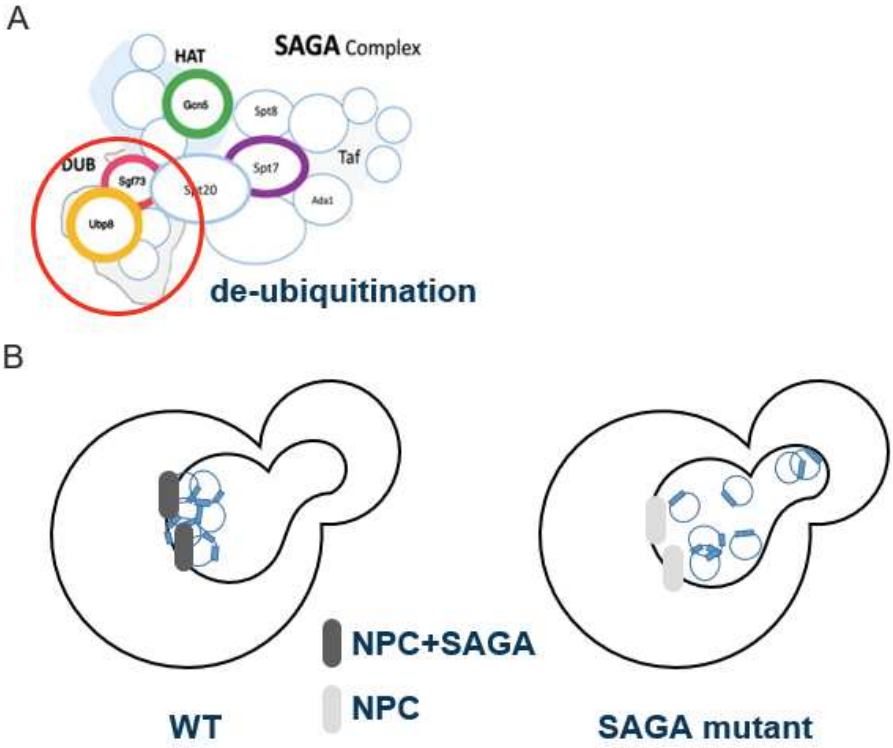

Figure 3.10 SAGA complex and schematic figure of SAGA mutant adapted from (Denoth-Lippuner, Krzyzanowski et al. 2014)
A: mDUB module of SAGA complex (adapted from Canzoneta et al., 2016).
B: Schematic figure showing ERC retention capacity in WT and SAGA mutants. In WT, SAGA complex helps to tether ERC on the NPC and prevent the ERC propagation. In SAGA mutant, the ERC are not tethered to NPC, therefore propagation of ERC to the daughter cell is more frequent in SAGA mutant.

ERC asymmetric segregation can also be regulated by the diffusion barrier located to the bud neck between mother and daughter. It has been proved that Bud6-dependent diffusion barrier serve to confine ERC segregation in mother cell (Shcheprova, Baldi et al. 2008). Hence, bud6 has been found to be a long-lived mutant due to ERC bud neck propagation from mother to daughter cells.

2.2 Result

2.2.1 RLS analysis for verification of long-lived mutants

Above mentioned mutants: sgf73Δ, ubp8Δ and bud6Δ are monitored for time lapse ageing experiment. Bud6Δ mutant shows a similar RLS to WT in our hand (Figure 3.11). Probabilistic SEP is not observed in this mutant. From statistical test between the bud6Δ and WT, both RLS and SEP are similar. This mutant does not show longer RLS in microfluidic system. In addition, both cell cycle duration, SEP probability (proportion of with-SEP and no-SEP cells) are similar compare to WT. Therefore, no further analysis was performed in this mutant.

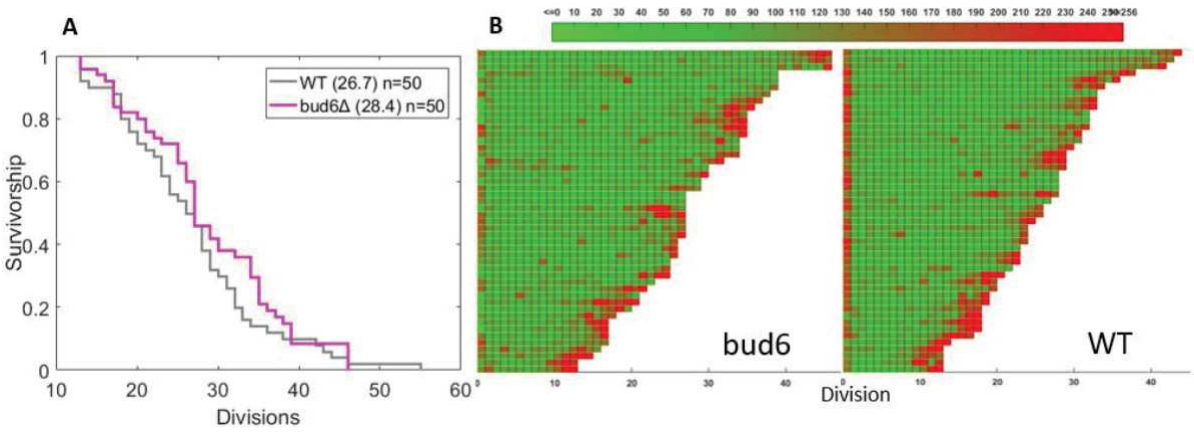

Figure 3.11 RLS and cell cycle duration trajectories in bud6Δ mutant compare to WT

A. RLS survival curve is observed in bud6Δ mutant and WT. (N=50)

B. Color-coded cell cycle duration trajectories of WT and bud6Δ. The probability for SEP onset (~80%) and cell cycle duration (80 min) do not show significant difference.

For the other 2 SAGA mutants, RLS extension can be measured (Figure 3.12). The median RLS of the three strains WT, sgf73Δ and ubp8Δ are respectively 27.5 (±0.8), 34 (±1) and 31.5 (±0.9). Using boxplot graphic to present the RLS and combining with statistical test, sgf73Δ seems to exhibit more longevity extension compare to ubp8Δ.

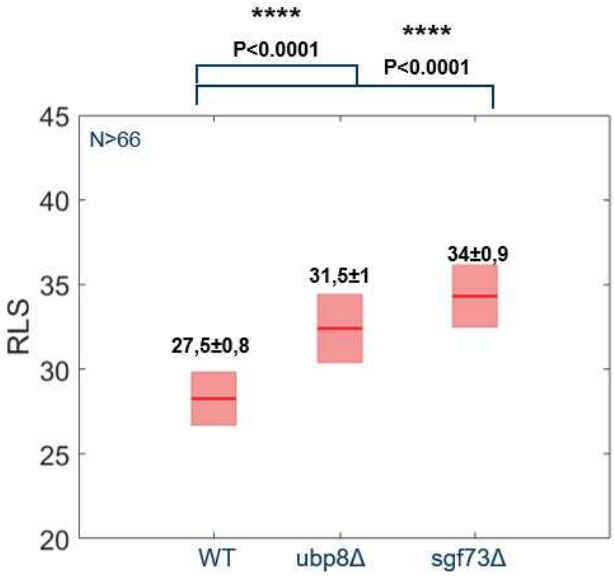

Figure 3.12 RLS extension observed in sgf73Δ and upb8Δ mutants

Boxplot graph of RLS of WT and SAGA mutants. SAGA mutants show extended RLS. Average RLS for sgf73Δ (N=85) is 34 and upb8Δ (N=102). The legend indicates the mean ±standard error on mean. Statistical test has been performed, when comparing with WT RLS, sgf73Δ shows significant increase of RLS whereas ubp8Δ shows less significant increase.

When investigating the SEP in SAGA mutants, I found surprisingly the no-SEP population which indicate that SEP is under the regulation of SAGA mDUB function as well. The probabilistic SEP event among all the mothers and the onset of SEP in with-SEP subpopulation are analyzed (Figure 3.13).

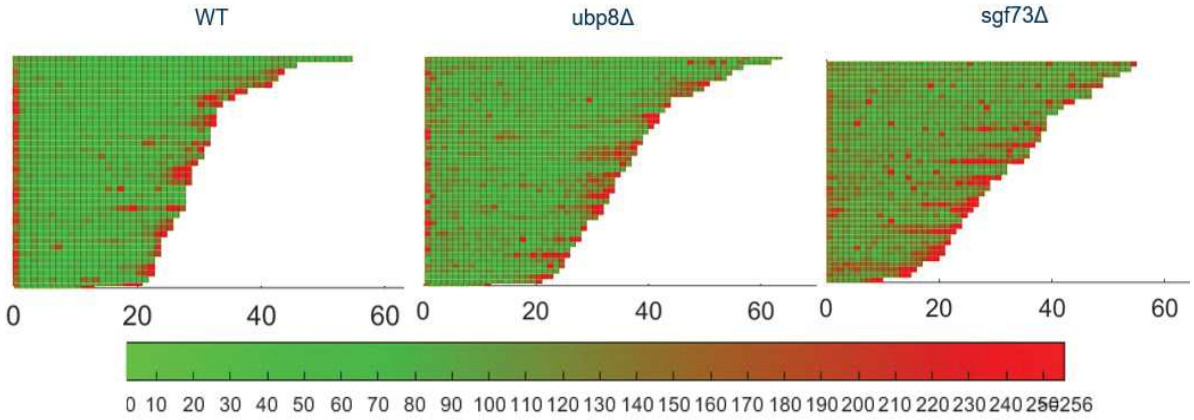

Figure 3.13 Cell cycle duration trajectory of WT and SAGA mutants

The representative color-coded cell cycle duration trajectories for WT, sgf73Δ and ubp8Δ mutants (N>36). Erratic and spontaneous long cell cycle in red can be observed in sgf73Δ mutant.

2.2.2 Alternative SEP determination approach for sgf73Δ SAGA mutant

The spontaneous long cell cycle duration represented in red can be seen in color coded cell cycle duration trajectories. Comparing SAGA mutants with WT, the both ubp8Δ and sgf73Δ seem to show spontaneous and erratic long cell cycle during early age. And the most severe phenotype with spontaneous long cell cycle at early stage is the sgf73Δ mutant. I then focus on sgf73Δ mutant for further analysis solely, since the two SAGA mutants are involved in the same enzymatic function. Not only cell cycle duration become irregular, the young mother cell shows prolonged cell cycle as well. When analyzing the SEP based on the cell cycle sudden extension, it become difficult and inaccurate due to irregular and extended pre-SEP cell cycle duration (Figure 3.14A).

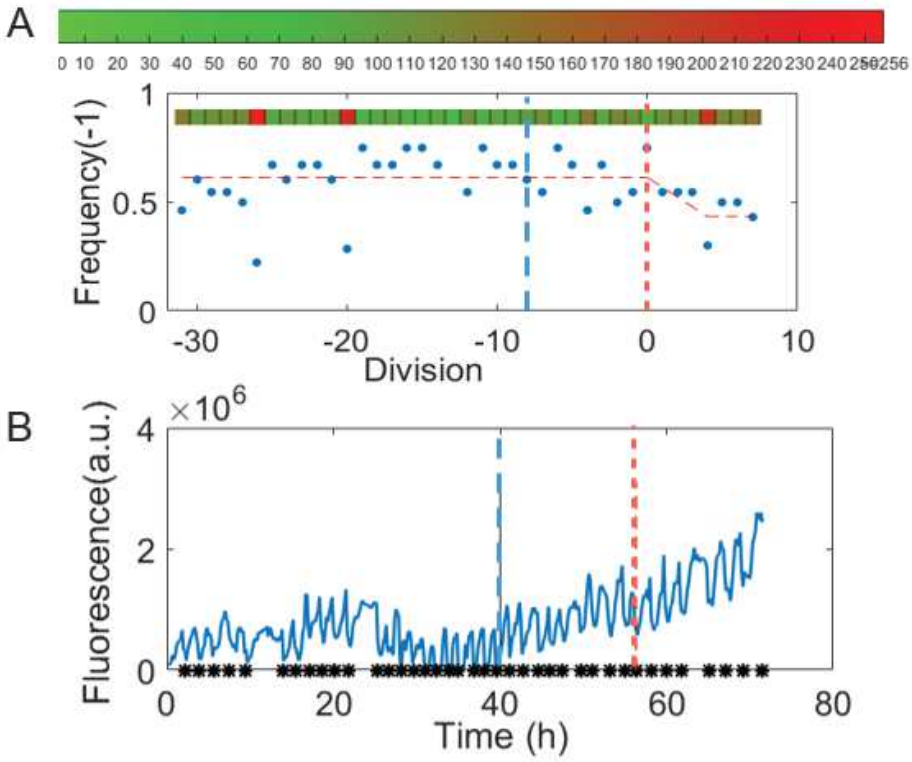

Figure 3.14 Determination of SEP in sgf73Δ mutant

A: Color-code cell cycle duration trajectory and corresponding cell dividing frequency are plotted on the figure. Erratic and extended long cell cycle duration perturb the SEP determination based on dividing frequency. The red dashed line indicates the linear regression using previously described 'findSEP' code. The SEP found at '0' is indicated by bold red dashed line.

B: HTB2-sfGFP fluorescence signal evolution during ageing of the same cell. Each asterisk indicates a cell division. The blue dashed line indicate the SEP determined by fluorescence increase breaking point, the red line indicate the SEP determined by cell cycle duration breaking point.

It also worth noting that both cell cycle duration and histone protein expression level increase upon SEP. When plotting the H2b histone protein fluorescence evolution of the same cell (Figure 3.14B), the cell shows fluorescence level increase as well. Therefore, based on the linear regression principle of SEP determination, I developed an alternative method of SEP determination based on fluorescence level increment. Since the basal fluorescence level increase at SEP, the fluorescence-based SEP is indicated by blue dashed line (Figure 3.14B). Based on the SEP determination, I pooled all the pre-SEP cells and found that sgf73Δ show much longer cell cycle duration in sgf73Δ mutant (105 ± 15 min) compare to WT (80 ± 10 min). The abnormally long cell cycle before SEP can also be a reason that blur the sudden cell cycle extension and influence the SEP determination by cell cycle duration.

The decoupling of H2b protein accumulation and cell cycle duration upon SEP may be due to loss of random ERC copies in sgf73Δ mutants. It seems that ERC accumulation is more tightly linking to the histone protein level rather than the cell cycle duration.

2.2.3 SAGA mutant extend RLS partly by promoting genome stability

I then focus on sgf73Δ to investigate the SEP dynamic in with-SEP subpopulation. Surprisingly, sgf73Δ mutants also show SEP probabilistic event like the fob1Δ strain. Both no-SEP and with-SEP subpopulations can be observed (Figure 3.15). There are about 59% cells showing SEP and 41% without SEP. The no-SEP subpopulation (36.7±1.3) shows similar lifespan longevity to the WT no-SEP subpopulation (37±1.7). And the withSEP sub-population again shows slightly increased lifespan than to the WT. I then asked how the SEP changed in sgf73Δ mutant, whether the pre-SEP period or the post-SEP period?

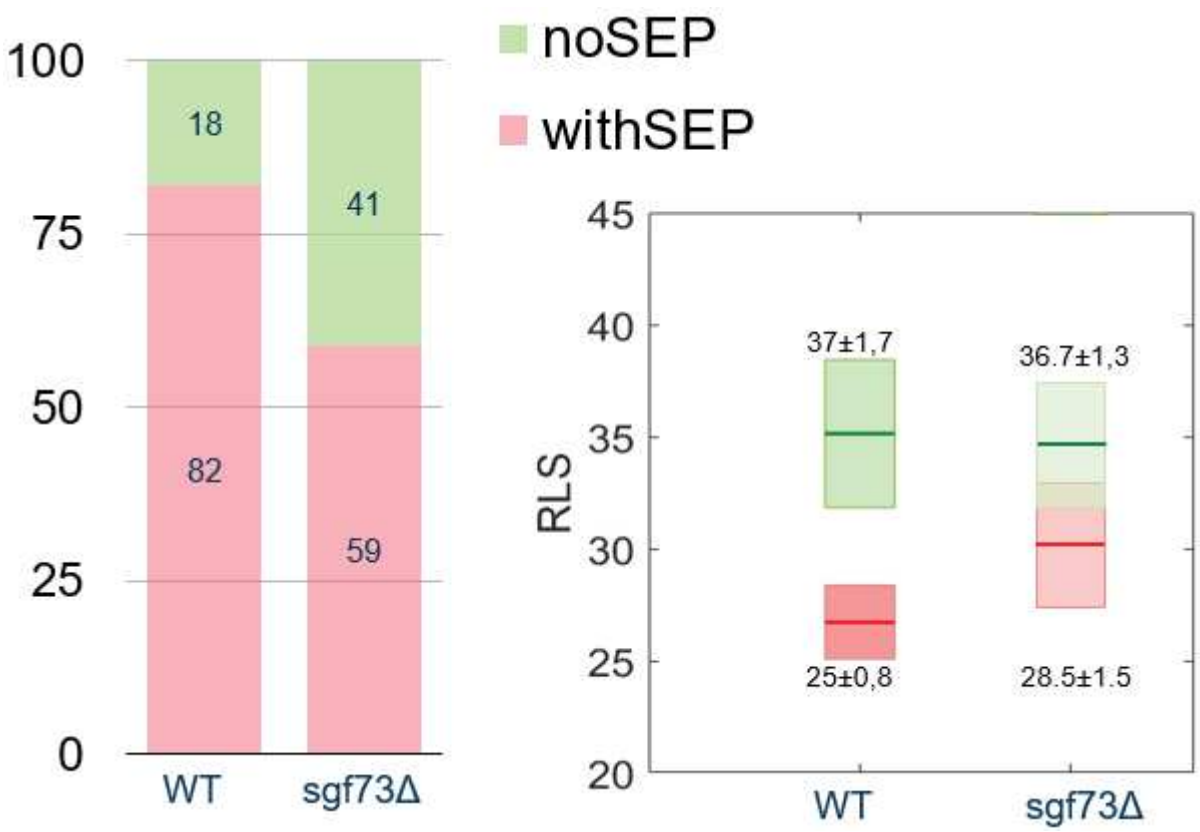

Figure 3.15 Distribution of with-SEP and no-SEP population

The histogram distribution of with-SEP and no-SEP population in both WT and sgf73Δ mutant. The legend indicates the percentage proportion of the two subpopulations. The boxplot figure indicates each subpopulation replicative lifespan. The color is set to be transparent for sgf73Δ for better visualization. The legend indicates the mean ±standard error on mean. (N>85)

From the boxplot, the replicative lifespan does not seem to be extended in a large scale. The extended with-SEP subpopulation lifespan contributes mostly to the lifespan extension, along with increased proportion of no-SEP population.

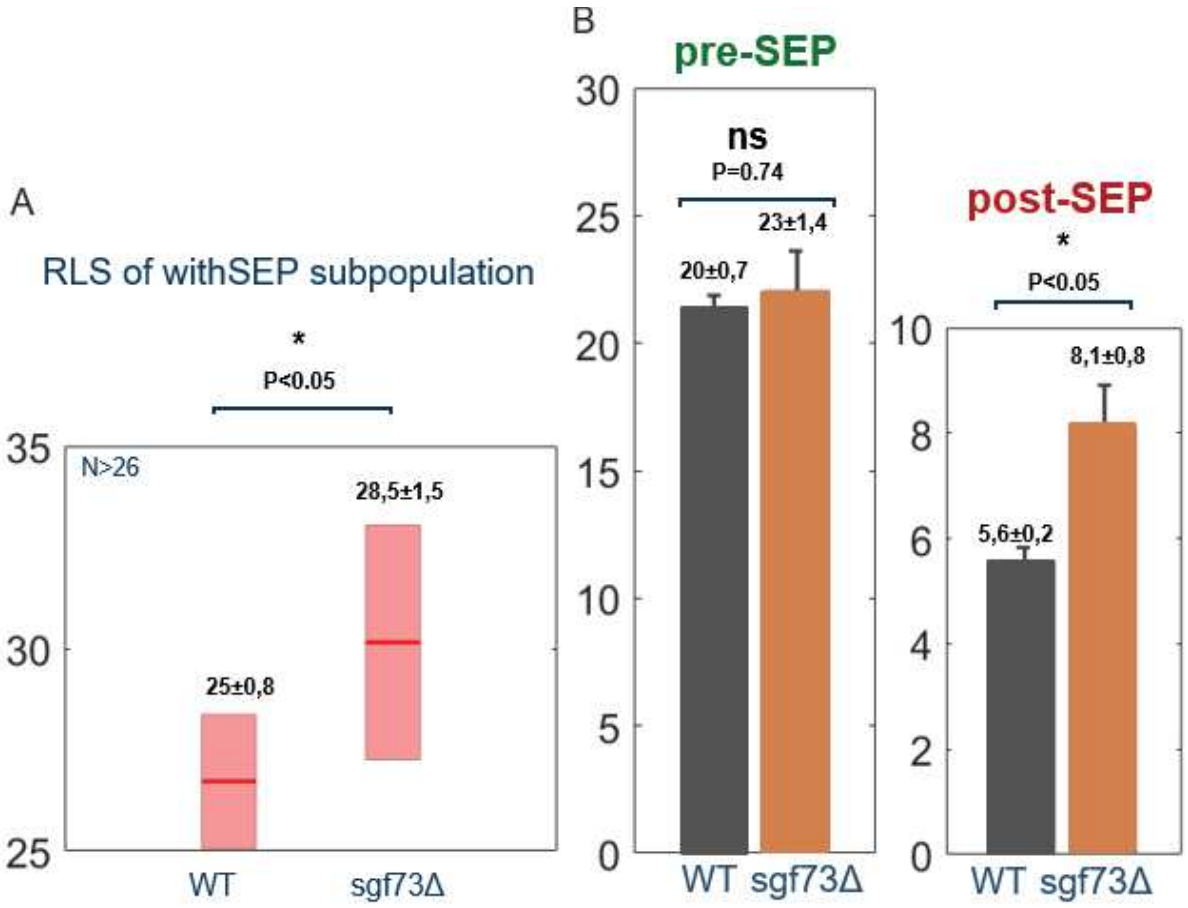

Figure 3.16 Comparison of SEP onset and RLS of subpopulation

A: The boxplot graph of with-SEP subpopulation in both WT and sgf73Δ. The with-SEP cells of sgf73Δ strain show slightly longevity extension. The legend indicates the mean ±standard error on mean. (N>26)
B; The histogram graph of SEP comparison in both sgf73Δ and WT. The SEP of sgf73Δ mutant (24) is prolonged compare to WT (21). The post-SEP lifespan is identical in both backgrounds. The legend indicates the mean ±standard error on mean.

When looking at the SEP onset, the SEP of sgf73Δ is like WT (Figure 3.16). From statistical test, the SEP is identical. A post-SEP extension can be observed in sgf73Δ mutant. Due to the pattern observed previously in fob1Δ, the mechanism involved in longevity extension for the two mutants seems different. Indeed, the Sgf73 protein is involved in ERC retention, it may be less involved in ERC formation and accumulation before it reaches the crucial threshold. According to the extended post-SEP lifespan, the loss of ERC maybe key for lifespan extension. It strongly suggests that ERC quantity is key for RLS and ERC retention is one of the mechanisms that regulate the ERC quantity.

2.2.4 SEP characterization in with-SEP subpopulation of sgf73Δ

Like the case of fob1Δ mutant, nuclear size, histone protein expression level and N/C ratio are compared in with-SEP population for sgf73Δ and WT. In sgf73Δ mutant, this nuclear size increase and fluorescence increase seems to be less pronounced compare to WT. After looking into the fluorescence increasing dynamic no significant difference can be observed. To better investigate the dynamic transition upon SEP, it would be preferable to use shorter time for time-lapse experiments.

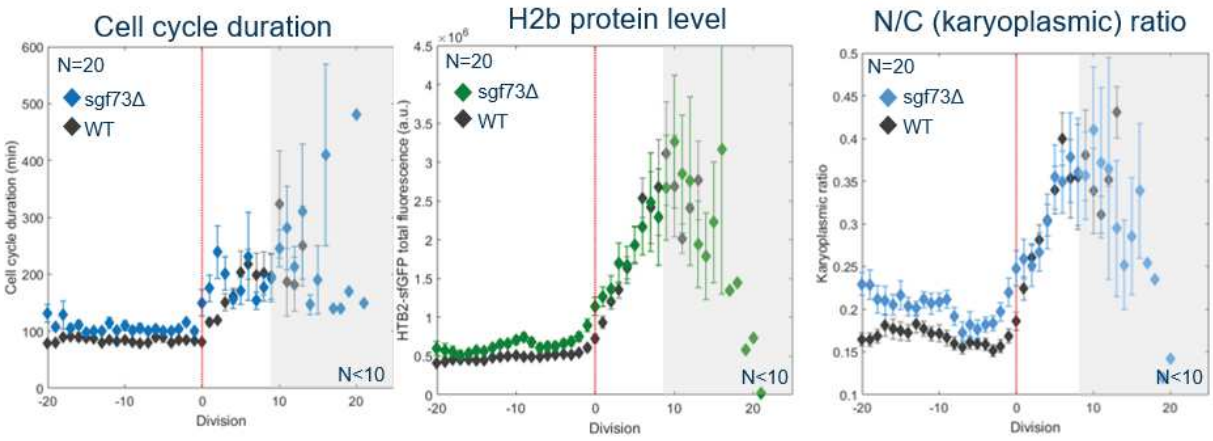

Figure 3.17 Comparison of SEP characteristics in sgf73Δ and WT

The evolution of cell cycle duration, HTB2-sfGFP and N/C ratio in sgf73Δ and WT (aligned by SEP). The error bar indicates ±standard error on mean. (N=20 for both strains) The SEP is indicated by a dashed red line and located to the zero of x-axe. The grey area indicates less effective at late life due to mother cell death.

Based on the fluorescence-determined SEP, we can observe that both sgf73Δ and WT how similar increase of all the parameters, including cell cycle duration, H2b protein expression level and N/C ratio (Figure 3.17). Using the nuclear marker, it is difficult to understand how the ERC copy number evolves during the ageing process.

From previously study that sgf73Δ extend RLS via Sir2 function by reducing rDNA recombination (McCormik et al., 2015), I speculate that sgf73Δ mutant show two major functions: less ERC formation and weaker ERC retention capacity. Taking these functions together, the increasing number of no-SEP subpopulation in sgf73Δ may be due to rDNA increasing silencing status which reduce the ERC formation rate. This speculation is based on the fob1Δ mutant with very low ERC formation rate exhibiting much higher proportion of no-SEP subpopulation compare to WT. The weakening of ERC retention in sgf73Δ could be

the reason for post-SEP extension due to loss of excessive ERC and propagate to daughter cells. The fact that I can observe a SEP by H2b protein fluorescence increase suggesting that the ERC retention capacity of the mother cell is not totally abolished, for instance the nuclear barrier may still function between mother and daughter for preventing the equal ERC distribution. To confirm the speculation above, directly using the rDNA/ERC reporter can provide more and direct evidence to understand SEP dynamic when ERC copy numbers show more variety in SAGA mutants.

As a conclusion, the long-lived mutants show a different SEP probability and dynamic by regulating potentially the ERC quantity leads to a direct causal relationship between ERC and SEP.

3 Asymmetric nuclear segregation between old age mother and daughter

3.1 Background

3.1.1 SEP phenotype inheritance from post-SEP mother

Based on the characterization of SEP in previous investigation, I observe the H2b histone protein overexpression along with nuclear size enlargement and cell cycle prolongation. It can be asked whether such phenotype can be inherited to the daughter cell?

3.2 Result

3.2.1 Rejuvenation analysis in daughters issued from post-SEP mothers

Mother yeast starts to show nuclear enlargement by the onset of SEP. This nuclear enlargement is not only characterized by the increment of nuclear size but also the nuclear content. For instance, the histone density is also increased. In addition, not only the H2b protein become abundant after SEP, the other histone protein H4 encoded by HHF2 also show increase upon SEP (Figure 3.18). Though the cell is very sick and sensitive to stress, the histone protein level has been seen increased upon SEP before cell death. Such observation leads to speculation that general nucleosome expression may be increased after SEP.

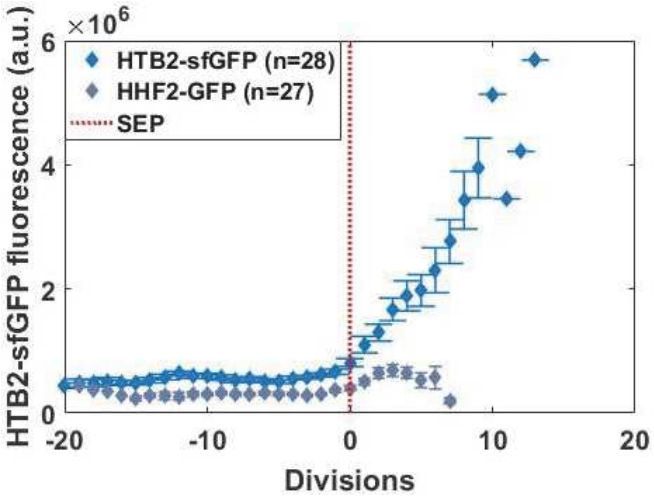

Figure 3.18 Histone proteins H2b and H4 accumulate upon SEP

The fluorescence signal evolution of H2b and H4 histone proteins are aligned by SEP during ageing. Both HTB2 encoded H2b protein and HHF2 encoded H4 protein show an increase of total fluorescence level after SEP can be observed. Due to the sick cell phenotype of HHF2-GFP reporter strain, the cell shows abnormal cell cycle and is very short-lived, the post-SEP period is only about 3 generations on average. The error bar indicates ±standard error on mean.

Whether post-SEP mother showing enlarged nuclear size and increased ERC copy number (Morlot, Song et al. 2019) would inherit the ageing phenotype to daughter cell or not. To answer the question above, I take advantage of the microfluidic device which allows the observation of the daughter cells for some time before they were removed by medium flood. The cell cycle duration, nuclear size and histone protein expression level of daughters are measured (Figure 3.19).

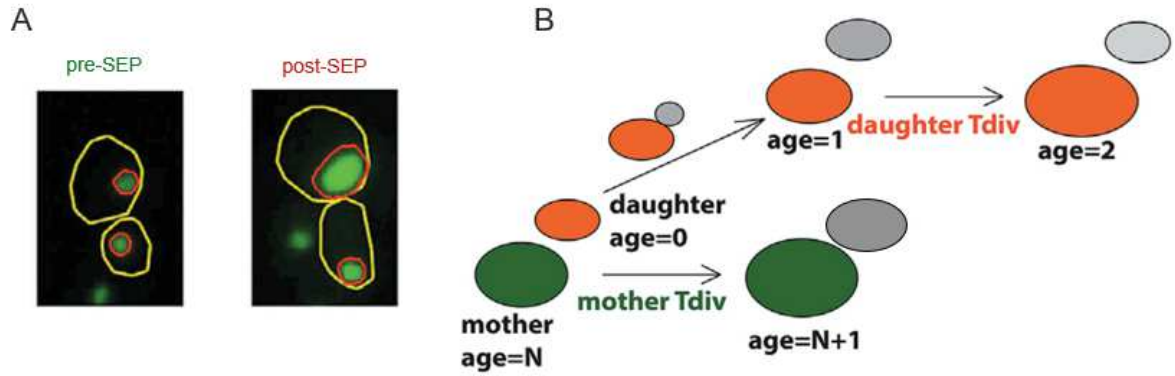

Figure 3.19 Rejuvenation analysis measurement (adapted from (Morlot, Song et al. 2019)
A: Representative images of pre-SEP and post-SEP mother and daughter cells. Using the HTB2-sfGFP reporter strain, the nuclear size, histone protein expression level can be monitored.
B: Schematic description for the quantification method. Daughters generated by corresponding aged mothers are monitored. To avoid cell-size-variation induced cell cycle difference, only the daughter cells' second cell cycle is counted for rejuvenation analysis.

The cell cycle duration of daughter cells originated from mother at different ages is the first time that has been investigated. The daughter generation issued from post-SEP mothers show similar short and regular cell cycle duration identical to the pre-SEP mother cells (Figure 3.20).

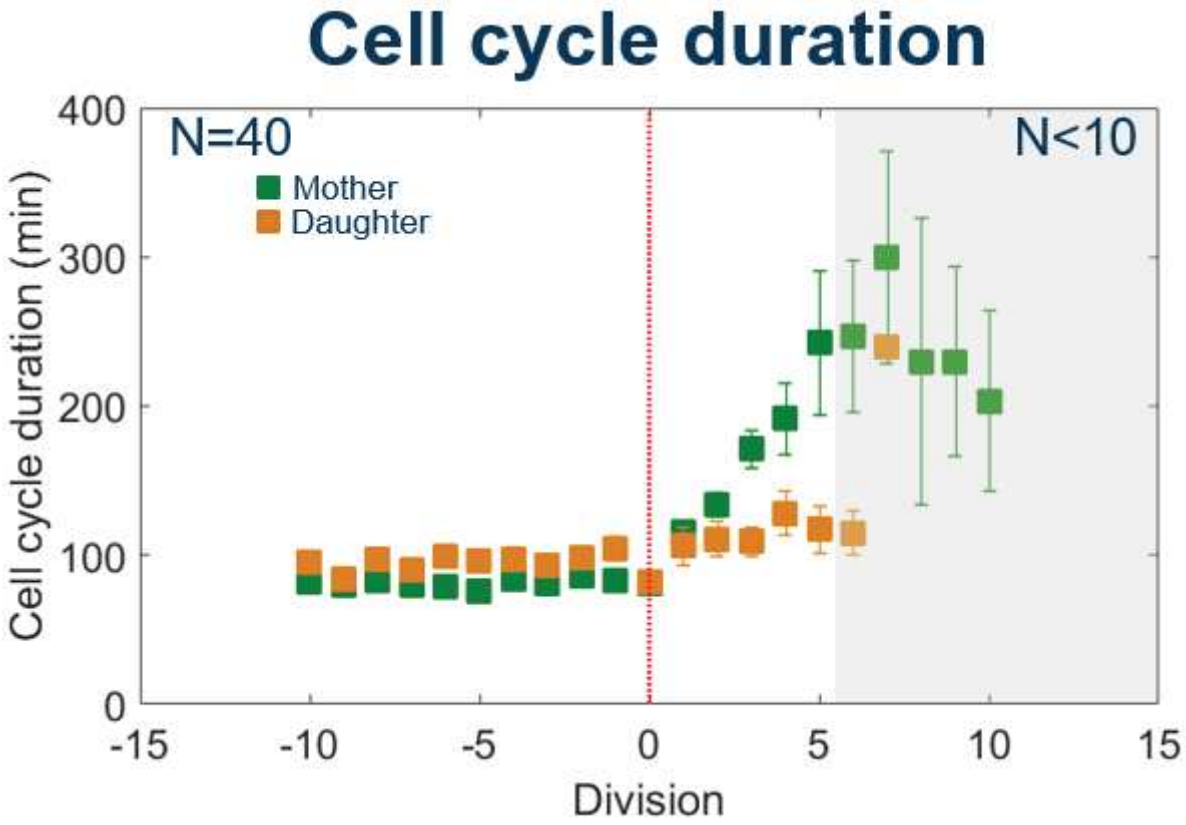

Figure 3.20 Rejuvenation analysis of cell cycle duration

The cell cycle duration measured in mothers at different age (aligned by SEP) and compare to the cell cycle duration measured in daughters issued from these mother cells. The SEP is indicated by red dashed line. The error bar indicates ±standard error on mean. (N=40 for mother cells)

This result shows that corresponding daughters generated at different ages show relatively constant cell cycle duration, it indicates the rejuvenation phenotype of daughter cells.

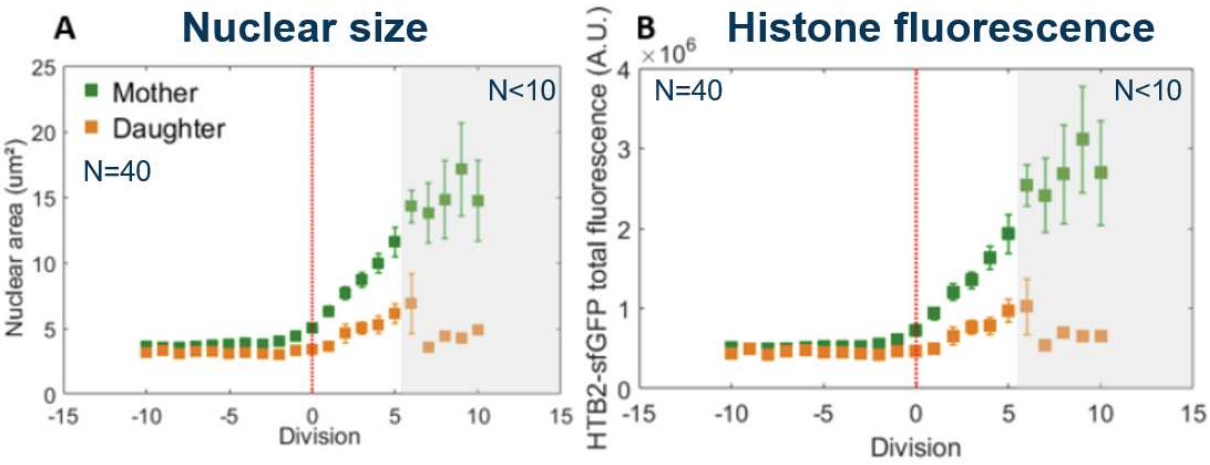

Figure 3.21 Rejuvenation analysis on mother bearing SEP transition

A: Nuclear size evolution of mothers and corresponding daughter (Mother in green, daughter in orange, SEP in red). The error bar indicates ±standard error on mean. (N=40 for mother cells)
B: Histone total fluorescence level of mothers enduring SEP of mothers and corresponding daughters (Mother in green, daughter in orange, SEP in red). The error bar indicates ±standard error on mean. (N=40 for mother cells)

Mother nuclear size and H2b histone protein level both increase abruptly from SEP. The daughters nuclear size increase slightly simultaneously (Figure 3.21). Not only the nuclear size, the histone protein total expression level also increases. However, the daughter seems to inherit less histone compare to mother cell. To better compare the rejuvenation between mother and daughter, the increased cell-size must consider avoiding the size-induced variation. Therefore, N/C ratio (karyoplasmic ratio) a key nuclear homeostasis index is measured.

As an important index for nuclear homeostasis is the karyoplasmic ratio. This ratio is defined by the nuclear volume/cellular volume. Due to the 2D constraint of images, we quantify the karyoplasmic ratio by nuclear/cellular area (Figure 3.22). It has been demonstrated in other study that nuclear size is highly consistent to the DNA copy and cytoplasmic factors (cell size).This karyoplasmic ratio measured shows constant N/C ratio in daughters, which strongly suggests that SEP ageing phenotype is not inherited to the daughters.

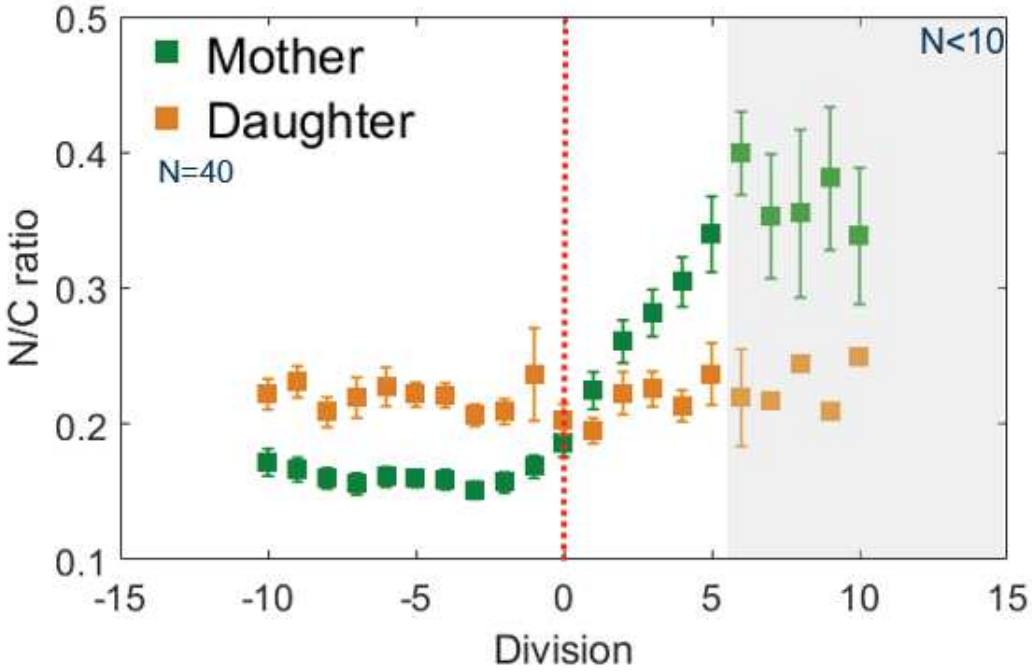

Figure 3.22 Rejuvenation analysis of N/C ratio

The N/C ratio measured in mothers and corresponding daughters, the result is aligned by SEP (Mother in green, Daughter in orange, SEP in red dashed line). The error bar indicates ±standard error on mean. (N=40 for mother cells)

3.2.2 Loss of rejuvenation in extremely old mother showing multi-nucleate inheritance

When mother ages to extremely old age, multi-nuclei phenotype is a typical ageing phenotype indicating a loss of nuclear homeostasis (Neurohr, Terry et al. 2018). We noticed that this phenotype is observed in old mothers especially before death (Figure 3.23). As the mother age pass SEP, linearly increased frequency of multi-nucleated mother phenotype can be observed.

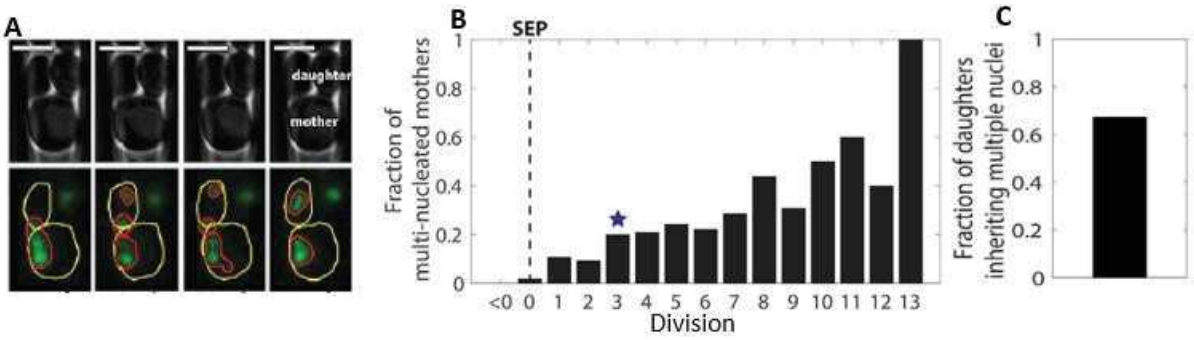

Figure 3.23 Inheritance of multi-nucleated ageing phenotype in daughter issued from post-SEP mother

A: Phase-contrast and fluorescence micrographs of a representative multi-nucleated mother cell transmitting two nuclei to its daughter.
B: Fraction of multi-nucleated mother as a function of age. The 0 of x-axe indicate the SEP moment. The cell from image A is marked by the blue star.
C: Inheritance rate of multi-nucleated phenotype to the daughter (31 of 46 cells).

Very old mothers may inherit multi-nucleated phenotype to daughters. This observation suggests that at late life, the asymmetric retention of ageing factors in mother yeast may be disrupted and result in forming daughters containing multi-nucleated phenotype.

Due to technical limitation, full RLS of old daughters generated from post-SEP mother cannot be followed. However, in a previous study, daughters generated from extremely old mother yeast show very short RLS (Kennedy, Austriaco et al. 1994). This group of multi-nucleated daughters inheriting ageing phenotype from old mothers could be the candidates contributing to the shortened RLS.

4 Characterization of SEP in long-lived intervention condition by H2O2 hormetic treatment

4.1 Specific background

4.1.1 Hormetic H2O2 concentration induce RLS extension

One of the long-lived interventions for budding yeast has been previously investigated in the host laboratory using H2O2 treatment (Goulev, Morlot et al. 2017). By growing cells under a

series of stable H2O2 concentrations throughout full RLS, we confirmed the hormetic effect of H2O2. The hormetic effect describes that toxic substance H2O2 can shorten RLS at a certain concentration (>50μM), whereas under mild concentration (<50μM), the same substance H2O2, can induce opposite effect to prolong the lifespan.

This is the first time that experiment on full RLS under oxidative stress has been performed. This is mainly due to the obstacle of maintaining H2O2 concentration at a stable and very low concentration. This molecule is chemically unstable and can be easily reduce to H2O and O2. Yet, using microfluidic system and peristaltic pumping system, fresh stable H2O2 medium can be provided and allowing the performance of full RLS ageing process.

4.2 Result

4.2.1 SEP is significantly delayed under long-lived H2O2 hormetic condition

By comparing the occurrence of SEP, we can understand potential mechanisms for promoting the longevity under H2O2 oxidative stress condition. For instance, if pre-SEP period is prolonged, mother yeast may be able to better maintain stable rDNA repetitive loci and prevent the ERC formation. If post-SEP period is prolonged, the mother yeast may be involved in less ERC duplication mechanism for instance. I firstly perform the RLS to repeat the experiment that has been published previously and I obtained similar hormetic effect (Figure 3.24)

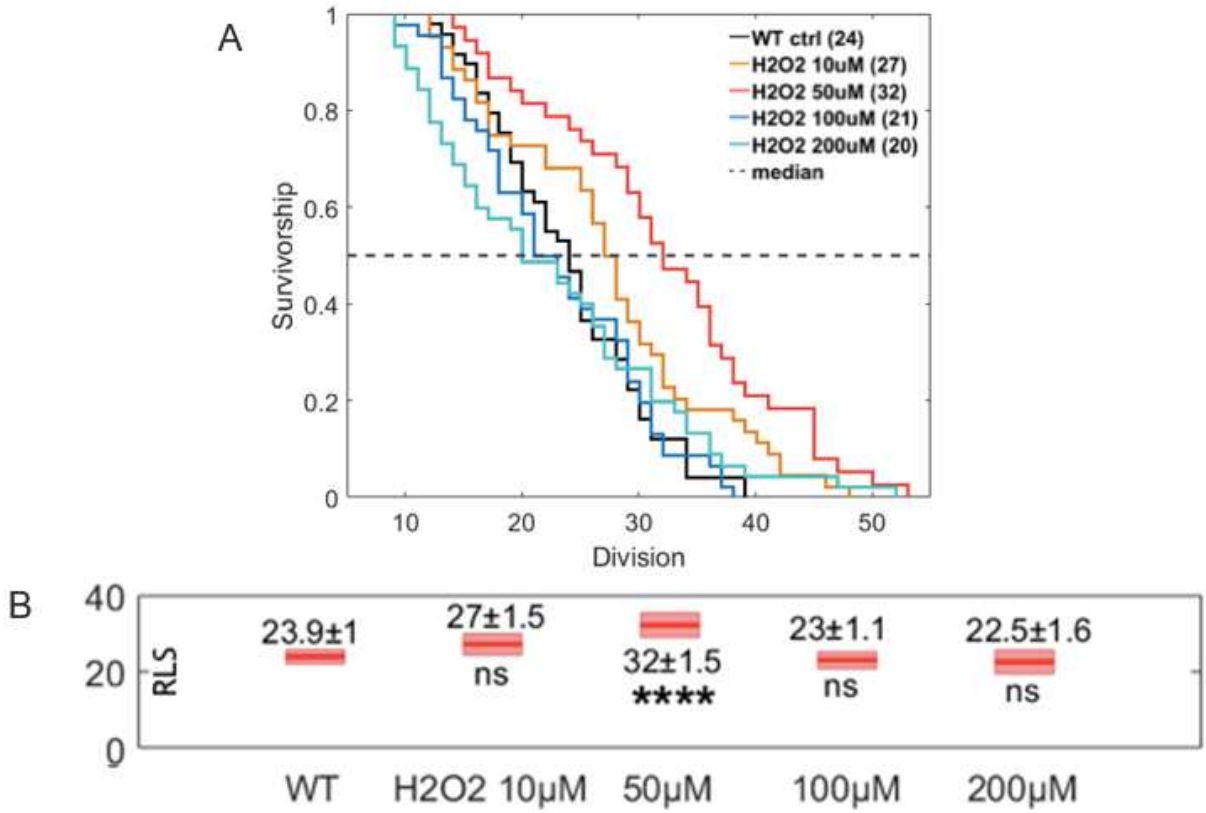

Figure 3.24 RLS analysis shown in survival curve and boxplot for hormesis ageing

A: The RLS result shown by survival curve, the median RLS is indicated on the legend.
B: The RLS result shown by boxplot, the error bar indicates ±standard error on mean. The statistical test shows most significant beneficial condition for RLS extension is under H2O2 50μM (N>40).

The RLS of various H2O2 concentration and corresponding pre-SEP and post-SEP division numbers are compared (Figure 3.25). Based on statistical test, the most significant increase of RLS can be observed at 50μM of H2O2 treatment, which is like the result of Dr. Goulev (Goulev, Morlot et al. 2017).

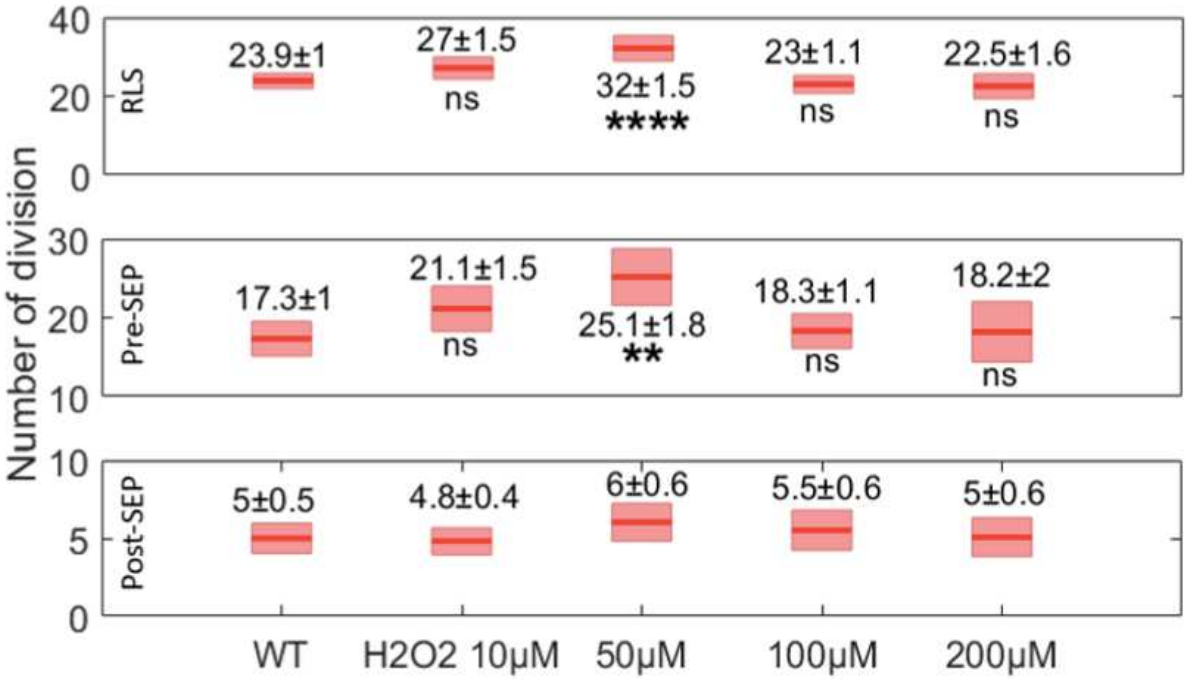

Figure 3.25 The lifespan compared before and after SEP under hormetic ageing condition

The boxplot graphic of hormetic ageing cells showing pre-SEP and post-SEP lifespan. The first panel is the full RLS box plot comparison; the second panel is the pre-SEP cell divisions under hormetic condition; the third panel is the post-SEP cell divisions under each hormetic condition. The error bar indicates ±standard error on mean. (N>40)

The lifespan before SEP seems contribute mostly to the longevity extension (Figure 3.25). The post-SEP lifespan remains relatively stable a show no statistical difference among these conditions.

The result indicates that hormetic stress promote longevity through better genome stability maintenance. Which further suggests a relationship between H2O2 and genome stability, especially the rDNA region. It requires more detail to illustrate the underlying mechanism.

5 Characterization of SEP in long-lived mutant by overexpressing antioxidant enzyme

5.1 Specific background

5.1.1 One of the most abundant antioxidant enzymes – Tsa1

To better understand the response of budding yeast against ROS accumulation, the oxidative stress defense mechanism has been extensively studied in budding yeast (Fridovich 1989, Wemmie, Szczypka et al. 1994, Kuge, Arita et al. 2001, Delaunay, Pflieger et al. 2002, Outten, Falk et al. 2005, Gross, Sevier et al. 2006). The cell respond to H2O2 is majorly based on the Yap1 regulon (Kuge and Jones 1994, Lee, Godon et al. 1999). Yap1 is a transcription factor that shuttles between cytoplasm and nucleus and predominantly in cytoplasm under normal condition. When encountering the oxidative stress such as H2O2, the Yap1 is oxidized and its exportation is blocked (Kuge, Toda et al. 1998). The nuclear accumulation of Yap1 leads to the expression of subset of genes that controlled by Yap1 (Lee, Godon et al. 1999). Among these genes, most of them are involved in antioxidant defense, some also involved in metabolism and heat shock response (Gasch, Spellman et al. 2000, Vandenbroucke, Robbens et al. 2008). In 2017, the host laboratory has studied comprehensively the core adaptive mechanism of budding yeast under H2O2 oxidative stress (Goulev, Morlot et al. 2017). By gradually increasing the external H2O2 concentration without activation transient defense mechanism (the ramp experiments). A key point that needs to be stressed out for this special framework is that it provides a unique insight for what may happen during ageing. Ageing is described as a gradual and accumulative decline of physiological functions. Therefore, the accumulation of oxidative stress is more likely to be a gradual pattern but not in a robust or sharp manner. Hence, the classical way that have been implicated for studying the stress response may not be suitable for mimicking the ageing context. However, using the small dose of increasing H2O2 concentration gradually, we observed the growth rate of various mutants downstream to Yap1 regulon under this condition. Eventually, we identified that the group of peroxiredoxin (Prx) antioxidant enzymes are very sensitive to the redox homeostasis imbalance and playing core roles for the H2O2 mild stress adaptability. Among the Prxs tested, one of the most abundant antioxidants scavenging protein Tsa1 is especially important (Goulev, Morlot et al. 2017). Upon oxidative stress, Tsa1 protein expression show dose-dependent increment.

5.1.2 Dual functions of Tsa1

Tsa1 is one of the most abundant antioxidants scavenging Prx enzyme in budding yeast (Gygi, Rochon et al. 1999). It has the thiol-bearing cysteine residues that are sensitive to oxidative stress. Tsa1 has 2-functional cysteine thiols (C48 and C171) that can be oxidized (Figure 3.26). When under small dose of H2O2 stress, Tsa1 C48 the peroxidatic cysteine can form a sulfenic acid –SOH. The oxidized form of Tsa1 can further form a disulfide bond with another Tsa1 at its C171 resolving cysteine residue. The dimer can then be reduced by a thioredoxin (Trx). There are Trx1 and Trx2 in the budding yeast that can reduce the Tsa1 oxidation. And the reductive energy source is root from NADPH (Ross, Findlay et al. 2000). This peroxidatic cycle can scavenge the oxidant rapidly. When the cells are stressed by a more pronounced H2O2 concentration, the Tsa1 may be hyper-oxidized and form a sulfonic acid (-SO_2H) at C48 residue. When under hyper-oxidative state, the tsa1 protein tends to form higher molecular weight oligomers (HMW) (Jang, Lee et al. 2004). This form of Tsa1 oligomers alter its peroxidase activity to protein chaperone holdase function which bind to the misfolded protein aggregates and correct protein folding under the assist of Hsp70 chaperone. This hyper-oxidized form of TSA1 is reversible by Sulfiredoxin (Srx) (Biteau, Labarre et al. 2003) by using ATP as the root of energy source (Figure 3.26).

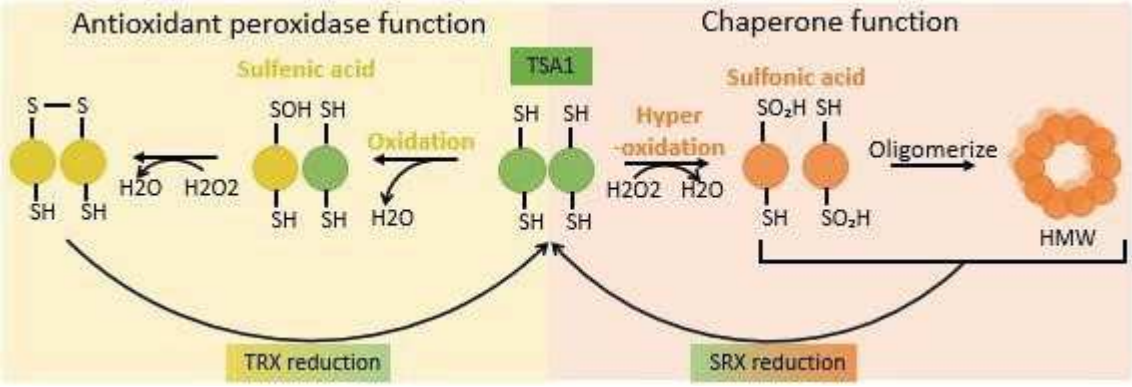

Figure 3.26 Tsa1 moonlighting functions: peroxidase and protein chaperone

Tsa1 can detoxify H2O2 by the redox cycle involving Trx reduction. When Tsa1 is oxidized to sulfenic acid form (C48 -SOH), it can then form a disulfide bond with another Tsa1 (C171). Thiol redoxin can then be recruited to complete the reductive cycle. When under massive H2O2 stress, the tsa1 can be hyper-oxidized to form sulfinic acid (C48 –SO2H) and assemble as high molecular weight oligomers and switch to a protein chaperone function.

As a conclusion, Tsa1 as a 2-Cys Prx is a moonlighting enzyme that can alter between two functions: H2O2 scavengers or protein chaperone holdase, according to its oxidation status (Figure 3.27).

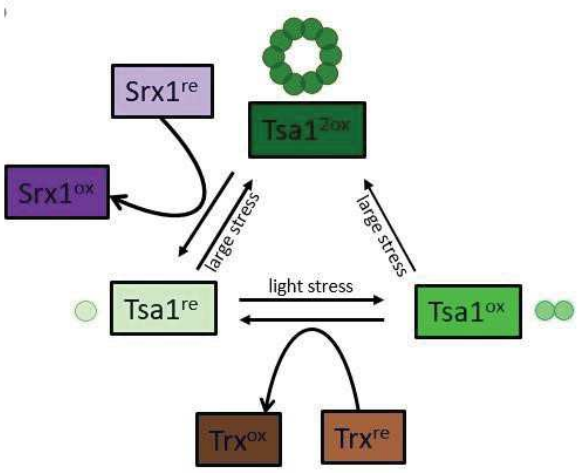

Figure 3.27 Schematic presentation for Tsa1 redox function cycle

5.2 Result

5.2.1 RLS analysis for determination of long-lived mutant TSA1OE

According to H2O2 hormetic ageing experiment, we speculate that Tsa1 protein may play a key role to promote longevity by its dual protective functions. It has been previously shown in other study that overexpression Tsa1 protein can prolong longevity (Hanzén, Vielfort et al. 2016). We then tested the TSA1OE mutant's longevity in the microfluidic system.

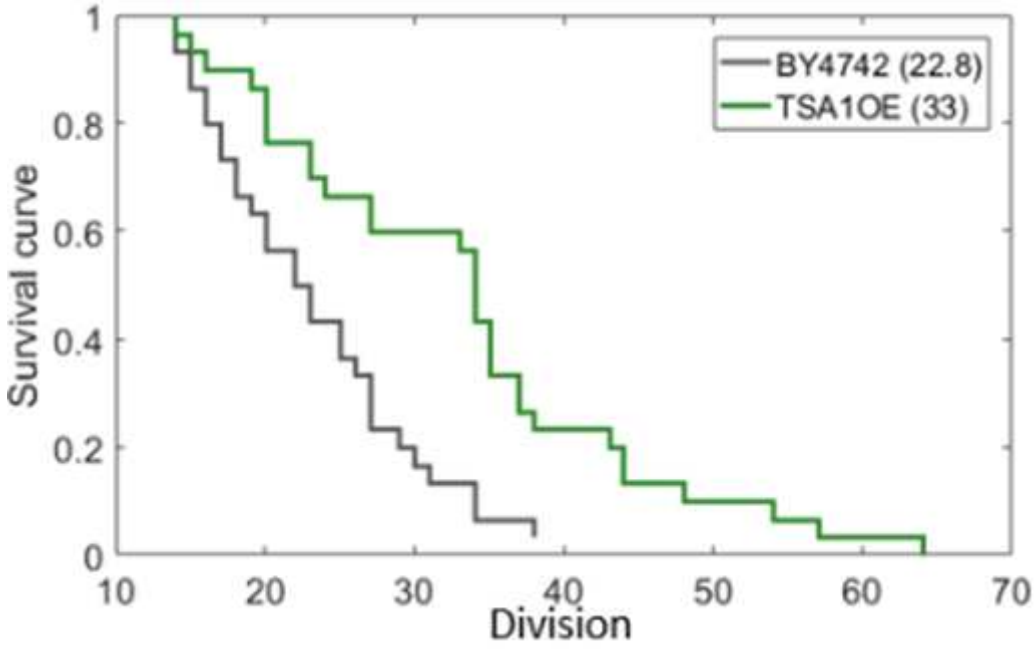

Figure 3.28 RLS analysis of TSA1OE

The survival curve of TSA1OE and WT, the median RLS is indicated on the legend. (N>35)

The increased RLS has been observed in microfluidic system (Figure 3.28). It is worth noting that in this mutant and H2O2 hormetic condition, most cells show with-SEP phenotype before death which is like WT (Figure 3.29). The probabilistic SEP event is not significantly different from control condition. This observation suggests that beneficial hormetic effect and TSA1OE mutant has different mechanism compare to the probabilistic SEP observed in fob1Δ and SAGA mutants. Based on previous speculation that ERC excision rate is crucial for inducing probabilistic SEP, the ERC excision rate might not be influenced under hormetic effect or in TSA1OE mutant. Yet, this hypothesis requires further experimental proof.

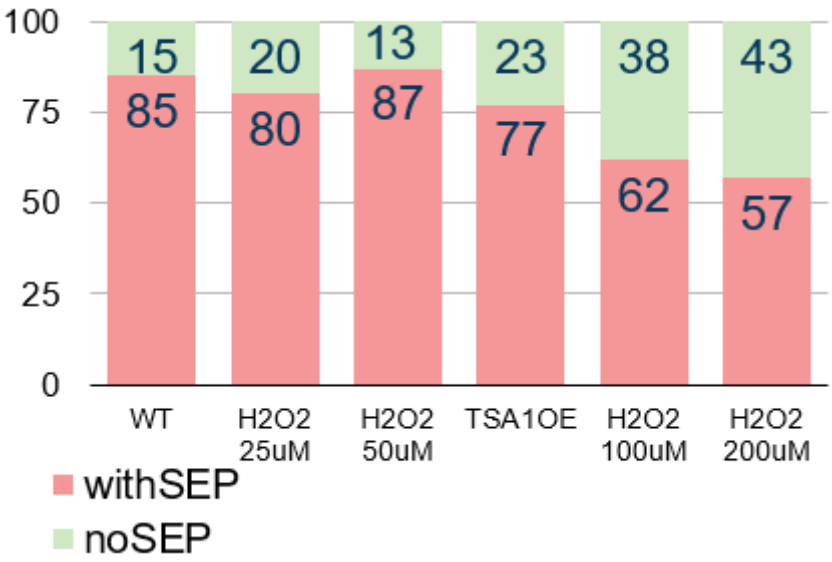

Figure 3.29 Distribution of with-SEP and no-SEP hormetic and TSA1OE condition

The histogram showing with-SEP and no-SEP subpopulation proportion in different ageing condition. the fraction is indicated on the histogram. (N>44)

5.2.2 SEP transition is delayed in TSA1OE mutant

I then compare the pre-SEP and post-SEP distribution for TSA1OE and H2O2 50µM condition, since these two conditions show the most significantly extended RLS. After comparing the pre-SEP and post-SEP distribution (Figure 3.30), I found that like the H2O2 hormetic effect, the TSA1OE also significantly increase for pre-SEP. Indicating that under these longevity extension mechanisms, similarly SEP is delayed. In addition, the post-SEP of TSA1OE mutant is also increased compare to WT and hormetic effect. This further suggests that TSA1OE promote the longevity also during the post-SEP period.

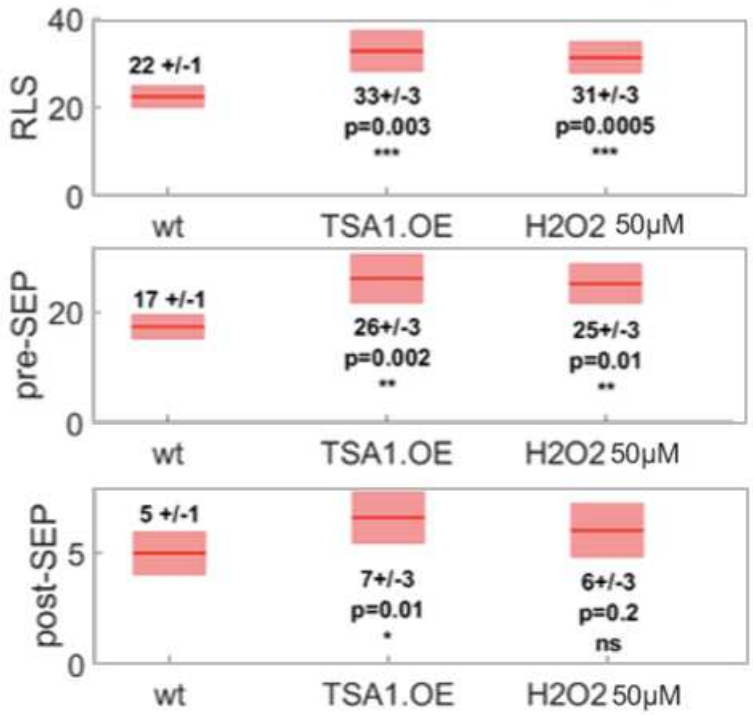

Figure 3.30 Distribution of pre-SEP and post-SEP divisions in TSA1OE mutant and H2O2 hormetic condition

The box plot comparison of RLS, pre-SEP and post-SEP lifespan in TSA1OE mutant and H2O2 50µM hormetic condition. The error bar indicates ±standard error on mean. (N>44)

As a conclusion, the hormetic beneficial effect on longevity extension under H2O2 50µM treatment might be mimic by TSA1OE mutant. Both show similar longevity extension and SEP delay. In addition, overexpression Tsa1 protein can also post-SEP before death. It then worth investigating how oxidative stress and antioxidant enzyme promote ageing? Is genome stability a downstream effect of antioxidant protective response?

Chapter IV

Result part 3

Preliminary study of redox homeostasis during replicative ageing

1 Specific background:

1.1 Evolution of redox state during replicative ageing process

Increasing oxidative stress and oxidative damages have been observed during ageing process, yet the dynamic of internal [ROS] evolution has been rarely studied. Most of the study is performed in a population level to provide stronger signal. Using the microfluidic device, I investigated the redox state during the ageing process and whether redox state can be related to SEP transition?

1.2 Potential redox state reporter strains for RLS monitoring

To monitor the redox state in live cell, fluorescence reporters are needed for following the dynamic of redox homeostasis throughout the full RLS.

Based on previously described oxidative stress defense mechanisms of Yap1 regulon. Proteins involved in the antioxidant defense mechanism are tested. These reporter strains are YAP1-GFP, TSA1-GFP and SRX1-GFP. (Figure 4.1).

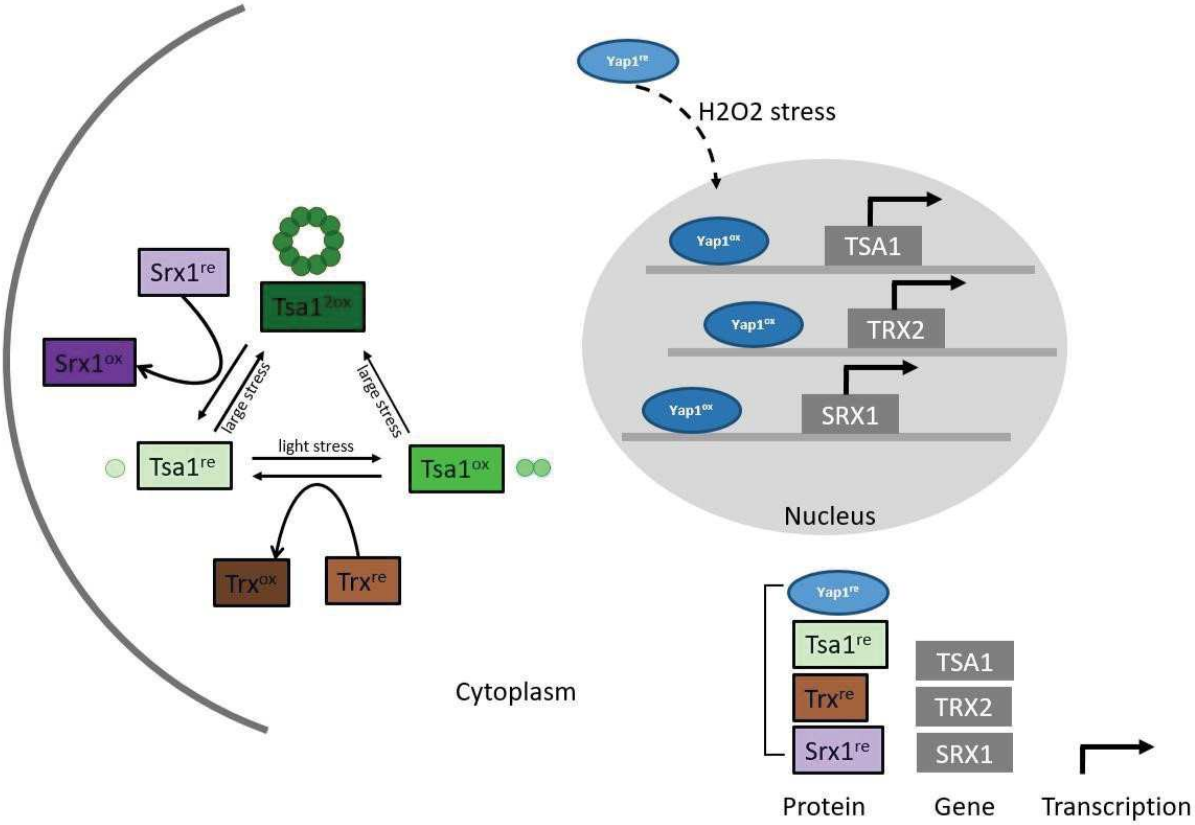

Figure 4.1 Potential redox state reporter strains involved in redox homeostasis

Schematic interactions between antioxidant proteins are drawn in the graphic. The Yap1 protein oxidized form can activate downstream gene expression. The genes are translated to protein and they are involved in redox homeostasis maintenance.

2 Result:

2.1 Selection of redox state reporter marker for monitoring ageing in microfluidic system

Above mentioned reporter strains are tested in microfluidic system to monitor its expression level upon an external oxidative stress. The minimum concentration for the yeast cell reaching the maximum defense activation magnitude is 0.2µM H2O2 (Goulev, Morlot et al. 2017). This concentration is thus used to test the reporter strain in ageing microfluidic system as the positive control. Since these reporters will be used for ageing experiment, the positive control is monitored under ageing experimental set-up.

The fluorescence signal of these markers indicates that all of them are overexpressed when encountering oxidative stress. YAP1-GFP reporter, as the most sensitive reporter that may be involved in the oxidative stress signaling pathway, it shows very weak fluorescence signal upon oxidative stress. Therefore, this strain is not used for ageing experiment. As for the other reporters, they all show significant increase of magnitude upon oxidative stress (Figure 4.2). Thus, the reporter strains selected for ageing experiment are: SRX1-GFP and TSA1-GFP.

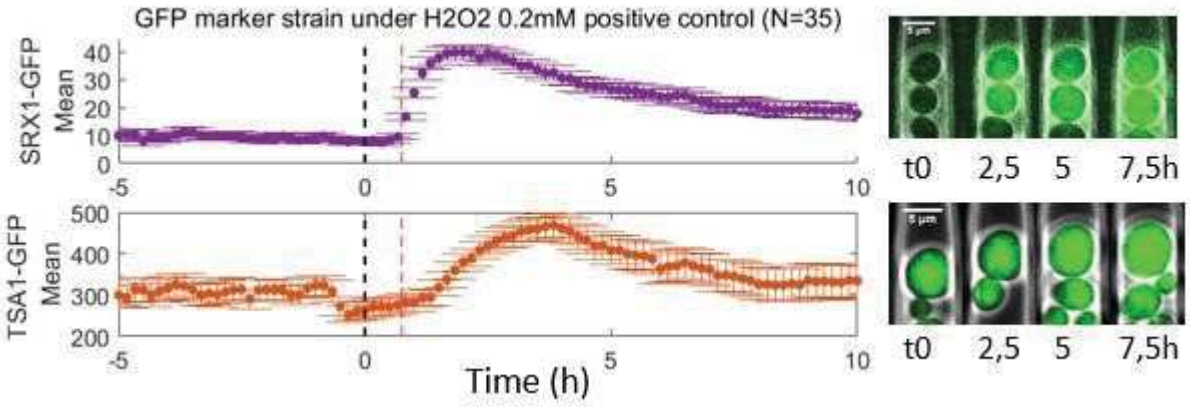

Figure 4.2 Oxidative stress positive control for testing potential redox marker

The fluorescence evolution upon oxidative stress in oxidative stress reporter strain. The black bold dashed line indicates the medium change of H2O2 0.2mM, the purple dashed line indicates the onset of oxidative stress response. The sequential images of reporters at different time point are shown to the right. (N=35)

These two markers are then monitored for ageing experiment to study the redox state evolution.

2.2 Redox imbalance can be observed at the beginning of RLS

After the ageing experiment, the mother yeast full RLS fluorescence trajectories are collected (Figure 4.3).

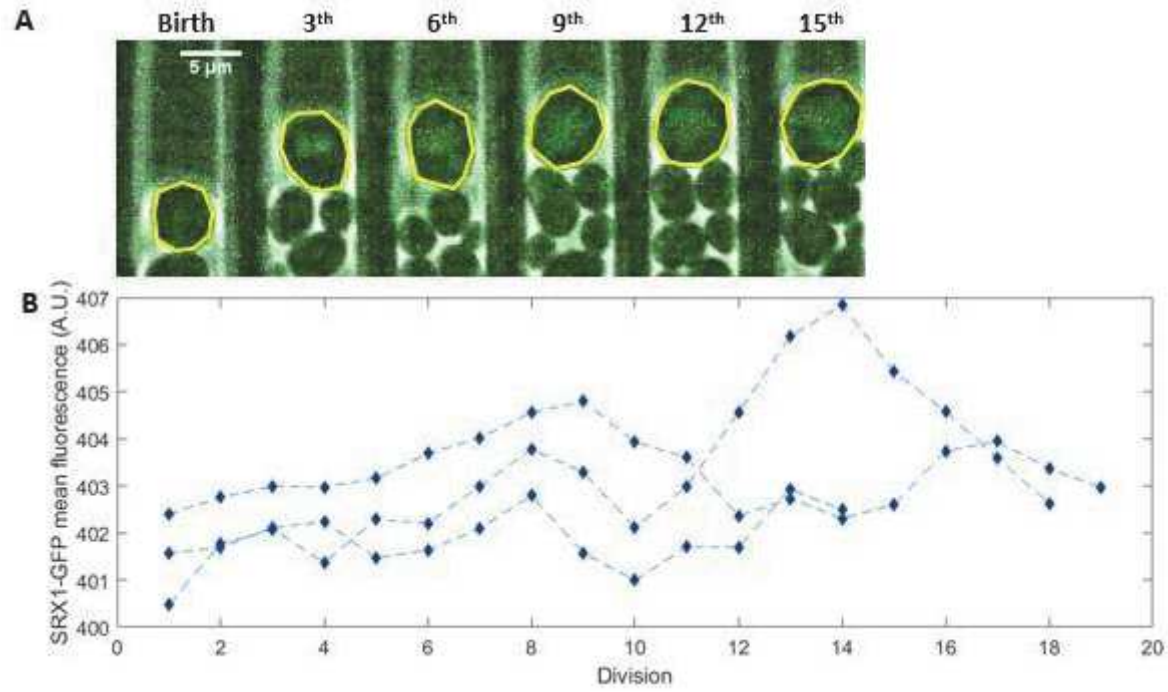

Figure 4.3 Trajectories of mother yeast RLS for SRX1-GFP reporter strain

A: Sequential images of reporter strain SRX1-GFP ageing process. The yellow indicates the cell contour.
B: Three trajectories of fluorescence signal evolution started from birth. The fluorescence is very weak, which is almost comparable to background noise.

After collecting data from SRX-GFP cells, due to lack of continuous experimental data, the SEP for this reporter strain cannot be determined. Therefore, only the data of early age can be used for further analysis. From this ageing experiment, we can see that Srx1 show relatively weak expression level which is comparable to the background noise. Therefore, to better compare the fluorescence evolution and avoid the cell to cell variety, mother yeasts are aligned by birth (Figure 4.4). The background noise is removed.

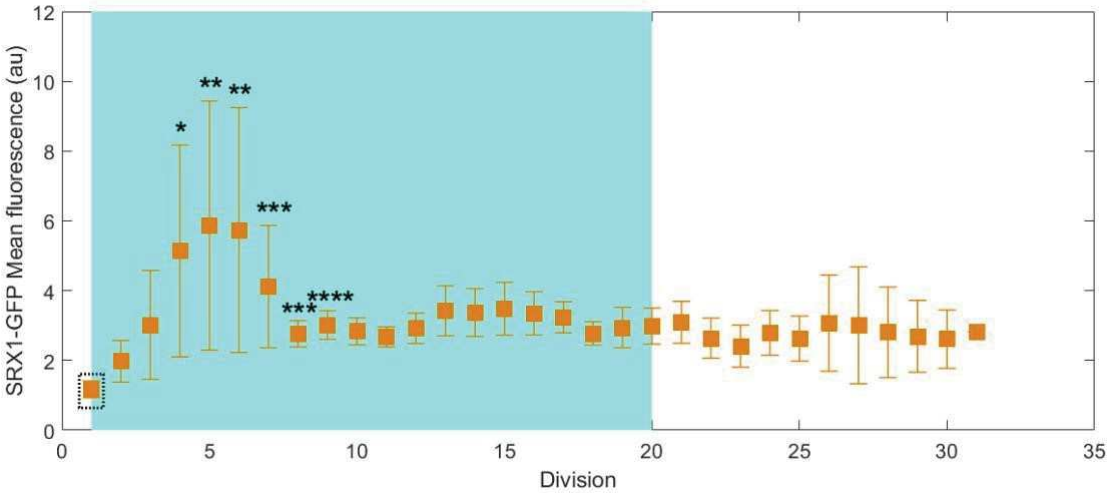

Figure 4.4 Pooled SRX1-GFP mean fluorescence evolution aligned by birth
Mean fluorescence SRX1-GFP during ageing process aligned by birth. The light blue rectangle indicates that more than half of the cells are viable. The first cell cycle SRX1-GFP shows average fluorescence level is set as basal level. Statistical test is performed for each cell cycle compare to the previous cell cycle. The significance of P-value is indicated. The error bar indicates ±standard error on mean.

Burst of SRX1-GFP fluorescence level increase can be monitored several divisions after birth. However, the increasing level of burst is less than 5 a.u on average. To better confirm the significance of the burst, statistical test of fluorescence is compared between each division. The significance of Mann–Whitney–Wilcoxon statistical test indicates that as cell grows, the fluorescence level become more and more significantly different starting from the 4-9th division. This increment suggests an increase of Srx1 expression at early stage of RLS. Then the internal Srx1 protein level become stable and remains in a significantly different level compare to the newborn daughters. I proposed that Srx1 protein may be actively synthesized after cell birth, which suggests an accumulation of oxidative stress after birth. This observation supports the previous study that has been revealed by roGFP2 redox state reporter strain that has been used in the same replicative ageing context (Knieß and Mayer 2016). In their study, the mother yeast starts to increase the oxidative fraction of roGFP2, suggesting that mother yeast starts to accumulate [ROS] after birth. The daughter cells show stable and relatively low level of oxidative roGFP2 marker ratio compare to mother cells.

The data of SRX1-GFP fluorescence level is not used for SEP alignment due to a corruption of time-lapse ageing experiment. The SEP cannot be determined without enough cells and fully

continuous RLS. Therefore, more ageing experiment is needed to further confirm the redox homeostasis at SEP moment in this reporter strain.

2.3 Internal [ROS] concentration could be revealed via TSA1-GFP reporter strain

The Tsa1 protein expression level correlates to the H2O2 concentration. This has been proved in the work of Dr. Goulev previously (Goulev, Morlot et al. 2017).

Ageing experiment is performed to TSA1-GFP reporter strain (Figure 4.5). By following the cell cycle duration of mother yeast trajectories, the SEP is determined by cell cycle sudden extension.

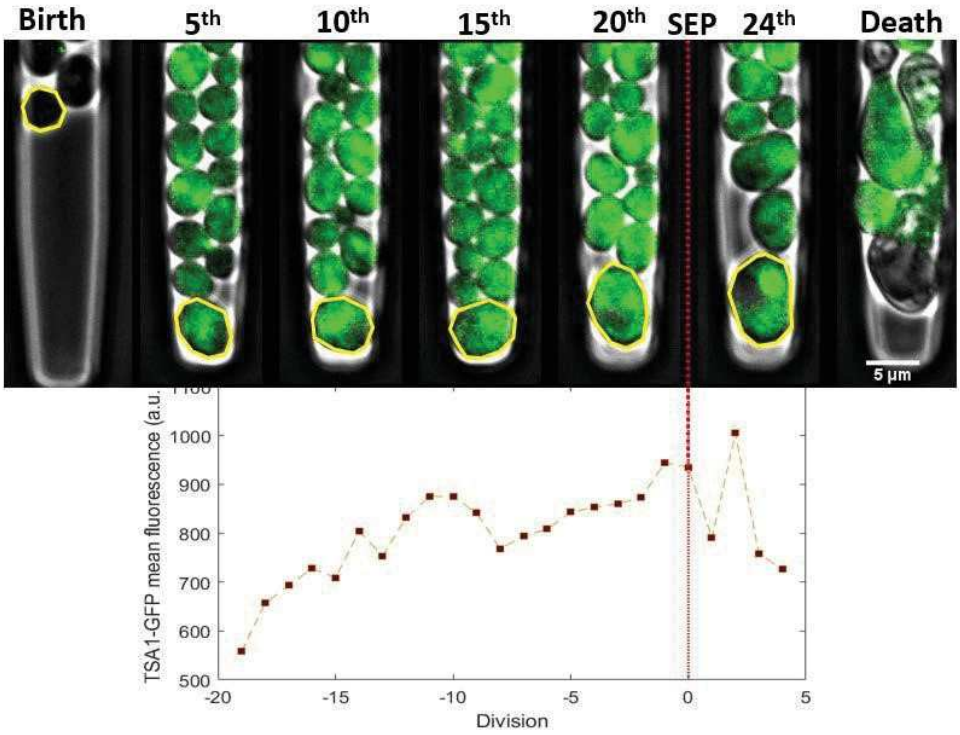

Figure 4.5 Trajectory of ageing process in representative TSA1-GFP reporter strain
The sequential images of TSA1-GFP ageing process. The yellow indicates cell contour. The SEP is indicated by red dashed line. The corresponding fluorescence evolution of the same cell is shown below. The fluorescence level is averaged for each cell cycle.

From the ageing experiment of TSA1-GFP, the data of mother cells are collected. Due to the abundance of Tsa1 expression level, the daughter cells born with less fluorescence and the mother cells age with more fluorescence can be observed by eye nude significantly (Figure 4.5). This observation is in line with the result from previous SRX1-GFP reporter. To better

compare the evolution of fluorescence at birth and SEP. Alignment of fluorescence evolution based on birth and SEP are measured (Figure 4.6A). The background noise is removed.

When cells are aligned by birth, the TSA1-GFP fluorescence show almost linear increase from 0-7th divisions and followed by a slow down to 10th division, this increment reaches the maximum level around the 10th division (Figure 4.6A). An unsynchronized decrease can be observed after the maximum peak after 10th division. This result corresponds to the SRX1-GFP reporter strain that significant increase of oxidative stress emerges after birth.

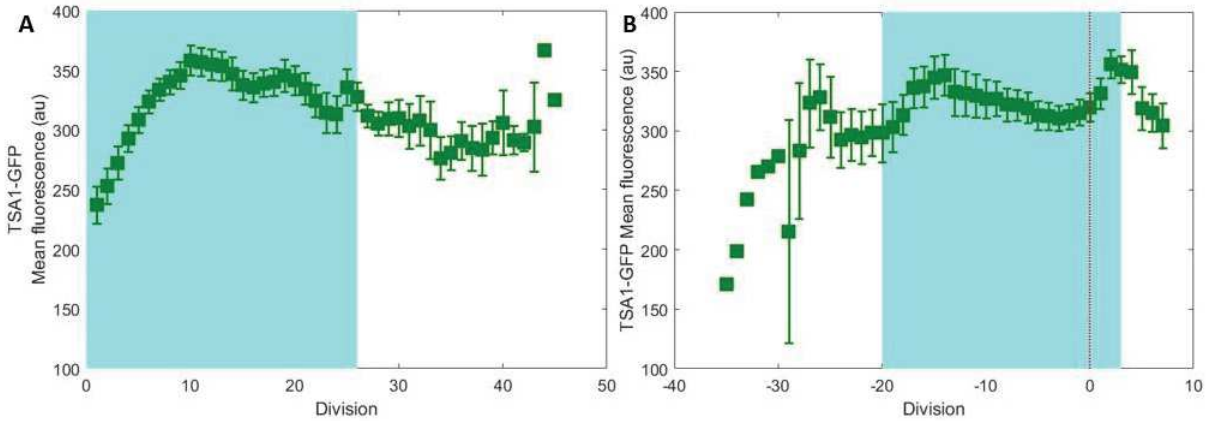

Figure 4.6 Fluorescence evolution of TSA1-GFP reporter strain with different alignment

A: The fluorescence evolution of TSA1-GFP cells aligned from birth. The blue rectangle indicates the range that more than 50% cells are viable. The error bar indicates ±standard error on mean. (N=20)
B: The fluorescence evolution of TSA1-GFP cells aligned by SEP. The SEP is indicated by dashed red line. The blue rectangle indicates the range that more than 50% cells are viable. The error bar indicates ±standard error on mean. (N=20)

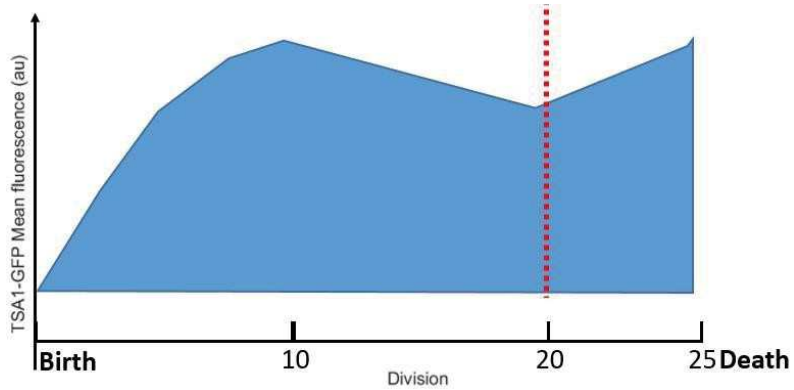

Figure 4.7 Schematic TSA-GFP fluorescence expression evolution

According to the Tsa1 protein fluorescence data, schematic TSA1-GFP fluorescence evolution is proposed. The total RLS is estimated to 25, the SEP is estimated at 20th division and indicated by red dashed line.

When cells are aligned by SEP, the fluorescence show a slight synchronized decrease before SEP and then increase after SEP onset (Figure 4.6B).

Combining with the fluorescence profile when aligned by birth, it seems that after reaching a maximum expression at early stage, the Tsa1 protein expression level decreased gradually until two to three divisions before SEP. Upon SEP transition, Tsa1 protein expression level is increased slightly for the second time (Figure 4.7). Approximately the average of RLS is around 25 divisions. The RLS can be separated into three phases: early pre-SEP stage which defined by the fast oxidative stress accumulation for around 10 divisions; late pre-SEP stage which corresponding to the presumption that oxidative stress decreased gradually when TSA1-GFP decrease; post-SEP stage which corresponds to the second slight rase of oxidative stress. Both SRX1-GFP and TSA1-GFP reporter strain show a rapid and significant oxidative stress accumulation at the beginning of RLS. This increase is more significant for Tsa1 protein, which lasts 10 cell cycles starting from birth while the it happens from 4-9th divisions for Srx1 protein. It seems that TSA1-GFP reporter strain maybe more sensitive to the redox balance variation compare to SRX1-GFP reporter strain. This suggests that after birth, the daughter cell may endure an oxidative stress accumulation. When cell ages to SEP, the slight increase of TSA1-GFP fluorescence suggests another redox imbalance at this moment. Alternative method for intracellular ROS quantification at various mother ages by using other markers is required for further confirmation.

2.4 Internal oxidative stress may be investigated via Tsa1 protein oxidative state

Dual protective Tsa1 protein functions are implicated face with different level of oxidative stress. When undergo strong external oxidative stress, the Tsa1 protein can be hyper-oxidized to form high molecular weight (HMW) aggregates and perform chaperon protein holdase function to prevent the protein aggregation (Noichri, Palais et al. 2015, Hanzén, Vielfort et al. 2016). When in TSA1-GFP reporter strain, this HMW form of Tsa1 could be observed as extremely brilliant fluorescence pixel signal. When Tsa1 protein is oxidized by a mild oxidative stress, it forms disulfide bond dimers, the fluorescence signal in TSA1-GFP reporter strain could be detected as like other free Tsa1 protein signal. It has been described in other literature using mathematical method to isolate the aggregated protein fluorescence signal. They considered that fluorescence values higher than two standard deviation of background noise are HMW aggregated (Marvin, Scholl et al. 2018). I then measured the aggregates and free Tsa1 protein fluorescence level and thus we could study the fraction of different oxidative state proteins during the ageing process.

The fluorescence measured for total Tsa1 protein and HMW Tsa1 aggregates are measured. Due to the cell-to-cell variety, these data are aligned by birth and SEP separately to monitor its evolution upon these important events (Figure 4.8).

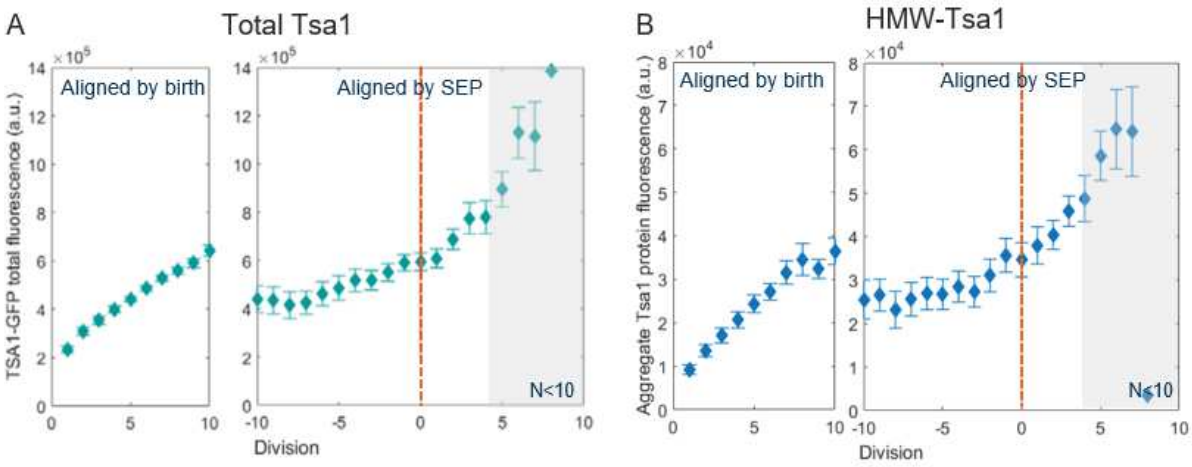

Figure 4.8 Fluorescence evolution of Tsa1 total protein expression and HMW-Tsa1 level

A: Total Tsa1 expression level fluorescence evolution. Both birth and SEP alignement are shown. The SEP is indicated by red dashed line, the grey area indicates less than 50% viable cells. The error bar indicates ±standard error on mean.
B: HMW aggregate form of Tsa1 level fluorescence evolution. Both birth and SEP alignement are shown. The SEP is indicated by red dashed line, the grey area indicates less than 50% viable cells. The error bar indicates ±standard error on mean.

It seems that total fluorescence profile and Tsa1 HMW aggregate fluorescence profile are very similar. The aggregate form of Tsa1 protein maybe proportional to the total protein expression level. Both show steady linear increase at early age after birth and another slight increase after SEP.

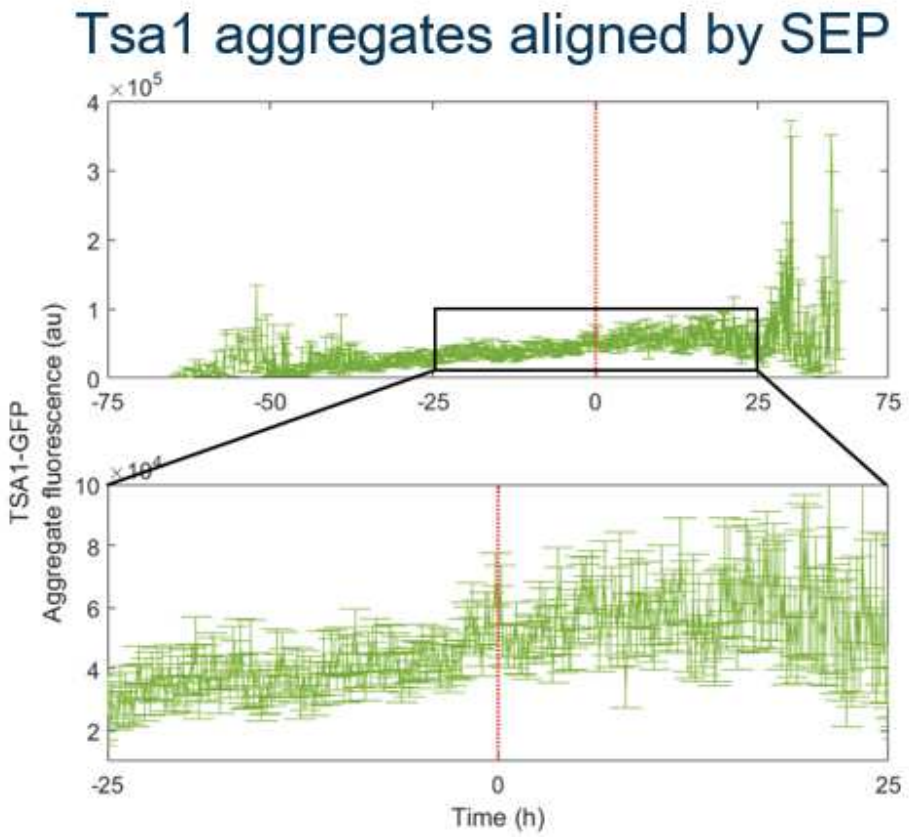

Figure 4.9 HMW-Tsa1 fluorescence signal aligned by SEP

The HMW aggregated form of Tsa1 fluorescence level is aligned by SEP, the SEP is indicated by red dashed line. The error bar indicates ±standard error on mean.

Previous fluorescence quantification is averaged for each cell cycle, it can provide more detail when analyzing the fluorescence quantification by each frame. The Tsa1 HMW aggregates is thus quantified based on each frame for more detail analysis (Figure 4.9).

It seems that the HMW Tsa1 aggregates show a linear accumulation as cell ages. It then worth comparing the fraction of Tsa1 aggregates compare to the total Tsa1 protein. It has been speculated in other study that Tsa1 is crucial due to their HMW function to dissolve protein aggregates as protein holdase (Hanzén, Vielfort et al. 2016). If the Tsa1 HMW fraction become significantly decreased, then it suggests that the holdase protective enzymatic function if indeed key for maintaining longevity at late life.

The fraction of HMW-Tsa1 aggregates during the ageing process in total Tsa1 protein is compared (Figure 4.10).

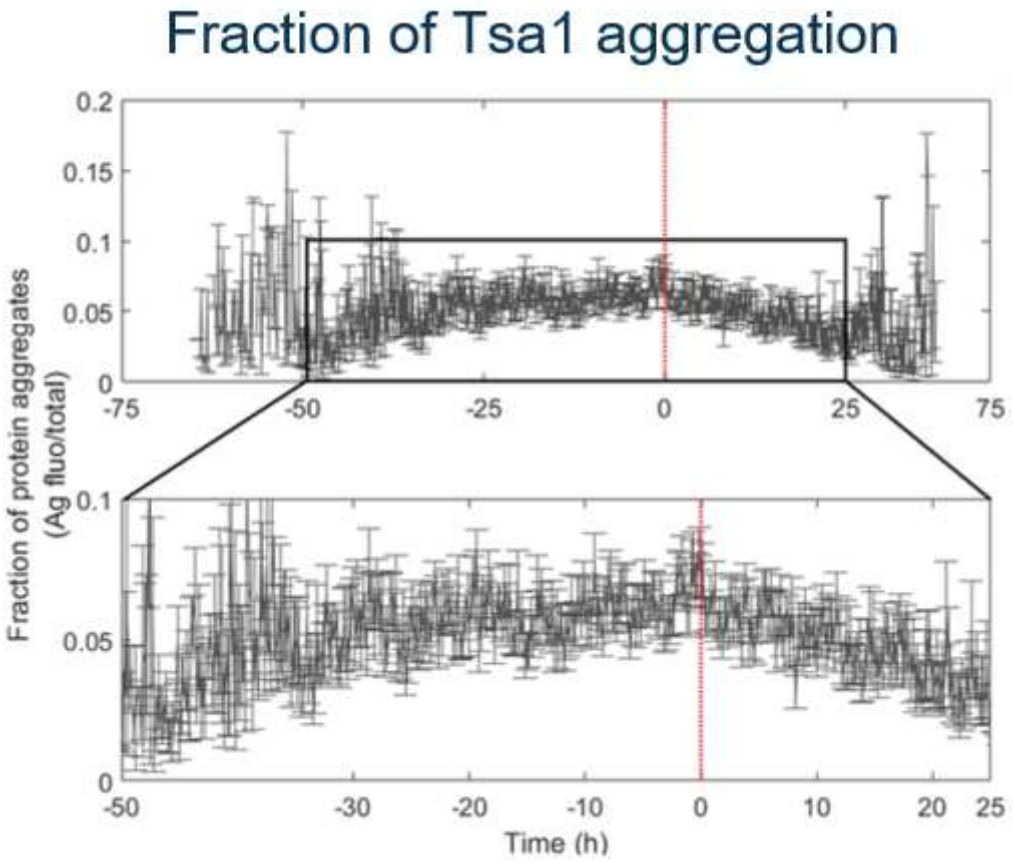

Figure 4.10 The evolution of HMW-Tsa1 aggregate form fraction during ageing over time

The HMW aggregated form of Tsa1 fraction is aligned by SEP, the SEP is indicated by red dashed line. The error bar indicates ±standard error on mean.

The fraction of HMW-Tsa1 aggregates is only about 6% of total Tsa1 protein. It seems that the fraction of HMW-Tsa1 is decreased since SEP. Even though the HMW-Tsa1 aggregate protein fraction is very low, we observe a significant decrease upon SEP, this partially supports the idea that protein holdase function is crucial for later life survivorship.

The free fraction of non-aggregate protein is on average 94% throughout the whole RLS. This observation highly suggests the abundance of non-aggregate Tsa1 protein, and probably free Tsa1 plays a more important protective function for redox homeostasis than HMW-Tsa1 during ageing. Taking all the information together, a theoretical scheme of Tsa1 protein expression profile during ageing can be deduced (Figure 4.11).

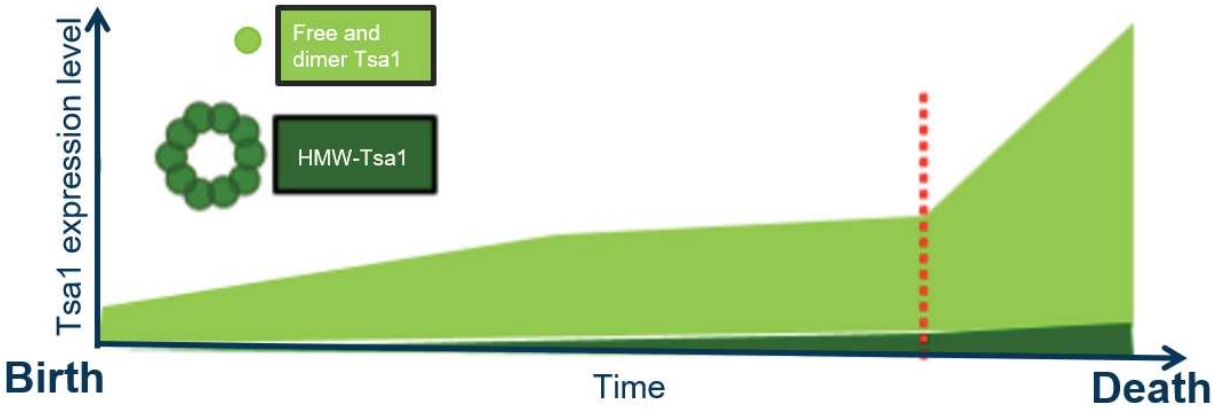

Figure 4.11 Schematic Tsa1 protein evolution profile during ageing

Hypothetical scheme predicting Tsa1 protein expression profile showing theoretically the two-protein fraction over time. The light green indicates the free and dimer form of Tsa1; the dark green indicates the HMW-Tsa1. The Tsa1 expression level is aligned according to the SEP. The SEP is indicated by red dashed line.

Previously, it has been suggested that protein chaperon function is more crucial for preventing ageing, especially for late life. From this result, this is true due to the reduced fraction of Tsa1 aggregation after SEP. However, if we consider the abundance of free Tsa1, the result suggests probably a more importance role of Tsa1 as peroxidatic function over the protein holdase function. So far, the understanding of redox homeostasis during ageing remains preliminary, other markers can be used for further and more detail analysis. However, if Tsa1 protein expression is following a [ROS] dose-dependent manner, this theoretical scheme may provide a primitive impression for [ROS] evolution during ageing. This study also indicates the using antioxidant GFP-fused reporter may reveal intracellular redox evolution in microfluidic system. It may help further understanding on intracellular redox homeostasis under mild hormetic ageing and even in TSA1OE mutant.

Chapter V

Conclusion

During my thesis, I have worked on 3 projects. These three projects may provide more insightful understanding on the replicative ageing process of budding yeast regarding ERC ageing factor and oxidative stress evolution.

From cell cycle point of view, the cell cycle phase-specific cell cycle checkpoint is not activated for cell cycle slowdown at SEP. When following the DDR activation, more DNA damage signal is detected at later life after SEP. As a conclusion, a general physiological cellular function breakdown may be linking to SEP onset.

The dynamic of SEP is investigated in long-lived mutants and intervention. Both Fob1 and SAGA mDUB module functions by regulating the ERC formation/excision trigger probabilistic SEP. For these two mutants, the longevity extension is largely contributed by the long-lived subpopulation live longer without SEP. The regulatory mechanism involved in ERC formation for both protein function is still not clear.

When yeast ages under H2O2 mild stress (hormetic effect), the onset of SEP is delayed, to prolong the RLS. The overexpression of antioxidant Tsa1 protein can partially reproduce the H2O2 hormetic by extending SEP and RLS. It can be speculated the when under hormetic H2O2 concentration, the antioxidant defense mechanism promotes Tsa1 protein expression and induce genome stability by less ERC formation and accumulation, thus extend the SEP. The molecular mechanism between Tsa1 and rDNA stability is unknown.

Understanding the evolution of oxidative stress and Tsa1 protein function contributing to longevity may further help to understand the H2O2 hormetic effect. Based on the readout of SRX1-GFP and TSA1-GFP redox state reporter strains, [ROS] may be rapidly accumulated after birth for around ten divisions. A slight redox state imbalance can be observed upon SEP by TSA1-GFP reporter strain as well, yet further confirmation is needed.

Tsa1 protein has dual protective functions to prevent ageing. One is the peroxidatic activity for [ROS] scavenging when Tsa1 is free or dimer, the other is the protein chaperon holdase for dissolving protein aggregates when Tsa1 is aggregated. After investigating the fraction of Tsa1 protein forms during ageing, on average 94% of Tsa1 shows scavenging function,

whereas 6% of Tsa1 shows chaperon function. From the perspective of quantity, it seems that Tsa1 antioxidant scavenging function is more important for preventing ageing.

Chapter VI

Discussion and Perspective

1. The relationship between histone (nucleosome) and excess ERC

Histone is well scaled with ERC/DNA level both before and after SEP. The tight scaling may be a reason for neutralizing and stabilizing negatively charged excess ERC. There is probably a structure formed between ERC and nucleosome. Hence, we could speculate that loss of histone may be accompanied with ERC loss at old age. This hypothesis can be supported by the observation on SAGA mutant (Figure 6.1), when less histone accumulation rate is observed during post-SEP period, the toxicity induced by ERC accumulation become less pronounced and exhibit a prolonged post-SEP lifespan in sgf73Δ mutant.

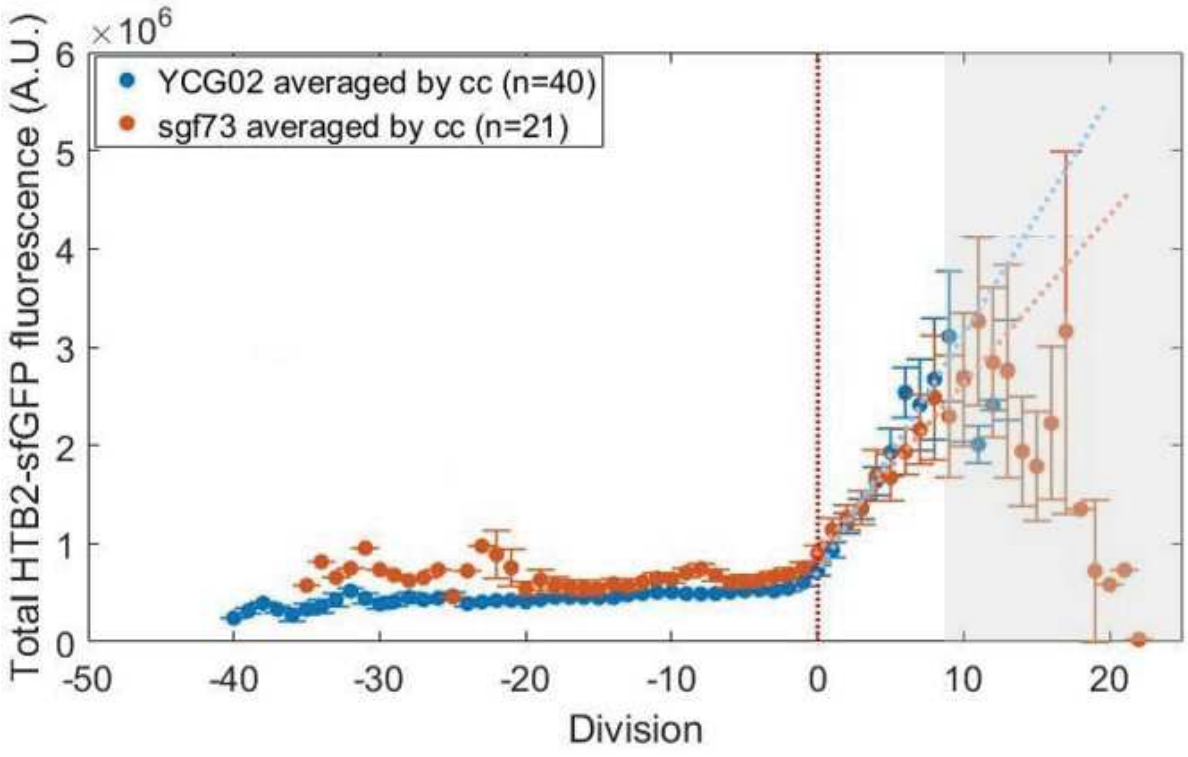

Figure 6.1 Histone protein fluorescence evolution during ageing aligned by SEP

Fluorescence evolution of HTB2-sfGFP reporter strain in both WT and sgf73Δ mutant. For WT, on average post-SEP lifespan is 5 division. The WT histone fluorescence level in blue dashed line shows a linear fit of increasing kinetic of about 23600. Whereas in sgf73Δ mutant, the average post-SEP lifespan is 8. The linear fit of orange dashed line for sgf73Δ histone protein show increasing kinetic 18410. The SEP is represented in red dashed line, the grey area indicates less than 50% viable cells. The error bar indicates ±standard error on mean.

In the result of sgf73Δ, we have observed specifically post-SEP division extension. For pre-SEP period, the number of ERC is unable to assume due to lack of direct reporter and the tolerance of mother yeast before the ERC reach a threshold for triggering SEP. However, after SEP, the ERC become excessive and may require SAGA anchorage function for ERC retention. Therefore, the ERC loss during post-SEP period could be explained.

There is another relative but indirect result from another study. It shows that old mother become rejuvenated showing faster cell cycle duration after inheriting excess Whi5 protein (along with nuclear content) to daughter cell (Figure 6.2) (Neurohr, Terry et al. 2018). This observation may provide supportive evidence that loss of excess nuclear content (probably along with ERC) may trigger rejuvenation in old mother.

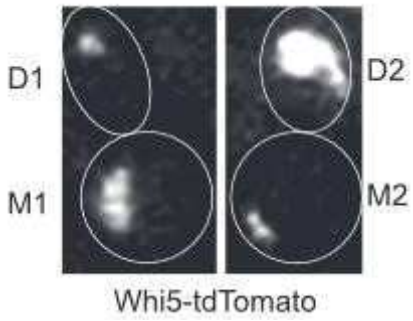

Figure 6.2 Mother asymmetric inheritance of Whi5 to daughter (adapted from Neurohr, Terry et al. 2018)
M1 old mother accumulate Whi5 for delaying G1 phase. Whereas M2 mother segregated whi5 into the daughter cell and undergo fast cell cycle duration for being 'rejuvenated'.

The asymmetric heritage of Whi5 from mother to daughter may also include other nuclear content. Therefore, we could assume that in this case, modifying the histone level after SEP may reduce the ERC accumulation in mother yeast. Yet no direct ERC copy number statistic to support this hypothesis and specific marker to distinguish the histone binding to the ERC or the histone binding to the chromosomal DNA. We could perform ageing experiment on SAGA mutant with ERC reporter markers to verify the hypothesis instead by taking advantage of random ERC loss in SAGA mutant.

2. Oxidative stress related rDNA stability induction and less ERC formation

Longevity extension observed in ERC-related mutants (fob1Δ, SAGA mutants) prolong RLS by less ERC formation and induce a portion of cells live longer without SEP. Whereas, H2O2 hormetic treatment and Tsa1 protein over expression extend RLS by delay SEP which probably through overall better rDNA stability maintenance.

The underlying mechanisms seems different between the two groups of longevity extension intervention. This observation has not been described before, the no-SEP subpopulation contributing to the longevity extension and its mechanism of death without cell cycle arrest are interesting questions that can be asked.

For the hormetic effect and Tsa1 overexpression, we could investigate what may be the potential mechanism between oxidative stress response and genome stability. We could speculate that when facing an oxidative stress, many mechanisms involved in protecting protein, DNA and altering metabolism are activated through Tsa1 overexpression. It then worth investigating the Tsa1 overexpression-induced protective downstream mechanisms involved in genome stability maintenance. The mechanism underlying maybe already unclosed, for instance: the DNA repair mechanism activation, which efficiently maintain the genome stability in TSA1OE mutant. It could also be an unknown mechanism which has been unclosed and unrelated to DNA regulation directly, for instance: through a specific fermento-respiratory metabolism which stabilize genome through an unexpected epigenetic molecular pathway. Many possibilities that can be proposed for another big project.

3. Evidence for genome stability maintenance under oxidative pre-stress

Based on the observation of hormetic H2O2 longevity extension, it has been proposed that multiple protective defense mechanisms may be pre-activated to repair damages, ensure protein functions and prevent ageing. One proof of principle experiment has been performed using ERC reporter strain (GFP binding to the rDNA/ERC marker). When cells are cultured in the microfluidic chamber, the population may reach a limit when the space

become limited and cell may sense environmental stress due to this space crisis. Two groups of cells are compared for their responses to the environmental stress, the control group with normal medium (Video 6.3A), another group of cells under hormetic H2O2 concentration (Video 6.3B).

vid_6.3A.avi

Video 6.3A Induction of rDNA instability and ERC formation facing environmental stress

ERC fluorescence evolution when facing environmental stress. Control cells without pre-treatment of oxidative stress show abrupt ERC formation upon space constraints. ERC reporter strain shows direct rDNA/ERC formation dynamic.

vid_6.3B.avi

Video 6.3B Pretreatment of mild H2O2 hormetic stress stabilize rDNA and prevent from other stress

Evolution of ERC fluorescence level in cells cultured in 50µM H2O2 concentration. rDNA/ERC fluorescence signal show less increase in front of space constraints. The ERC reporter strain shows direct rDNA/ERC formation dynamic.

When facing an environmental stress, the ERC signal of control group cells increases significantly, show abrupt ERC formation upon space-induced stress. This suggests that ERC formation/excision and ribosomal biogenesis may be important (by protein biosynthesis) to activate stress defense mechanisms. Less increase and relatively stable ERC signal are observed in the cells incubated in hormetic H2O2 concentration. This observation confirm that a relationship exists between stress and ERC formation/rDNA instability. And mild oxidative stress can be beneficial to prevent ageing by better maintenance of ERC formation/rDNA stability.

In the same experiment, another group of cells are also exposed to a massive oxidative stress of 0.5mM H2O2 (Video 6.4). This video shows cells under large dose of stress, the rDNA instability and ERC formation starts to increase before the space become constrained.

vid_6.4.avi

Figure 6.4 Evolution of ERC fluorescence when cells are cultured under massive H2O2 stress at 0.5mM concentration

Another supportive observation is provided by fob1Δ mutant. This mutant is long-lived compare to WT yet was not 'evolutionary selected'. It must be pointed out that two main resources that are necessary for microorganisms' survivorship: nutrient and space (Ghoul and Mitri 2016). When I noticed that this mutant shows more stable ERC level (relatively less than WT) (Ganley, Ide et al. 2009) and its cell cycle duration is slightly but significantly longer than WT. I proposed two reasons for 'not been selected' compare to WT. Firstly, by shorter cell cycle duration, WT may rapidly increase in population for space and nutrient occupation. Secondly, when facing various environmental stress from the wild, WT may be more responsive (by inducing rDNA instability/ERC formation) than fob1Δ mutant (less ERC inducing) for activating stress defense mechanisms.

As a conclusion, the rDNA instability/ERC formation/ribosomal biogenesis may be crucial for stress defense mechanism. Pre-activation of stress defense mechanism by mild oxidative stress may provoke defense and protective response which eventually result in less rDNA instability/ERC formation.

4. Discovery of an unknown Tsa1 function

The dual protective functions of Tsa1 have both been reported for its impact on preventing ageing (Hanzén, Vielfort et al. 2016). From the proportion of both free (96%) and aggregate (6%) forms of protein, we could conclude that peroxidatic activity of protein may be a more important function. This speculation is then verified by tsa1-variant mutants. By changing the key cysteine residues of Tsa1 protein, Tsa1 mutant protein variants can respectively exhibit two separate functions. These Tsa1-variant mutants can be expressed under the regulation of endogenous promoter. These Tsa1-variant mutants' RLS are then measured (Figure 6.5) and the result suggests that chaperon function may be more important than peroxidative function for preventing ageing.

Mutant	Peroxidatic	Chaperon
WT	++	++
TSA1OE	+++	+++
DYF	+++	-
DYF.C171S	+	-
C171S	-	++
C48S	-	-
tsa1Δ	-	-

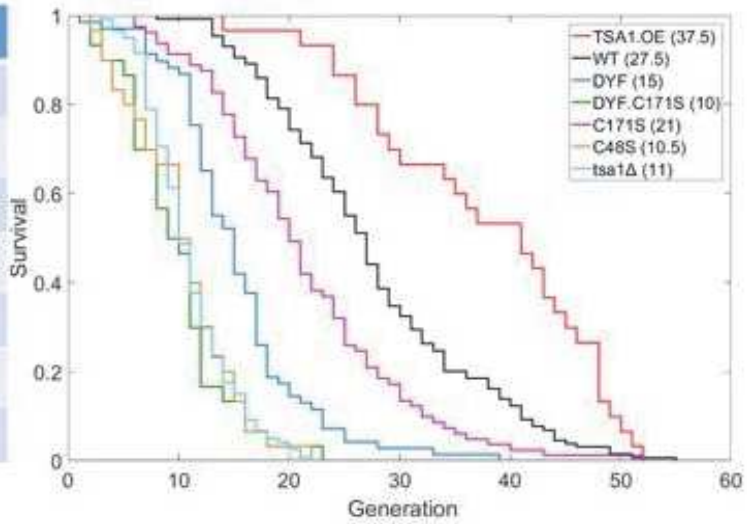

Figure 6.5 Tsa1-variant mutants and their RLS analysis

The list of Tsa1-variant mutants is tested and their RLS analysis is shown to the right by survival curve. The TSA1OE show 37.5 median RLS; WT 27.5; DYF 15; DYC.C171S 10; C171S 21; C48S 10.5; tsa1Δ 11.

From the RLS analysis result, we observe that surprisingly, C171S mutant live longer than DYF mutant. This suggests that chaperon function may override the peroxidatic function for preventing ageing. However, the chaperon protein fraction is so little (6%), plus this small fraction of HMW Tsa1 become less after SEP.

In addition to this observation, a genome stability maintenance function of Tsa1 can be assumed. From the result that tsa1Δ mutant shows very short replicative lifespan (Figure 6.5), plus the Tsa1 protein increase its expression level at the beginning of RLS up to two-fold. We could speculate that Tsa1 is crucial for early stage growth when cell producing massive [ROS]. On the contrary, overexpress Tsa1 in TSA1OE show delayed SEP by less ERC accumulation/better rDNA stability, we could speculate that Tsa1 protein may contribute to a mechanism for genome stability maintenance. Yet the potential mechanisms contributing to the genome stability maintenance remain unclear? One of the mechanisms that contributing to genome stability is through slow cell growth (Vinton and Weinert 2017), therefore I measured the growth rate between tsa1Δ, WT and TSA1OE (Figure 6.6). Surprisingly, the growth rate meets the speculation, the TSA1OE indeed better maintain the genome stability through a slower growth phenotype. This leads to further question, what may be the regulatory mechanism?

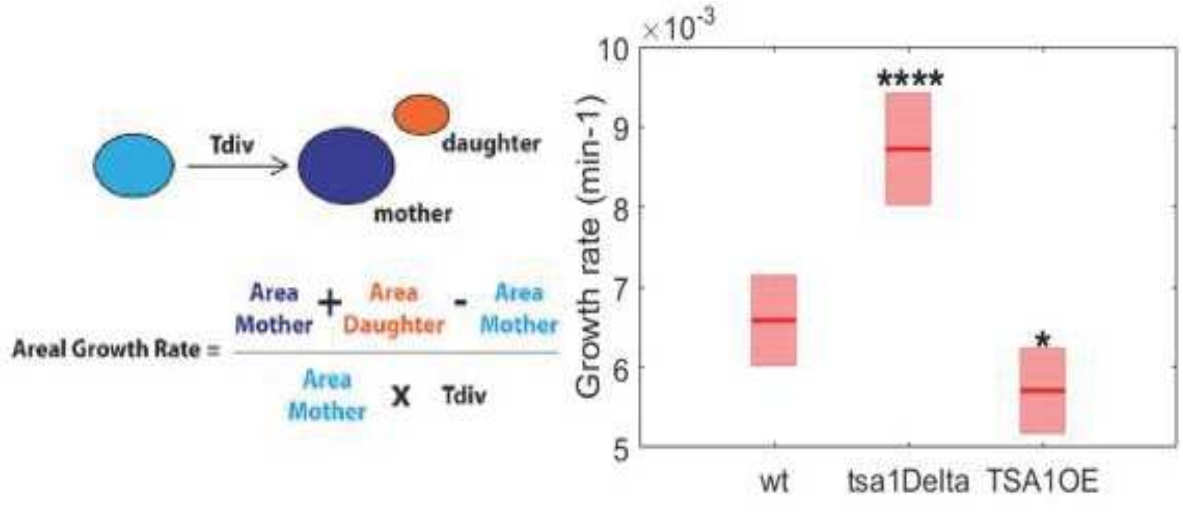

Figure 6.6 Growth rate measurement in WT, tsa1Δ and TSA1OE mutants

The schematic growth rate measurement is drawn to the left. The boxplot of growth rate is shown to the right, the measurement is then verified with statistical test.

5. Accumulation of oxidative stress at the beginning of RLS

Real-time monitoring for molecular dynamic of redox homeostasis is performed under replicative ageing background. Though the result is very preliminary, the increment of redox reporter signal after birth seems to be positive. Both SRX1-GFP and TSA1-GFP reporters show significant increasing signal during first ten generations. Other study has observed similar read out (Figure 6.7) (Knieß and Mayer 2016).

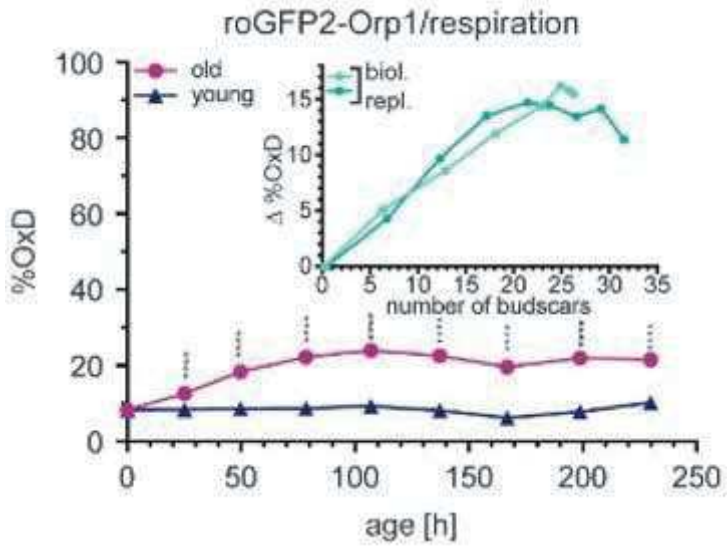

Figure 6.7 Evolution of intracellular H2O2 (revealed by Orp1-roGFP2) under respiratory condition over time

The curve in green measures the accumulation of [ROS] by counting bud scars (divisions). In the graphic below, the mother population measured in red dot and corresponding offspring is shown in blue triangle.

In their work, they use the Orp1-roGFP2 redox reporter to reveal H2O2 quantity. Increasing redox potential at early age can be related to the similar linear increase that has been observed in our quantification. This result correlates further with the result of TSA1-GFP, if aligned by birth, slight fluorescence fluctuation around SEP maybe blurred due to the cell-to-cell heterogeneity. This observation suggests that redox balance could be studied using proper endogenous GFP reporter strain in microfluidic system. This tool can be developed for more study regarding the hormetic longevity extension and in long-lived TSA1OE mutant.

Ageing is a complex and multifactorial network. The fundamental understanding of cellular ageing process may be just a small brick in front of a big wall. Yet all great buildings are built up from small bricks.

Chapter VII

Materials and Methods

1. Yeast strains and media

All strains used are congenic to S288c, unless specified. Htb2-sfGFP strain was generated by classical PCR-mediated genome editing from previous work (Garmendia-Torres et al.,2018). All GFP-labelled strains were from the Yeast GFP Clone Collection provided by Michael Knop (Huh et al., 2003). fob1Δ, tsa1Δ strains were purchased from Euroscarf and sgf73Δ, ubp8Δ, bud6Δ knock-out collection from Sylvie Friant's lab. These strains are then crossed with strains containing the relevant sfGFP markers and genotyped by PCR. LacO-rDNA & LacI-GFP strain (Miyazaki and Kobayashi, 2011) was BY backcrossed strain from TMY8 strain by Dr. Sandrine Morlot (Morlot et al., 2019). Tsa1-variant mutants were provided by Prof. Michel Toledano. The list of strains used in my thesis report can be found in the table below (Table 7.1).

Table 7.1 Table of strains

Strains/Name	Genotype	Reference/Source
WT/BY4742	MATalpha; ADE2; his3D1; leu2D0; lys2D0; MET15; ura3D0; TRP1	Euroscarf
Htb2-sfGFP/YCG01	MATa; ADE2; his3D1; leu2D0; lys2D0; met15D0; ura3D0; TRP1; Htb2-sfGFP-KANMX	(Garmendia-Torres et al.,2018)
Htb2-sfGFP/YCG02	MATalpha; ADE2; his3D1; leu2D0; lys2D0; met15D0; ura3D0; TRP1; HTB2-sfGFP-KANMX	(Garmendia-Torres et al.,2018)
Whi5-GFP	MATa; Whi5-GFP-HIS3MX; ADE2; leu2D0; LYS2; met15D0; ura3D0; TRP1	Yeast GFP Clone Collection/ Thermo Fischer scientific
Rnr3-GFP	MATa; Rnr3-GFPHIS3MX; ADE2; leu2D0; LYS2; met15D0; ura3D0; TRP1	Yeast GFP Clone Collection/ Thermo Fischer scientific
fob1Δ	MATalpha; ADE2; his3D1; leu2D0; lys2D0; MET15; ura3D0; TRP1; fob1::kanMX4	Euroscarf
ubp8Δ	MATalpha; ADE2; his3D1; leu2D0; lys2D0; MET15; ura3D0; TRP1; ubp8::kanMX4	Euroscarf
sgf73Δ	MATalpha; ADE2; his3D1; leu2D0; lys2D0; MET15; ura3D0; TRP1; sgf73::kanMX4	Euroscarf
bud6Δ	MATalpha; ADE2; his3D1; leu2D0; lys2D0; MET15; ura3D0; TRP1; bud6::kanMX4	Euroscarf

Strains/Name	Genotype	Reference/Source
fob1Δ; Htb2-sfGFP	MATalpha; ADE2; his3D1; leu2D0; lys2D0; MET15; ura3D0; TRP1; fob1::kanMX4; Htb2-sfGFP-KANMX	This work
ubp8Δ; Htb2-sfGFP/SJ1.18	MATalpha; ADE2; his3D1; leu2D0; lys2D0; MET15; ura3D0; TRP1; ubp8::kanMX4; Htb2-sfGFP-KANMX	This work
sgf73Δ; Htb2-sfGFP/SJ1.18	MATalpha; ADE2; his3D1; leu2D0; lys2D0; MET15; ura3D0; TRP1; sgf73::kanMX4; Htb2-sfGFP-KANMX	This work
Tsa1-GFP	MATa; Tsa1-GFPHIS3MX; ADE2; leu2D0; LYS2; met15D0; ura3D0; TRP1	Yeast GFP Clone Collection/ Thermo Fischer scientific
Yap1-GFP	MATa; Yap1-GFPHIS3MX; ADE2; leu2D0; LYS2; met15D0; ura3D0; TRP1	Yeast GFP Clone Collection/ Thermo Fischer scientific
Srx1-GFP	MATa; Srx1-GFPHIS3MX; ADE2; leu2D0; LYS2; met15D0; ura3D0; TRP1	Yeast GFP Clone Collection/ Thermo Fischer scientific
BY4742 vector/YMM130	MATalpha; his3D1::pRS403; leu2D0; lys2D0; ura3D0;	(Hanzen et al., 2016)
tsa1Δ	MATalpha; ADE2; his3D1; leu2D0; lys2D0; MET15; ura3D0; TRP1; tsa1::kanMX4	Euroscarf
TSA1OE	MATalpha; his3D1::pRS403-Myc-TSA1; leu2D0; lys2D0; ura3D0	(Hanzen et al., 2016)
tsa1ΔC48S/YMM145	MATalpha; his3D1::pRS403; leu2D0; lys2D0; ura3D0; tsa1C48S	(Bodvard et al., 2017)
tsa1ΔC171S/YMM146	MATalpha; his3D1::pRS403; leu2D0; lys2D0; ura3D0; tsa1C171S	(Bodvard et al., 2017)
tsa1ΔYF/YMM147	MATalpha; his3D1::pRS403; leu2D0; lys2D0; ura3D0; tsa1(1-184)	(Bodvard et al., 2017)
tsa1C171SΔYF/YMM148	MATalpha; his3D1::pRS403; leu2D0; lys2D0; ura3D0; tsa1(1-184)C171S	(Bodvard et al., 2017)
TMY8	MATa; ade2::pAFS144-wtGFP(ADE2); rDNA::pTM-lacO50 (URA3) amplified ~150 copies; NET1-mCherry-spHIS5; leu2-3,112; trp1-1; can1-100; ura3-1; ade2-1; his3-11,1	(Miyazaki and Kobayashi, 2011)

Strains/Name	Genotype	Reference/Source
LacOrDNA & LacI-GFP strain	MATa; ade2::pAFS144-wtGFP(ADE2); rDNA::pTM-lacO50 (URA3) amplified ~150 copies; NET1-mCherry-spHIS5; leu2D0; LYS2; MET15; TRP1	(Morlot et al., 2019)

The DNA oligo nucleotide used for PCR amplification and verification are also listed below in Table 7.2.

Table 7.2 Table of DNA oligo used for PCR verification

Oligo name	Sequence	goal
KanC	TGATTTTGATGACGAGCGTAAT	Deleting collection KanMX4 gene verification
fob1Δ_C	TTCCTACTATCAAACTCTGGAATCG	fob1Δ mutant verification
fob1Δ_D	GCCTCTTGTAATATTGTTCAAGGAA	
sgf73Δ-F	AATGCAAGAATCAAATCAAGATAGC	sgf73Δ mutant verification
sgf73Δ-R	TGGCATTTATAAAAATTCTACCCAA	
ubp8Δ-F	CTCCTTGGAAAGTTCTATTGTGTGT	ubp8Δ mutant verification
ubp8Δ-R	TAAAGAAAAACATGATGGAAACGAT	
bud6Δ-F	AGACTTGGGTAAGGCATTAGAAACT	bud6Δ mutant verification
bud6Δ-R	TATGCAATTTCATTCGTTCTTACAA	
tsa1Δ_C	ACTGTCTTGCCATGTAACTGGA	tsa1Δ mutant verification
tsa1Δ_D	GGTTTACGCGTTTTAGAGCCAG	
Myc_F	GAACAAAAACCTCATCTCAGAAGAGGAT	Tsa1 gene insertion verification on the genome
tsa1_F	ATACGCTACCCAAGTACAGAAGATGG	
tsa1_R	TTATTTGTTGGCAGCTTCGAAG	
Myc_F_new	ATGGAACAAAAGTTGATTTCTGAAGA	Tsa1 gene insertion verification at alternative position
tsa1_R_new	GGAGTTTGGAAGCTTCCTTCC	
qPCR_tsa1_F	GTCTTTGACGAAGTCTCCTT	qPCR verification for number of genes inserted in TSA1OE
qPCR_tsa1_R	AAGGAGACTTCGTCAAAGAC	

One night before loading into microfluidic device, freshly thawed cells were grown overnight in synthetic complete (SC) liquid medium with 2% dextrose and then diluted in the morning for exponentially growing healthy cells. The cell cycle phase (CCP) quantification and ageing experiments is performed in microfluidic chip system under freshly prepared SC+2%dextrose medium. For H2O2 hormetic ageing experiment, due to the fast degradation of H2O2, the highly concentrated H2O2 (Hydrogen peroxide solution 35wt. % in H2O, 349887–500 ML, Sigma) is diluted to suitable H2O2 concentration. The media bottle is placed in ice box for maintaining a low temperature to avoid H2O2 degradation. The microfluidic experiment and the media do not affect the experiment since the media reached room temperature before entering the chip (Goulev et al., 2017). The H2O2 medium is freshly prepared and changed every 48hrs. The H2O2 at suitable concentration is used for hormesis ageing experiment. The H2O2 concentration was measured using a colometric H2O2 assay kit (OxiSelect Hydrogen Peroxide Assay Kit (Colorimetric), STA-343, EUROMEDEX, France) in media samples taken from the freshly prepared media.

2. Micro-fabrication and microfluidic setup

2.1 Micro-fabrication procedure

The micro-fabrication was performed using the soft lithography approach (Figure 7.1). After the improving the microfluidic design, a photolithography mask with custom design is then used as the template to construct 3D structure. By spin coating, the photoresist (Selba) is homogeneously covering the silicon wafer. Then followed by a step of soft baking. Both spin coating parameters and the soft baking are controlling the height from 1µm to 1mm. The soluble photoresist resin become polymerized after exposing to the UV light. Therefore, the desired 3D relief is curved by UV light and to avoid the photo-diffraction the photolithography mask is uniformly covered on the resin. Non-polymerized resin can then be removed. By applying several times such steps, different layers can be applied in order to achieve the desired mold. Finally, for better conservation of the origin mold precision (made by wafer and SU-8 resin), the negative of the mold is duplicated using the PDMS resin. Using Epoxy resin and harder mix in a ratio of 1:3 after remove bubbles by vacuum pumping, the mix is poured onto the PDMS motif (Burgoyne 2009). Putting the mold under the hood at room temperature for 24hrs, the mold can be cured and it is more resistant than wafer motif and suitable for repetitive use. For more detailed description of the multi-layer

photolithography micro-fabrication, thesis of previous doctorate student can be conferred (Ferhman et al., 2013; Paoletti C., 2014).

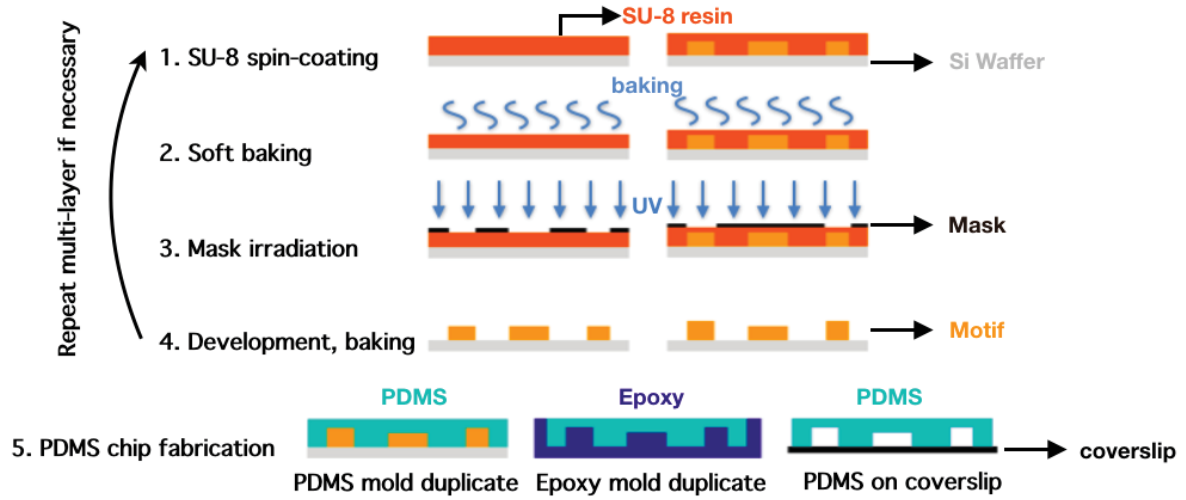

Figure 7.1 Micro-fabrication steps and the microfluidic chip photo
The height is controlled by both SU-8 photoresist spin-coating and soft baking. Then the region exposed to UV irradiation through a mask is polymerized. These steps can be repeated to build up multi-layer micro-structure. Finally using PDMS polymerized mold (turquoise), the micro-structure can be negatively duplicated. The mold is conserved in Epoxy (violet) mold by PDMS duplication.

2.2 Microfluidic device design optimization

The microfluidic chips used for long-term observation was designed based on the previous publication (Figure 7.2) (Fehrmann et al., 2013). Such design allows the capture of one single

cell at the tip of the cavity and based on the polar budding pattern of haploid yeast cells, the lifespan can be monitored.

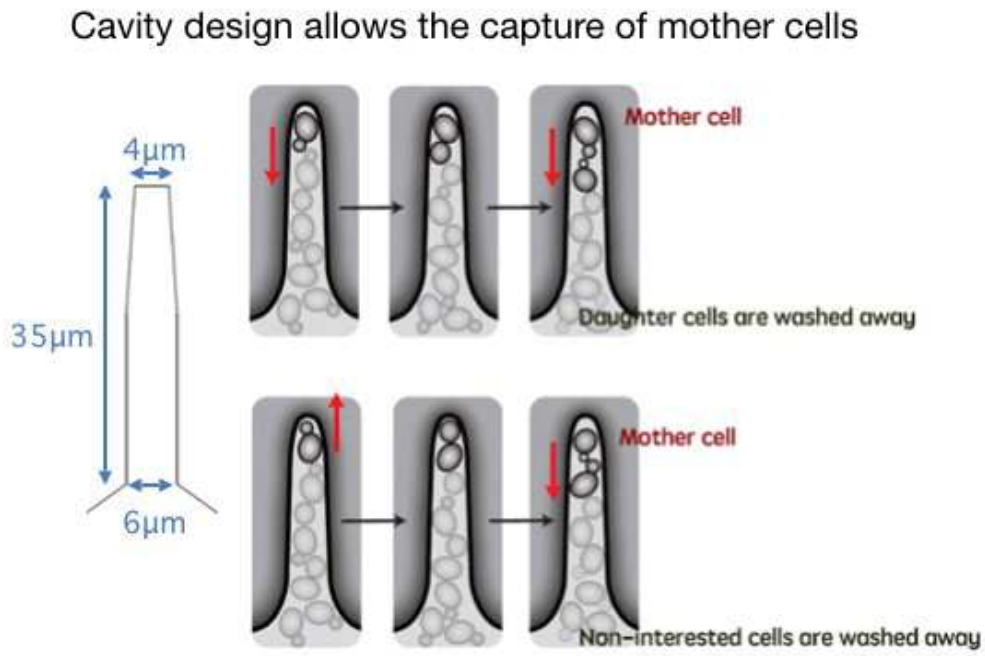

Figure 7.2 Previous microfluidic design for ageing experiment (Fehrmann et al., 2013)

The cavity design that has been published from previous host lab work (Fehrmann et al., 2013). The budding yeast with an average diameter around 4µm can be trapped at the tip of the cavity. Due to the polar budding pattern, the daughter cells to be pushed outside of the cavity then of the trapping area and finally washed away by flow media.

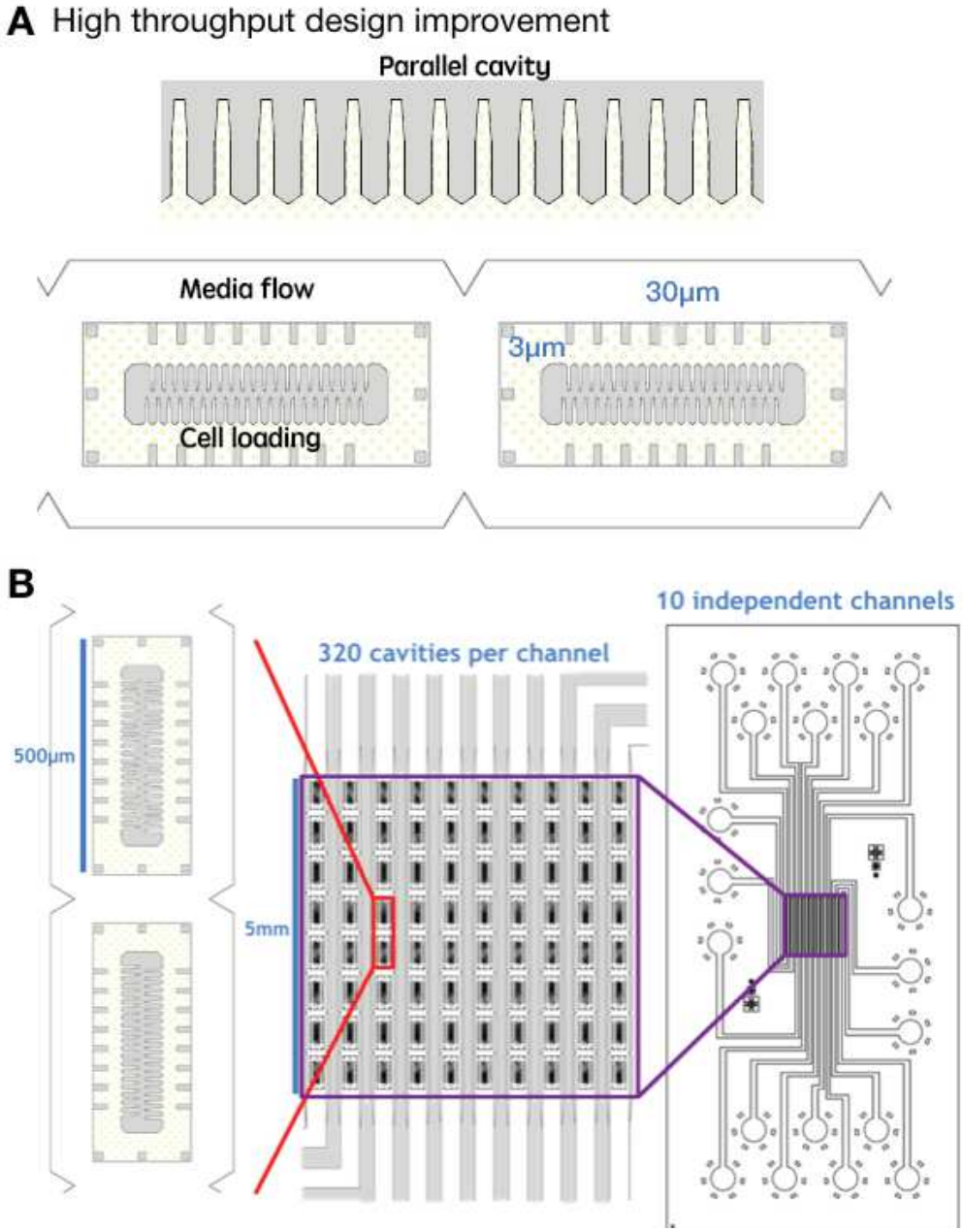

Figure 7.3 The high-throughput and 10 independent channel-optimization design allowing to monitor more conditions within one experiment

A: To increase the number of mother cells that can be captured within one experiment, more cavities are added and the grey area indicating the regions where the PDMS chip is covalently bound to the coverslip glass., The cell trapping area presenting a height of 3µm is shown by light yellow dots, which allowing a single layer of cells be trapped in this area. The white area with a height of 30µm allowing the media to go through and wash away the excessive cells and avoid cell clogging.

B: 10 independent channels are designed for independent medium and strain experiment.

To optimize the design, more cavities are added to observe more mother cells at one time for high throughput improvement (Figure 7.3A); 10 independent channels are designed on the same chip for more media condition improvement (Figure 7.3B). 10 independent channels are designed on the chip. There are 320 cavities per channel. Taking together, within one experiment, 10 different conditions or strains can be observed in one experiment. 320 cavities/mother cells can be captured for each channel. Comparing to previous design 'CLiC' (Fehrmann et al., 2013), around 60 cavities can be monitored for each experiment. The efficiency for observing various strains and various conditions within one experiment on a single microfluidic chip is improved. This improvement is designed and micro-fabricated by Dr. Morlot Sandrine of the host lab (Morlot et al., 2018). The design improvement and micro-fabrication of microfluidic chip were not performed by me during my thesis, the device has been already prepared for use (Figure 7.4).

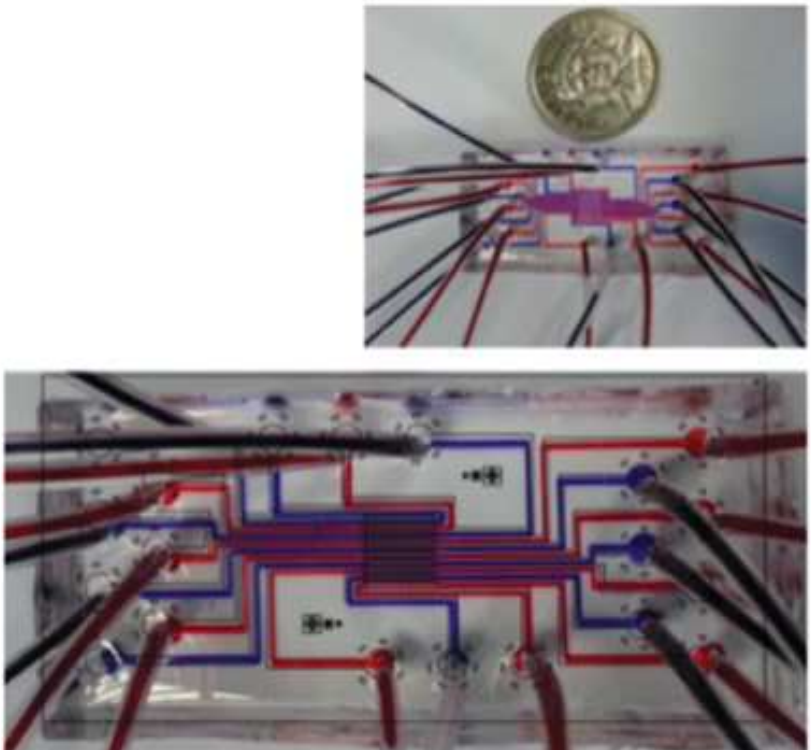

Figure 7.4 Microfluidic chip photo showing independent channels

The microfluidic chip used for long-term cell growth and ageing experiment. The chip shows a size of 24*50 mm. The different ink colors indicate that the different media can be used for cell growth. The liquid medium is controlled by peristaltic pump connected to the input. A big trash bottle is needed for output.

2.3 Protocol for microfluidic chip preparation

The micro-channels were cast by curing PDMS (Sylgard 184, 10:1 mixing ratio) and then covalently bound to a 24*50 mm coverslip using plasma surface activation (Diener, Germany). Chips were baked for 1hr at 60°C to consolidate bonding between the glass and PDMS and then perfused with media using Tygon tubing and a peristaltic pump (Ismatec, Switzerland) at an 8μL/s speed. After 2h of PDMS rehydration, yeast cells were loaded into the chip with a 1mL syringe and a 23G needle.

3. The principle of image analysis of Matlab pipeline

After time-lapse acquisition, NIS raw data were analyzed using the custom MATLAB software 'phylocell' and 'autotrack' function developed by the host lab (Fehrmann et al., 2013). The nd2 format images are converted to Matlab jpeg project format. This format allows to be analyzed using the custom software Phylocell. For the image processing step, the cell contour recognition and segmentation is achieved by setting appropriate threshold in phase contrast channel； combining with the classic 'watershed' image processing algorithm, the cell contour can be delineated from the cell masks returned by the watershed program. (Beucher & Lantuéjoul, 1979; Fehrmann et al., 2013). The nuclear contour can be revealed using the fluorescence fused nuclear protein, for instance the strain Htb2-sfGFP in my thesis report. The image processing procedure is like the cell contour segmentation. Firstly a 'top-hat' classic filter is applied to abstract the background noise based on the fluorescence threshold. Then like the cellular contour segmentation, a 'watershed' image analysis is applied for correct nuclear contour segmentation. The GUI allows to visualize the segmentation and perform manual corrections if necessary (Fehrmann et al., 2013). This image processing routine has been applied and published in the article Fehrmann et al., 2013 (Paoletti, 2014).

To monitor the continuous dynamic within the cell, a step of 'cell tracking' is applied to associate a number to the same cell or the same nucleus of different images. This step is also called 'cell tracking'. It is achieved by optimizing the contour position and cell size globally by using Hungarian algorithm calculation. This step of cell 'mapping' allows to numerate the same cell from frame 'a' (birth) to frame 'z' (death) and along with manual correction. This

step facilitates the quantification of consequent dynamic of a single cell during the ageing process (Fehrmann et al., 2013; Paoletti, 2014).

Based on the above described image processing pipeline, the functions 'cellfluo' and 'incellfluo' can be used to quantify the total, average fluorescence signal and contour parameters within both cellular and nuclear contours.

4. Microfluidic time-lapse experiments and data analysis (a. experiment b. analysis)

4.1 Common section for all the equipment:

Cells were imaged using an inverted Nikon Ti-E microscope. Fluorescence illumination was achieved using LED light (Lumencor) and emitted light was collected using a 60X N.A. 1.4 objective and a CMOS camera Hamamatsu Orca Flash 4.0. An automated stage was used to follow different fields of view over the course of the experiment. Focus was maintained using the Nikon Perfect Focus System. A constant temperature of 30°C was maintained on the chip using a custom sample holder with thermoelectric modules, an objective heater with heating resistors, and a PID controller (5C7-195, Oven Industries).

Table 7.3 Table of microfluidic experiments and time-lapse microscopic settings

Section	Microfluidic experiments & settings	Strain	Phase	GFP	DAPI	min/frame	duration (h)
4.2	Ageing experiment	Htb2-sfGFP	x	x		10	>140h
4.4	DAPI staining experiment	Htb2-sfGFP	x	x	x	1	2min
4.5	CCP quantification (Htb2-sfGFP)	Htb2-sfGFP	x	x		3	50h
4.6	CCP quantification (Whi5-GFP)	Whi5-GFP	x	x		3	50h
4.7	DNA damage positive control test	Ddc2-GFP	x	x		10	10h (24h-incubation)

4.7	DNA damage positive control test	Rnr3-GFP	x	x		10	10h (24h-incubation)
4.2	Ageing experiment	Rnr3-GFP	x	x		10	>140h
4.2	Ageing experiment	fob1Δ;	x			10	>140h
4.2	Ageing experiment	fob1Δ. Htb2-sfGFP	x	x		10	>140h
4.2	Ageing experiment	sgf73Δ	x			15	>140h
4.2	Ageing experiment	sgf73Δ. Htb2-sfGFP	x	x		10	>140h
4.2	Ageing experiment	ubp8Δ	x			15	>140h
4.2	Ageing experiment	ubp8Δ. Htb2-sfGFP	x	x		10	>140h
4.2	Ageing experiment	bud6Δ	x			15	>140h
4.3	H2O2 hormetic ageing experiment	Htb2-sfGFP	x	x		10	>140h
4.7	H2O2 0.4mM oxidative stress activation experiment	Tsa1-GFP	x	x		10	12h (24h-incubation)
4.7	H2O2 0.4mM oxidative stress activation experiment	Yap1-GFP	x	x		10	12h (24h-incubation)
4.7	H2O2 0.4mM oxidative stress activation experiment	Srx1-GFP	x	x		10	12h (24h-incubation)
4.2	Ageing experiment	TSA1OE	x			10	>140h
4.2	Ageing experiment	tsa1Δ	x			10	>140h
4.2	Ageing experiment	Tsa1 mutant variants	x			10	>140h
4.2	Ageing experiment	Srx1-GFP	x	x		10	>70h
4.2	Ageing experiment	Tsa1-GFP	x	x		10	>140h

4.2a. ageing time-lapse experiment

The ageing time-lapse experiment is by monitoring the whole replicative ageing process of the strain to analyze its RLS, cell cycle duration for SEP determination and in the case of fluorescence measurement, the fluorescence levels are also quantified throughout the replicative lifespan. The acquisition starts just after the cell loading; therefore, the birth event will not be missed.

2 channels are mainly used for ageing time-lapse experiment: phase contrast: 20ms exposure time, no binning; GFP channel is optional depending on the strain used: 5% laser excitation for Htb2-sfGFP reporter strains and 7% for Rnr3-GFP strain (wavelength 470nm): 50ms exposure time and binning 2*2.

4.2b. analysis of ageing time-lapse experiment

4.2b.1 RLS analysis

The RLS is measured by counting successive daughter cells generated from single mother yeast from birth to death (till cell lysis). The time-lapse ageing experiment images are transformed to video by using custom MATLAB function 'exportmontage' code. The Nikon format images (nd2) are converted into Matlab jpeg and then into avi movie. This code belongs to the 'autotrack' function that has been developed by Dr. Gilles CHARVIN. These videos are opened in ImageJ and analyzed by directly counting the number of daughters generated from one single mother yeast. After analyzing enough number of mother cells (usually N>50), survival curves can be generated using 'ecdf' MATLAB function. Alternatively, using 'NotBoxPlot' function, the RLS distribution can also be shown by box with the median and standard error. The code 'notBoxPlot' function was published by Rob Campbell.

4.2b.2 Cell cycle duration trajectory analysis

The cell cycle duration is quantified by counting the number of frames between each cell division directly by ImageJ. After collecting all the cell cycle duration trajectory of a single mother cell, the trajectory can be represented by color-code bar using 'Tabtrajiso_Jia' function which is customized based on the original 'Tabtrajiso' function developed by Dr. Gilles CHARVIN. The new function can add the color bar agenda.

4.2b.3 SEP determination based on cell cycle duration

The SEP is determined based on the breaking point determined by cell cycle duration extension. The sudden cell cycle extension corresponding to a decrease of cells dividing frequency. Using 'findSEP_Jia' customized function which was originally developed by Dr. Gilles CHARVIN, the piece-wise linear regression can detect the most abrupt cell cycle extension, the SEP. Compare to conventional 'findSEP' function, the customized function limit the SEP by a slightly more abrupt cell cycle extension and reject the SEP when the last cell cycle duration is less than 120 minutes.

4.2b.4 Fluorescence analysis

The nuclear Htb2-sfGFP fluorescence is measured by firstly nuclear segmentation threshold at '600' fluorescence density. A round of manual correction for the contour segmentation is necessary for the data precision. After segmenting the nuclear contour, the mother cells monitored from birth to death are analyzed using 'incellfluo' function for collecting the nuclear data.

The cellular Rnr3-GFP fluorescence is measured after the cellular contour segmentation. After a round of manual contour segmentation correction, the mother cells monitored from birth to death are analyzed using 'cellfluo' function for analyzing the cellular fluorescence data.

4.2b.5 SEP determination based on Htb2-sfGFP fluorescence signal

The SEP can also be determined based on the breaking point of fluorescence increment for sgf73Δ mutant. Firstly, use the customized 'findPEAKbyflu' function to locate the fluorescence basal level after each cell division based on 'findpeaks' function. Then a round of manual correction is required to locate the fluorescence signal and verify the cell division event. Lastly, based on the piece-wise linear regression principle, the increasing point where fluorescence starts to increase can be determined and defined as SEP. The function is called 'findSEP_flonly'.

4.3a. H2O2 hormetic ageing time-lapse experiment

The H2O2 hormetic ageing time-lapse experiment is the ageing experiment performed under the media containing various H2O2 mild concentration. The cells are cultured in SC+2% dextrose condition before injecting into the microfluidic chip. The frame interval is 10 minutes and the total time-lapse experiment lasts for more than 140hrs. However, these cells are not included for ageing analysis, the cells analyzed are born in the H2O2 media without an induction of oxidative stress.

The parameters of 2 channels are identical to the ageing time-lapse experiment: phase contrast: 20ms exposure time, no binning; GFP channel is optional depending on the strain used: 5% laser excitation (wavelength 470nm): 50ms exposure time and binning 2*2.

4.3b. RLS and SEP determination analysis (refer to part 4.2b)

4.4a. DAPI staining for DNA quantification at the end of time-lapse experiment

The DAPI staining time-lapse an additional experiment is by performing the DAPI staining at the end of ageing time-lapse experiment. The ageing time-lapse experiment allows to monitor the replicative ages of the mother cells in the microfluidic device. The DAPI fluorescence allows to measure the DNA quantity in both pre-SEP and post-SEP mother cells. The freshly prepared DAPI solution 2.5µg/mL is used for cell incubation in microfluidic system for 35 minutes under the flow rate 5µL/min right after the ageing time-lapse experiment. Then the cells are washed 10 minutes with SC+2%Dextrose medium at 5µL/min and 20-minute at 10µL/min. 2 rounds of images are taken for each position continuously, 5 stacks are taken to ensure the total DAPI fluorescence signal (Figure 7.4). The five stacks are determined according to the middle plane, then equally distributed 4 extra planes so that the highest and lowest planes show a range of 3µm height. The DNA is not homogeneously distributed in the nucleus region, therefore, by constructing max projection of 5 stacks, the signal of DNA within the nucleus can be better quantified.

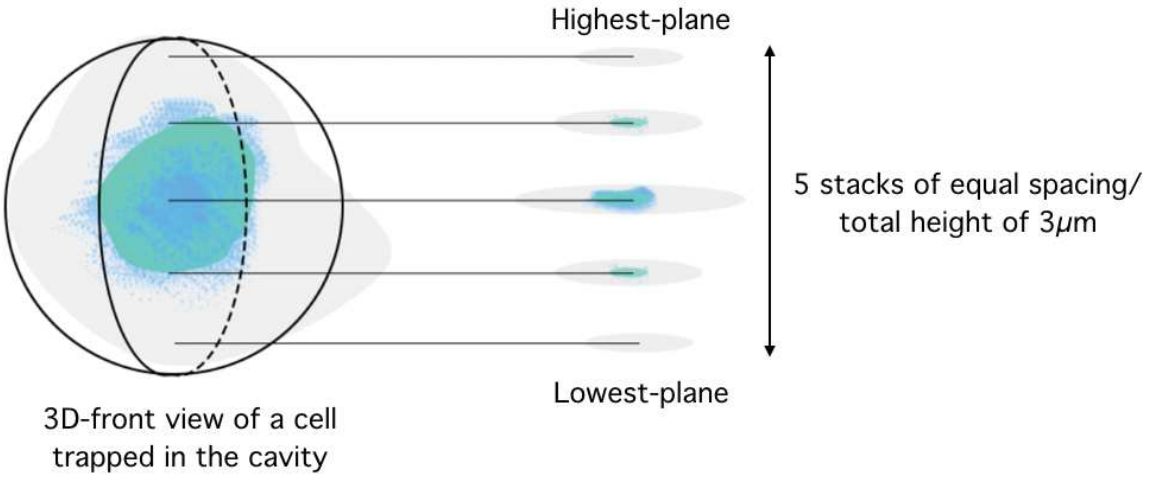

Figure 7.4 Five stacks are taken for DAPI fluorescence max-projection quantification

The cell trapped in the cavity show a nuclear volume containing DNA. The green indicates the nuclear volume of a mother cell. The blue incites the DAPI stained DNA both in nucleus and mitochondrion. Five stacks are taken for DAPI fluorescence signal precise quantification. Using the perfect focus system of NIS, based on the middle plane 4 extra planes equally distributed so that the highest and lowest planes show the range of 3µm height. In total, five planes are taken for DAPI maxi-projection quantification. The DAPI fluorescence is collectively projected to a single plane and analyzed.

Three channels are used for this experiment: phase contrast: 20ms exposure time, no binning; GFP: 7% laser excitation (wavelength 470nm): 50ms exposure time and binning 2*2; DAPI: 50% laser excitation (wavelength 350nm): 100ms exposure time and binning 2*2. Two frames are taken continuously for each position.

4.4b. DAPI fluorescence/ DNA quantification analyses

The images of Nikon (nd2) format is firstly converted to Matlab jpeg format, the DAPI fluorescence channel is collectively analyzed by projecting the five stacks using the 'tiffToMatlabProject' function. Secondly, the nuclear contour is automatically segmented by '720' Htb2-sfGFP fluorescence density threshold. A round of manual correction for the contour segmentation is necessary for the data precision. Thirdly, using the 'analysedapi'

function, both Htb2-sfGFP and DAPI fluorescence within the nuclear contour of each cell can be quantified.

Based on the video of ageing experiment, the age and the SEP status of each mother cell can be analyzed. Lastly, the DAPI and Htb2-sfGFP fluorescence data are analyzed and compared between pre-SEP and post-SEP mother cells.

4.5a. Htb2-sfGFP CCP quantification time-lapse experiment

To quantify the CCP duration, the fluorescence of H2b protein is measured each 3 minutes for a precise temporal precision compare to ageing time-lapse experiment. To avoid large file stockage and the photo-toxicity induced above 50hrs under such high laser excitation frequency, the number of frames taken within each time-lapse experiment is usually limited within 1000 frames. Therefore, a total of 50-hour cell ageing process can be monitored for each time-lapse experiment. It takes about 24hrs for the microfluidic chip to be filled with budding yeast and yeast cells may be trapped in the cavity. The acquisition starts after 1 days of cell growth in microfluidic chip when most cavities are filled with cells.

Two channels are used for time-lapse experiment: phase contrast: 20ms exposure time, no binning; GFP: 7% laser excitation (wavelength 470nm): 50ms exposure time and binning 2*2.

4.5b. Htb2-sfGFP CCP quantification analyses

4.5b.1 Cell cycle duration, SEP determination for CCP quantification analysis (automated)

Firstly, the sequence of Nikon images (nd2) are converted into Matlab jpeg project and video. This code belongs to the ‘autotrack’ function that was developed by Dr. Gilles CHARVIN. Secondly, the cellular and nuclear contours are automatically detected by phase contrast and green fluorescence threshold at ‘1000’. A round of manual correction for the contour segmentation is necessary for the data precision. Thirdly, the Htb2-sfGFP nuclear fluorescence data can be quantified by ‘incellfluo’ function. Then two different approaches of analyses are used in the thesis report.

Automated cell cycle duration and SEP determination is performed using ‘plotFLuo’ function. This approach is based on Htb2-sfGFP fluorescence signal exclusively (Figure 7.5A). The cell

cycle duration is determined based on the anaphase nuclear separation by automated fluorescence signal using 'findpeaks' function, the detected fluorescence peaks are represented by yellow arrows. The SEP is thus calculated based on the cell cycle duration by conventional 'findSEP' custom function (more detail for SEP determination confer 4.2b section). However, as shown from the figure 7.5A, the detected fluorescence peaks could be erratic due to irregular fluorescence signal at the end of cell cycle. The good detection is shown in yellow arrow, whereas the erratic detection is circled by dashed red circles. Therefore, without a round of manual correction, the cell cycle duration result may be not precise already.

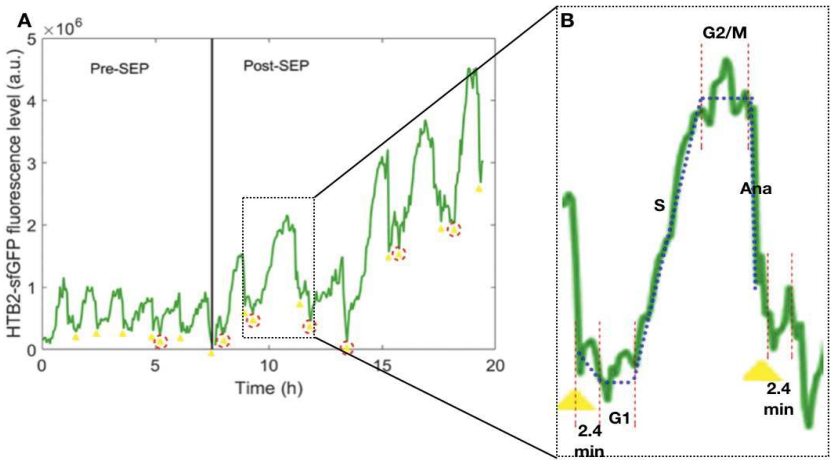

Figure 7.5 CCP quantification exclusively based on fluorescence and piece-wise linear regression

A: The Htb2-sfGFP fluorescence oscillatory signal showing 5 divisions before and after SEP. The SEP is indicated by the black line. The yellow arrow corresponding to the potential automated detection of fluorescence peaks by 'findpeaks' function. The yellow arrows correspond to the correct anaphases and the incorrect anaphases are circled by red dashed line.

B: The quantification of CCP based on the fluorescence detected anaphase. The corresponding linear pattern for each phase is shown in blue dashed line. Each phase is segmented by the red dashed line.

Next step, the cell cycles are cut into single cell cycles according to the previous detection and the CCPs are measured based on piece-wise linear regression using 'BFSK' function. As shown in the figure 7.5B, the fluorescence signal is fitted into the different 'shape' pattern corresponding to different phases as shown in blue dashed line. The yellow arrow indicates the nuclear separation determined at anaphase, the duration between anaphase and cytokinesis has been measured using the Cdc10-mCherry reporter strain (unpublished data) which is on average 2.4 minutes. Therefore, the cell cycle starts from the determined fluorescence peak (yellow arrow) + 2.4 minutes, then followed by the piece-wise linear

regression corresponding to the horizontal G1 phase, increasing kinetic S phase, horizontal G2/M phase and lastly anaphase and the cytokinesis (decreasing kinetic + 2.4 minutes). Each CCP can be thus quantified.

The CCP duration corresponding to the 5 divisions before and after SEP are compared and analyzed (Figure 7.6). The kinetic of each CCP can is represented. This approach shows less precise cell cycle duration which is shorter than previous result (Garmendia-Torres, Tassy et al. 2018). The mother cells die five divisions after SEP on average, the number of divisions post-SEP is much less than pre-SEP cell cycles. In addition, after ruling out irregular fluorescence pattern of certain post-SEP cell cycles, the result is measured based on much less effective for post-SEP mothers.

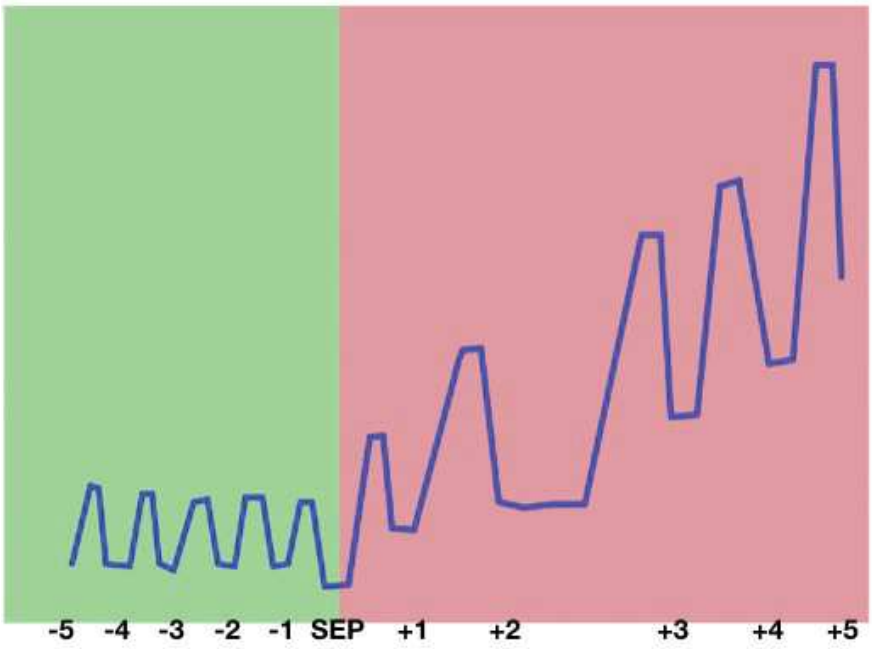

Figure 7.6 CCP quantification using automated fluorescence-based approach

Five divisions before and after SEP are *analyzed* for CCP comparison. The dynamic of each CCP evolution from SEP-5 division to SEP+5 division is *measured,* respectively.

4.5b.2 Cell cycle duration, SEP determination for CCP quantification analysis (manual)

To increase the precision and improve the measurement, an alternative approach is applied for CCP quantification using manual analysis for cell cycle determination. Using ImageJ, the cell division is determined at the end of mitosis which is represented by nuclear detachment

(Figure 7.7). This morphological signature allows to delimitate the cytokinesis closer than the fluorescence peak (anaphase) determined by automated approach.

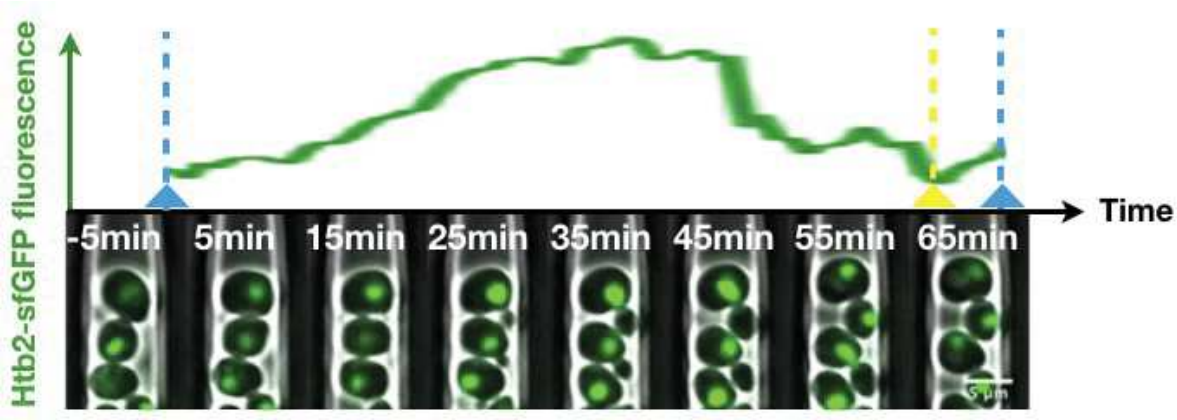

Figure 7.7 Cell cycle determination using manual determination in ImageJ

The cell division is defined by nuclear detachment morphology between mother and daughter cell (indicated by blue dashed line) analyzed by ImageJ. The Htb2-sfGFP fluorescent signal is cut according to the cell division as shown in green. The fluorescence-determined cell division is indicated by yellow arrow and dashed line.

The SEP is then analyzed using 'findSEP' function as previously described in section 4.2b. Then each cell cycle can be separated and analyzed for CCP quantification. As shown in the figure 7.8A, the cell division can be defined by blue arrow. As for single cell cycle, similar piece-wise linear regression method is applied for CCP quantification based on fluorescence signal pattern. The cell cycle starts as determined manually, then followed by the horizontal G1 phase, increasing kinetic S phase, then the horizontal G2/M phase, lastly the anaphase before next cell cycle, this mitosis and cytokinesis is quantified by the duration between the G2/M phase and next cell cycle. As shown in the figure 7.8B, each CCP is delimitated by red dashed line.

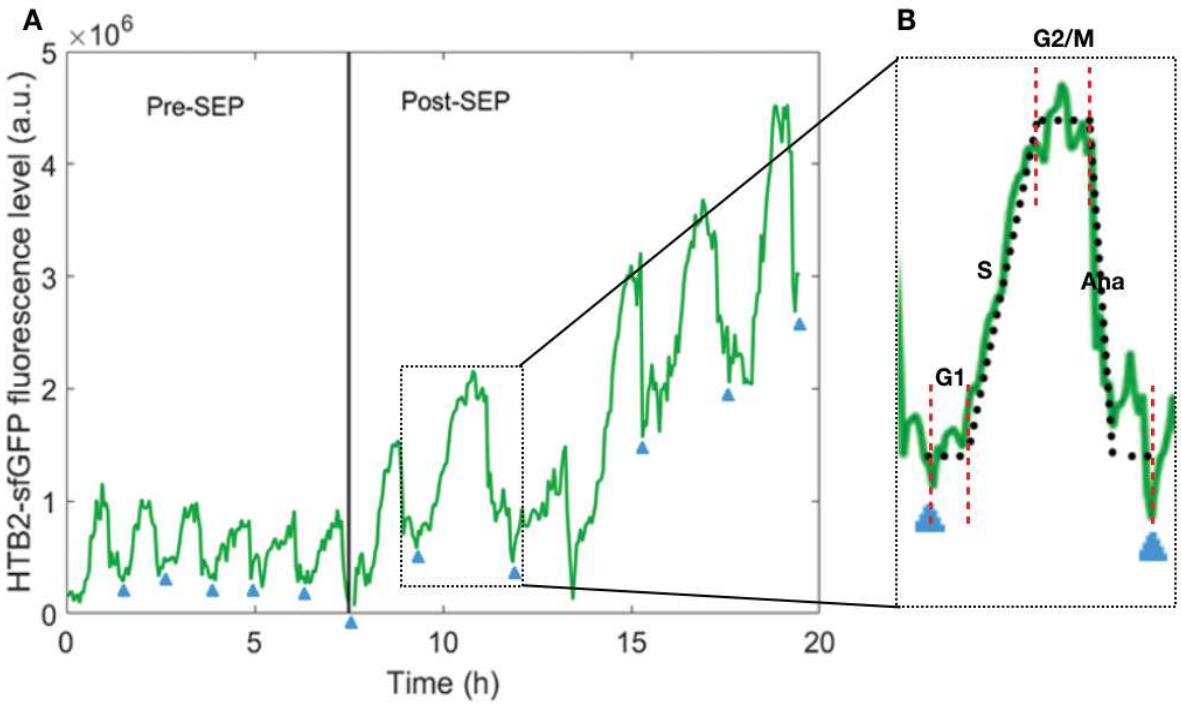

Figure 7.8 CCP quantification based on piece-wise linear regression

A: The blue arrows indicate the cell division determined by ImageJ manual analysis based on nuclear detachment between mother and daughter cells. The SEP is defined based on the cell cycle duration.

B: Each cell division is cut based on the blue arrow, each CCP is quantified using 'BFSK' function based on piece-wise linear regression. The linear regression fitting is shown in black dashed line, each phase is separated by red dashed line. The G1 and G2/M phases correspond to the horizontal duration, the increasing line for S phase and the rest is the anaphase until early cytokinesis (nuclear detachment after mitosis).

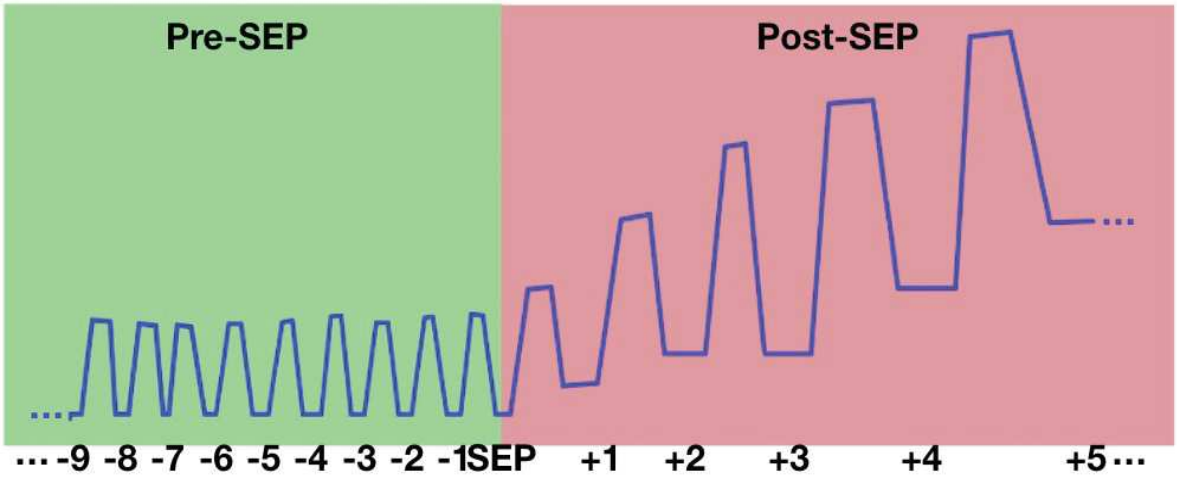

Figure 7.9 Comparison between pre-SEP and post-SEP cells

The cell cycles before and after SEP are compared by pooling two group of data. More cell cycles allowing a more accurate quantification between each CCP.

The comparison of CCP is performed between pre-SEP and post-SEP cells as shown in figure 7.9.

4.6a. Whi5-GFP CCP quantification time-lapse experiment

This time-lapse experiment with Whi5-GFP is for comparing the G1 phase duration before and after SEP by using Whi5-GFP reporter strain. To quantify the CCP duration, the images are taken for each 3 minutes. A total of 50-hour cell ageing process is monitored for each time-lapse experiment (1000 frames).

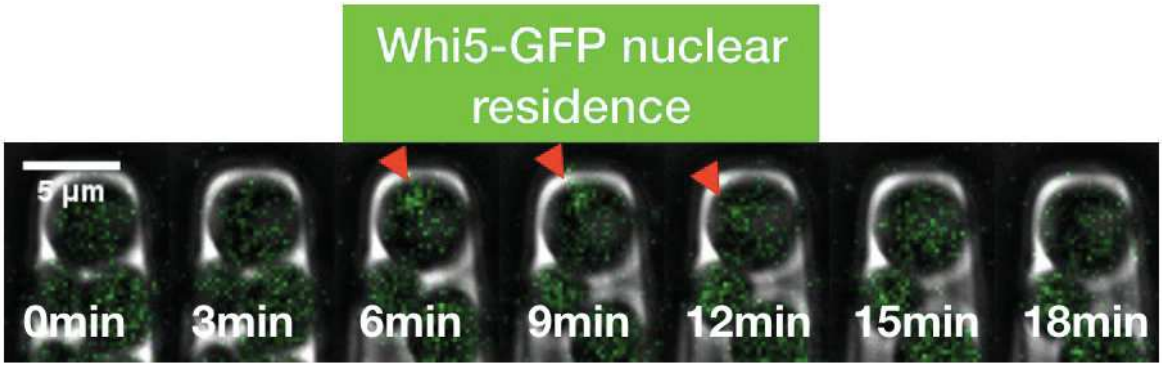

Figure 7.10 Whi5-GFP nuclear residence analysis in ImageJ

The G1 phase measured by Whi5-GFP protein nuclear residence is analysed directly by eye in ImageJ. The duration corresponds to the number of frames showing Whi5-GFP nuclear fluorescence accumulation which indicated by red arrow.

Two channels are used for time-lapse experiment:

phase contrast: 20ms exposure time, no binning. Due to the weak Whi5-GFP signal and meanwhile avoid the photo-damage, the GFP channel is set to 8% laser excitation (wavelength 470nm): 80ms exposure time, binning 2*2.

4.6b. Whi5-GFP nuclear residence CCP quantification

The images (nd2) are converted to Matlab jpeg format and avi video. The Manual cell cycle duration and SEP determination is performed using ImageJ as previously described by counting the number of frames between each cell division the video clip. The SEP is determined using 'findSEP_Jia' function as described in section 4.2b.

The Whi5-GFP nuclear residence state is analyzed by eyes on ImageJ directly (Figure 7.10). The number of frames showing significant nuclear fluorescence accumulation correspond to

the relative-G1 phase duration. To increase the precision of CCP quantification, the pre-SEP and post-SEP cell cycles are pooled to quantify the average CCP duration in Whi5-GFP reporter strain.

4.7a. DNA damage positive control time-lapse experiment

This time-lapse experiment is performed in microfluidic chip for testing the DNA damage reporter for 10hrs. The Rnr3-GFP and Ddc2-GFP are the strains tested (7.11A). 24hrs after injecting cells into the microfluidic device, the cells are filled in the cavities. The time-lapse experiment is set to take each image every 10 minutes, identical to the ageing experiment. For the first 5hrs, the growth of cells is monitored under normal SC+2% dextrose media as the control. Then the cells are incubated under DNA damaging agents such as H2O2 0.4mM (which induce most various cell fates according to Goulev et al., 2017) and 1000µg/mL zeocin antibiotic for up to 5hrs.

Another DNA damage positive control is performed by H2O2 0.2mM (which induce maximal magnitude of Yap1-regulated oxidative stress defense activation from Goulev et al., 2017) for testing the oxidative stress response in microfluidic device. The Srx1-GFP and Tsa1-GFP are firstly injected into microfluidic chip and grow under SC+2% dextrose media for 24hrs. Then the time-lapse acquisition is set to take each image every 10 minutes, identical to the ageing experiment. For the first 2hrs, the cells are monitored for control condition, then incubated under H2O2 0.2mM for more than 10 hrs (to monitor the stable state under oxidative stress).

2 channels are used throughout this experiment, the parameters for each channel were set as below: phase contrast: 20ms exposure time, no binning; GFP: 7% laser excitation (wavelength 470nm): 50ms exposure time and binning 2*2.

4.7b. DNA damage response (DDR) activation analysis and fluorescence analysis

Firstly, the images (nd2) of both strains are converted into Matlab jpeg format and avi video using the code developed by Dr. Gilles CHARVIN in 'autotrack'. Secondly the cellular contour is segmented by phase contrast threshold. A round of manual correction for the contour segmentation is necessary for the data precision. Thirdly, the fluorescence signal of interested mother cells are analyzed by eye for Ddc2-GFP reporter strain or using 'cellfluo' function for Rnr3-GFP reporter strain.

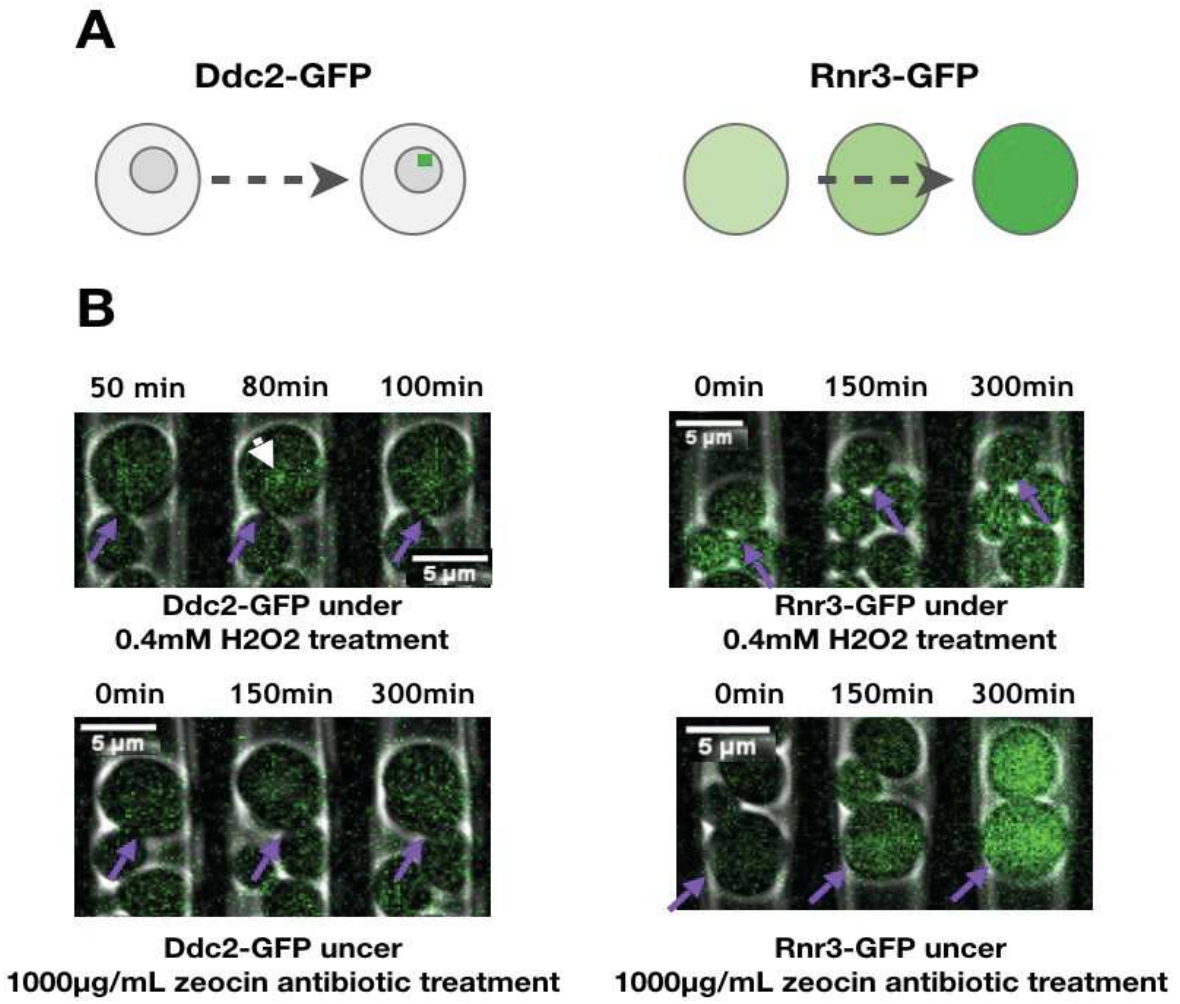

Figure 11 DDR activation induced in Ddc2-GFP and Rnr3-GFP reporter strains by DNA damaging agents

A: Schematic DDR activation fluorescence evolution in both reporter strains.

B: Two strains are treated under both 0.4mM H2O2 media and 1000µg/mL zeocin antibiotic for 5hrs. The images show representative fluorescence evolution in both strains. The interested mother cells are indicated by violet arrows. The nuclear foci may be observed in Ddc2-GFP strain under both condition yet the nuclear foci (indicated by white arrow) is not stable and can be lost easily from the view. The fluorescence burst can be observed mostly in Rnr3-GFP under zeocin antibiotic treated condition.

The persistence of nuclear foci cannot be observed in Ddc2-GFP reporter strain after the DNA damaging agent-treatment (7.11B). In addition, to avoid the photo-damage, the excitation fluorescence signal cannot be increased, which lead to weak fluorescence signal. Therefore, this reporter strain is not suitable for monitoring the DDR activation in microfluidic ageing experiment.

The Rnr3-GFP reporter strain under zeocin antibiotic treatment show most significant fluorescence burst which last more than 1hr (Figure 7.11B). Rnr3-GFP is therefore used for studying the DDR activation during ageing process in microfluidic device in the next step.

However, the cellular Rnr3-GFP fluorescence show heterogeneous basal level without stress due to its oscillatory expression pattern involved in DNA synthesis. The Rnr3-GFP strain also shows a large variety of DDR activation kinetic under zeocin antibiotic treatment. Therefore, the basal zeocin fluorescence level is compared with 5-hour-treated Rnr3-GFP fluorescence for deterring the DDR activation threshold (Figure 7.12A). The threshold of DDR activation in Rnr3-GFP reporter strain is set by DNA damage maximum fluorescence level minus the median basal level, which equals to 26 a.u. (Figure 7.12B).

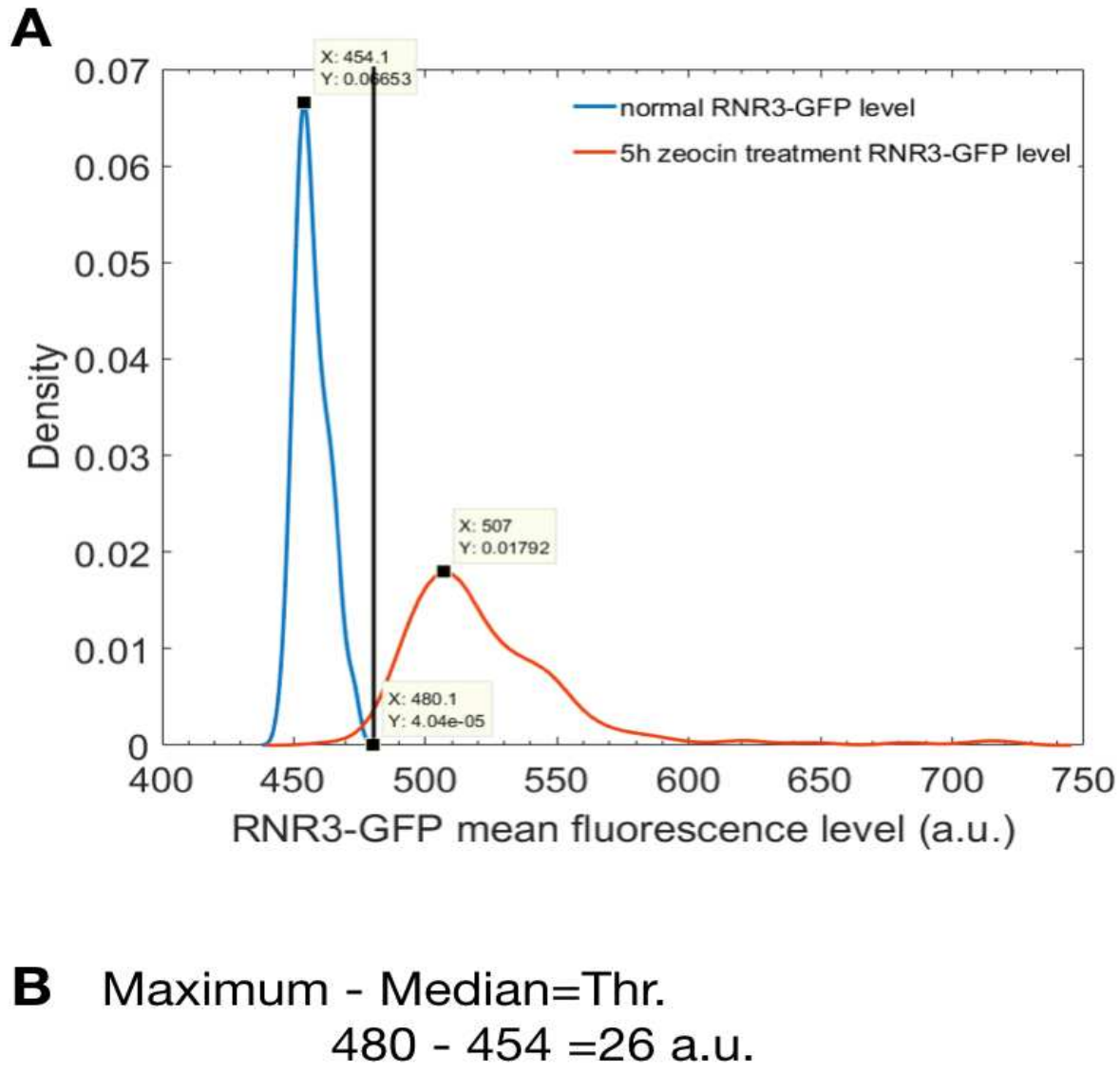

Figure 7. 12 Threshold determination for Rnr3-GFP DDR activation under zeocin antibiotic treatment

A: The smoothed density distribution of control (in blue) and positive control (in orange) (5h under zeocin treatment) comparison.

B: The threshold for DDR activation is set to 26 a.u. measured by maximum minus median control fluorescence signal.

Table 7.4 Summary table of image processing analyses and Matlab functions

Summary of analysis procedure	nd2/tiff to jpeg Matlab project	jpeg to avi video and ImageJ analysis	cellular & nuclear segmentation and cell tracking	fluorescence quantification
Function	nd2ToMatlabProject4/ tiffToMatlabProject	exportMontage/ ecdf/NotBoxPlot/ Tabtrajiso(_Jia)/ findSEP (_Jia)	autotrack (at_batch)	phyloCell_mainGUI/ cellfluo/ incellfluo/ analysedapi/ plotFLuo (findpeaks/BFSK)/ findPEAKbyflu/ findSEP_flonly'
Analysis		RLS analysis/ survival curve/ boxplot of RLS/ cell cycle duration trajectory/ SEP determination/ CCP quantification (in Whi5-GFP0/	cellular & nuclear segmentation and cell tracking	Manual correction by GUI; cellular and nuclear contour-measurement/ DAPI fluorescence quantification/ CCP quantification/ SEP determination (for sgf73 Δ)

5. Code Annex

5.1 Online published resources

'Phylocell' and 'autotrack' functions has been developed by Dr. Gilles CHARVIN (Fehrmann et al., 2013) , the code can be found from the link: https://github.com/gcharvin/autotrack.

'ecdf' function belongs to the Matlab code (see link: https://www.mathworks.com/help/stats/ecdf.html).

'NotBoxPlot' function has been published by Rob Campbell (see link: https://www.mathworks.com/matlabcentral/fileexchange/26508-notboxplot).

5.2 unpublished code that has been developed by other authors (request the lab for more information)

'nd2ToMatlabProject', 'exportMontage', 'cellfluo' and 'incellfluo', 'Tabtrajiso','findSEP', 'findPEAK (findPEAKbyflu)', 'tiffToMatlabProject', 'analysedapi', 'plotFLuo' and 'plotFLuo_noSEP', functions were developed by the lab members.

5.3 customized code in this work

'Tabtrajiso_Jia':

```
function tabtrajiso_Jia(tab)
%tab=matrix, each line corresponds to a cell with successive values of cell
%cycle duration in min
ytick=[];
 h=figure;
map=zeros(256,3);
% map(1,:)=[0,1,0];
% map(256,:)=[1,0,0];
R0to256=linspace(0,1,256);
G0to256=1-R0to256;
```

```
map(:,1)=R0to256;
map(:,2)=G0to256;
col2=colormap(map);
cc2=1;
 for i=1:size(tab,1)
       tabtemp1(i,:)=[length(tab(i,:))-sum(isnan(tab(i,:))) tab(i,:)];
 end
%  tabtemp2=tabtemp1';
%  [values,order]=sort(tabtemp2(:,1));
%  tabsort=tabtemp2(order);
%  tabsort=tabsort'
[values,order]=sort(tabtemp1(:,1));
tabsort=tabtemp1(order,:);
for i=1:size(tabsort,1)
       startY=i;
       ytick=[ytick startY];
  cindex=ones(1,length(tabsort(i,:))-1-sum(isnan(tabsort(i,:))));
 T=numel(cindex);
 R=ones(T,1);
      for j=1:(length(tabsort(i,:))-2-sum(isnan(tabsort(i,:))))
        t=uint8(round(255*(tabsort(i,j+1))/250));
        cindex(j)=max(1,t);
        R(j+1)=R(j)+R(j+1);
      end
   tf=uint8(round(255*(tabsort(i,length(tabsort(i,:))-sum(isnan(tabsort(i,:))))/250)));
   cindex(length(tabsort(i,:))-1-sum(isnan(tabsort(i,:))))= max(1,tf) ;
   temp2=[0;R];
```

```
   R1=temp2(1:(size(R)));

   rec=[R1 R];

   Traj(rec,'Color',col2,'colorindex',cindex,'tag',['Cell ' ],h,'width',0.95,'startX',0,'startY',start
Y,'sepColor',[0.1 0.1 0.1],'sepwidth',0.07,'gradientwidth',0);

end

  set(gca,'YTick',ytick);

   axis tight;

   hold on

%    colorbar('Units','pixels',...

%     'Ticks',[0 0.0625 0.125 0.1875 0.25 0.3125 0.375 0.4375 0.5 0.5625 0.625 0.6875 0.75
0.8125 0.875 0.9375 1],...

%    'TickLabels',{'<=0','16','32','48','64','80','96','112','128','144','160','176','192','208','224',
'240','>=256'});

   caxis([0,1])

colorbar('southoutside','Units','pixels',...
```

‘findSEP_Jia’:

```
function [t1 t2 mid x y tdiv fdiv]=findSEP_Jia(tab,l,display)

%dau=[tcells(cellindex).daughterList];

t1=[];

t2=[];

x=[];

y=[];

tdiv=[];

fdiv=[];

%    if numel(dau)==0

%       return;

%    end

tdiv=tab(l,:);
```

```
tdiv=tdiv(tdiv>0);
if numel(tdiv)==0
    return;
end
   fdiv=1./tdiv;
    test=fdiv;
    %test(end+1)=0.001;
    [t1 t2 level1 level2 curve]=fitSenescenceModel(test,0,0);

   % [sp v] = spaps(1:length(fdiv),fdiv,0.002);
    %
   % t1,t2,level1,level2
    %
    if level2<=0.08 %0.09
        % senesence case
        %mid=(t1+t2)/2
        mid=find(curve<level1-0.0,1,'first'); % 0.03
        mid=t1;
        if numel(mid)==0
            mid=round((t1+t2)/2);
        end
        mid=min(length(fdiv),mid);
        %mid=t1;
        %mid=t1;
        x=1:1:length(fdiv);
        x=x-mid;
        % x=x-length(x);
```

```
        y=1./fdiv(1:end);
        % mid
        % plot(x,y,'Color',col(i,:)); hold on;
      else
        %continue
        x=1:1:length(fdiv);
        mid=length(x)+1;
        x=x-length(x);
        y=1./fdiv(1:end);
        t2=mid; t1=mid-1;
        %if length(fdiv
        %figure(h3); plot(x,1./y,'Color',col(i,:));
        %hold on;
       % plotFit(fdiv,t1,t2)
      end
      %plot(x,1./y,'Color',col(i,:));
     %%% plotFit(x,fdiv,t1,t2)
    %  return;
      if nargin==3
    h= plotFit(x,fdiv*6,t1,t2); %plot(x,v,'Color','g');
      end
function [t1 t2 level1 level2 curve]=fitSenescenceModel(fdiv,thr1,thr2)
chi2=zeros(size(fdiv));
fdiv(fdiv>0.2)=0.15;
for i=1:length(fdiv)-1
   for j=i+1:length(fdiv)
      %chi2=0;
```

```
        level1=mean(fdiv(1:i));
        level2=mean(fdiv(j:end));
        chi2(i,j)= sum((fdiv(1:i)-level1).^2)+sum((fdiv(j:end)-level2).^2);
        if j>i+1
           arrx=i:1:j;
           arry=(level1-level2)/(i-j)*arrx+(level2*i-level1*j)/(i-j);
           chi2(i,j)= chi2(i,j) + sum( (fdiv(i+1:j-1)- arry(2:end-1)).^2 );
        end
%          if i>8
%          plotFit(1:1:length(fdiv),fdiv,i,j);
%         a=chi2(i,j),i,j
%          pause
%          close
%          end
    end
end
pix=find(chi2==0);
chi2(pix)=max(max(chi2));
[m pix]=min(chi2(:));
%figure, plot(chi2(:));
[i j]=ind2sub(size(chi2),pix);
t1=i;
t2=j;
 %plotFit(1:1:length(fdiv),fdiv,i,j);
level1=mean(fdiv(1:i));
level2=mean(fdiv(j:end));
curve(1:i)=level1*ones(1,i);
```

```
%length(fdiv)-j
curve(j:length(fdiv))=level2*ones(1,length(fdiv)-j+1);
arrx=i:1:j;
arry=(level1-level2)/(i-j)*arrx+(level2*i-level1*j)/(i-j);
curve(i+1:j-1)=arry(2:end-1);
function h=plotFit(x,fdiv,i,j)
h=figure;
% h=subplot(2,1,1);
level1=mean(fdiv(1:i));
level2=mean(fdiv(j:end));
line1x=1:i; line1y=level1*ones(1,length(line1x));
line2x=j:length(fdiv); line2y=level2*ones(1,length(line2x));
if j>=i+1
   arrx=i:1:j;
   arry=(level1-level2)/(i-j)*arrx+(level2*i-level1*j)/(i-j);
end
plot(x,fdiv,'Marker','.','LineStyle','none','MarkerSize',20); hold on;
plot(line1x+x(1)-1,line1y,'Color','r','LineStyle','--'); hold on;
plot(line2x+x(1)-1,line2y,'Color','r','LineStyle','--');  hold on;
if j>=i+1
   plot(arrx+x(1)-1,arry,'Color','r','LineStyle','--'); hold on;
end
k = arry(2)-level1
if k <= -0.0025;
elseif k > -0.0025
   disp('no SEP was found due to k > -0.0025')
   return
```

```
end
if fdiv(j-1) < 1/120 && fdiv(j) < 1/120;
   disp( 'no SEP was found due to 120 min cell cycle')
   return
end
```

‘findSEP_fluonly’:

```
function findSEP_flonly(Min,flu,ibf);%find out the SEP moment by fluorescence
%based on the peaks of fluorescence valeys, find out the increasing point
%where fluorescence starts to increase
%Min is the result of findPEAK containing two vectors corresponding to
%peaks and their locations
%ibf is the minutes in between frame
[~,n] = size(Min);
pks=(Min(1,:)) ;
dd=diff(pks); %diff of peaks
cc=diff(Min(2,:)*ibf);
% figure; findchangepts(pks,'Statistic','std')
% count=findchangepts(pks,'Statistic','std'); %Find potential SEP by std variation
% %Generally, the result is later than the real SEP.
% count
if cc(n-2)<120 && cc(n-1)<120;      %the last 2 cell cycles are less than 120 minutes.
  display 'no SEP is found'
elseif cc(n-2)>=120 && cc(n-1)>=120;
end
% for j=count;
%     if dd(j)>=m_ddpre+err_ddpre;  %if the fluo level is excluded of the mean domain, then
```

```
%                       %SEP could be the previous cell cycle; else if the
%                       %fluo level is included in the mean domain, then SEP
%                       %could be the current cell cycle.
%
%           count=count-1;
%    elseif m_ddpre-err_ddpre<dd(j)<m_ddpre+err_ddpre;
%    end
% end
%
% i=count;
%    if dd(i)<=dd(i-1);
%      count=count-1;
%
%    elseif dd(i)>dd(i-1);%if the fluo level is greater than previous, then
%                  %SEP could be the current cell cycle.
%    end
%
% for k=count;
%    if cc(k)>m_ccpre+err_ccpre;  %if current cell cycle duration is larger than the
%                       %previous one, the SEP could be the previous
%                       %cell cycle; else if current cell cyce duratio
%                       %is less than the previous one, the SEP could
%                       %be the next cell cycle.
%      count = count -1;
%    elseif cc(k)< m_ccpre-err_ccpre;
%      count = count+1;
%    elseif m_ccpre-err_ccpre<=cc(k)<=m_ccpre+err_ccpre;  %if the cell cycle
```

```
%                                       %duration is within
%                                       %normal range then
%                                       %compare with next
%                                       %cell cycle
%       if cc(k)>=cc(k+1);          %cell cycle duration is increased at
%                               %SEP+1 moment,so next cell cycle
%                               %duration of SEP must be longer.
%          count =count+1;
%       elseif cc(k)<cc(k+1);
%       end
%
%    end
% end
X=Min(2,:);
plot(X,pks,'Marker','.','LineStyle','none','MarkerSize',20); hold on;
      nknots = 2;
      fixknots = [];
      k = 2;
      clear shape
      % function horizonal
      lo(1) = 0; up(1) = 0;
      lo(2) = 0; up(2) = +inf;
      % Function forced to have followh values
      %    s(0)=1, s(3/2)=1, s(2)=2
      %    s'(0)=1 s'(3)=1
%       pntcon(1) = struct('p', 0, 'x', [0 1.5 3], 'v', [0 1 2]);
%       pntcon(2) = struct('p', 1, 'x', [0 3], 'v', 1);
```

```
      shape = struct('p',1,'lo',lo,'up',up);
%       options = struct('animation', 1, ...
%           'figure', 1, ...
%           'waitbar', 1, ...
%           'display', 1, ...
%           'd', 1, 'lambda', 0e-3, 'regmethod', 'c', ...
%           'qpengine', '', ...
%           'sigma', [], ...
%           'shape', shape);
pp = BSFK(X, pks, k, nknots, fixknots)  %piecewise linear fit (2 knots)
[ d, ix ] = min( abs( X- pp.breaks(2) ) ); ix %the nearest index of X(cc)
line1y=ones*mean(pks(1:ix));  %mean fluo before SEP
plot([X(1) X(ix)],[line1y line1y],'Color','r','LineStyle','--'); hold on;
plot([X(ix) X(n)],[line1y pks(n)],'Color','r','LineStyle','--');  hold on;
%plot((flu(1,:)*6),flu(3,:),'Color','g','LineStyle','-');
plot(flu ,'Color','g','LineStyle','-');
% Create xlabel
xlabel('Frame');
% Create ylabel
ylabel('Fluorescence (A.U.)');   hold off
```

Bibliography

Aguilaniu, H., et al. (2003). "Asymmetric inheritance of oxidatively damaged proteins during cytokinesis." Science 299(5613): 1751-1753.

Carbonylated proteins were visualized in single cells of the budding yeast Saccharomyces cerevisiae, revealing that they accumulate with replicative age. Furthermore, carbonylated proteins were not inherited by daughter cells during cytokinesis. Mother cells of a yeast strain lacking the sir2 gene, a life-span determinant, failed to retain oxidatively damaged proteins during cytokinesis. These findings suggest that a genetically determined, Sir2p-dependent asymmetric inheritance of oxidatively damaged proteins may contribute to free-radical defense and the fitness of newborn cells.

Allshire, R. C., et al. (1989). "Human telomeres contain at least three types of G–rich repeat distributed non-randomly." Nucleic Acids Research 17(12): 4611-4627.

Allsopp, R. C., et al. (1995). "Telomere shortening is associated with cell division in vitro and in vivo." Experimental cell research 220(1): 194-200.

Allsopp, R. C., et al. (1992). "Telomere length predicts replicative capacity of human fibroblasts." Proceedings of the National Academy of Sciences 89(21): 10114-10118.

Anderson, R. M., et al. (2009). "Caloric restriction and aging: studies in mice and monkeys."

Toxicologic pathology 37(1): 47-51.

Arlia-Ciommo, A., et al. (2018). "Caloric restriction delays yeast chronological aging by remodeling carbohydrate and lipid metabolism, altering peroxisomal and mitochondrial functionalities, and postponing the onsets of apoptotic and liponecrotic modes of regulated cell death." Oncotarget 9(22): 16163.

Arlia-Ciommo, A., et al. (2014). "Quasi-programmed aging of budding yeast: a trade-off between programmed processes of cell proliferation, differentiation, stress response, survival and death defines yeast lifespan." Cell Cycle 13(21): 3336-3349.

Ashrafi, K., et al. (1999). "Passage through stationary phase advances replicative aging in Saccharomyces cerevisiae." Proceedings of the National Academy of Sciences 96(16): 9100-9105.

Austad, S. N. (2010). "Cats,“rats,” and bats: the comparative biology of aging in the 21st

century." Integrative and comparative biology 50(5): 783-792.

Ayala, A., et al. (2014). "Lipid peroxidation: production, metabolism, and signaling mechanisms of malondialdehyde and 4-hydroxy-2-nonenal." Oxidative medicine and cellular longevity 2014.

Baccolo, G., et al. (2018). Mitochondrial metabolism and aging in yeast. International review of cell and molecular biology, Elsevier. 340: 1-33.

Baker, D. J., et al. (2016). "Naturally occurring p16 Ink4a-positive cells shorten healthy lifespan." Nature 530(7589): 184-189.

Ball, D. A., et al. (2011). "Oscillatory dynamics of cell cycle proteins in single yeast cells analyzed by imaging cytometry." PloS one 6(10): e26272.

Bassett Jr, D. E., et al. (1996). "Exploiting the complete yeast genome sequence." Current Opinion in Genetics & Development 6(6): 763-766.

Baumbach, L. L., et al. (1987). "Regulation of human histone gene expression: transcriptional and posttranscriptional control in the coupling of histone messenger RNA stability with DNA replication." Biochemistry 26(19): 6178-6187.

Baur, J. A., et al. (2001). "Telomere position effect in human cells." Science 292(5524): 2075-2077.

Bean, J. M., et al. (2006). "Coherence and timing of cell cycle start examined at single-cell resolution." Molecular cell 21(1): 3-14.

Ben-Porath, I. and R. A. Weinberg (2004). "When cells get stressed: an integrative view of

cellular senescence." The Journal of clinical investigation 113(1): 8-13.

Birben, E., et al. (2012). "Oxidative stress and antioxidant defense." World Allergy Organization Journal 5(1): 9-19.

Biteau, B., et al. (2003). "ATP-dependent reduction of cysteine–sulphinic acid by S. cerevisiae sulphiredoxin." Nature 425(6961): 980.

Bitterman, K. J., et al. (2003). "Longevity regulation in Saccharomyces cerevisiae: linking metabolism, genome stability, and heterochromatin." Microbiol. Mol. Biol. Rev. 67(3): 376-399.

Borodkina, A., et al. (2018). "“Social life” of senescent cells: what is SASP and why study it?" Acta Naturae (англоязычная версия) 10(1 (36)).

Borodkina, A., et al. (2014). "Interaction between ROS dependent DNA damage, mitochondria and p38 MAPK underlies senescence of human adult stem cells." Aging (Albany NY) 6(6): 481.

Bringold, F. and M. Serrano (2000). "Tumor suppressors and oncogenes in cellular senescence☆." Experimental gerontology 35(3): 317-329.

Buck, S. W., et al. (2002). "RNA polymerase I propagates unidirectional spreading of rDNA silent chromatin." Cell 111(7): 1003-1014.

The ribosomal DNA (rDNA) tandem array in Saccharomyces cerevisiae induces transcriptional silencing of RNA polymerase II-transcribed genes. This SIR2-dependent form of repression (rDNA silencing) also functions to limit rDNA recombination and is involved in life span control. In this report, we demonstrate that rDNA silencing spreads into the centromere-proximal unique sequence located downstream of RNA polymerase I (Pol I) transcription but fails to enter the upstream telomere-proximal sequences. The preading of silencing correlates with SIR2-dependent histone H3 and H4 deacetylation and can be extended by SIR2 overexpression. Surprisingly, rDNA silencing required transcription by RNA polymerase I and the direction of spreading was controlled by the direction of Pol I transcription.

Buffenstein, R. (2005). "The naked mole-rat: a new long-living model for human aging

research." The Journals of Gerontology Series A: Biological Sciences and Medical Sciences 60(11): 1369-1377.

Burtner, C. R., et al. (2011). "A genomic analysis of chronological longevity factors in budding yeast." Cell Cycle 10(9): 1385-1396.

Campisi, J. (2005). "Senescent cells, tumor suppression, and organismal aging: good citizens,

bad neighbors." Cell 120(4): 513-522.

Campisi, J. (2013). "Aging, cellular senescence, and cancer." Annual review of physiology 75:

685-705.

Campisi, J. and F. D. A. Di Fagagna (2007). "Cellular senescence: when bad things happen to good cells." Nature reviews Molecular cell biology 8(9): 729-740.

Case, A. and A. Deaton (2017). "Mortality and morbidity in the 21st century." Brookings papers on economic activity 2017(1): 397-476.

Chance, B. and H. Sies (1979). "Boveris a. Hydroperoxide metabolism in mammalian organs." Physiol. Rev 59: 527-605.

Chang, F. and D. G. Drubin (1996). "Cell division: why daughters cannot be like their mothers." Current biology 6(6): 651-654.

Chapagain, D., et al. (2018). "Cognitive aging in dogs." Gerontology 64(2): 165-171.

Chen, K. L., et al. (2017). "Microfluidic technologies for yeast replicative lifespan studies." Mechanisms of ageing and development 161: 262-269.

Chondrogianni, N. and E. S. Gonos (2004). "Proteasome inhibition induces a senescence-like phenotype in primary human fibroblasts cultures." Biogerontology 5(1): 55-61.

Collado, M., et al. (2007). "Cellular senescence in cancer and aging." Cell 130(2): 223-233.

Colman, R. J. (2018). "Non-human primates as a model for aging." Biochimica et Biophysica Acta (BBA)-Molecular Basis of Disease 1864(9): 2733-2741.

Colman, R. J., et al. (2009). "Caloric restriction delays disease onset and mortality in rhesus monkeys." Science 325(5937): 201-204.

Conrad, M., et al. (2014). "Nutrient sensing and signaling in the yeast Saccharomyces cerevisiae." FEMS microbiology reviews 38(2): 254-299.

Coppé, J.-P., et al. (2010). "The senescence-associated secretory phenotype: the dark side of tumor suppression." Annual Review of Pathology: Mechanisms of Disease 5: 99-118.

Coppé, J.-P., et al. (2008). "Senescence-associated secretory phenotypes reveal cell-nonautonomous functions of oncogenic RAS and the p53 tumor suppressor." PLoS biology 6(12).

Correia-Melo, C. and J. F. Passos (2015). "Mitochondria: are they causal players in cellular senescence?" Biochimica et Biophysica Acta (BBA)-Bioenergetics 1847(11): 1373-1379.

Davidson, J. F., et al. (1996). "Oxidative stress is involved in heat-induced cell death in Saccharomyces cerevisiae." Proceedings of the National Academy of Sciences 93(10): 5116-5121.

De Bruin, R. A., et al. (2004). "Cln3 activates G1-specific transcription via phosphorylation of the SBF bound repressor Whi5." Cell 117(7): 887-898.

Defossez, P.-A., et al. (1999). "Elimination of replication block protein Fob1 extends the life span of yeast mother cells." Molecular cell 3(4): 447-455.

Delaunay, A., et al. (2002). "A thiol peroxidase is an H2O2 receptor and redox-transducer in gene activation." Cell 111(4): 471-481.

Denoth-Lippuner, A., et al. (2014). "Role of SAGA in the asymmetric segregation of DNA circles during yeast ageing." Elife 3: e03790.

di Fagagna, F. d. A. (2008). "Living on a break: cellular senescence as a DNA-damage response." Nature reviews cancer 8(7): 512-522.

di Fagagna, F. d. A., et al. (2003). "A DNA damage checkpoint response in telomere-initiated senescence." Nature 426(6963): 194-198.

di Fagagna, F. d. A., et al. (2004). "Functional links between telomeres and proteins of the DNA-damage response." Genes & development 18(15): 1781-1799.

Di Leonardo, A., et al. (1994). "DNA damage triggers a prolonged p53-dependent G1 arrest and long-term induction of Cip1 in normal human fibroblasts." Genes & development 8(21): 2540-2551.

Di Talia, S., et al. (2007). "The effects of molecular noise and size control on variability in the budding yeast cell cycle." Nature 448(7156): 947.

Dimri, G. P., et al. (1995). "A biomarker that identifies senescent human cells in culture and in aging skin in vivo." Proceedings of the National Academy of Sciences 92(20): 9363-9367.

Doncic, A., et al. (2011). "Distinct interactions select and maintain a specific cell fate." Molecular cell 43(4): 528-539.

Egilmez, N. K. and S. Jazwinski (1989). "Evidence for the involvement of a cytoplasmic factor in the aging of the yeast Saccharomyces cerevisiae." Journal of bacteriology 171(1): 37-42.

Epel, E. S., et al. (2004). "Accelerated telomere shortening in response to life stress." Proceedings of the National Academy of Sciences 101(49): 17312-17315.

Erjavec, N., et al. (2007). "Accelerated aging and failure to segregate damaged proteins in Sir2 mutants can be suppressed by overproducing the protein aggregation-remodeling factor Hsp104p." Genes & development 21(19): 2410-2421.

Fabian, D. and T. Flatt (2011). "The evolution of aging." Nature Education Knowledge 3(3): 1-10.

Fabrizio, P., et al. (2010). "Genome-wide screen in Saccharomyces cerevisiae identifies vacuolar protein sorting, autophagy, biosynthetic, and tRNA methylation genes involved in life span regulation." PLoS genetics 6(7).

Fehrmann, S., et al. (2013). "Aging yeast cells undergo a sharp entry into senescence unrelated to the loss of mitochondrial membrane potential." Cell reports 5(6): 1589-1599.

Freund, A., et al. (2011). "p38MAPK is a novel DNA damage response-independent regulator of the senescence-associated secretory phenotype." The EMBO journal 30(8): 1536-1548.

Fridovich, I. (1989). "Superoxide dismutases. An adaptation to a paramagnetic gas." Journal of Biological Chemistry 264(14): 7761-7764.

Ganley, A. R., et al. (2009). "The effect of replication initiation on gene amplification in the rDNA and its relationship to aging." Molecular cell 35(5): 683-693.

Garmendia-Torres, C., et al. (2018). "Multiple inputs ensure yeast cell size homeostasis during cell cycle progression." Elife 7: e34025.

Gasch, A. P., et al. (2000). "Genomic expression programs in the response of yeast cells to environmental changes." Molecular biology of the cell 11(12): 4241-4257.

Gehlen, L. R., et al. (2011). "Nuclear geometry and rapid mitosis ensure asymmetric episome segregation in yeast." Current biology 21(1): 25-33.

Ghoul, M. and S. Mitri (2016). "The ecology and evolution of microbial competition." Trends in microbiology 24(10): 833-845.

Giaever, G. and C. Nislow (2014). "The yeast deletion collection: a decade of functional

genomics." Genetics 197(2): 451-465.

Giri, D. and M. Ittmann (2000). "Interleukin-1α is a paracrine inducer of FGF7, a key epithelial growth factor in benign prostatic hyperplasia." The American journal of pathology 157(1): 249-255.

González, A. and M. N. Hall (2017). "Nutrient sensing and TOR signaling in yeast and mammals." The EMBO journal 36(4): 397-408.

Goulev, Y., et al. (2017). "Nonlinear feedback drives homeostatic plasticity in H2O2 stress response." Elife 6: e23971.

Greider, C. W. and E. H. Blackburn (1987). "The telomere terminal transferase of Tetrahymena is a ribonucleoprotein enzyme with two kinds of primer specificity." Cell 51(6): 887-898.

Griffith, J. D., et al. (1999). "Mammalian telomeres end in a large duplex loop." Cell 97(4):

503-514.

Gross, E., et al. (2006). "Generating disulfides enzymatically: reaction products and electron acceptors of the endoplasmic reticulum thiol oxidase Ero1p." Proceedings of the National Academy of Sciences 103(2): 299-304.

Gygi, S. P., et al. (1999). "Correlation between protein and mRNA abundance in yeast." Molecular and cellular biology 19(3): 1720-1730.

Hahn, W. C. and R. A. Weinberg (2002). "Rules for making human tumor cells." New England Journal of Medicine 347(20): 1593-1603.

Hanahan, D. and R. A. Weinberg (2000). "The hallmarks of cancer." Cell 100(1): 57-70.

Hanzén, S., et al. (2016). "Lifespan control by redox-dependent recruitment of chaperones to misfolded proteins." Cell 166(1): 140-151.

Harbour, J. W. and D. C. Dean (2000). "The Rb/E2F pathway: expanding roles and emerging

paradigms." Genes & development 14(19): 2393-2409.

Harman, D. (1992). "Free radical theory of aging." Mutation Research/DNAging 275(3-6): 257-266.

Hartwell, L. H. (1971). "Genetic control of the cell division cycle in yeast: II. Genes controlling

DNA replication and its initiation." Journal of Molecular Biology 59(1): 183-194.

Hartwell, L. H. and T. A. Weinert (1989). "Checkpoints: controls that ensure the order of cell

cycle events." Science 246(4930): 629-634.

Hayflick, L. (1965). "The limited in vitro lifetime of human diploid cell strains." Experimental cell research 37(3): 614-636.

Hayflick, L. and P. S. Moorhead (1961). "The serial cultivation of human diploid cell strains." Experimental cell research 25(3): 585-621.

He, Y. and H. Jasper (2014). "Studying aging in Drosophila." Methods 68(1): 129-133.

Heintz, N., et al. (1983). "Regulation of human histone gene expression: kinetics of accumulation and changes in the rate of synthesis and in the half-lives of individual histone mRNAs during the HeLa cell cycle." Molecular and cellular biology 3(4): 539-550.

Hemann, M. T., et al. (2001). "The shortest telomere, not average telomere length, is critical for cell viability and chromosome stability." Cell 107(1): 67-77.

Henderson, K. A., et al. (2014). "Mother-daughter asymmetry of pH underlies aging and rejuvenation in yeast." Elife 3: e03504.

Herbig, U., et al. (2006). "Cellular senescence in aging primates." Science 311(5765): 1257-1257.

Holmes, D. J. and S. N. Austad (1995). "Birds as animal models for the comparative biology of aging: a prospectus." The Journals of Gerontology Series A: Biological Sciences and Medical Sciences 50(2): B59-B66.

Honda, S. and M. Matsuo (1992). "Lifespan shortening of the nematode Caenorhabditis elegans under higher concentrations of oxygen." Mechanisms of ageing and development 63(3): 235-246.

Hu, Z., et al. (2014). "Nucleosome loss leads to global transcriptional up-regulation and genomic instability during yeast aging." Genes & development 28(4): 396-408.

Huang, J. and D. Moazed (2003). "Association of the RENT complex with nontranscribed and coding regions of rDNA and a regional requirement for the replication fork block protein Fob1 in rDNA silencing." Genes & development 17(17): 2162-2176.

Silencing within the yeast rDNA repeats inhibits hyperrecombination, represses transcription from foreign promoters, and extends replicative life span. rDNA silencing is mediated by a Sir2-containing complex called RENT (regulator of nucleolar silencing and telophase exit). We show that the Net1 (also called Cfi1) and Sir2 subunits of RENT localize primarily to two distinct regions within rDNA: in one of the nontranscribed spacers (NTS1) and around the Pol I promoter, extending into the 35S rRNA coding region. Binding to NTS1 overlaps the recombination hotspot and replication fork barrier elements, which have been shown previously to require the Fob1 protein for their activities. In cells lacking Fob1, silencing and the association of RENT subunits are abolished specifically at NTS1, while silencing and association at the Pol I promoter region are unaffected or increased. We find that Net1 and Sir2 are physically associated with Fob1 and subunits of RNA polymerase I. Together with the localization data, these results suggest the existence of two distinct modes for the recruitment of the RENT complex to rDNA and reveal a role for Fob1 in rDNA silencing and in the recruitment of the RENT complex. Furthermore, the Fob1-dependent associations of Net1 and Sir2 with the recombination hotspot region strongly

suggest that Sir2 acts directly at this region to carry out its inhibitory effect on rDNA recombination and accelerated aging.

Huh, W.-K., et al. (2003). "Global analysis of protein localization in budding yeast." Nature 425(6959): 686-691.

Irani, K., et al. (1997). "Mitogenic signaling mediated by oxidants in Ras-transformed fibroblasts." Science 275(5306): 1649-1652.

Itahana, K., et al. (2001). "Regulation of cellular senescence by p53." European Journal of Biochemistry 268(10): 2784-2791.

Jang, H. H., et al. (2004). "Two enzymes in one: two yeast peroxiredoxins display oxidative stress-dependent switching from a peroxidase to a molecular chaperone function." Cell 117(5): 625-635.

Jang, W., et al. (1999). "Comparative sequence of human and mouse BAC clones from the mnd2 region of chromosome 2p13." Genome Research 9(1): 53-61.

Janzen, D. H. (1976). "Why bamboos wait so long to flower." Annual Review of Ecology and systematics 7(1): 347-391.

Jazwinski, S. M. (1990). "An experimental system for the molecular analysis of the aging process: the budding yeast Saccharomyces cerevisiae." Journal of gerontology 45(3): B68-B74.

Jeyapalan, J. C. and J. M. Sedivy (2008). "Cellular senescence and organismal aging." Mechanisms of ageing and development 129(7-8): 467-474.

Jin, S. and A. J. Levine (2001). "The p53 functional circuit." Journal of cell science 114(23):

4139-4140.

Jurk, D., et al. (2012). "Postmitotic neurons develop a p21-dependent senescence-like phenotype driven by a DNA damage response." Aging cell 11(6): 996-1004.

Kawanishi, S. and S. Oikawa (2004). "Mechanism of telomere shortening by oxidative stress." Annals of the New York Academy of Sciences 1019(1): 278-284.

Keeley, J. E. and W. J. Bond (1999). "Mast flowering and semelparity in bamboos: the bamboo fire cycle hypothesis." The American Naturalist 154(3): 383-391.

Kennedy, B. K., et al. (1994). "Daughter cells of Saccharomyces cerevisiae from old mothers display a reduced life span." The Journal of cell biology 127(6): 1985-1993.

Khan, S. S., et al. (2017). "Molecular and physiological manifestations and measurement of aging in humans." Aging cell 16(4): 624-633.

Kirkwood, T. B. (1977). "Evolution of ageing." Nature 270(5635): 301.

Kirkwood, T. B. and R. Holliday (1979). "The evolution of ageing and longevity." Proceedings of the Royal Society of London. Series B. Biological Sciences 205(1161): 531-546.

KISHI, S. (2004). "Functional aging and gradual senescence in zebrafish." Annals of the New York Academy of Sciences 1019(1): 521-526.

Kiyono, T., et al. (1998). "Both Rb/p16 INK4a inactivation and telomerase activity are required to immortalize human epithelial cells." Nature 396(6706): 84-88.

Knieß, R. A. and M. P. Mayer (2016). "The oxidation state of the cytoplasmic glutathione redox system does not correlate with replicative lifespan in yeast." npj Aging and Mechanisms of Disease 2: 16028.

Kniess, R. A. and M. P. Mayer (2016). "The oxidation state of the cytoplasmic glutathione redox system does not correlate with replicative lifespan in yeast." npj Aging and Mechanisms of Disease 2.

What is cause and what is consequence of aging and whether reactive oxygen species (ROS) contribute to this phenomenon is debated since more than 50 years. Notwithstanding, little is known about the cellular buffer and redox systems in aging Saccharomyces cerevisiae, which is a model for aging stem cells. Using genetically encoded fluorescent sensors, we measured pH, H2O2 levels and the glutathione redox potential compartment-specific in the cytosol of living, replicatively aging yeast cells, growing under fermenting and respiratory conditions until the end of their lifespan. We found that the pH decreases under both conditions at later stages of the replicative lifespan. H2O2 levels increase in fermenting cells

in the post-replicative stage, but increase continuously with age in respiring cells. The glutathione redox couple becomes also more oxidizing in respiring cells but surprisingly more reducing under fermenting conditions. In strains deleted for the gene encoding glutathione reductase Glr1, such a reduction of the glutathione redox couple with age is not observed. We demonstrate that in vivo Glr1 is activated at lower pH explaining the reduced glutathione potential. The deletion of glr1 dramatically increases the glutathione redox potential especially under respiratory conditions but does not reduce lifespan. Our data demonstrate that pH and the glutathione redox couple is linked through Glr1 and that yeast cells can cope with a high glutathione redox potential without impact on longevity. Our data further suggest that a breakdown of cellular energy metabolism marks the end of replicative lifespan in yeast.

Kobayashi, T. (2003). "The replication fork barrier site forms a unique structure with Fob1p and inhibits the replication fork." Molecular and cellular biology 23(24): 9178-9188.

Kobayashi, T., et al. (2004). "SIR2 regulates recombination between different rDNA repeats, but not recombination within individual rRNA genes in yeast." Cell 117(4): 441-453.

It is known that mutations in gene SIR2 increase and those in FOB1 decrease recombination within rDNA repeats as assayed by marker loss or extrachromosomal rDNA circle formation. SIR2-dependent chromatin structures have been thought to inhibit access and/or function of recombination machinery in rDNA. We measured the frequency of FOB1-dependent arrest of replication forks, consequent DNA double-strand breaks, and formation of DNA molecules with Holliday junction structures, and found no significant difference between sir2Delta and SIR2 strains. Formal genetic experiments measuring mitotic recombination rates within individual rRNA genes also showed no significant difference between these two strains. Instead, we found a significant decrease in the association of cohesin subunit Mcd1p (Scc1p) to rDNA in sir2Delta relative to SIR2 strains. From these and other experiments, we conclude that SIR2 prevents unequal sister-chromatid recombination, probably by forming special cohesin structures, without significant effects on re-combinational events within individual rRNA genes.

Kobayashi, T. and M. Sasaki (2017). "Ribosomal DNA stability is supported by many ‘buffer genes’—introduction to the Yeast rDNA Stability Database." FEMS yeast research 17(1).

Kõks, S., et al. (2016). "Mouse models of ageing and their relevance to disease." Mechanisms of ageing and development 160: 41-53.

Kozmin, S., et al. (2005). "UVA radiation is highly mutagenic in cells that are unable to repair 7, 8-dihydro-8-oxoguanine in Saccharomyces cerevisiae." Proceedings of the National Academy of Sciences 102(38): 13538-13543.

Kraikivski, P., et al. (2015). "From START to FINISH: computational analysis of cell cycle

control in budding yeast." NPJ systems biology and applications 1(1): 1-9.

Krishnamurthy, J., et al. (2004). "Ink4a/Arf expression is a biomarker of aging." The Journal of clinical investigation 114(9): 1299-1307.

Kuge, S., et al. (2001). "Regulation of the yeast Yap1p nuclear export signal is mediated by redox signal-induced reversible disulfide bond formation." Molecular and cellular biology 21(18): 6139-6150.

Kuge, S. and N. Jones (1994). "YAP1 dependent activation of TRX2 is essential for the response of Saccharomyces cerevisiae to oxidative stress by hydroperoxides." The EMBO journal 13(3): 655-664.

Kuge, S., et al. (1998). "Crm1 (XpoI) dependent nuclear export of the budding yeast transcription factor yAP-1 is sensitive to oxidative stress." Genes to Cells 3(8): 521-532.

Kuilman, T., et al. (2010). "The essence of senescence." Genes & development 24(22): 2463-2479.

Kuilman, T. and D. S. Peeper (2009). "Senescence-messaging secretome: SMS-ing cellular

stress." Nature reviews cancer 9(2): 81-94.

Kulaeva, O. I., et al. (2003). "Epigenetic silencing of multiple interferon pathway genes after cellular immortalization." Oncogene 22(26): 4118-4127.

Labuschagne, C. F. and A. B. Brenkman (2013). "Current methods in quantifying ROS and oxidative damage in Caenorhabditis elegans and other model organism of aging." Ageing research reviews 12(4): 918-930.

Lee, J., et al. (1999). "Yap1 and Skn7 control two specialized oxidative stress response regulons in yeast." Journal of Biological Chemistry 274(23): 16040-16046.

Lee, K. W., et al. (2011). "Lower ataxia telangiectasia mutated (ATM) mRNA expression is correlated with poor outcome of laryngeal and pharyngeal cancer patients." Annals of Oncology 22(5): 1088-1093.

Background: Ataxia telangiectasia mutated (ATM) kinase is a critical regulator in initiating DNA damage response and activating DNA repair. However, the correlation between ATM expression and the outcome of laryngopharyngeal cancer patients is unknown. We hypothesize that ATM expression is correlated with a worse outcome in laryngopharyngeal cancer patients.

Patients and methods: The ATM messenger RNA (mRNA) expression of 80 tumors of laryngeal and pharyngeal cancer was examined by real-time quantitative RT-PCR. Overall survival rates were measured using Kaplan-Meier estimates and the log-rank tests. The adjusted hazard rate ratios (HRRs) were computed by multivariate Cox regressions.

Results: Reduced ATM mRNA was found in 65 of 80 studied cases. Lower ATM expression [tumor/normal < 0.3, HRR = 2.49; 95% confidence interval (CI) 1.27-4.88], younger age (< 55 years, HRR = 2.71; 95% CI 1.16-6.32), and larger tumor (T-3/T-4, HRR = 2.21; 95% CI 1.10-4.44) were independent risk factors for survival. Patients with lower ATM and younger age (HRR = 6.51; 95% CI 2.05-20.66) or with lower ATM and T-3/T-4 tumor (HRR = 5.23; 95% CI 2.04-13.40) exhibited the poorest outcome.

Conclusion: The expression of ATM mRNA, which is frequently downregulated in laryngeal and pharyngeal cancers, could be a valuable prognostic marker.

Lee, S. S., et al. (2012). "Whole lifespan microscopic observation of budding yeast aging through a microfluidic dissection platform." Proceedings of the National Academy of Sciences 109(13): 4916-4920.

Leonov, A., et al. (2017). "Caloric restriction extends yeast chronological lifespan via a mechanism linking cellular aging to cell cycle regulation, maintenance of a quiescent state, entry into a non-quiescent state and survival in the non-quiescent state." Oncotarget 8(41): 69328.

Lindstrom, D. L. and D. E. Gottschling (2009). "The mother enrichment program: a genetic system for facile replicative life span analysis in Saccharomyces cerevisiae." Genetics 183(2): 413-422.

Liu, X., et al. (2015). "Reliable cell cycle commitment in budding yeast is ensured by signal integration." Elife 4: e03977.

Longo, V. D., et al. (1996). "Superoxide dismutase activity is essential for stationary phase survival in Saccharomyces cerevisiae Mitochondrial production of toxic oxygen species in vivo." Journal of Biological Chemistry 271(21): 12275-12280.

Longo, V. D., et al. (2012). "Replicative and chronological aging in Saccharomyces cerevisiae." Cell metabolism 16(1): 18-31.

López-Lluch, G. and P. Navas (2016). "Calorie restriction as an intervention in ageing." The Journal of physiology 594(8): 2043-2060.

Luo, H., et al. (2017). "Nutrient sensing and the oxidative stress response." Trends in Endocrinology & Metabolism 28(6): 449-460.

MacLean, M., et al. (2001). "Chronological lifespan of stationary phase yeast cells; a model for investigating the factors that might influence the ageing of postmitotic tissues in higher organisms." Yeast 18(6): 499-509.

Magalhães, J. P. d., et al. (2007). "An analysis of the relationship between metabolism, developmental schedules, and longevity using phylogenetic independent contrasts." The Journals of Gerontology Series A: Biological Sciences and Medical Sciences 62(2): 149-160.

Magiera, M. M., et al. (2014). "DNA replication and spindle checkpoints cooperate during S phase to delay mitosis and preserve genome integrity." J Cell Biol 204(2): 165-175.

Maldonado, J. L., et al. (2004). "Mechanisms of cell-cycle arrest in Spitz nevi with constitutive activation of the MAP-kinase pathway." The American journal of pathology 164(5): 1783-1787.

Marvin, J. S., et al. (2018). "Stability, affinity, and chromatic variants of the glutamate sensor iGluSnFR." Nature methods 15(11): 936-939.

McCormick, M. A., et al. (2014). "The SAGA histone deubiquitinase module controls yeast replicative lifespan via Sir2 interaction." Cell reports 8(2): 477-486.

Mehta, I. S., et al. (2007). "Alterations to nuclear architecture and genome behavior in senescent cells." Annals of the New York Academy of Sciences 1100: 250-263.

Mercken, E. M., et al. (2013). "Calorie restriction in humans inhibits the PI 3 K/AKT pathway and induces a younger transcription profile." Aging cell 12(4): 645-651.

Meydani, S. N., et al. (2016). "Long-term moderate calorie restriction inhibits inflammation without impairing cell-mediated immunity: a randomized controlled trial in non-obese humans." Aging (Albany NY) 8(7): 1416.

Morgan, C. C., et al. (2013). "Molecular adaptation of telomere associated genes in mammals." BMC evolutionary biology 13(1): 251.

Morlot, S., et al. (2019). "Excessive rDNA transcription drives the disruption in nuclear homeostasis during entry into senescence in budding yeast." Cell reports 28(2): 408-422. e404.

Mortimer, R. K. and J. R. Johnston (1959). "Life span of individual yeast cells." Nature 183(4677): 1751-1752.

Moyzis, R. K., et al. (1988). "A highly conserved repetitive DNA sequence,(TTAGGG) n, present at the telomeres of human chromosomes." Proceedings of the National Academy of Sciences 85(18): 6622-6626.

Murphy, M. P. (2009). "How mitochondria produce reactive oxygen species." Biochemical Journal 417(1): 1-13.

Narita, M. (2007). "Cellular senescence and chromatin organisation." British Journal of Cancer 96(5): 686-691.

Nelson, D. M., et al. (2002). "Coupling of DNA synthesis and histone synthesis in S phase independent of cyclin/cdk2 activity." Molecular and cellular biology 22(21): 7459-7472.

Neurohr, G. E., et al. (2018). "Deregulation of the G1/S-phase transition is the proximal cause of mortality in old yeast mother cells." Genes & development 32(15-16): 1075-1084.

Noichri, Y., et al. (2015). "In vivo parameters influencing 2-Cys Prx oligomerization: The role

of enzyme sulfinylation." Redox biology 6: 326-333.

Novarina, D., et al. (2017). "Increased genome instability is not accompanied by sensitivity to DNA damaging agents in aged yeast cells." DNA repair 54: 1-7.

Okada, M., et al. (2017). "Proteomics analysis for asymmetric inheritance of preexisting proteins between mother and daughter cells in budding yeast." Genes to Cells 22(6): 591-601.

Olovnikov, A. M. (1971). "[Principle of marginotomy in template synthesis of polynucleotides]." Dokl Akad Nauk SSSR 201(6): 1496-1499.

Outten, C. E., et al. (2005). "Cellular factors required for protection from hyperoxia toxicity in Saccharomyces cerevisiae." Biochemical Journal 388(1): 93-101.

Park, P. U., et al. (1999). "Effects of Mutations in DNA Repair Genes on Formation of Ribosomal DNA Circles and Life Span inSaccharomyces cerevisiae." Molecular and cellular biology 19(5): 3848-3856.

Partridge, L. and D. Gems (2002). "Mechanisms of aging: public or private?" Nature Reviews

Genetics 3(3): 165-175.

Passos, J. F., et al. (2010). "Feedback between p21 and reactive oxygen production is necessary for cell senescence." Molecular systems biology 6(1).

Pearl, R. (1928). "The Rate of Living University of London Press." London, UK.

Pearson, M., et al. (2000). "PML regulates p53 acetylation and premature senescence induced by oncogenic Ras." Nature 406(6792): 207-210.

Pifferi, F., et al. (2018). "Caloric restriction increases lifespan but affects brain integrity in grey mouse lemur primates." Communications biology 1(1): 1-8.

Pollard, T. D., et al. (2016). Cell Biology E-Book, Elsevier Health Sciences.

Prieur, A. and D. S. Peeper (2008). "Cellular senescence in vivo: a barrier to tumorigenesis."

Current opinion in cell biology 20(2): 150-155.

Prothero, J. (1993). "Adult life span as a function of age at maturity." Experimental gerontology 28(6): 529-536.

Reis, R. J. S., et al. (2009). "Extreme-longevity mutations orchestrate silencing of multiple signaling pathways." Biochimica et Biophysica Acta (BBA)-General Subjects 1790(10): 1075-1083.

Ren, B., et al. (2002). "E2F integrates cell cycle progression with DNA repair, replication, and G2/M checkpoints." Genes & development 16(2): 245-256.

Righolt, C. H., et al. (2011). "Robust nuclear lamina-based cell classification of aging and senescent cells." Aging (Albany NY) 3(12): 1192.

Rinnerthaler, M., et al. (2012). "Yno1p/Aim14p, a NADPH-oxidase ortholog, controls extramitochondrial reactive oxygen species generation, apoptosis, and actin cable formation in yeast." Proceedings of the National Academy of Sciences 109(22): 8658-8663.

Robles, S. J. and G. R. Adami (1998). "Agents that cause DNA double strand breaks lead to

p16 INK4a enrichment and the premature senescence of normal fibroblasts." Oncogene 16(9):

1113-1123.

Rodier, F. and J. Campisi (2011). "Four faces of cellular senescenceFour faces of senescence." The Journal of cell biology 192(4): 547-556.

Roninson, I. B. (2003). "Tumor cell senescence in cancer treatment." Cancer research 63(11):

2705-2715.

Ross, S. J., et al. (2000). "Thioredoxin peroxidase is required for the transcriptional response to oxidative stress in budding yeast." Molecular biology of the cell 11(8): 2631-2642.

Rubner, M. (1908). "Das Problem det Lebensdaur und seiner beziehunger zum."

Saarikangas, J. and Y. Barral (2015). "Protein aggregates are associated with replicative aging without compromising protein quality control." Elife 4: e06197.

Salehi, F., et al. (2018). "Oxidative DNA damage induced by ROS-modulating agents with the ability to target DNA: A comparison of the biological characteristics of citrus pectin and apple pectin." Scientific reports 8(1): 13902.

Santivasi, W. L. and F. Xia (2014). "Ionizing radiation-induced DNA damage, response, and repair." Antioxidants & redox signaling 21(2): 251-259.

Sedelnikova, O. A., et al. (2004). "Senescing human cells and ageing mice accumulate DNA lesions with unrepairable double-strand breaks." Nature cell biology 6(2): 168-170.

Serrano, M., et al. (1997). "Oncogenic ras provokes premature cell senescence associated with accumulation of p53 and p16INK4a." Cell 88(5): 593-602.

Shay, J. W., et al. (1991). "A role for both RB and p53 in the regulation of human cellular senescence." Experimental cell research 196(1): 33-39.

Shay, J. W. and W. E. Wright (2005). "Senescence and immortalization: role of telomeres and

telomerase." Carcinogenesis 26(5): 867-874.

Shcheprova, Z., et al. (2008). "A mechanism for asymmetric segregation of age during yeast budding." Nature 454(7205): 728-734.

Shelton, D. N., et al. (1999). "Microarray analysis of replicative senescence." Current biology 9(17): 939-945.

Shiels, P. G., et al. (1999). "Analysis of telomere lengths in cloned sheep." Nature 399(6734):

316-317.

Sinclair, D. A. (2013). Studying the replicative life span of yeast cells. Biological Aging, Springer: 49-63.

Sinclair, D. A. and L. Guarente (1997). "Extrachromosomal rDNA circles—a cause of aging in yeast." Cell 91(7): 1033-1042.

Sinclair, D. A., et al. (1997). "Accelerated aging and nucleolar fragmentation in yeast sgs1 mutants." Science 277(5330): 1313-1316.
Sitte, N., et al. (1998). "Proteasome-dependent degradation of oxidized proteins in MRC-5 fibroblasts." FEBS letters 440(3): 399-402.

Sittman, D. B., et al. (1983). "Histone mRNA concentrations are regulated at the level of transcription and mRNA degradation." Proceedings of the National Academy of Sciences 80(7): 1849-1853.

Sohal, R. S., et al. (1994). "Oxidative damage, mitochondrial oxidant generation and antioxidant defenses during aging and in response to food restriction in the mouse." Mechanisms of ageing and development 74(1-2): 121-133.

Sohal, R. S. and R. Weindruch (1996). "Oxidative stress, caloric restriction, and aging." Science 273(5271): 59-63.

Srivastava, R., et al. (2016). "The Epigenetic Pathways to Ribosomal DNA Silencing." Microbiology and Molecular Biology Reviews 80(3): 545-563.

Heterochromatin is the transcriptionally repressed portion of eukaryotic chromatin that maintains a condensed appearance throughout the cell cycle. At sites of ribosomal DNA (rDNA) heterochromatin, epigenetic states contribute to gene silencing and genome stability, which are required for proper chromosome segregation and a normal life span. Here, we focus on recent advances in the epigenetic regulation of rDNA silencing in Saccharomyces cerevisiae and in mammals, including regulation by several histone modifications and several protein components associated with the inner nuclear membrane within the nucleolus. Finally, we discuss the perturbations of rDNA epigenetic pathways in regulating cellular aging and in causing various types of diseases.

Steffen, K. K., et al. (2009). "Measuring replicative life span in the budding yeast." JoVE (Journal of Visualized Experiments)(28): e1209.

Steinkraus, K., et al. (2008). "Replicative aging in yeast: the means to the end." Annual review

of cell and developmental biology 24: 29-54.

Symonds, H., et al. (1994). "p53-dependent apoptosis suppresses tumor growth and progression in vivo." Cell 78(4): 703-711.

Takai, H., et al. (2003). "DNA damage foci at dysfunctional telomeres." Current biology 13(17): 1549-1556.

Tchkonia, T., et al. (2013). "Cellular senescence and the senescent secretory phenotype:

therapeutic opportunities." The Journal of clinical investigation 123(3): 966-972.

Toussaint, O., et al. (2000). "Cellular and molecular mechanisms of stress-induced premature senescence (SIPS) of human diploid fibroblasts and melanocytes." Experimental gerontology 35(8): 927-945.

Trimarchi, J. M. and J. A. Lees (2002). "Sibling rivalry in the E2F family." Nature reviews Molecular cell biology 3(1): 11-20.

Tyler, J. K. and J. E. Johnson (2018). "The role of autophagy in the regulation of yeast life span." Annals of the New York Academy of Sciences 1418(1): 31.

Valdes, A. M., et al. (2005). "Obesity, cigarette smoking, and telomere length in women." The lancet 366(9486): 662-664.

Vandenbroucke, K., et al. (2008). "Hydrogen peroxide–induced gene expression across kingdoms: A comparative analysis." Molecular Biology and Evolution 25(3): 507-516.

Vasconcellos, L. R., et al. (2016). "Protein aggregation as a cellular response to oxidative stress induced by heme and iron." Proceedings of the National Academy of Sciences 113(47): E7474-E7482.

Vaziri, H., et al. (1993). "Loss of telomeric DNA during aging of normal and trisomy 21 human lymphocytes." American journal of human genetics 52(4): 661.

Venable, M. E., et al. (1995). "Role of ceramide in cellular senescence." Journal of Biological Chemistry 270(51): 30701-30708.

Victorelli, S. and J. F. Passos (2017). "Telomeres and cell senescence-size matters not." EBioMedicine 21: 14-20.

Vinton, P. J. and T. Weinert (2017). "A slowed cell cycle stabilizes the budding yeast genome." Genetics 206(2): 811-828.

Von Zglinicki, T. (2002). "Oxidative stress shortens telomeres." Trends in biochemical sciences 27(7): 339-344.

von Zglinicki, T., et al. (1995). "Mild hyperoxia shortens telomeres and inhibits proliferation of fibroblasts: a model for senescence?" Experimental cell research 220(1): 186-193.

Wang, L., et al. (2018). "Enriched physical environment attenuates spatial and social memory impairments of aged socially isolated mice." International Journal of Neuropsychopharmacology 21(12): 1114-1127.

Watson, J. D. (1972). "Origin of concatemeric T7 DNA." Nat New Biol 239(94): 197-201.

Wemmie, J. A., et al. (1994). "Cadmium tolerance mediated by the yeast AP-1 protein requires the presence of an ATP-binding cassette transporter-encoding gene, YCF1." Journal of Biological Chemistry 269(51): 32592-32597.

Werner-Washburne, M., et al. (1996). "Stationary phase in Saccharomyces cerevisiae." Molecular microbiology 19(6): 1159-1166.

Wloka, C., et al. (2011). "Evidence that a septin diffusion barrier is dispensable for cytokinesis in budding yeast." Biological chemistry 392(8-9): 813-829.

Xie, K., et al. (2017). "Every-other-day feeding extends lifespan but fails to delay many symptoms of aging in mice." Nature communications 8(1): 1-19.

Xie, Z., et al. (2015). "Early telomerase inactivation accelerates aging independently of telomere length." Cell 160(5): 928-939.

Xu, H. J., et al. (1993). "Loss of Rb Protein Expression in Primary Bladder-Cancer Correlates with Loss of Heterozygosity at the Rb Locus and Tumor Progression." International Journal of Cancer 53(5): 781-784.

RB-protein status as determined by immunohistochemical analysis was compared with loss of heterozygosity (LOH) at the RB locus in 68 primary transitional-cell carcinomas of the bladder. Absence of RB-protein expression was found in 15 of 17 tumors in which LOH at the RB locus was identified, whereas 31 of 36 tumors from informative patients which showed no LOH had a normal

RB-protein pattern ($p < 0.001$). Altered RB-protein expression was also more frequently seen in muscle-invasive and high-grade tumors ($p < 0.003$ and < 0.005, respectively). Our results indicate that LOH at the RB locus is highly correlated with loss of RB-protein expression in primary bladder carcinomas and further strengthens the notion that loss of RB function may be associated with more aggressive bladder tumors.

Yan, M. and C. Wolberger (2015). "Uncovering the role of Sgf73 in maintaining SAGA deubiquitinating module structure and activity." Journal of Molecular Biology 427(8): 1765-1778.

Yang, J., et al. (2015). "Systematic analysis of asymmetric partitioning of yeast proteome between mother and daughter cells reveals “aging factors” and mechanism of lifespan asymmetry." Proceedings of the National Academy of Sciences 112(38): 11977-11982.

Yang, L., et al. (2016). "Long-Term Calorie Restriction Enhances Cellular Quality-Control Processes in Human Skeletal Muscle." Cell reports 14(3): 422-428.

Calorie restriction (CR) retards aging, acts as a hormetic intervention, and increases serum corticosterone and HSP70 expression in rodents. However, less is known regarding the effects of CR on these factors in humans. Serum cortisol and molecular chaperones and autophagic proteins were measured in the skeletal muscle of subjects on CR diets for 3-15 years and in control volunteers. Serum cortisol was higher in the CR group than in age-matched sedentary and endurance athlete groups (15.6 +/- 4.6 ng/dl versus 12.3 +/- 3.9 ng/dl and 11.2 +/- 2.7 ng/dl, respectively; $p <= 0.001$). HSP70, Grp78, beclin-1, and LC3 mRNA and/or protein levels were higher in the skeletal muscle of the CR group compared to controls. Our data indicate that CR in humans is associated with sustained rises in serum cortisol, reduced inflammation, and increases in key molecular chaperones and autophagic mediators involved in cellular protein quality control and removal of dysfunctional proteins and organelles.

Article annex

Morlot, Sandrine, et al. "Excessive rDNA transcription drives the disruption in nuclear homeostasis during entry into senescence in budding yeast." Cell reports 28.2 (2019): 408-422.

Cell Reports

Excessive rDNA Transcription Drives the Disruption in Nuclear Homeostasis during Entry into Senescence in Budding Yeast

Graphical Abstract

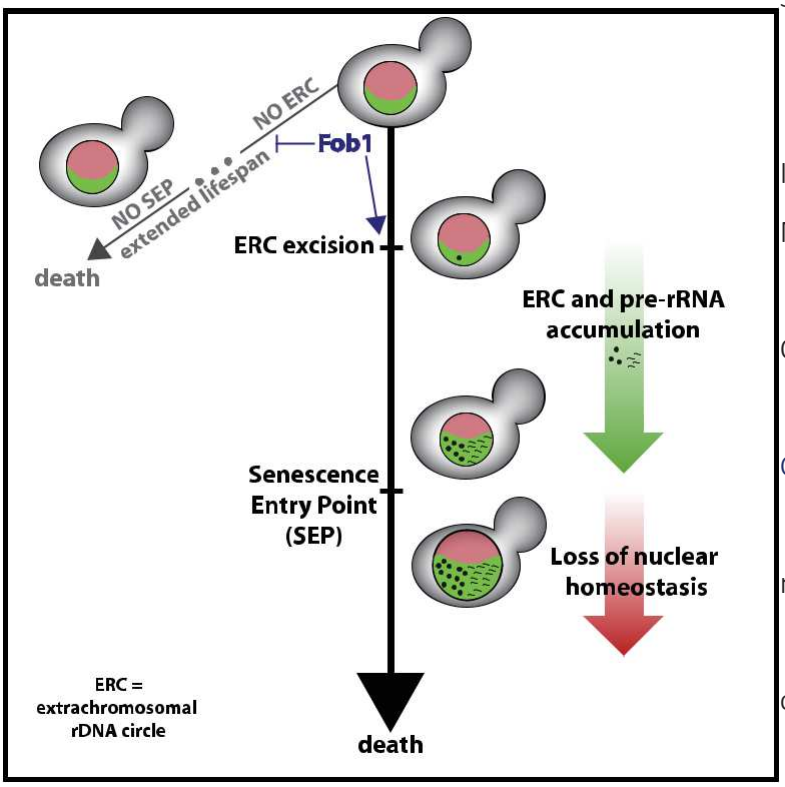

Authors

Sandrine Morlot, Jia Song, Isabelle Le´ger-Silvestre, Audrey Matifas, Olivier Gadal, Gilles Charvin

Correspondence

morlot@igbmc.fr (S.M.), charvin@igbmc.fr (G.C.)

In Brief

The accumulation of extrachromosomal rDNA circles (ERCs) is a hallmark of aging in budding yeast. Morlot et al. show that ERCs accumulate ahead of senescence onset and fuel an excessive rDNA transcription, ultimately leading to impaired nuclear homeostasis and an irreversible cell cycle slowdown.

Highlights

- Single-cell monitoring shows that ERC accumulation starts well before senescence
- ERC accumulation drives a large upregulation in pre-rRNA, but not ribosome, synthesis
- A strong loss of nuclear homeostasis occurs downstream of nucleolar defects
- Rejuvenation of daughters is ensured by asymmetrical nuclear partitioning

Morlot et al., 2019, Cell Reports 28, 408–422

July 9, 2019 ª 2019 The Authors.
https://doi.org/10.1016/j.celrep.2019.06.032

OPEN ACCESS
CellPress

Cell Reports

Ar ticle

Excessive rDNA Transcription Drives the Disruption in Nuclear Homeostasis during Entry into Senescence in Budding Yeast

Sandrine Morlot,[1,2,3,4,*] Jia Song,[1,2,3,4] Isabelle Le´ger-Silvestre,[5] Audrey Matifas,[1,2,3,4] Olivier Gadal,[5] and Gilles Charvin[1,2,3,4,6,*]

[1]Developmental Biology and Stem Cells Department, Institut de Ge´ne´tique et de Biologie Mole´culaire et Cellulaire, Illkirch 67400, France
[2]Centre National de la Recherche Scientifique, UMR7104, Illkirch 67400, France
[3]Institut National de la Sante´ et de la Recherche Me´dicale, U1258, Illkirch 67400, France
[4]Universite´ de Strasbourg, Illkirch 67400, France

[5]Laboratoire de Biologie Mole´culaire Eucaryote, Centre de Biologie Inte´grative (CBI), Universite´ de Toulouse, CNRS, UPS, Toulouse 31000, France
[6]Lead Contact
*Correspondence: morlot@igbmc.fr (S.M.), charvin@igbmc.fr (G.C.)

https://doi.org/10.1016/j.celrep.2019.06.032

SUMMARY

Budding yeast cells undergo a limited number of divi-sions before they enter senescence and die. Despite recent mechanistic advances, whether and how molecular events are temporally and causally linked during the transition to senescence remain elusive. Here, using real-time observation of the accumulation of extrachromosomal rDNA circles (ERCs) in single cells, we provide evidence that ERCs build up rapidly with exponential kinetics well before any physiolog-ical decline. We then show that ERCs fuel a massive increase in ribosomal RNA (rRNA) levels in the nucle-olus, which do not mature into functional ribosomes. This breakdown in nucleolar coordination is followed by a loss of nuclear homeostasis, thus defining a chronology of causally related events leading to cell death. A computational analysis supports a model in which a series of age-independent processes lead to an age-dependent increase in cell mortality, hence explaining the emergence of aging in budding yeast.

INTRODUCTION

Budding yeast cells undergo a limited number of asymmetrical divisions before entering senescence and dying, a phenomenon known as replicative aging (Mortimer and Johnston, 1959). Although the replicative age of mother cells increases at each di-vision, the newborn daughter cells are ''rejuvenated,'' meaning that they have full replicative potential (Kennedy et al., 1994). To explain this phenomenon, it has long been proposed that ag-ing cells accumulate detrimental factors that are lethal to the mother but are not inherited by daughter cells (Egilmez and Jaz-winski, 1989). Since that hypothesis was first proposed, a large body of literature has established that yeast cell aging is accom-panied by breakdown of many cellular functions, resulting in the loss of proteostasis (Erjavec et al., 2007), sterility (Smeal et al.,

1996), genomic instability (McMurray and Gottschling, 2003), impairment in mitochondrial function (Veatch et al., 2009), cell cycle dysregulation (Neurohr et al., 2018), and nucleolar enlarge-ment and fragmentation (Sinclair et al., 1997), among other defects.

Based on these observations, a consensus has emerged in which cellular aging is viewed as a progressive phenomenon involving gradual deterioration of physiological functions, lead-ing to cell death. In contrast to this classical view, which is largely based on observations of cells in bulk culture, longitudinal tracking of individual cells from birth to death revealed the exis-tence of a well-defined time point in cellular lifespan beyond which the cell cycle duration rapidly increases before cell death, which is a time point previously referred to as the senescence entry point (SEP) (Fehrmann et al., 2013). The origin of the discrepancy between single-cell versus population measure-ments originates from cell-cell variability in the time of death. Indeed, even if the appearance of a given hallmark of age is abrupt during cellular lifespan, it was shown that pooling of data from individual cells with heterogeneous lifespans consid-erably attenuate the average dynamics of this marker (Fig-ure S1A) (Fehrmann et al., 2013). Hence, bulk measurements do not faithfully capture the true kinetics of aging markers during the entry into senescence, and this may lead to misleading inter-pretations. Similarly, an analysis of bulk populations of cells with heterogeneous lifespans would limit our ability to temporally order the onset of aging marks, thus precluding the identification of their causal relationships (Figure S1B). This explains in part why, despite numerous correlations between age and accumu-lation of diverse factors (for example, protein aggregates [Erja-vec et al., 2007], mitochondrial defects [Veatch et al., 2009], and genomic instability [McMurray and Gottschling, 2003]) in Saccharomyces cerevisiae and other model organisms, a clear and causal chain of events explaining entry into senescence re-mains to be unraveled.

In yeast, one factor proposed to regulate aging is the accumu-lation of extrachromosomal rDNA circles (ERCs) within mother cells (Sinclair and Guarente, 1997) that are asymmetrically apportioned and retained in the mother upon cell division

(Denoth Lippuner et al., 2014b; Shcheprova et al., 2008). ERCs are self-replicating sequences formed by the excision of repeats from the rDNA cluster, a genomic region located on chromo-some XII that contains about 150–200 repeats of rRNA genes. Formation of ERCs is favored by these repeated sequences and by the presence of a replication fork barrier mediated by Fob1, which prevents collision between the DNA replication and rDNA transcription machineries, thereby favoring double-strand breaks and recombination events (Brewer and Fangman, 1988; Kobayashi, 2003). However, it is not yet known whether and how ERC accumulation is detrimental to cells (Ganley et al., 2009) or whether ERC excision, a potentially stochastic event, is temporally and mechanistically related to the onset of cell cycle slowdown (SEP) observed in aging mothers.

To address these questions, we monitored the replicative life-span (RLS) of individual yeast cells by using a microfluidics-based imaging system (Goulev et al., 2017). We quantitatively analyzed the sequence of events driving both the entry into senescence in mother and the rejuvenation in daughter cells. Importantly, our experimental data support a model in which a series of age-independent processes lead to an age-dependent increase in cell mortality, hence explaining the emergence of aging in a simple unicellular organism.

RESULTS

ERCs Accumulate Exponentially before Entry into Senescence

To test the hypothesis that ERCs may be involved in driving the abrupt onset of SEP in aging mother cells, we measured the total number of rRNA gene copies (i.e., chromosomal and ERC rRNA gene repeats) in single yeast cells over their entire lifespans. To this end, we used a previously described microfluidics device in which individual mother cells are trapped in cavities and imaged at the single-cell level from birth to death (Goulev et al., 2017). To track rDNA copy number, we used a strain in which 50 repeats of the LacO sequence are inserted into each repeat of the nucleolar rRNA gene cluster (Miyazaki and Kobaya-shi, 2011). Thus, by co-expressing a GFP-LacI fusion protein and the nucleolar marker Net1-mCherry, the total size of the rDNA loci can be quantified (Figure 1A). Fluorescence imaging of these cells showed the presence of nucleolar-localized GFP throughout the cell lifespan, as expected (Figure 1B; Video S1), with a marked increase in GFP toward the end of the lifespan that was concomitant with the SEP (Figure 1C). We calculated the time of onset of SEP for each trajectory based on piecewise linear fitting to the dynamics of the individual cell cycle durations (as previously reported [Fehrmann et al., 2013] see also STAR Methods and Figure S2), which enabled alignment of the nucle-olar GFP-LacI fluorescence signal and confirmed the marked accumulation of rDNA copies preceding the SEP (Figure 1D). This analysis revealed an almost 10-fold increase in the number of rRNA gene copies in post-SEP compared with pre-SEP cells (Figure 1E), which was paralleled by a large increase in total Net1-mCherry fluorescence (Figures S3A and S3B).

By further quantifying the dynamics of the average GFP-LacI fluorescence signal over time, we found an excellent agreement to an exponential fit with a doubling time t of 1.6 ± 0.5 genera-tions, providing direct evidence that a rapid multiplicative pro-cess governs the accumulation of the rDNA copy number (see Figure 1E and STAR Methods for details). Instead, when we analyzed average data after alignment of single-cell trajectories from birth (Figures S3E and S3F) or death (Figures S3G and S3H), rather than at the SEP, we obtained markedly slower esti-mates of the dynamics of rDNA copies (8.6 ± 2.2 and 3.4 ± 0.5 generation doubling time, respectively). Fitting single-cell GFP-LacI data, rather than the average signal displayed in Figure 2E, confirmed a median 1.5 ± 0.2 doubling time (Figures S3C and S3D). Thus, alignment of trajectories from birth or death lead to a strong and systematic underestimate of the true kinetics of the amplification of rDNA copies.

Because the chromosomal rDNA copy number is known to be tightly regulated at 200 throughout the cell cycle (Ide et al., 2013; Mansisidor et al., 2018), we assumed that the baseline level of GFP-LacI fluorescence in the early part of the lifespan (i.e., well ahead of the SEP) is likely to correspond to chromo-somal rDNA repeats, and the exponential increase in GFP-LacI fluorescence coincident with the SEP is likely due to the self-replication of ERCs. In strong support of this, the GFP signal above baseline segregates asymmetrically between mother and daughter cells, which would be inconsistent with the equal partitioning of chromosomal rDNA (see below, Figures 5A and 5B). Along these lines, it is interesting to note that GFP-LacI fluo-rescence appeared in aging cells as a diffuse signal rather than as a single foci in the nucleolus (Figure 1B), which is more consis-tent with GFP-LacI binding to multiple ERCs throughout the nucleolus than with binding to a discrete cluster of rRNA genes in the chromosomal DNA.

To better characterize the specific kinetics of ERC accumula-tion in mother cells, we subtracted the baseline GFP-LacI fluo-rescence signal (assuming it corresponded to 200 chromosomal rDNA copies), calculated the number of gene copies represented by the remaining GFP-LacI signal, and plotted the data in semi-log scale (Figure 1E, inset). This analysis confirmed the striking exponential increase in ERCs over about 15 generations, fol-lowed by a plateau representing saturation of the amplification process at 1,500 ERC copies/cell, which is an order of magni-tude higher than the chromosomal rDNA copy number and could be underestimated due to the potential titration of GFP-LacI. Importantly, extrapolating the exponential fit allowed us to esti-mate that the first ERC excision (defined by ERC copy number equal to 1; Figure 1E, inset) occurred an average of about 13 divisions before the SEP, i.e., long before any decline in physio-logical function is manifest. In addition, the number of ERCs at the SEP was 360, indicating that aging cells can tolerate a large increase in extra rDNA copies before cell division is perturbed (Figure 1E, inset). Taken together, these results provide direct evidence for the exponential accumulation of ERCs in the mother cell and demonstrate that it is an early event that precedes by far the onset of SEP that characterizes entry into replicative senescence.

ERC Accumulation Leads to a Massive Increase in Pre-rRNA Levels Prior to Entry into Senescence

ERCs have long been speculated to be toxic to aging cells by titrating the DNA replication machinery and/or rDNA-specific

Cell Reports 28, 408–422, July 9, 2019

409

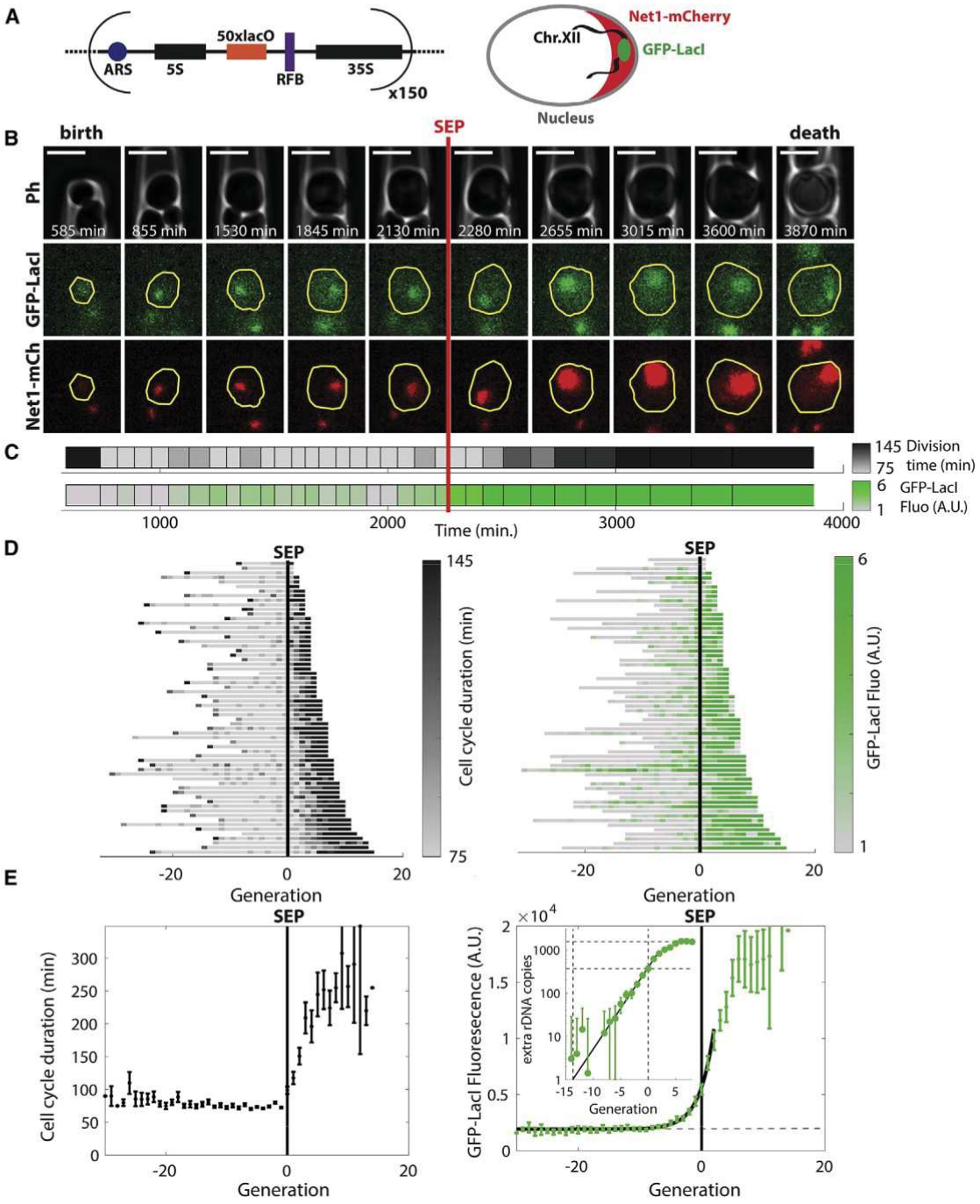
A
ARS
5S
50xlacO
RFB
35S
x150
Chr.XII
Net1-mCherry
GFP-LacI
Nucleus
B
birth
SEP
death
Ph
GFP-LacI
Net1-mCh
585 min
855 min
1530 min
1845 min
2130 min
2280 min
2655 min
3015 min
3600 min
3870 min
C
145 Division
75 time (min)
6 GFP-LacI
1 Fluo (A.U.)
1000
2000
3000
4000
Time (min.)
D
SEP
145
75
Cell cycle duration (min)
6
1
GFP-LacI Fluo (A.U.)
-20
0
20
Generation
E
SEP
Cell cycle duration (min)
300
250
200
150
100
50
0
GFP-LacI Fluorescence (A.U.)
×10^4
2
1.5
1
0.5
0
extra rDNA copies
1000
100
10
1
-15
-10
-5
0
5
Generation

Figure 1. rDNA Copy Numbers (ERCs) Increase Exponentially before Entry into Senescence

(A) Schematic showing LacO insertion into each rDNA repeat in TMY8-BY4B strain also co-expressing GFP-LacI and Net1-mCherry.

(B) Phase contrast (top), GFP-LacI fluorescence (middle), and Net1-mCherry fluorescence (bottom) images of a mother cell trapped in a cavity of the microfluidic device from birth to death. The mother cell is delimited by yellow contours. Scale bars: 5 mm.

(C) Schematic showing trajectory of cell cycle duration (gray scale) and GFP-LacI signal (green scale). Black and green density is proportional to the cell cycle duration and nucleolar GFP-LacI fluorescence (rDNA copy number), respectively, for the cell shown in (B).

(D) Single-cell trajectories of cell cycle duration (left) and nucleolar GFP-LacI fluorescence (right) shown as a function of age. Trajectories are aligned to the SEP (black vertical bar).

(E) Cell cycle duration (left) and nucleolar GFP-LacI fluorescence (right) in SEP-aligned cells as a function of age. Inset: Number of presumptive extrachromosomal rDNA (ERCs) as a function of age, calculated from the GFP-LacI signal. The plot shows the exponential rise in ERC number preceding the SEP. N = 64 mother cells. Data are represented as mean ± SEM.

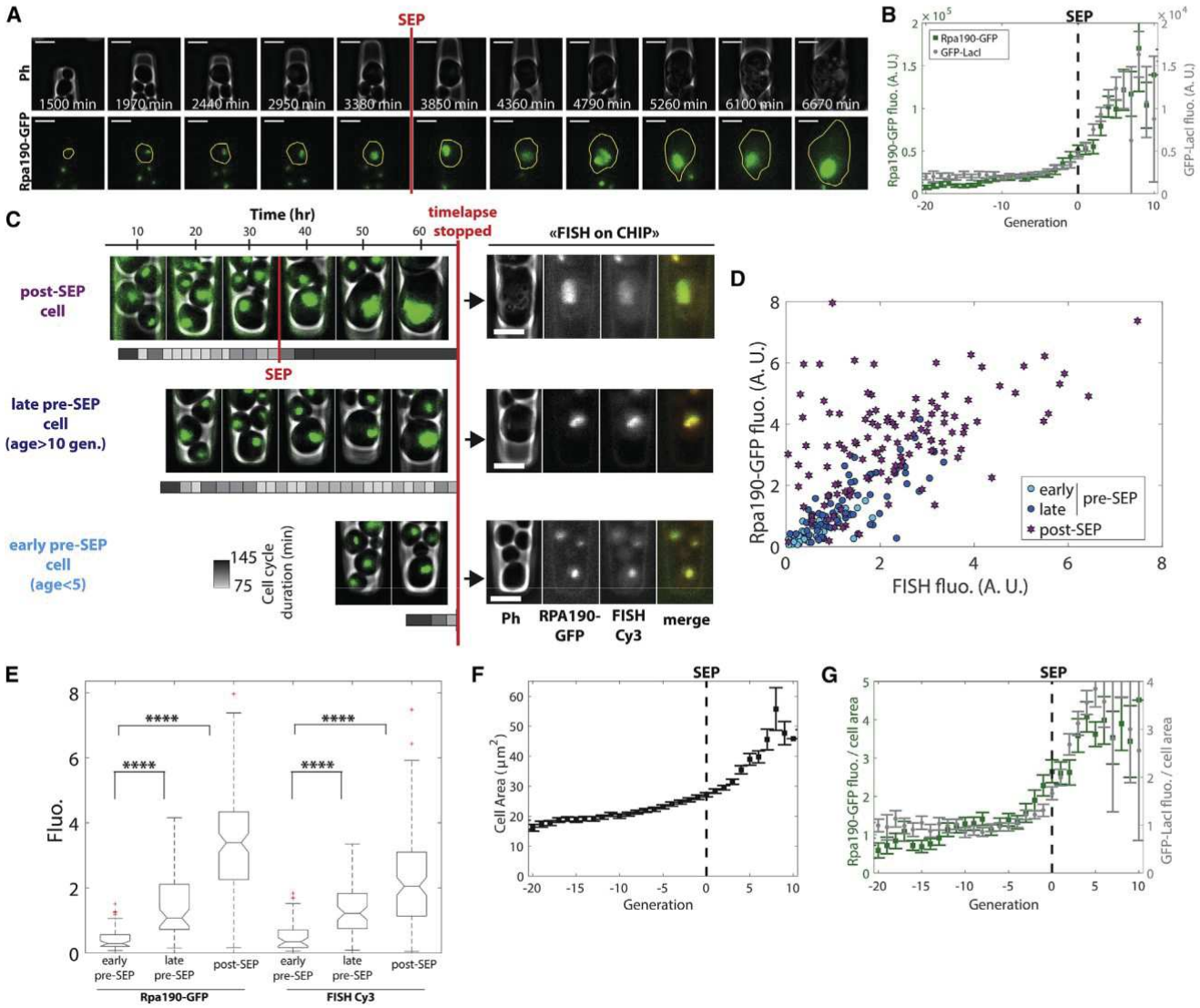
A
SEP
Ph
Rpa190-GFP
1500 min
1970 min
2440 min
2950 min
3380 min
3850 min
4360 min
4790 min
5260 min
6100 min
6670 min
B
SEP
Rpa190-GFP
GFP-LacI
Rpa190-GFP fluo. (A.U.)
GFP-LacI fluo. (A.U.)
Generation
C
Time (hr)
timelapse stopped
«FISH on CHIP»
post-SEP cell
SEP
late pre-SEP cell (age>10 gen.)
early pre-SEP cell (age<5)
145
75
Cell cycle duration (min)
Ph
RPA190-GFP
FISH Cy3
merge
D
Rpa190-GFP fluo. (A. U.)
FISH fluo. (A. U.)
early
late
pre-SEP
post-SEP
E
Fluo.
****
early pre-SEP
late pre-SEP
post-SEP
Rpa190-GFP
FISH Cy3
F
SEP
Cell Area (μm²)
Generation
G
SEP
Rpa190-GFP fluo. / cell area
GFP-LacI fluo. / cell area
Generation

Figure 2. Pre-rRNAs Accumulate Concomitantly with ERCs before Entry into Senescence

(A) Phase contrast and GFP fluorescence micrographs of an Rpa190-GFP-expressing mother cell. The mother cell is delimited by yellow contours.

(B) Total Rpa190-GFP fluorescence (N = 61 cells) and nucleolar GFP-LacI fluorescence (N = 64 cells) in SEP-aligned cells as a function of age.

(C) FISH-on-CHIP. Left: Three examples of Rpa190-GFP-expressing cells tracked for different generation times before RNA FISH labeling. The number of di-visions and their durations are represented in trajectories (gray scale) below the corresponding images for each cell tracked. Right: Cells shown on the left were subjected to FISH with a Cy3-tagged probe detecting all pre-rRNAs.

(D) Rpa190-GFP fluorescence as a function of FISH-Cy3 fluorescence for early pre-SEP (N = 45, light blue), late pre-SEP (N = 68, dark blue), and post-SEP (N = 123, magenta) cells.

(E) Rpa190-GFP and FISH-Cy3 fluorescence for the cells shown in (D).

(F) Cell area calculated from SEP-aligned Rpa190-GFP-expressing mother cells as a function of age (N = 61).

(G) Total Rpa190-GFP fluorescence (green) and nucleolar GFP-LacI (gray) normalized to the cell area of SEP-aligned cells plotted as a function of age.

Scale bars: 5 mm for all images. Data are represented as mean ± SEM except in (E), which are medians. ****p < 0.0001, t-test.

RNA polymerase 1 (Pol I) (Defossez et al., 1998; Denoth Lippuner et al., 2014a); however, the latter has never been experimentally verified. Here, we tested this hypothesis by examining Pol I and rDNA transcription levels.

To assess Pol I levels throughout the cell lifespan, we moni-tored cells expressing a fusion protein of GFP and Rpa190, the largest subunit of Pol I. Unexpectedly, we observed a large increase in total Rpa190-GFP fluorescence levels, starting before the SEP and continuing to death (Figures 2A and 2B; Video S2). By the end of the lifespan, the average Rpa190-GFP fluorescence reached a level approximately 10-fold higher than that in young cells, which paralleled the dynamics of ERC accu-mulation (Figure 2B). This finding suggests that, in contrast to the titration hypothesis, Pol I level may not be a limiting factor of

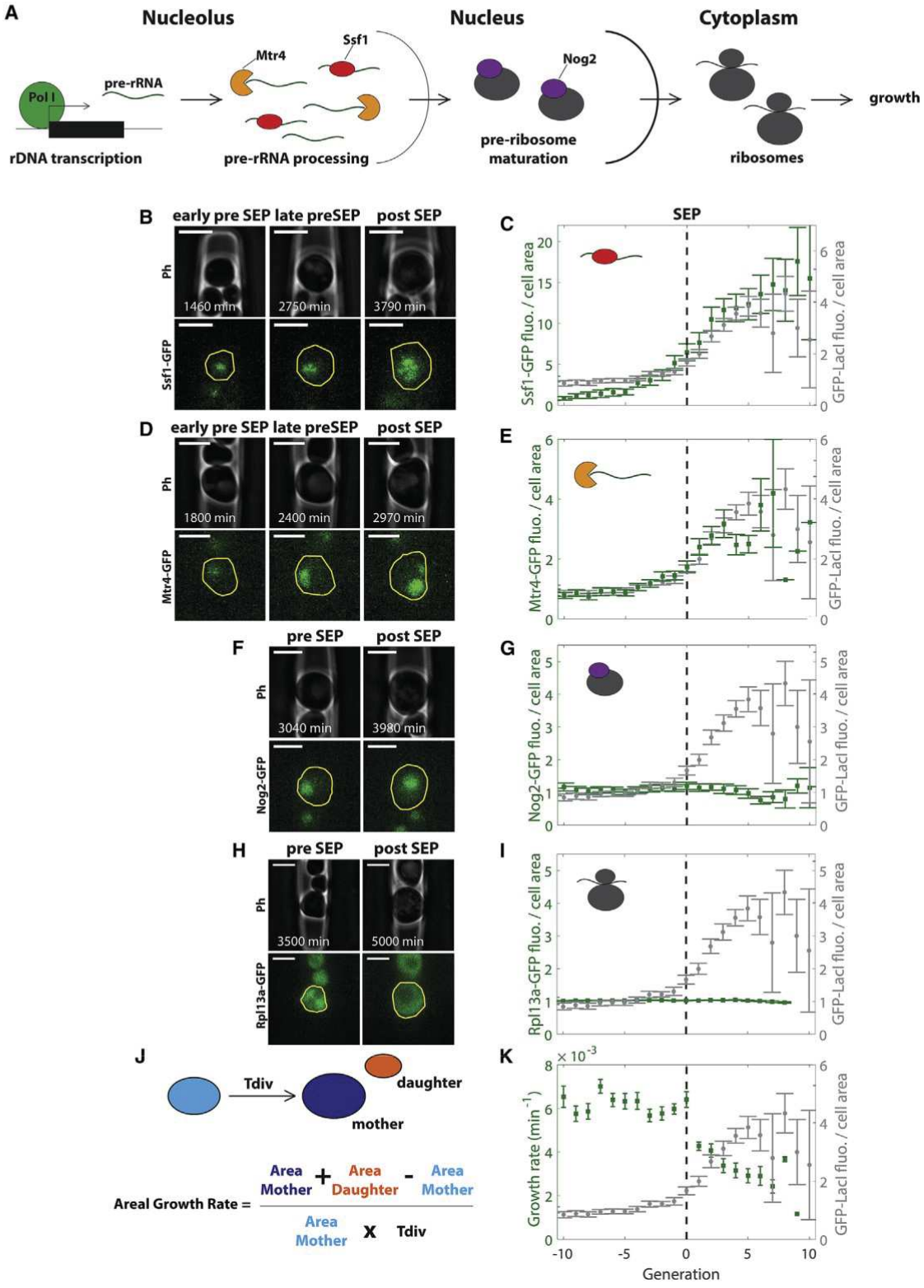

Figure 3. Early and Late Steps of Ribosome Biogenesis Are Uncoupled before Entry into Senescence

(A) Schematic of the steps involved in ribosome biogenesis.

(B) Phase contrast and fluorescence micrographs of an Ssf1-GFP-expressing mother cell at early and late pre-SEP and post-SEP stages.

(legend continued on next page)

rDNA transcription in aging cells because it increases alongside ERCs in a stoichiometric manner.

To directly assess rDNA transcription, we developed a fluores-cence in situ hybridization protocol to measure total pre-rRNA levels in cells growing in the microfluidic chip cavities (fluores-cence in situ hybridization [FISH]-on-CHIP). After monitoring Rpa190-GFP-expressing mother cells for 65 h, RNA FISH was performed using a 35S RNA-targeting probe sequence that labels all nucleolar pre-rRNAs from 35S to 20S. Because mother cell birth was not synchronized in all cavities, we used the history of cell division to classify the cells as in pre-SEP or post-SEP stages when RNA FISH was performed (Figure 2C). Using this methodology, we found that the RNA FISH and Rpa190-GFP fluorescence signals were not only colocalized (Figure 2C) but also correlated quantitatively (Figure 2D), albeit less strongly in post-SEP compared with pre-SEP cells (Pearson correlation coefficients = 0.5 and 0.8, respectively; Figure 2D). This result clearly indicated that the high amount of Pol I is functional and effectively produces increased levels of pre-rRNA. Moreover, based on the assumption that pre-SEP cells that achieved a larger number of generations are more likely to be close to the SEP, we further discriminated between early pre-SEP cells (<5 generations from birth) and late pre-SEP cells (>10 genera-tions). Using this distinction, we confirmed that the increase in pre-rRNA levels preceded the SEP and coincided with the in-crease in Pol I levels (Figure 2E) and, thus, with the timing of ERC accumulation (Figure 2B).

To rule out the possibility that the observed upregulation in pre-rRNA levels simply reflected the characteristic increase in cell size over the lifespan (Figure 2F), we normalized Rpa190-GFP signal to cell area. The kinetics of Pol I accumulation were comparable with or without normalization to cell area (Figure 2B versus Figure 2G), confirming that pre-rRNA levels accumulate before senescence independently of cell growth. Therefore, un-less specified otherwise, all of the following fluorescence data were normalized by cell area.

To sum up, the comparable scale and timings of increase in ERC and pre-RNA levels suggest that the large excess in rDNA transcription is fueled by ERC accumulation.

Increased rDNA Transcription Prior to Entry into Senescence Is Uncoupled from Ribosome Production and Compromises Growth Homeostasis

Given the striking increase in pre-rRNAs before the SEP, we next asked whether ribosome biogenesis was also elevated in these cells and its consequence for the cellular growth rate. Therefore, we used a series of fluorescent reporter proteins to investigate whether successive steps from pre-rRNA processing to ribo-some assembly were coordinated with the increase in pre-rRNA levels (Figure 3A).

To quantify pre-rRNA processing, we expressed a GFP fusion protein with Ssf1, which is a component of 66S pre-ribo-somal particles that contain functionally processed rRNAs (Fatica et al., 2002). Monitoring of Ssf1-GFP fluorescence throughout the lifespan revealed similar dynamics to that of GFP-LacI (Figures 3B and 3C; Video S3). As a second pre-rRNA processing proxy, we monitored Mtr4, which is a compo-nent of the nuclear exosome required for RNA degradation during pre-rRNA processing (de la Cruz et al., 1998). Interest-ingly, Mtr4-GFP fluorescence also increased when the cells went through the SEP transition (Figures 3D and 3E). These data, therefore, indicate that components of the pre-rRNA maturation machinery were concomitantly upregulated with Pol I, suggesting that the increase in pre-rRNA levels was due to increased rDNA transcription rather than a defect in pre-rRNA processing.

To monitor the later steps associated with pre-ribosome nuclear export, we used a Nog2-GFP fusion protein. Nog2 is required for the nucleoplasmic steps of pre-60S maturation (Baßler et al., 2001; Saveanu et al., 2001), and its expression level is assumed to mirror the export rate. However, in contrast to the dynamics of Rpa190, Ssf1, and Mtr4, we found that the total nuclear Nog2-GFP signal (normalized to cell area) was remark-ably stable throughout the cellular lifespan (Figures 3F and 3G; Video S4). Moreover, the average total ribosome content (normalized to cell area), monitored using GFP-fused Rpl13a, a component of the 60S ribosomal subunit, was also maintained at a near constant level until cell death (Figures 3H and 3I; Video S5). Taken together, these data indicate that the abundance of components of the late nuclear steps of ribosome biogenesis was relatively unaffected by cell age, suggesting that the pre-SEP excess in rDNA transcription does not lead to more ribo-some assembly. Because ribosome biogenesis is finely tuned to support cell growth under physiological conditions, we hypothesized that the lack of coordination between rDNA tran-scription and ribosome biogenesis might be detrimental to growth in the post-SEP part of the cellular lifespan. Consistent with this, the cell growth rate actually declined in post-SEP (Fig-ures 3J and 3K), confirming that the failure to coordinate rDNA transcription and ribosome assembly could be deleterious to cell growth.

A Loss of Nuclear Homeostasis Drives the Decline in Cellular Physiology in Post-SEP Cells

The observation of a dramatic increase in nucleolar size, which is likely to originate from the accumulation of pre-RNAs prior to

(C) Ratios of Ssf1-GFP fluorescence (green, N = 56 cells) and GFP-LacI fluorescence (gray, N = 64 cells) to cell area in SEP-aligned cells as a function of age. (D and E) Same as (B) and (C), respectively, for Mtr4-GFP-expressing cells (N = 40 cells).

(F and G) Same as (B) and (C), respectively, except for pre-SEP and post-SEP Nog2-GFP-expressing cells (N = 33 cells). (H and I) Same as (B) and (C), respectively, except for Rpl13a-GFP-expressing cells (N = 32 cells).

(J) Schematic showing calculation of growth rate based on segmented contouring of the mother cells before (light blue) and after (dark blue) division and the newborn daughter (orange).

(K) Growth rate (green, measured as in J, N = 36 cells) and ratio of GFP-LacI fluorescence to cell area (gray, N = 64 cells) of SEP-aligned mother cells as a function of age.

Scale bars: 5 mm for all images. Data are represented as mean ± SEM.

A

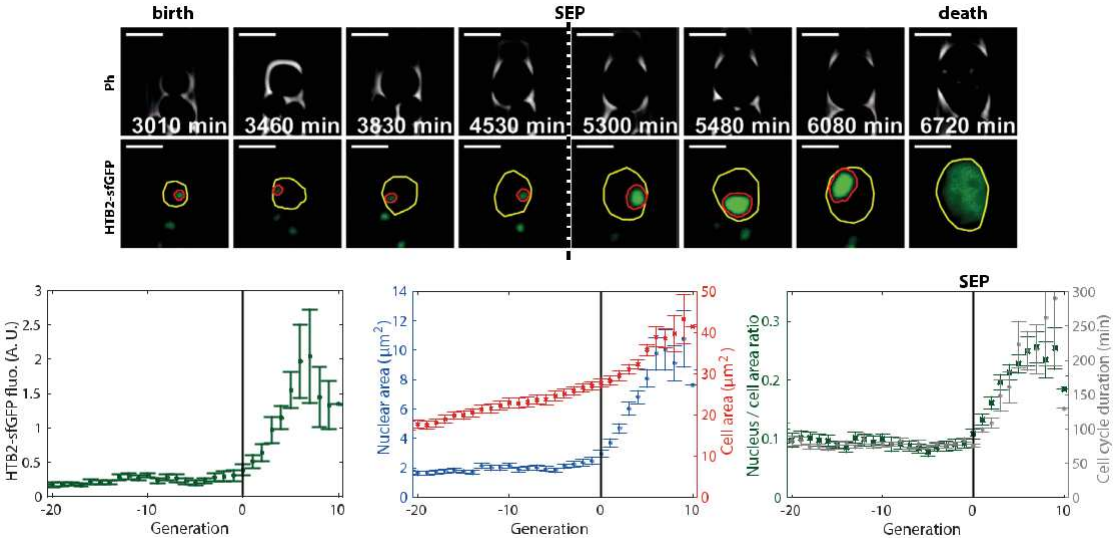
birth
SEP
death
Ph
HTB2-sfGFP
3010 min
3460 min
3830 min
4530 min
5300 min
5480 min
6080 min
6720 min
HTB2-sfGFP fluo. (A. U.)
Nuclear area (μm²)
Cell area (μm²)
Nucleus / cell area ratio
Cell cycle duration (min)
Generation

B C D

E

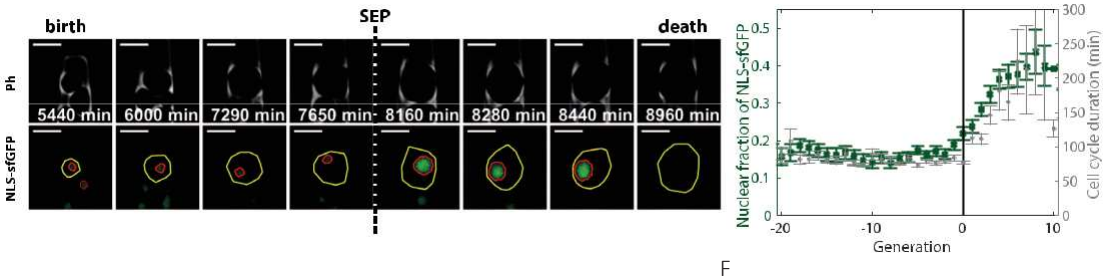
birth
SEP
death
Ph
NLS-sfGFP
5440 min
6000 min
7290 min
7650 min
8160 min
8280 min
8440 min
8960 min
Nuclear fraction of NLS-sfGFP
Cell cycle duration (min)
Generation

F

Figure 4. Loss of Nuclear Homeostasis Occurs Concomitantly with Entry into Senescence

(A) Phase contrast and fluorescence micrographs of a mother cell expressing the nuclear marker Htb2-sfGFP.

(B) Total Htb2-sfGFP fluorescence in SEP-aligned cells as a function of age. (N = 23 cells).

(C) Nuclear area (left axis [blue]) and cellular area (right axis [red]) of SEP-aligned cells as a function of age. (N = 23 cells).

(D) Ratio of the nuclear to cell area (left axis [green]) and cell cycle duration (right axis [gray]) of SEP-aligned cells as a function of age. (N = 23 cells).

(E) Phase contrast and fluorescence micrographs of a mother cell expressing NLS-sfGFP.

(F) Fraction of NLS-sfGFP fluorescence localized to the nucleus (left axis [green]) and cell cycle duration (right axis [gray]) in SEP-aligned cells as a function of age (N = 24 cells).

Scale bar: 5 mm for all images. Data are represented as mean ± SEM.

the SEP, prompted us to investigate how it may be linked to the subsequent decline in cell division rate. To this end, we wondered whether the overall nuclear size scales with that of the nucleolus in aging mothers. We used the histone 2B reporter Htb2-sfGFP as a nuclear reporter (Figure 4A; Video S6). Strik-ingly, this analysis revealed an important increase in total histone levels, the onset of which was concomitant with the SEP. Simi-larly, the cells underwent a dramatic increase in nuclear area (the nuclear contours were delineated using the Htb2-sfGFP marker), which could not be attributed to the age-dependent in-crease in cell size (Figure 4C). Indeed, the nucleus-to-cell area ratio (N/C ratio), which was remarkably stable before the SEP despite a progressive increase in cellular size, went up by about 150% in post-SEP cells (Figure 4D; Video S6) (Rempel et al., 2019). This result was unexpected knowing that the N/C ratio is tightly regulated and is relatively unaffected by mutations that perturb either cell cycle progression or cell size (Jorgensen et al., 2007; Kume et al., 2017; Neumann and Nurse, 2007). In addition, we noticed the increase in N/C ratio was clearly poste-rior to pre-SEP increase in rDNA transcription and ERC accumu-lation and, yet, was strikingly identical to the evolution of the cell cycle duration (Figure 4D). This suggests a direct relationship be-tween dysregulation of nuclear size and the onset of physiolog-ical decline.

To check whether other proteins targeted to the nucleus would tend to undergo an increased accumulation in the nucleus after the SEP, we investigated the localization of sfGFP proteins fused with a nuclear localization signal (NLS-sfGFP) (Figure 4E). The fraction of NLS-sfGFP localized to the nucleus increased consid-erably as the cells passed the SEP (from 14% to 40%; Figure 4F). This increase was not due to an upregulation of NLS-sfGFP expression with age, as the total cellular fluorescence of sfGFP was almost identical throughout cellular lifespan with or without NLS (Figures S4A and S4B). These results suggested that nu-clear transport was dramatically affected by age, in agreement with a recent study (Rempel et al., 2019). Altogether, these re-sults clearly unravel a loss in nuclear homeostasis in post-SEP cells characterized by an enlargement of the nucleoplasm and the accumulation of nuclear proteins, which quantitatively coin-cides with the decline in cellular function.

Asymmetrical Nuclear and Nucleolar Division Enables the Rejuvenation of Daughters of Senescent Mother Cells

It has long been observed that ERCs are primarily inherited by mother cells upon nuclear division (Sinclair and Guarente, 1997), and this asymmetrical inheritance is thought to drive daughter cell rejuvenation (Kennedy et al., 1994). However, neither asymmetrical partitioning of ERCs nor rejuvenation of daughter cells has been demonstrated by live single-cell tracking.

To address this, we examined the fate of the GFP-LacI fluores-cence signal in aging mother cells upon nuclear division. Although GFP-LacI was equally partitioned into the daughter cells of young (i.e., pre-SEP) mothers, the fluorescence signal was disproportionately retained by older (i.e., post-SEP) mothers, and the daughters exhibited only basal GFP-LacI levels, consistent with asymmetrical segregation of ERCs (Fig-ures 5A and 5B) (Shcheprova et al., 2008). This further confirms that the increase in rDNA copies observed in aged mothers is due to an accumulation of ERCs rather than to an expansion of the chromosomal rDNA array, which would be inherited by daughters.

To determine whether the recovery of basal ERC levels was associated with a recovery of physiological function in daugh-ters, we examined their cell cycle duration. The first division time of yeast cells is highly dependent on cell volume (Hartwell and Unger, 1977), which varies considerably with age (Figure 2F); therefore, we began monitoring from the second cell division (i.e., the first division of the daughter cell as a mother; Figure 5C). We observed that the cell cycle duration of daughter cells was comparable to that of pre-SEP mother cells (Figure 5D), suggest-ing that the deleterious hallmarks of aging are not inherited by the daughter cells.

Therefore, to further investigate whether daughters were born clear of the other aging markers identified in this study, we exam-ined the nucleolar size (Figure 5E), Pol I levels (Rpa190-GFP; Fig-ures 5F and 5G), N/C ratio (Figures 5H and 5I), and Ssf1-GFP fluorescence levels (Figures S4C–S4E) of daughters born to mothers of young and old replicative ages (from 10 generations pre-SEP to 10 generations post-SEP). Notably, monitoring of each of these phenotypes over multiple generations indicated that the daughter cells displayed a rejuvenated phenotype, regardless of the age of the mother (Figures 5E–5I). These data suggest that asymmetrical partitioning of the entire nucleolus and nuclear content is involved in the rejuvenation process, thus freeing the daughters from the effects of dysregulated rDNA transcription and pre-ribosomal assembly and increased N/C ratio observed in aged mother cells.

A previous study found that daughters of very old mothers (i.e., more than 90% of the lifespan) display a very short RLS (Ken-nedy et al., 1994), suggesting the existence of mechanisms that limit the efficiency of the rejuvenation process, which is in contradiction with the daughter clearance of aging markers re-ported here. Technical limitations preclude tracking of the RLS of daughters born from post-SEP mothers within the microflui-dics device. However, we observed the appearance of a multi-nucleated cell phenotype, a reflection of whole-genome instability, the frequency of which linearly increased with replica-tive age after the SEP (Figures 5J and 5K) (Neurohr et al., 2018). Importantly, we found that this phenotype, which is likely to be detrimental to cellular function, was faithfully inherited by daughter cells (about 60% exhibiting the multi-nucleated pheno-type; Figures 5J and 5L). This observation suggests that, despite efficient epigenetic segregation of aging markers by asymmet-rical nucleolar and nuclear division, mother cells are likely to un-dergo genetic alterations following the loss in nuclear homeosta-sis, which ultimately compromise daughter cell rejuvenation. Collectively, the results shown here contribute to explain the mechanism, the chronology, and the limitations associated with daughter cell rejuvenation in aging mothers.

A Probabilistic Event Drives the Transition into Replicative Senescence

Previous work proposing that accumulation of ERCs is asso-ciated with entry into senescence is supported by the fact that fob1D mutants, which show defects in ERC excision (De-fossez et al., 1999; Kobayashi, 2003; Mansisidor et al., 2018) and, hence, have lower ERC levels than wild-type (WT) cells, also have much longer lifespans (Defossez et al., 1999). Conversely, sir2D mutants, which accumulate high levels of ERCs, are relatively short-lived (Kaeberlein et al., 1999). Therefore, we asked whether and how the reduced and elevated levels of ERCs in fob1D and sir2D mutants, respec-tively, modified the scenario of entry into senescence described in this study.

We observed that the median lifespans of fob1D and sir2D mutants were indeed much longer and shorter, respectively, than that of WT cells (36, 13, and 29 generations, respectively; Figure 6A). Most (87%) of sir2D cells experienced a SEP prior to cell death, similarly to WT (Figures S5B and S5C). However, a detailed analysis of the trajectory of individual fob1D cells revealed that the majority (68.3%) did not undergo a slow-down in the cell cycle before death (referred to as No-SEP cells; Figures 6C and 6D) compared with only 7% of WT cells (Figure 1D). We also did not observe accumulation of GFP-LacI fluorescence during cellular lifespans of the No-SEP fob1D subpopulation (Figures 6E and 6F), which is in contrast to the remaining fob1D population that did experience the SEP (referred to as With-SEP), which displayed a similar in-crease in GFP-LacI (Figures 6E and 6F) and Net1-mCherry fluorescence signals (Figures S6A–S6C) as observed in WT cells.

This observation suggested that ERCs do not accumulate in No-SEP fob1D cells; therefore, they must die through an ERC-independent mechanism. To investigate this further and to establish the precise relationship between ERC levels and concomitant or downstream events, we monitored Pol I levels (using Rpa190-GFP), the N/C ratio (Htb2-GFP), and the growth rate in the No-SEP and With-SEP fob1D sub-populations. Notably, the Pol I content (Figures 6B and 6G; Video S7), N/C ratio (Figure 6H; Figure S6D), and growth rate (Figure S6F) of the No-SEP subpopulation were nearly constant throughout the lifespan, whereas the phenotypes of the With-SEP fob1D subpopulation and WT cells were virtually indistinguishable (Figures 6B, 6G, and 6H; Figures S6E and S6F; Video S8). A recent study suggested that excessive

Cell Reports 28, 408–422, July 9, 2019

415

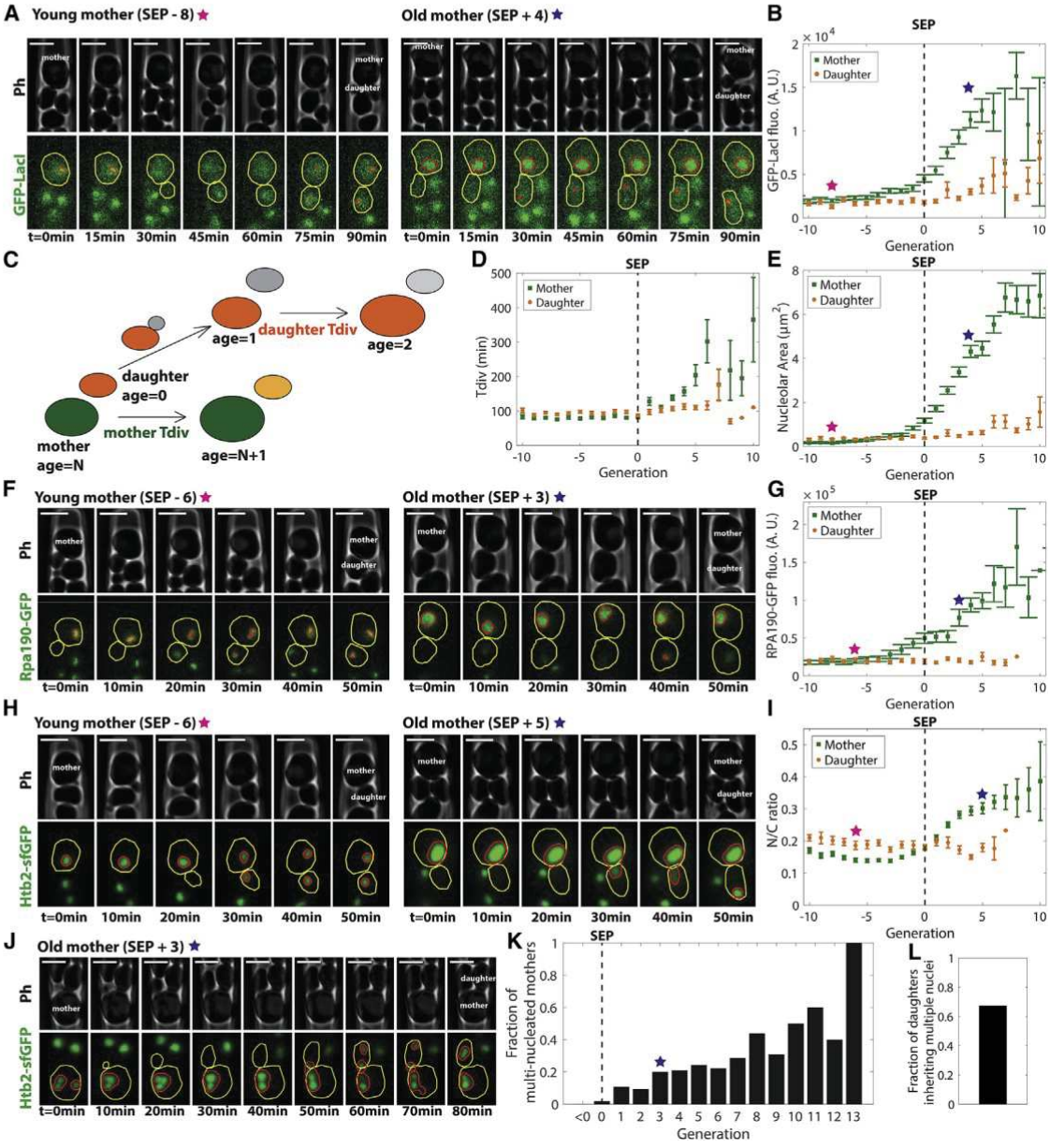

Figure 5. Rejuvenated Daughter Cells of Aging Mothers Show Basal Levels of ERCs and Pre-rRNA Synthesis

(A) Phase contrast and fluorescence micrographs of a dividing GFP-LacI-expressing mother cell at a young age (8 divisions before SEP, left, pink star) and at an old age (4 divisions after SEP, right, blue star).

(B) Nucleolar GFP-LacI fluorescence in SEP-aligned mother (green) and daughter (orange) cells as a function of age (N = 23–64 cells). Pink and blue stars indicate the stages corresponding to the cells shown in (A).

(C) Schematic showing calculation of the cell cycle duration for the daughter cell shown in orange.

(D) Cell cycle duration of SEP-aligned mother (green) and daughter (orange) cells as a function of age (N = 29 cells).

(E) Nucleolar area in SEP-aligned mother (green) and daughter (orange) cells as a function of age (N = 23–64 cells).

(F and G) Same as (A) and (B), respectively, except showing Rpa190-GFP fluorescence (N = 21–61 cells).

(H) Same as (A) except showing Htb2-sfGFP-expressing cells.

(I) Nuclear to cellular area (N/C) ratio in SEP-aligned mother (green) and daughter (orange) cells as a function of age (N = 42 cells).

(J) Phase-contrast and fluorescence micrographs of a multi-nucleated mother cell transmitting two nuclei to its daughter.

(K) Fraction of multi-nucleated mothers as a function of age.

(L) Fraction of daughters inheriting nuclear defects (31 of 46 cells).

Scale bars: 5 mm for all images. Data are represented as mean ± SEM.

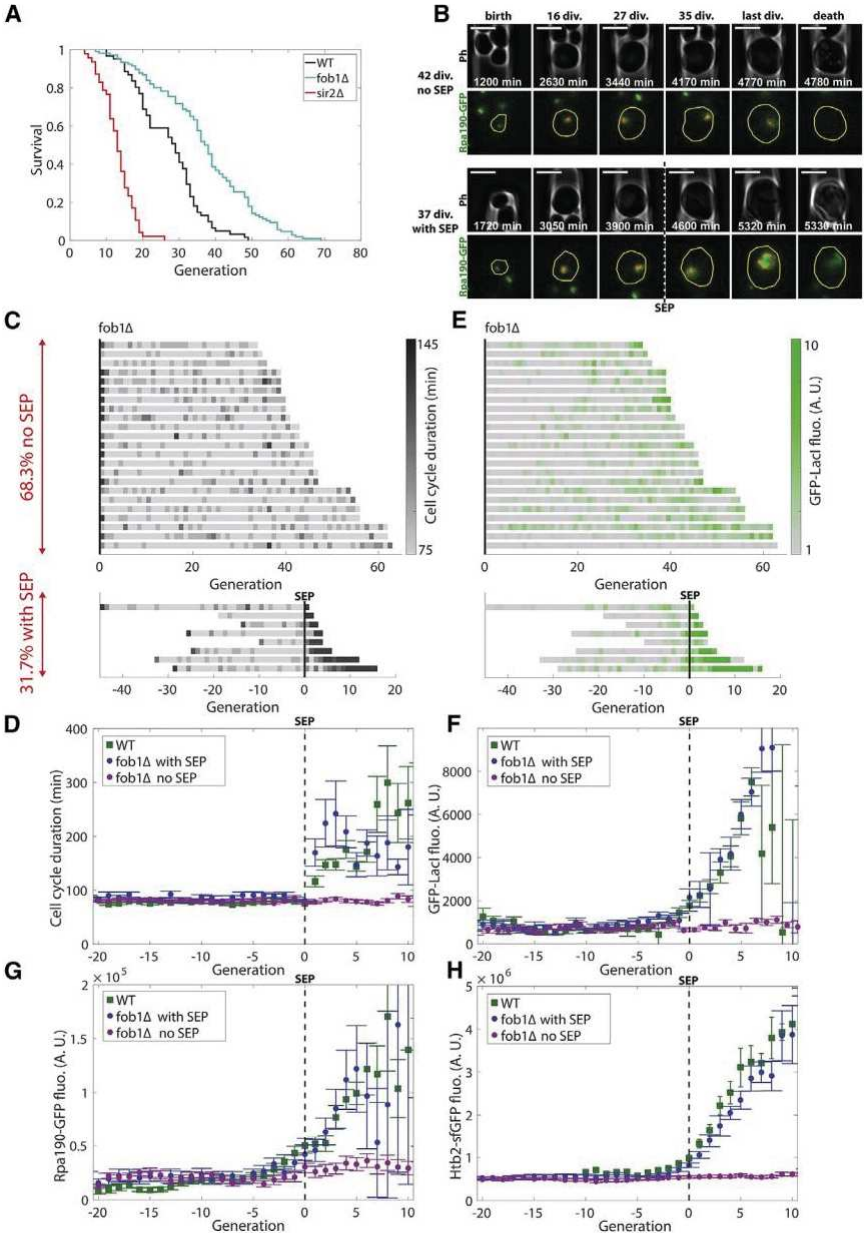
A
Survival
Generation
WT
fob1Δ
sir2Δ
B
birth
16 div.
27 div.
35 div.
last div.
death
42 div.
no SEP
1200 min
2630 min
3440 min
4170 min
4770 min
4780 min
37 div.
with SEP
1720 min
3050 min
3900 min
4600 min
5320 min
5330 min
Ph
Rpa190-GFP
SEP
C
fob1Δ
68.3% no SEP
31.7% with SEP
Cell cycle duration (min)
Generation
SEP
E
fob1Δ
GFP-LacI fluo. (A. U.)
Generation
SEP
D
WT
fob1Δ with SEP
fob1Δ no SEP
Cell cycle duration (min)
Generation
SEP
F
WT
fob1Δ with SEP
fob1Δ no SEP
GFP-LacI fluo. (A. U.)
Generation
SEP
G
WT
fob1Δ with SEP
fob1Δ no SEP
Rpa190-GFP fluo. (A. U.)
Generation
SEP
H
WT
fob1Δ with SEP
fob1Δ no SEP
Htb2-sfGFP fluo. (A. U.)
Generation
SEP

Figure 6. Senescence Entry Is Controlled by a FOB1-Dependent Stochastic Process That Dysregulates Nucleolar Activity

(A) Survival curves of WT cells (black, RLS = 29, N = 61), fob1D cells (cyan, RLS = 36, N = 126), and sir2D cells (red, RLS = 13, N = 55 cells).

(B) Phase-contrast and fluorescence micrographs of two Rpa190-GFP-expressing fob1D mother cells: one that never experiences a SEP (RLS = 42 generations; top) and one that experiences a SEP after 33 divisions (RLS = 37 generations; bottom). Scale bars: 5 mm.

(C) Trajectories of cell cycle durations for fob1D No-SEP (top) and With-SEP (bottom) sub-populations.

(D) Cell cycle duration of SEP-aligned WT cells (green, N = 57), With-SEP fob1D cells (blue, N = 40), and No-SEP fob1D cells (magenta, N = 84).

(E) Trajectories of GFP-LacI fluorescence for the same cells represented in (C).

(F–H) GFP-LacI (F), Rpa190-GFP (G), and Htb2-sfGFP (H) fluorescence in SEP-aligned WT cells (green), With-SEP fob1D cells (blue), and No-SEP fob1D cells (magenta). No-SEP cells were aligned from birth with generation 0 set at the median SEP of the corresponding With-SEP fob1D cells (30 for D, 25 for F, 21 for G, and 27 for H) (N = 20–61 cells). Data are represented as mean ± SEM.

cell growth could contribute to senescence by diluting cyto-plasm (Neurohr et al., 2019). Although it is not excluded that this process could impair cell survival at very late stages of lifespan, cytoplasm dilution does not seem to be involved in ERC accumulation and to trigger the SEP, as cell size increased very similarly throughout the lifespan in fob1D cells (Figure S6G) despite different cell fates (With-SEP or No-SEP).

In contrast to fob1D, sir2D cells presented a shorter lifespan than WT (Figure 6A) and an early entry into senescence (Fig-ure S5B), which is consistent with ERC accumulation being the driver of SEP. However, GFP-LacI fluorescence signal aligned at SEP exhibited very similar trends in WT and sir2D populations (Figures S5A, S5D, and S5E), suggesting that the process of exponential accumulation of ERCs is identical in sir2D and WT (doubling time, 1.9 ± 1.4 generations). Thus, the early entry into senescence observed in sir2D is likely due to a higher rate of ERC excision rather than to a faster accumulation of ERCs.

These data further support the hy-pothesis that ERC accumulation may contribute, at least in part, to the loss of nuclear homeostasis in aging cells. In addition, the heterogeneity in cell fate observed in the fob1D mutant sug-gests that the ERC-dependent entry into senescence is a stochastic pro-cess, the probability of which is greatly reduced by the fob1D mutation and increased by the sir2D mutation, and

that an ERC-independent mechanism sets the subsequent limit of replicative longevity.

A Quantitative Model of Entry into Replicative Senescence in Budding Yeast

Our results thus far support a clear order of events in the transi-tion to replicative senescence in yeast. The probabilistic excision of an ERC leads to the exponential accumulation of rDNA copies over a multi-generation timescale and precedes the onset of SEP and loss of nuclear homeostasis that likely causes cell death (Figure 7A).

Because this interpretation derives from quantitative experi-mental results (ERC accumulation, cell cycle duration, and life-span measurements), we sought to build a computational model

Cell Reports 28, 408–422, July 9, 2019

417

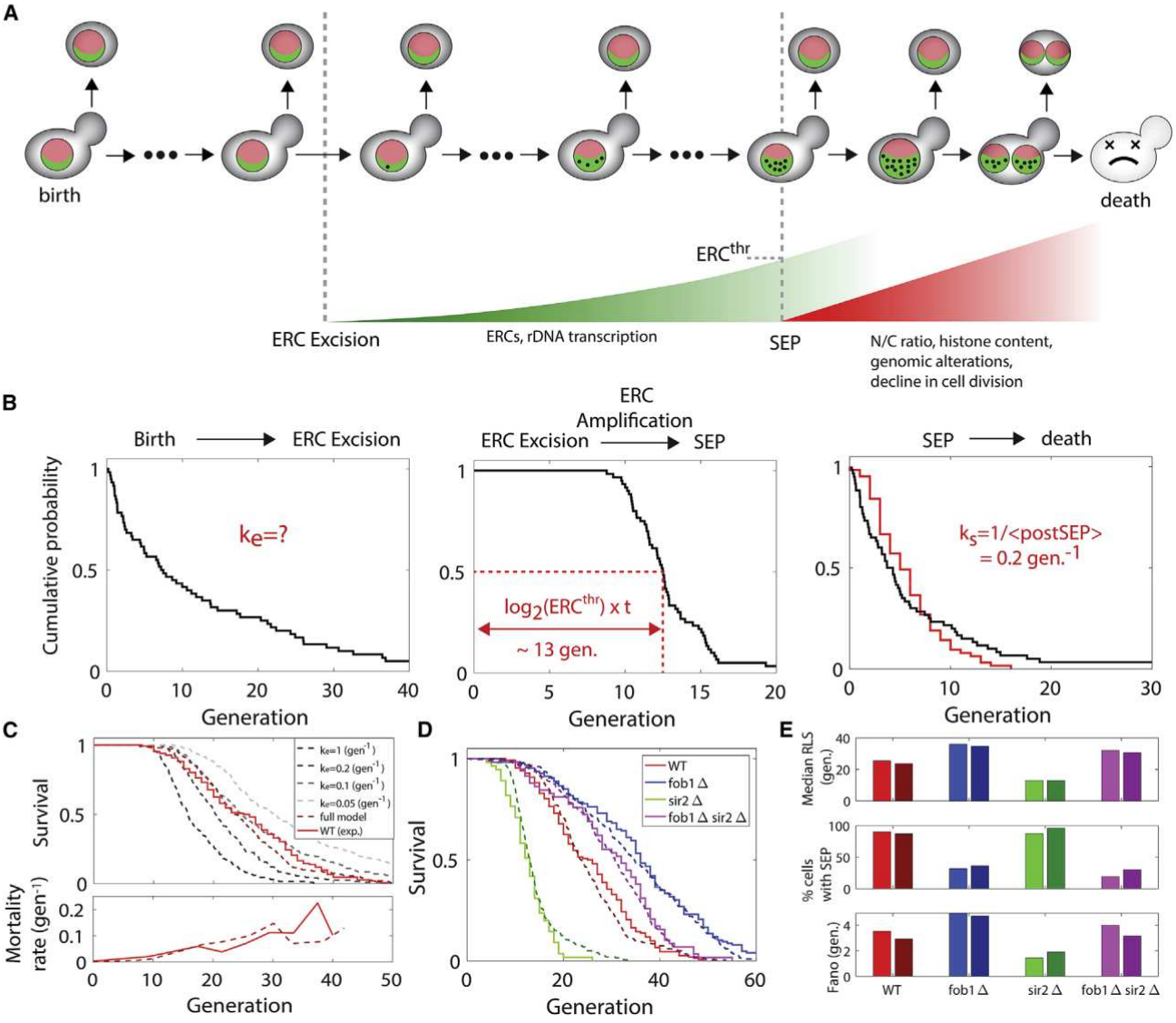
A
birth
death
ERC^thr
ERC Excision
ERCs, rDNA transcription
SEP
N/C ratio, histone content, genomic alterations, decline in cell division
B
Birth → ERC Excision
ERC Amplification
ERC Excision → SEP
SEP → death
Cumulative probability
ke=?
log2(ERC^thr) x t
~ 13 gen.
ks=1/<postSEP>
= 0.2 gen.^-1
Generation
C
Survival
Mortality rate (gen^-1)
ke=1 (gen^-1)
ke=0.2 (gen^-1)
ke=0.1 (gen^-1)
ke=0.05 (gen^-1)
full model
WT (exp.)
D
WT
fob1 Δ
sir2 Δ
fob1 Δ sir2 Δ
E
Median RLS (gen.)
% cells with SEP
Fano (gen.)
WT
fob1 Δ
sir2 Δ
fob1 Δ sir2 Δ

Figure 7. Biological and Computational Model of Entry into Senescence

(A) Schematic showing the three steps involved in ERC-dependent senescence (ERC excision, ERC self-replication, and post-SEP interval).

(B) Cumulative probability (black lines) associated with each step shown in (A), as defined by the computational model (see STAR Methods), by using experimentally determined parameter values (indicated in red; see Table S1). Left: Cumulative distribution of times from birth to the first ERC excision. Middle: Cumulative distribution of the duration of accumulation of ERCs from 1 to ERC^{thr} copies. The median (red dashed line) corresponds to the experimentally measured value reported in Figure 2E. Right: Cumulative distribution of times from SEP to cell death. The red line represents the experimentally measured distribution in WT.

(C) Top: Experimentally determined RLS of WT cells (solid line) and the influence of the excision rate k_e on RLS, as predicted by the computational model (gray dashed lines). The dark red line indicates the numerical RLS obtained by adding an ERC-independent cause of death (referred to as the ''full model,'' see A Quantitative Model of Entry into Replicative Senescence in Budding Yeast). Bottom: Mortality rate (i.e., probability of live cells to die per generation) as a function of age calculated for both experimental (solid red line) and full model (red dashed line).

(D) Experimentally determined (solid lines) and computationally predicted (dashed lines) RLS for WT cells and the indicated mutants.

(E) Experimentally determined (light bars) and computationally predicted (dark bars) median RLS (top), fractions of cells experiencing a SEP (middle) and Fano factor (bottom) obtained for WT cells and each indicated mutant.

N = 200 cells for all computationally determined curves.

based on this scenario to determine whether it could recapitulate the distribution of lifespans and the fraction of cells experiencing the SEP in WT cells as well as in the mutant strains in which the ERC excision rate is perturbed.

We designed a stochastic numerical model with continuous time—inspired from a previous study (Gillespie et al., 2004)— whereby the cellular lifespan is the convolution of three steps (see Figure S7A and STAR Methods for details): the stochastic

excision of the first ERC (rate k_e; Figure 7B, left); the self-replica-tion of ERCs (with a doubling time t; Figure 7B, middle) until a threshold number ERC^{thr} is reached that corresponds to the SEP; and an interval between SEP and cell death, which is asso-ciated with the loss of nuclear homeostasis (rate k_s; Figure 7B, right).

Most parameter values could be estimated experimentally from single-cell measurements: the number of generations achieved by the cells in the post-SEP interval was close to an exponential distribution with a mean post-SEP around 5 genera-tions (Figure 7B), in agreement with a random death rate k_s =

1/(post-SEP) = 0.2 generation (gen) ^{1} (Figure 7B). The ERC doubling time t = 1.5 gen and the threshold number ERC^{thr} =
360 were measured from the exponential increase in GFP-LacI fluorescence signal (Figure 1D). These two parameters set the timescale of the ERC self-replication phase, i.e., $\log_2(ERC^{thr})$ 3 t 13 generations (Figure 7B). k_e was the only free parameter to fit the model to the data. Interestingly, k_e = 0.1 gen ^{1} provided good agreement with the experimental RLS in WT cells (Fig-ure 7C, top panel), except for the prolongation of survival observed at advanced ages. Importantly, this indicates that the increased mortality with age (which is the formal definition of ag-ing, see bottom panel on Figure 7C) can be well accounted for by the sequence of three age-independent kinetic steps. In this sce-nario, replicative aging appears to derive from a stochastic trig-gering event related to rDNA instability, the outcome of which is protracted due to the long period over which ERC amplification occurs as well as substantial cellular buffering against the dele-terious consequences of ERC accumulation occurring in post-SEP. This result differs from the model of Gillespie et al. (2004), in which a quadratic increase of the probability of ERC excision with age was required to obtain a good fit to the data. The differ-ence comes from the fact that a substantial part of the variability in survival is due to the post-SEP interval (Figure S7), which could not be taken into account in the Gillespie et al. model.

Based on this model, lowering the rate of ERC excision k_e should recapitulate the lifespan extension observed in fob1D cells. However, it is much less clear how a refined model could quantitatively capture the partitioning of individual fob1D life-spans into ERC-dependent versus ERC-independent cell fates. To investigate this, we included in the model the possibility that cell death could also occur due to a competing ERC-independent cause following a standard Gompertz law (i.e., dictated by a mor-tality rate l given by l[age] = l_0 3 exp[m 3 age], where l_0 and m are constant parameters). Assuming that the parameters associated with the Gompertz law (l_0 and m) were identical in the fob1D mutant and WT, fitting k_e, l_0, and m to the data provided reason-able agreement with the RLS curves for WT cells (k_e = 0.1 gen ^{1}) and fob1D cells (k_e = 0.02 gen ^{1}) (Figure 7D), suggesting that the mutant has a 5-fold lower ERC excision rate than WT cells. Most importantly, the model also accurately captured the fraction of cells experiencing an ERC-dependent SEP in both WT and fob1D cells (Figure 7E; Figures S7B and S7C). In addition, intro-ducing the Gompertz law improved the agreement of the model to the experimental RLS curve for WT cells by cutting the long tail in the survival curve (Figure 7C, top panel).

Conversely, we wondered under which assumption this model could capture the lifespan reduction observed in the sir2D back-

ground, which prematurely accumulates ERCs to high levels (Kaeberlein et al., 1999). A decent fit to the data required both a 20-fold higher ERC excision rate (k_e = 2 gen ^{1} in sir2D versus 0.1 gen ^{1} in WT) and a 3-fold larger basal mortality rate (l_0 =

0.03 gen ^{1} in sir2D versus l_0 = 0.01 gen ^{1} in WT) than in WT, showing that the premature death in this mutant has multiple origins (i.e., not only ERC-dependent), as suggested previously (Kaeberlein et al., 1999). The consequence of a high rate of ERC excision was to considerably reduce the influence of the interval time between the birth and ERC excision on the total lifespan, hence reducing the cell-cell variability therein. Using the Fano factor (Fano, 1947), which provides a mean-indepen-dent measurement of heterogeneity in a distribution, we found

a 3-fold reduction in lifespan variability in the sir2D strain compared to WT, which was successfully accounted for by the model (Figure 7E; Figure S7C). Conversely, the fob1D strain dis-played a marked increase in lifespan variability compared to WT (Figure 7E).

In contrast to sir2D, the experimental RLS of the fob1D sir2D double mutant was slightly higher than that of WT cells (Fig-ure 7D), which is in agreement with previous studies (Kaeberlein et al., 1999, 2004). As with the fob1D strain, only a minority of double mutant cells (18%) experienced a SEP, suggesting that the ERC excision rate was similar to that of the single fob1D mutant and that the sir2 mutation only governed the ERC-inde-pendent death rate. Indeed, a good agreement with experi-

mental data in the double mutant was found when using a low ERC excision rate (k_e = 0.02 gen ^{1}) with a high ERC-independent mortality rate, as in the sir2D mutant (l_0 = 0.03 gen ^{1}) (Fig-ure S7C). Altogether, this computational model provides support for a probabilistic scenario of entry into senescence, which quantitatively explains the origin of cell-cell variability in cellular lifespan. Furthermore, it suggests that a stochastic age-inde-pendent crisis associated with rDNA instability sets the first repli-cative limit and that a different mechanism may set subsequent replicative limits.

DISCUSSION

Heterogeneity in cellular lifespan within a population has long been a major impediment to understanding the mechanisms governing entry into senescence by blurring the chain of causal-ity. In this study, we used longitudinal tracking of individual cells coupled with quantitative analysis and computational methods to propose a comprehensive description of the sequence of events leading to replicative arrest in budding yeast. Our sin-gle-cell approach strongly suggests a temporal distinction between early and later hallmarks of senescence, thereby ques-tioning the classical view of a multifactorial aging process in which the causes and consequences of events are often re-ported to be tightly intertwined. Instead, our analysis establishes that ERC accumulation may drive an upregulation of rDNA tran-scription prior to the SEP and that entry into senescence is accompanied by a breakdown in nuclear homeostasis that is likely to trigger cell death. In this context, it appears that studies focusing on the last division preceding cell death are more likely to refine our understanding of cellular ''necrology'' than to explain the mechanisms that trigger replicative senescence.

Cell Reports 28, 408–422, July 9, 2019 419

Excision and accumulation of ERCs in mother cells are well-established events proposed to limit yeast lifespan (Sinclair and Guarente, 1997). A recently published study examined the cell cycle impairment during the last divisions before cell death by using the nucleolar marker Net1-mCherry as an indirect proxy for ERCs (Neurohr et al., 2018). By directly monitoring and quan-tifying the dynamics of rDNA copy number in living cells, throughout their whole lifespan, our study further reveals that ERCs follow a multiplicative self-replicative process with high ef-ficiency, finally providing evidence for a long-standing but previ-ously unverified hypothesis (Sinclair and Guarente, 1997). Then, we provide reliable estimates of the maximum number of ERCs (360) that can be tolerated by the cell before detrimental effects ensue. The large number of ERCs accumulated by the time of death (1,500) reveals the magnitude of the increase in rDNA content, which is comparable to the size of the entire genome (Neurohr et al., 2018; Sinclair and Guarente, 1997). The inability of cells to sustain exponential expansion of ERCs beyond the SEP might also be a hallmark of impairment of the DNA replica-tion machinery, a hypothesis that remains to be evaluated in future studies. Finally, we show that ERC accumulation is a lengthy process initiated long before the detection of any known hallmarks of senescence (with the exception of the loss in vacu-olar acidity [Hughes and Gottschling, 2012]) and the triggering signal is likely to occur about 10–15 generations before the onset of SEP, very early in life.

In addition to the hypothesis that ERCs limit RLS, it has also been proposed that rDNA instability, not ERCs themselves, drive entry into senescence (Ganley et al., 2009; Saka et al., 2013). Because we observed increased Pol I and pre-rRNA levels concomitant with the exponential accumulation of ERCs, we cannot exclude a scenario in which an unknown event that regulates chromosomal rDNA transcription initiates nucleolar stress, which then triggers ERC excision. However, in this case, it would be difficult to explain why the range of nucleolar markers examined here would all display sustained exponential kinetics of accumulation over close to 20 generations. Instead, this phenomenon seems easier to conceive if it is being driven by accumulation of self-replicating ERCs. In addition, a stochas-tic event, like ERC excision, can better explain the two subpop-ulations No-SEP and With-SEP emerging from an isogenic population growing in a well-controlled environment.

Under physiological conditions, the rate of rDNA transcription is buffered against variations in rDNA copy numbers (Dammann et al., 1993; French et al., 2003; Takeuchi et al., 2003). Based on this, it is usually assumed that increasing rDNA copies beyond physiological numbers (as in the case of ERCs here) should not impact on rDNA transcription rates. In that case, accumulating ERCs should not be transcribed. In contrast to this reasoning, we show that levels of pre-rRNAs and components of the rDNA transcription machinery are massively increased in cells about to enter senescence. This invalidates the assumption that rDNA transcription is under precise homeostatic regulation around the SEP and suggests that ERCs fuel excessive rDNA transcription in a mechanism that remains to be determined. Our study demonstrates that, despite a large increase in pre-rRNA synthesis and processing, senescent cells are unable to scale up ribosome production. This lack of coordination between RNA synthesis and ribosome biogenesis is consistent with a pre-vious study showing that transcription and translation of genes involved in protein biogenesis are uncoupled in aging cells (Jans-sens et al., 2015).

Recent studies have uncovered mechanistic links between aging and a number of physiological defects in nuclear pro-cesses, including the accumulation of nuclear pores (Denoth Lip-puner et al., 2014b), their functional decline (Rempel et al., 2019), and the dysregulation of cell cycle controllers such as the tran-scriptional repressor Whi5 (Neurohr et al., 2018). Our study re-vealed that entry into senescence is associated with a large increase in the N/C ratio and an overall accumulation of proteins targeted to the nucleus, thus raising the possibility of defective protein shuttling across the nucleus (Kume et al., 2017). The finding that nucleolar stress precedes the defects in protein shut-tling suggests a possible causal relationship; for example, nu-clear pores may become clogged by a buildup of pre-RNAs or ERCs, as proposed previously (Denoth Lippuner et al., 2014b).

Our study provides insights into the mechanism of daughter cell rejuvenation by demonstrating, in single cells, that asymmet-rical nucleolar and nucleoplasmic partitioning in post-SEP mother cells correlates with the rejuvenation of daughter cells. This observation provides further support to the model in which asymmetrical inheritance of ERCs accumulating in the nucleolus is a driver of the rejuvenation process. Similarly to autonomously replicating DNA circles, the asymmetrical nucleolar and nuclear division could be due to the diffusion barrier at the bud neck (Shcheprova et al., 2008). However, our results also reveal that genomic defects present in post-SEP mothers are largely inherit-able and are likely to prevent full recovery of the RLS in daughter of very old mothers, which has been reported long ago (Kennedy et al., 1994). Therefore, our study reconciles the epigenetic para-digm of daughter rejuvenation (i.e., daughters do not inherit the age of their mother) with the long-standing observation that old cells accumulate genomic alterations that must be inherited by the progeny (McMurray and Gottschling, 2003).

The nucleolar stress described in this study is likely conserved across species because similar observations have been re-ported in several studies in metazoans. In mouse embryonic fibroblasts, oncogenic stress induces rRNA transcription and triggers cellular senescence (Nishimura et al., 2015). Human fibroblasts were shown to accumulate rRNA precursors in the nucleolus and display defective ribosome biogenesis after in-duction of senescence by oncogenic Ras (Lessard et al., 2018). More recently, maintenance of nucleolar homeostasis was shown to alleviate senescence in human mesenchymal stem cells (Ren et al., 2019). Similarly, small nucleoli in post-mitotic cells were found to be a hallmark of extended longevity in Caenorhabditis elegans, Drosophila, mice, and human muscle tissue (Tiku et al., 2017). These results, together with the findings here, uncover a crucial role for the nucleolus in both replicative and chronological aging, suggesting that mechanisms ensuring rDNA stability are key regulators of longevity.

Finally, our computational model proposes a simple yet quantitative description of the steps leading to entry into senes-cence. Based on the main assumptions that excision and amplification of ERCs control

the onset of SEP, we can recapit-ulate the RLS in WT cells and in a number of mutants in which

the rate of ERC excision is affected. Most importantly, this ki-netic model of cellular lifespan is based on age-independent steps and fully supports a model in which senescence in budding yeast is driven by a purely stochastic event associated with rDNA instability, the physiological consequences of which are protracted due to the kinetics of ERC accumulation. Further experiments could further challenge this model. For example, inducing ERCs in the NO-SEP fob1D population should be suf-ficient to trigger the whole cascade of events (accumulation of pre-rRNAs, SEP, and loss of nuclear homeostasis). This sce-nario reveals how the process of aging—which manifests as an increase in the mortality rate—might be seen as an emerging property driven by a series of age-independent bio-logical processes.

STAR+METHODS

Detailed methods are provided in the online version of this paper and include the following:

- KEY RESOURCES TABLE
- LEAD CONTACT AND MATERIALS AVAILABILITY
- EXPERIMENTAL MODEL AND SUBJECT DETAILS
- METHOD DETAILS
  - Yeast strains, plasmids, and media
  - Microfluidics
  - RNA FISH-on-a-CHIP
  - Time-lapse microscopy
  - Image analysis
  - Data analysis
  - Computational simulations of replicative lifespan
- QUANTIFICATION AND STATISTICAL ANALYSIS
- DATA AND CODE AVAILABILITY

SUPPLEMENTAL INFORMATION

Supplemental Information can be found online at https://doi.org/10.1016/j.celrep.2019.06.032.

ACKNOWLEDGMENTS

We thank Denis Fumagalli and the MEDIAPREP facility of IGBMC for preparing media and Prof. Takehiko Kobayashi for providing the TMY8 strain. We are grateful to Theo Aspert, Renee Chow, Basile Jacquel, Alastair McEwen, Man-uel Mendoza, Sophie Quintin, and Zhou Xu for careful reading of the manu-script. This work was supported by the ATIP-Avenir program 2012-2017 (G.C.), a grant from the Fondation pour la Recherche Me´dicale FRM DEI20151234397 (G.C.), and by grant ANR-10-LABX-0030-INRT, a French State fund managed by the Agence Nationale de la Recherche under the frame program Investissements d'Avenir ANR-10-IDEX-0002–02. This work was partly supported by the French RENATECH network.

AUTHOR CONTRIBUTIONS

S.M., Conceptualization, Data curation, Formal analysis, Investigation, Visual-ization, Methodology, Project administration, Supervision, Writing— original draft. J.S., Data curation, Formal analysis, Investigation. I.L.-S., Methodology, Conceptualization. A.M., Resources. O.G., Conceptualization. G.C., Concep-tualization, Formal analysis, Methodology, Visualization, Project administra-tion, Software, Supervision, Funding acquisition, Writing— review & editing.

DECLARATION OF INTERESTS

The authors declare no competing interests.

Received: February 11, 2019

Revised: April 9, 2019

Accepted: June 7, 2019

Published July 9, 2019

REFERENCES

Baßler, J., Grandi, P., Gadal, O., Lessmann, T., Petfalski, E., Tollervey, D., Lechner, J., and Hurt, E. (2001). Identification of a 60S preribosomal particle that is closely linked to nuclear export. Mol. Cell 8, 517–529.

Brewer, B.J., and Fangman, W.L. (1988). A replication fork barrier at the 3^0 end of yeast ribosomal RNA genes. Cell 55, 637–643.

Dammann, R., Lucchini, R., Koller, T., and Sogo, J.M. (1993). Chromatin struc-tures and transcription of rDNA in yeast Saccharomyces cerevisiae. Nucleic Acids Res. 21, 2331–2338.

de la Cruz, J., Kressler, D., Tollervey, D., and Linder, P. (1998). Dob1p (Mtr4p) is a putative ATP-dependent RNA helicase required for the 3^0 end formation of 5.8S rRNA in Saccharomyces cerevisiae. EMBO J. 17, 1128–1140.

Defossez, P.-A., Park, P.U., and Guarente, L. (1998). Vicious circles: a mech-anism for yeast aging. Curr. Opin. Microbiol. 1, 707–711.

Defossez, P.-A., Prusty, R., Kaeberlein, M., Lin, S.-J., Ferrigno, P., Silver, P.A., Keil, R.L., and Guarente, L. (1999). Elimination of replication block protein Fob1 extends the life span of yeast mother cells. Mol. Cell 3, 447–455.

Denoth Lippuner, A., Julou, T., and Barral, Y. (2014a). Budding yeast as a model organism to study the effects of age. FEMS Microbiol. Rev. 38, 300–325.

Denoth-Lippuner, A., Krzyzanowski, M.K., Stober, C., and Barral, Y. (2014b). Role of SAGA in the asymmetric segregation of DNA circles during yeast ageing. eLife 3, e03790.

Egilmez, N.K., and Jazwinski, S.M. (1989). Evidence for the involvement of a cytoplasmic factor in the aging of the yeast Saccharomyces cerevisiae. J. Bacteriol. 171, 37–42.

Erjavec, N., Larsson, L., Grantham, J., and Nystro¨m, T. (2007). Accelerated aging and failure to segregate damaged proteins in Sir2 mutants can be sup-pressed by overproducing the protein aggregation-remodeling factor Hsp104p. Genes Dev. 21, 2410–2421.

Fano, U. (1947). Ionization Yield of Radiations. II. The Fluctuations of the Num-ber of Ions. Phys. Rev. 72, 26–29.

Fatica, A., Cronshaw, A.D., Dlakic,! M., and Tollervey, D. (2002). Ssf1p prevents premature processing of an early pre-60S ribosomal particle. Mol. Cell 9, 341–351.

Fehrmann, S., Paoletti, C., Goulev, Y., Ungureanu, A., Aguilaniu, H., and Char-vin, G. (2013). Aging yeast cells undergo a sharp entry into senescence unre-lated to the loss of mitochondrial membrane potential. Cell Rep. 5, 1589–1599.

French, S.L., Osheim, Y.N., Cioci, F., Nomura, M., and Beyer, A.L. (2003). In exponentially growing Saccharomyces cerevisiae cells, rRNA synthesis is determined by the summed RNA polymerase I loading rate rather than by the number of active genes. Mol. Cell. Biol. 23, 1558–1568.

Ganley, A.R., Ide, S., Saka, K., and Kobayashi, T. (2009). The effect of replica-tion initiation on gene amplification in the rDNA and its relationship to aging. Mol. Cell 35, 683–693.

Garmendia-Torres, C., Tassy, O., Matifas, A., Molina, N., and Charvin, G. (2018). Multiple inputs ensure yeast cell size homeostasis during cell cycle progression. eLife 7, e34025.

Gillespie, D.T. (1977). Exact stochastic simulation of coupled chemical reac-tions. J. Phys. Chem. 81, 2340–2361.

Gillespie, C.S., Proctor, C.J., Boys, R.J., Shanley, D.P., Wilkinson, D.J., and Kirkwood, T.B.L. (2004). A mathematical model of ageing in yeast. J. Theor. Biol. 229, 189–196.

Nature 183, 1751–1752.

Goulev, Y., Morlot, S., Matifas, A., Huang, B., Molin, M., Toledano, M.B., and Charvin, G. (2017). Nonlinear feedback drives homeostatic plasticity in H_2O_2 stress response. eLife 6, e23971.

Hartwell, L.H., and Unger, M.W. (1977). Unequal division in Saccharomyces cerevisiae and its implications for the control of cell division. J. Cell Biol. 75, 422–435.

Hughes, A.L., and Gottschling, D.E. (2012). An early age increase in vacuolar pH limits mitochondrial function and lifespan in yeast. Nature 492, 261–265.

Huh, W.K., Falvo, J.V., Gerke, L.C., Carroll, A.S., Howson, R.W., Weissman, J.S., and O'Shea, E.K. (2003). Global analysis of protein localization in budding yeast. Nature 425, 686–691.

Ide, S., Saka, K., and Kobayashi, T. (2013). Rtt109 prevents hyper-amplifica-tion of ribosomal RNA genes through histone modification in budding yeast. PLoS Genet. 9, e1003410.

Janssens, G.E., Meinema, A.C., Gonza´lez, J., Wolters, J.C., Schmidt, A., Gur-yev, V., Bischoff, R., Wit, E.C., Veenhoff, L.M., and Heinemann, M. (2015). Protein biogenesis machinery is a driver of replicative aging in yeast. eLife 4, e08527.

Jorgensen, P., Edgington, N.P., Schneider, B.L., Rupes, I., Tyers, M., and Futcher, B. (2007). The size of the nucleus increases as yeast cells grow. Mol. Biol. Cell 18, 3523–3532.

Kaeberlein, M., McVey, M., and Guarente, L. (1999). The SIR2/3/4 complex and SIR2 alone promote longevity in Saccharomyces cerevisiae by two different mechanisms. Genes Dev. 13, 2570–2580.

Kaeberlein, M., Kirkland, K.T., Fields, S., and Kennedy, B.K. (2004). Sir2-inde-pendent life span extension by calorie restriction in yeast. PLoS Biol. 2, E296.

Kennedy, B.K., Austriaco, N.R., Jr., and Guarente, L. (1994). Daughter Cells of Saccharomyces cerevisiae from Old Mothers Display a Reduced Life Span. J. Cell Biol 127, 1985–1993.

Kobayashi, T. (2003). The replication fork barrier site forms a unique structure with Fob1p and inhibits the replication fork. Mol. Cell. Biol. 23, 9178–9188.

Kume, K., Cantwell, H., Neumann, F.R., Jones, A.W., Snijders, A.P., and Nurse, P. (2017). A systematic genomic screen implicates nucleocytoplasmic transport and membrane growth in nuclear size control. PLoS Genet. 13, e1006767.

Lessard, F., Igelmann, S., Trahan, C., Huot, G., Saint-Germain, E., Mignacca, L., Del Toro, N., Lopes-Paciencia, S., Le Calve´, B., Montero, M., et al. (2018). Senescence-associated ribosome biogenesis defects contributes to cell cycle arrest through the Rb pathway. Nat. Cell Biol. 20, 789–799.

Mansisidor, A., Molinar, T., Jr., Srivastava, P., Dartis, D.D., Pino Delgado, A., Blitzblau, H.G., Klein, H., and Hochwagen, A. (2018). Genomic copy-number loss is rescued by self-limiting production of DNA circles. Mol. Cell 72, 583– 593.e4.

McMurray, M.A., and Gottschling, D.E. (2003). An age-induced switch to a hyper-recombinational state. Science 301, 1908–1911.

Miyazaki, T., and Kobayashi, T. (2011). Visualization of the dynamic behavior of ribosomal RNA gene repeats in living yeast cells. Genes Cells 16, 491–502.

Mortimer, R.K., and Johnston, J.R. (1959). Life span of individual yeast cells.

Neumann, F.R., and Nurse, P. (2007). Nuclear size control in fission yeast.

J. Cell Biol. 179, 593–600.

Neurohr, G.E., Terry, R.L., Sandikci, A., Zou, K., Li, H., and Amon, A. (2018). Deregulation of the G1/S-phase transition is the proximal cause of mortality in old yeast mother cells. Genes Dev. 32, 1075–1084.

Neurohr, G.E., Terry, R.L., Lengefeld, J., Bonney, M., Brittingham, G.P., Mor-etto, F., Miettinen, T.P., Vaites, L.P., Soares, L.M., Paulo, J.A., et al. (2019). Excessive Cell Growth Causes Cytoplasm Dilution And Contributes to Senes-cence. Cell 176, 1083–1097.e18.

Nishimura, K., Kumazawa, T., Kuroda, T., Katagiri, N., Tsuchiya, M., Goto, N., Furumai, R., Murayama, A., Yanagisawa, J., and Kimura, K. (2015). Perturba-tion of ribosome biogenesis drives cells into senescence through 5S RNP-mediated p53 activation. Cell Rep. 10, 1310–1323.

Rempel, I.L., Crane, M.M., Thaller, D.J., Mishra, A., Jansen, D.P., Janssens, G., Popken, P., Aksxit, A., Kaeberlein, M., van der Giessen, E., Steen, A., Onck, P.R., Lusk, C.P., and Veenhoff, L.M. (2019). Age-dependent deteriora-tion of nuclear pore assembly in mitotic cells decreases transport dynamics. eLIFE. https://doi.org/10.7554/eLife.48186.

Ren, X., Hu, B., Song, M., Ding, Z., Dang, Y., Liu, Z., Zhang, W., Ji, Q., Ren, R., Ding, J., et al. (2019). Maintenance of Nucleolar Homeostasis by CBX4 Allevi-ates Senescence and Osteoarthritis. Cell Rep. 26, 3643–3656.e7.

Saka, K., Ide, S., Ganley, A.R., and Kobayashi, T. (2013). Cellular senescence in yeast is regulated by rDNA noncoding transcription. Curr. Biol. 23, 1794– 1798.

Saveanu, C., Bienvenu, D., Namane, A., Gleizes, P.E., Gas, N., Jacquier, A., and Fromont-Racine, M. (2001). Nog2p, a putative GTPase associated with pre-60S subunits and required for late 60S maturation steps. EMBO J. 20, 6475–6484.

Shcheprova, Z., Baldi, S., Frei, S.B., Gonnet, G., and Barral, Y. (2008). A mech-anism for asymmetric segregation of age during yeast budding. Nature 454, 728–734.

Sinclair, D.A., and Guarente, L. (1997). Extrachromosomal rDNA circles–a cause of aging in yeast. Cell 91, 1033–1042.

Sinclair, D.A., Mills, K., and Guarente, L. (1997). Accelerated aging and nucle-olar fragmentation in yeast sgs1 mutants. Science 277, 1313–1316.

Smeal, T., Claus, J., Kennedy, B., Cole, F., and Guarente, L. (1996). Loss of transcriptional silencing causes sterility in old mother cells of S. cerevisiae. Cell 84, 633–642.

Takeuchi, Y., Horiuchi, T., and Kobayashi, T. (2003). Transcription-dependent recombination and the role of fork collision in yeast rDNA. Genes Dev. 17, 1497–1506.

Tiku, V., Jain, C., Raz, Y., Nakamura, S., Heestand, B., Liu, W., Spa¨th, M., Suchiman, H.E.D., Muller,€ R.U., Slagboom, P.E., et al. (2017). Small nucleoli are a cellular hallmark of longevity. Nat. Commun. 8, 16083.

Veatch, J.R., McMurray, M.A., Nelson, Z.W., and Gottschling, D.E. (2009). Mitochondrial dysfunction leads to nuclear genome instability via an iron-sulfur cluster defect. Cell 137, 1247–1258.

STAR+METHODS

KEY RESOURCES TABLE

REAGENT or RESOURCE	SOURCE	IDENTIFIER
Chemicals, Peptides, and Recombinant Proteins		
Sylgard! 184 silicone polymer	World Precision Instruments LTD	Cat#SYLG184
Paraformaldehyde (PFA)16% ultra-pure methanol free	Electron Microscopy Sciences	Cat#50-980-487
Sorbitol	Sigma	Cat#S1876
Zymolyase 20T	Euromedex	Cat#UZ1000
Phenylmethylsulfonyl fluoride (PMSF)	Fischer Scientific	Cat#10485015
Vanadyl Ribonucleoside Complex (Vanadium)	Sigma	Cat#R3380
Mercaptoethanol-2 98% (bME)	Sigma	Cat#M3148
Formamide	Sigma	Cat#F-5786
Bovine Serum Albumin (BSA)	MP Biomedicals	Cat#841033
tRNA from E. coli	Roche Diagnostics	Cat# 10109541001
Triton X-100	Sigma	Cat#T8787
Experimental Models: Organisms/Strains		
S. cerevisiae: strain TMY8: MATa; ade2::pAFS144-wtGFP(ADE2); rDNA::pTM-lacO50 (URA3) amplified 150 copies NET1-mCherry-spHIS5, leu2-3,112 trp1-1 can1-100 ura3-1 ade2-1 his3-11,1	(Miyazaki and Kobayashi, 2011)	N/A
S. cerevisiae: strain TMY8-BY4B: MATa; ade2::pAFS144-wtGFP(ADE2); rDNA::pTM-lacO50 (URA3) amplified 150 copies NET1-mCherry-spHIS5; leu2D0; LYS2; MET15; TRP1	This study	N/A
S. cerevisiae: strain RPA190-GFP: from S288C, MATa; RPA190-GFP-HIS3MX; ADE2; leu2D0; LYS2; met15D0; ura3D0; TRP1	Thermo Fischer scientific	Yeast GFP Clone Collection
S. cerevisiae: strain SSF1-GFP: from S288C, MATa; SSF1-GFP-HIS3MX; ADE2; leu2D0; LYS2; met15D0; ura3D0; TRP1	Thermo Fischer scientific	Yeast GFP Clone Collection
S. cerevisiae: strain NOG2-GFP: from S288C, MATa; NOG2-GFP-HIS3MX; ADE2; leu2D0; LYS2; met15D0; ura3D0; TRP1	Thermo Fischer scientific	Yeast GFP Clone Collection
S. cerevisiae: strain RPL13A-GFP: from S288C, MATa; RPL13A-GFP-HIS3MX; ADE2; leu2D0; LYS2; met15D0; ura3D0; TRP1	Thermo Fischer scientific	Yeast GFP Clone Collection
S. cerevisiae: strain YCG01: from S288C, MATa; ADE2; his3D1;	(Garmendia-Torres et al.,	N/A

leu2D0; lys2D0; met15D0; ura3D0; TRP1; HTB2-sfGFP-KANMX	2018)	
S. cerevisiae: strain SJ164: from S288C, MATa; ADE2; his3D1; leu2D0; lys2D0; MET15; ura3D0; TRP1SP25::SP25-Act1p-NLS-sfGFP-STOP-Adh1t-NatMX	This study	N/A
S. cerevisiae: strain YAP160-1: from S288C, MATa; ADE2; his3D1; leu2D0; LYS2; met15D0; ura3D0; TRP1; SP25::SP25-Act1p-sfGFP-STOP-Adh1t-NatMX	This study	N/A
S. cerevisiae: strain SRP1-GFP: from S288C, MATa; SRP1-GFP-HIS3MX; ADE2; leu2D0; LYS2; met15D0; ura3D0; TRP1	Thermo Fischer scientific	Yeast GFP Clone Collection
S. cerevisiae: strain BY4742: from S288C, MATa; ADE2; his3D1; leu2D0; lys2D0; MET15; ura3D0; TRP1	Euroscarf	Cat#Y10000

S. cerevisiae: strain YCG02: from S288C, MATa; ADE2; his3D1; leu2D0; lys2D0; MET15; ura3D0; TRP1; HTB2-sfGFP-KANMX	N/A	(Garmendia-Torres et al., 2018)
S. cerevisiae: strain fob1D: from S288C, MATa; ADE2; his3D1; leu2D0; lys2D0; MET15; ura3D0; TRP1; fob1::kanMX4	Euroscarf	Cat#Y14044
S. cerevisiae: strain sir2D: from S288C, MATa; ADE2; his3D1; leu2D0; lys2D0; MET15; ura3D0; TRP1; sir2::kanMX4	Euroscarf	Cat#Y13738

(Continued on next page)

Continued

REAGENT or RESOURCE	SOURCE	IDENTIFIER
S. cerevisiae: strain SM627: same as TMY8-BY4B except MATa; lys2D0; fob1::KANMX	This study	N/A
S. cerevisiae: strain SM546: from S288C, MATa; RPA190-GFP-HIS3MX; fob1::KANMX; ADE2; leu2D0; LYS2; MET15; ura3D0; TRP1	This study	N/A
S. cerevisiae: strain SM345: from S288C, MATa; HTB2-sfGFP-KANMX; fob1::KANMX; ADE2; leu2D0; lys2D0; met15D0; ura3D0; TRP1	This study	N/A
S. cerevisiae: strain SM550: from S288C, MATa; ADE2; his3D1; leu2D0; lys2D0; MET15; ura3D0; TRP1; sir2::kanMX4; fob1::kanMX4	This study	N/A
S. cerevisiae: strain SM613: same as TMY8-BY4B except sir2::KANMX	This study	N/A
Oligonucleotides		
ITS1 FISH probe: GCACAGAAATCTCTCACCGTTTGGAATAGCAAG AAAGAAACTTACAAGC + 5^{0} Cy3	This study	N/A
Recombinant DNA		
pDM402: SIR2 in pRS315 backbone (CEN LEU2 AmpR)	From Moazed laboratory. Provided by Paola Fabrizio	N/A
Software and Algorithms		
NIS Element AR	Nikon	N/A
MATLAB R2016a	MathWorks	N/A
Phylocell	(Goulev et al., 2017)	https://www.github.com/gcharvin
Autotrack	(Goulev et al., 2017)	https://www.github.com/gcharvin

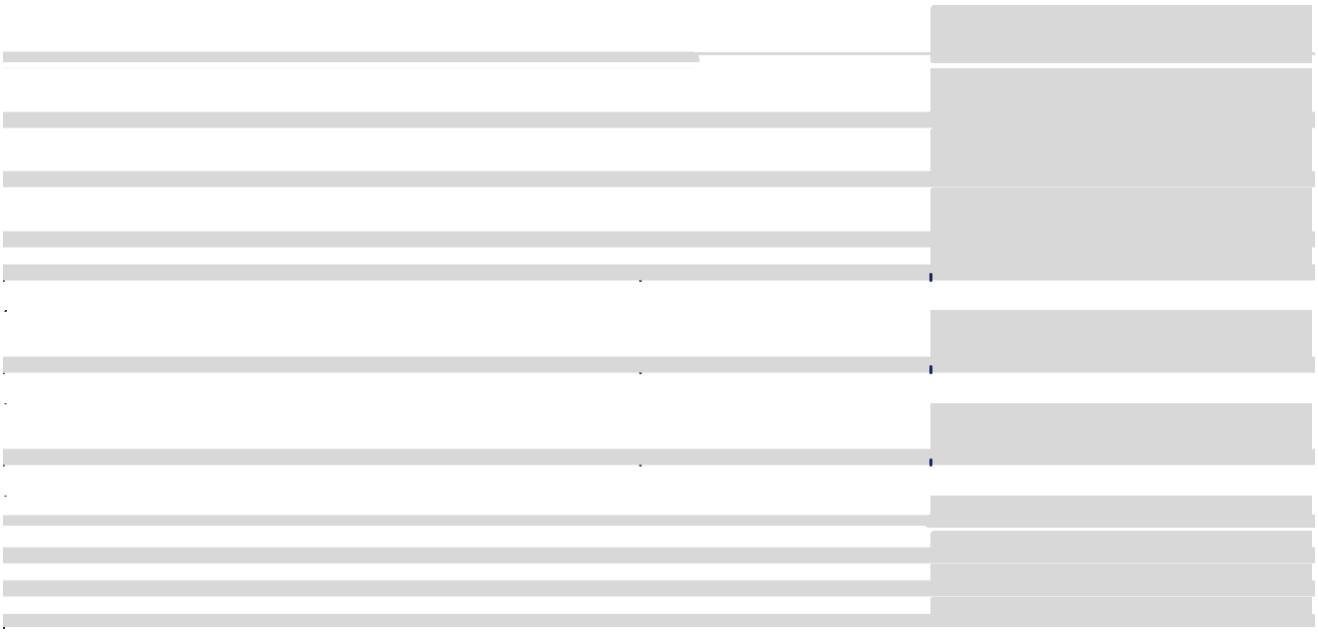

LEAD CONTACT AND MATERIALS AVAILABILITY

Further information and requests for resources and reagents should be directed to and will be fulfilled by the Lead Contact, Gilles Charvin (charvin@igbmc.fr).

EXPERIMENTAL MODEL AND SUBJECT DETAILS

Saccharomyces cerevisiae is the experimental model used in this study. All strains are congenic to S288C, except TMY8 and TMY8-BY4B, and listed in the Key Resources Table.

METHOD DETAILS

Yeast strains, plasmids, and media

TMY8-BY4B was obtained from backcrossing four times with BY4742/BY4741 the strain TMY8 provided by Prof. Takehiko Kobaya-shi. All GFP-labeled strains were from the Yeast GFP Clone Collection provided by Michael Knop (Huh et al., 2003). fob1D and sir2D strains were purchased from Euroscarf, crossed with strains containing the relevant GFP markers, and genotyped by PCR. As sir2D strain is sterile and in order to cross it, this strain was transformed with pDM402, a non-integrative plasmid containing SIR2 gene. After crossing, strains of interest were counter-selected for pDM402 plasmid loss by checking their inability to grow in synthetic dextrose (SD) medium without leucine. The Htb2-sfGFP (Garmendia-Torres et al., 2018), Act1pr-sfGFP (sfGFP), and Act1pr-NLS-sfGFP (NLS-sfGFP) strains were generated using DNA editing and yeast genetics classical techniques.

Prior to loading into microfluidic chips, freshly thawed cells were grown overnight in synthetic complete medium with 2% dextrose and then diluted in the morning to allow several divisions in exponential growth.

Microfluidics

The microfluidic master mold was made using standard soft-lithography techniques in the FEMTO-ST nanotechnology platform of the French Renatech network (Besanc¸on, France). Prototypic molds were replicated in epoxy to ensure long-term preserva-tion. The micro-channels were cast by curing PDMS (Sylgard 184, 10:1 mixing ratio) and then covalently bound to a 24 3 50 mm coverslip using plasma surface activation (Diener, Germany). The assembled chip was then baked for 1 h at 60 C to consolidate bonding between the glass and PDMS and then perfused with media using Tygon tubing and a peristaltic pump (Ismatec, Switzerland) at a 10 ml/min flow rate. After 2 h of PDMS rehydration, yeast cells were loaded into the chip with a 1 mL syringe and a 23G needle.

RNA FISH-on-a-CHIP

Time-lapse imaging was stopped after 65 h acquisition and the chip was perfused with 4% paraformaldehyde for 30 min at room temperature (RT) and then washed for 20 min with buffer B (1.2 M sorbitol, 0.1 M potassium phosphate, pH 7.5). The cell walls were digested by flowing a zymolyase mix (0.2mg/ml Zymolyase 20T, 0.2mM PMSF, 2mM Vanadium, 29mM bME) through the chip for 20 min at RT followed by a 20 min wash with buffer B. The chip was then rinsed with cold 70% ethanol for 5 min, with 2xSSC (saline-sodium citrate) for 15 min, and with 10% formamide in 2xSSC for 20 min. A hybridization mix containing 1 ng/ml FISH probe (in 2xSSC, 10% formamide, 10mM Vanadium, 0.5mg/ml BSA, 0.5mg/ml tRNA) was injected into the chip and the cells were incubated at 37 C for 3 h, protected from light. The cells were then rinsed with warm (37 C) 10% formamide in 2xSSC for 30 min, 1% Triton X-100 in 2xSSC for 20 min, and 1xSSC for 30 min. The cells were then imaged on a Nikon Ti-Eclipse with an mCherry filter to acquire the FISH probe signal (50% LED power, 300 ms exposure time, binning 2 3 2) and a GFP filter to acquire the Rpa190-GFP (20% led power, 100 ms exposure time, binning 2 3 2) as well as in phase contrast. The FISH probe (with a 5^0 Cy3 dye) targets the ITS1 region between the A2 cleavage site and the 18S coding region.

Time-lapse microscopy

Cells were imaged using an inverted Nikon Ti-E microscope. Fluorescence illumination was achieved using LED light (Lumencor) and emitted light was collected using a 60 3 N.A. 1.4 objective and a CMOS camera Hamamatsu Orca Flash 4.0. An automated stage was used to follow up to 60 different fields of view in parallel over the course of the experiment. Images were acquired every 10 or 15 min for a total duration of 140 h (full lifespan experiments) or 65 h (RNA FISH experiments) using NIS software. Focus was maintained using the Nikon Perfect Focus System. A constant temperature of 30 C was maintained on the chip using a custom sample holder with thermoelectric modules, an objective heater with heating resistors, and a PID controller (5C7-195, Oven Industries).

Image analysis

After acquisition, NIS raw data were analyzed using the custom MATLAB software phylocell and autotrack, available on https://www.github.com/gcharvin. Cell contours and fluorescent markers were segmented using a modified watershed algorithm and tracking was achieved with the Hungarian method, as previously described (Goulev et al., 2017). Cell area was measured from the segmen-tation of the phase contrast images (Figure 2F). Nuclear and nucleolar areas were measured from the segmentation of Htb2-sfGFP signal (Figures 4C, 4D, and 5I) and Net1-mCherry signal (Figure 5C) respectively.

Data analysis

As birth alignment blurs the dynamics of aging (Figure S1), we aligned single-cell trajectories from the onset of cell cycle slowdown (or SEP). To determine the SEP, we calculated the frequency of division for each individual cellular lifespan and we used piecewise linear model to determine the time beyond which the frequency of division rapidly declines (see Figure S2). Therefore, cells that have passed the SEP are not strictly in a senescent state, yet, they have started to undergo an irreversible physiological decline leading to cell death. The determination of the SEP is then systematically used as a reference of time to assess the average dynamics of specific markers throughout the manuscript, unless specified otherwise (e.g., Figures S3E-S3H).

A least-square minimization technique was used to fit GFP-LacI data to an exponential model (Figure 1E), excluding data points associated with late senescence (i.e., > SEP + 3 divisions), during which the GFP-LacI saturates.

Computational simulations of replicative lifespan

We designed a stochastic numerical model to describe the replicative lifespan of individual cells in which ERCs are excised and allowed to amplify, as previously described (Gillespie et al., 2004). For convenience, instead of discrete probability distributions, we used an analogy to a biochemical system with continuous time based on the following assumptions: 1) an ERC is randomly excised from the genome with a rate k_e per generation; Multiple ERC excisions are allowed during the course of the simulation, yet this does not much influence the exponential dynamics of ERCs, which is set by the first excision event; 2) Following a mechanism of self-replication, ERCs accumulate exponentially within the mother cell, with a doubling-time t (per generation), the value of which is measured experimentally. Hence, in the case of t > 1 generations, this rule assumes that the efficiency of replication may be lower than 100% or, alternatively, that some ERCs may

be inherited by daughter cells; 3) Once the number of ERCs within a mother cell overcomes a threshold ERC^{thr}, the cell division cycle starts to be impaired (SEP) and cell death occurs randomly with a rate k_s per generation, as observed experimentally (Figure 6).

We used the Gillespie algorithm (Gillespie, 1977) to generate 200 single cell trajectories according to this set of rules, in which the number of ERCs copies was simulated over time. Then, we extracted the numerical distribution of timings associated with the three main events that compose the lifespan of cells, i.e., the excision of the first ERC, the onset of entry into senescence (SEP), and cell death (Figure 7).

To account for the fact that a large fraction of fob1D cells die without any observable ERC accumulation, we used a Gompertz law to model an ERC-independent path to senescence, with a hazard rate l defined as:

$$l(age) = l_0 e^{m\ age}$$

where l_0 is the initial mortality rate and m is the rate of increase of the mortality rate with age. Therefore, the cells died either following excision and accumulation of ERC or from an alternative cause that did not lead to a cell cycle slow down (SEP), and the fraction of cells with SEP was calculated within the population of simulated cells.

QUANTIFICATION AND STATISTICAL ANALYSIS

All experiments have been replicated at least twice. Data are presented in Results and Figures as the mean ± SEM (curves) or median (boxplots). Boxplots show the median, the notch (95% confidence interval of the median), the 25^{th} quantile, the 75^{th} quantile, extreme data points and outliers. ****$p < 0.0001$, t test. Group means were compared using Two-sample t test. A P value of < 0.05 was considered significant.

DATA AND CODE AVAILABILITY

The custom MATLAB software phylocell and autotrack, used to analyze imaging data are available on https://www.github.com/ gcharvin.

Characterization of Senescence Entry Point using long-lived mutants and intervention related to ageing factors ERC and ROS

Résumé en français

Mon projet de thèse est d'étudier le processus de vieillissement réplicatif chez la levure. La levure en tant qu'organisme modèle conventionnel a été utilisée pour les études sur le vieillissement cellulaire. Elle se produise par bourgeonnement, cette division asymétrique implique une ségrégation asymétrique entre la mère et la fille. Des facteurs de vieillissement ont été découverts lors d'une division asymétrique. Son accumulation chez la mère induit un phénomène de vieillissement, tandis que les filles naissent sans dommages (facteurs de vieillissement) et sont rajeunies.

L'un des facteurs de vieillissement est les cercles extra-chromosomiques d'ADNr (ERC), qui proviennent de la région répétitive d'ADNr par recombinaison homologue. Cet ERC possède des gènes d'ADNr qui peuvent être utilisés comme matrice pour la synthèse d'ARNr et la ribogenèse. Il contient également une région auto-réplicative qui peut initier la réplication avec la progression du cycle cellulaire. Par conséquent, comme l'ERC se double et s'accumule chez la mère après chaque cycle, les cellules mères présentent une accumulation exponentielle d'ERC qui induit un phénotype vieillissant. Alors que les filles naissent sans ERC et sont rajeunies. L'oxygène réactif (ROS) est proposé comme facteur de vieillissement à accumuler pendant le processus de vieillissement.

Une étude antérieure du laboratoire a révélé un ralentissement brutal et irréversible du cycle cellulaire pendant la durée de vie réplicative (RLS). Ce point de rupture de l'extension du cycle cellulaire est défini comme le point d'entrée de la sénescence (SEP). Nous cherchons à comprendre le mécanisme sous-jacent au SEP et les facteurs de vieillissement potentiels liés à la régulation du SEP.

Pour étudier le processus de vieillissement chez la levure, j'utilise le système micro-fluidique pour capturer la levure mère unique et suivre ses divisions successives sous microscope time-lapse. En surveillant la dynamique des mécanismes moléculaires et l'évolution phénotypique à l'aide de mutants et d'interventions à longévité étendue, j'essaie de comprendre le SEP, ses mécanismes de régulation potentiels et ses conséquences sur le vieillissement.

En utilisant des mutants à longue durée de vie, je montre qu'un nouveau mécanisme de mort dont les cellules meurent sans ERC. Cette sous-population meurt sans accumulation d'ERC et SEP (ralentissement du cycle cellulaire). Finalement, ces mutants à longue durée de vie présentent une extension de la longévité grâce à un mécanisme d'induction d'un événement probabiliste SEP en perturbant l'accumulation du nombre de copies ERC (probablement par le taux d'excision ERC).

En utilisant une intervention à longue durée de vie sous une dose faible (50 µM) de H2O2 (ROS), le SEP est retardé, ce qui suggère que l'effet hormésis par le ROS peut retarder le SEP induit par l'ERC. L'extension de la longévité est obtenue grâce à un SEP retardé général qui est différent de l'ensemble des mutants précédents. Selon les résultats préliminaires, la cellule vit plus longtemps sous un léger stress de ROS en maintenant la stabilité de l'ADNr et déclenche moins de formation d'ERC. La stabilité du génome et la croissance cellulaire peuvent être impliquées dans le mécanisme. Ce résultat établit un lien entre le ROS stress (oxydant) et la formation de l'ERC (stabilité de l'ADNr).

Ce projet de thèse sert à fournir une compréhension complémentaire sur les mécanismes de régulation potentiels pour induire la SEP à travers la caractérisation du comportement phénotypique chez les mutants à longue durée de vie et l'intervention. Une relation entre ROS, ERC et SEP conduit à de nouvelles orientations de recherche.

Summary in English

My thesis project is to study replicative ageing process in budding yeast. Budding yeast as a conventional ageing model organism has been used for cellular ageing studies. Its asymmetric division budding pattern implies an asymmetric segregation between mother and daughter. Ageing factors have been uncovered during asymmetric division. Its accumulation in mother induce ageing phenomenon, while daughters are born free of damage (ageing factors) and are rejuvenated.

One of the ageing factors is the Extrachromosomal rDNA Circles (ERC), which arises from rDNA repetitive region by homologous recombination. This ERC has rDNA genes which can be used as template for rRNA and ribosome synthesis. It contains also auto-replicative region which can initiate replication along with cell cycle progression. Therefore, as ERC duplicate and accumulate in mother following each round of duplication, the mother cells shows exponential ERC accumulation which result in an ageing phenotype. Whereas the daughters are born ERC-free.

Reactive Oxygen Species (ROS) is proposed as an ageing factor to be accumulated during ageing process.

Previous study of the host laboratory has uncovered an abrupt irreversible cell cycle slowdown during Replicative Lifespan (RLS). This breaking point of cell cycle extension is defined as Senescence Entry Point (SEP). We seek to understand the mechanism underlying the SEP and potential ageing factors linking to the regulation of SEP.

To study the ageing process in budding yeast, I use the microfluidic system to capture single mother yeast and follow its successive divisions under time-lapse microscope. By monitoring the dynamic of molecular mechanisms and phenotypic evolution using longevity extended mutants and interventions, I try to understand the SEP, its potential regulatory mechanisms and consequences to ageing.

Using long-lived mutants, I show that a new mechanism of death which cells die in a ERC-free manner is uncovered. This subpopulation dies without ERC accumulation and SEP (cell cycle slowdown). Eventually, these long-lived mutants show longevity extension through a mechanism of inducing probabilistic SEP event by perturbing the ERC copy number accumulation (probably through ERC excision rate).

Using long-lived intervention under mild dose (50µM) of H2O2 (ROS) treatment, the SEP is delayed, suggesting hormetic effect by ROS can delay ERC induced SEP. Longevity extension is achieved through a general SEP elongation which is different from previous set of mutants. According to preliminary result, the cell lives longer under mild stress of ROS by maintenance of rDNA stability and trigger less ERC formation. Genome stability and cell growth maybe involved in the mechanism. This result establishes a link between (oxidative) stress and ERC formation (rDNA stability).

This thesis project serves to provide a complementary understanding on the potential regulatory mechanisms for inducing SEP through characterization the phenotypic behavior in long-lived mutants and intervention. A relationship between ROS, ERC and SEP leads to new research orientations.